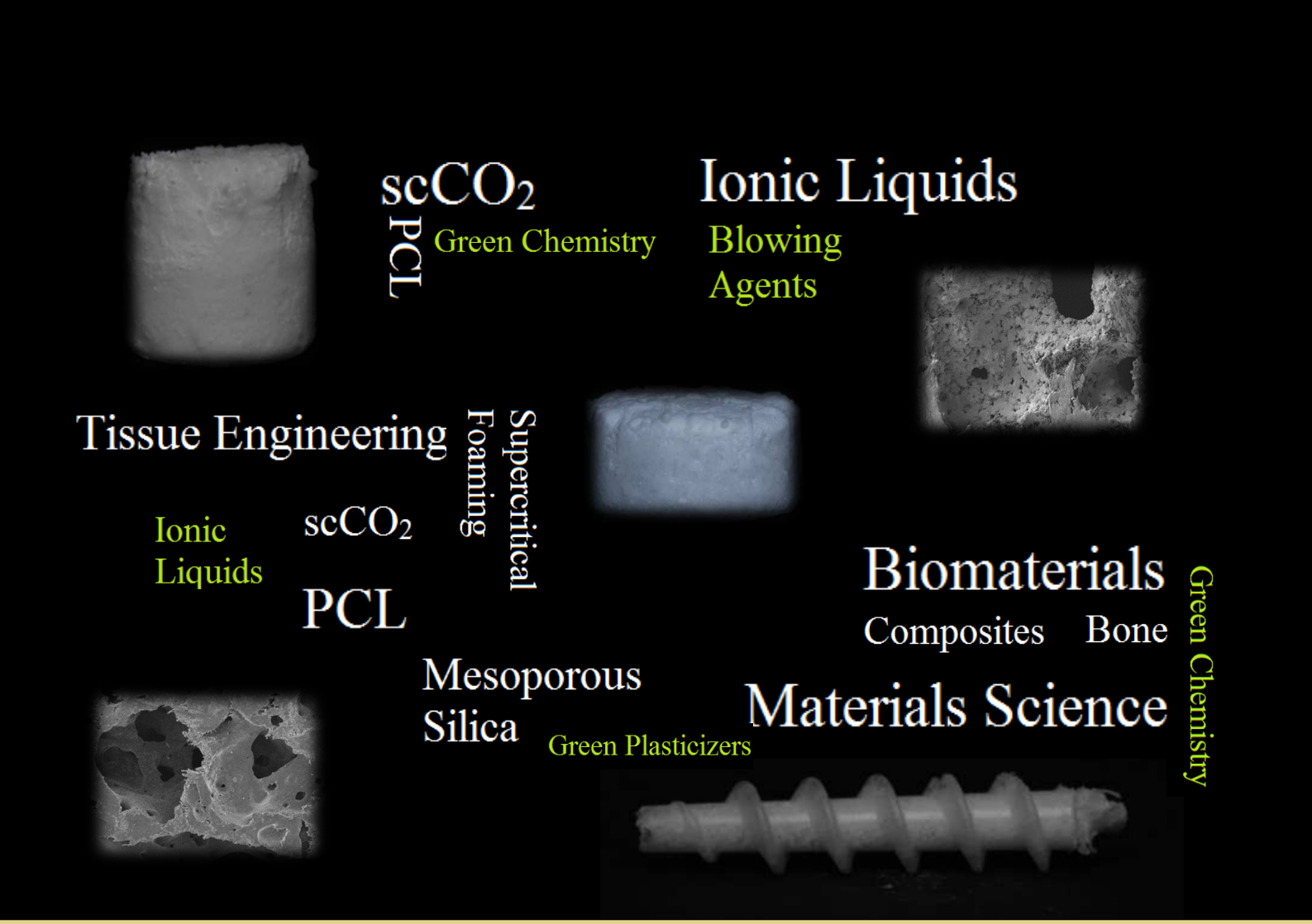

Rui Miguel Minhós Churro

Supercritical foaming/mixing on the preparation of PCL/mesoporous silica based composites for hard tissue engineering applications

Master's Thesis in Chemical Engineering
Presented to the Chemical Engineering Department of the Faculty of Sciences and Technology of University of Coimbra

September 2015

· U C ·

UNIVERSIDADE DE COIMBRA

Rui Miguel Minhós Churro

Supercritical foaming/mixing on the preparation of PCL/mesoporous silica based composites for hard tissue engineering applications

Dissertation submitted to Faculty of Science and Technology of University of Coimbra for attribution of Master's Degree in Chemical Engineering

Supervisors:

Prof. Dr. Hermínio José Cipriano de Sousa

Prof. Dr. Mara Elga Medeiros Braga

Coimbra
2015

· U C ·

UNIVERSIDADE DE COIMBRA

This page was intentionally left in blank

Acknowledgements

This works represents the end of a long journey during which lots of people were involved, helping me reaching my goals with success. The accomplishment of this work could not be possible without the help, contribution and incentive of everyone. I would like to take this opportunity to express my greater gratitude to each and every one of them.

Firstly, all my gratitude relies on my advisers, Professor Hermínio de Sousa and Professor Mara Braga, for all the availability, excellent guidance, excellent working ethics, expert advices and constructive critics and for always believing in me. This work is only possible because of their work and dedication.

My special thanks to António Rosa, for all the guidance, support and teaching in the lab from the very beginning of this work, to the very end.

To all of the research group members, António Rosa, Rita Chim, Luísa Filipe, Sofia Merceneiro and Dr. Ana Dias, for all the help, sympathy and availability at any time, I own them my gratitude.

To José Viegas from Escola Superior Agrária de Coimbra from Instituto Politécnico de Coimbra for all the help and assistance during the compression tests of the filler choice assays.

To Prof. António Alberto, from Department of Civil Engineering from University of Coimbra, for all the help and assistance during the compression tests with the oedometer and for the correction of the discussion of the obtained results.

To Rui Farias, for all the amazing professional-looking photographs and to Escola Superior de Artes Aplicadas from Instituto Politécnico de Castelo Branco, for the provision of the photographic study.

To my girlfriend, Stacy Morgado, who has always stood by my side no matter what, sorry for all the time that I have not spent with you and sorry for that times that I was not in my best mood due to work, you have been a breath of fresh air in my life, to you, all of my gratitude.

To Coimbra, and to all of the true friends that I have made in this marvellous city, who throughout this entire journey always gave all of their help and assistance, Fábio Branco, João Santos, André Gonçalves, José Lobo, for teaching me how to play PES and how to work with the higher standards, Daniel Marcos, for showing me and teaching me how to work and manage large groups and for showing me what Académica is all about, Pedro Sobral, it was an honour to work with you and to discuss football with. To you all I owe the man that I am today.

To all of my friends for and from life, Tiago Carrega, Bruno Penedo, Nuno Barata, Rui Gordino, “Bia” Rodrigues, João Bispo, Filipe Lobo and António Mingacho for everything that we have been trough and everything that we will be trough.

Last, but not least, all of my deepest gratitude is owed to all of my family members, my cousin, Ivo Ferreira and my brother, whom from the very beginning always believed in me and in my work, giving me unconditional help and assistance, especially my deepest gratitude to my mother and father, to whom I dedicate this work.

Abstract

Despite the chemical and biological properties, the success of processes towards the development of hard tissue engineering porous materials strongly relies on the control over physical properties such as, porosity, average pore diameter, surface area, surface roughness (tribological properties), compressive strength and crystallinity. Polymeric materials do not present sufficient mechanical properties for hard tissue engineering applications, so the incorporation of an inorganic filler, producing porous composite biomaterials arises as solution to adopt towards the development of mechanical improved materials. Conventional methods of polymer processing into porous materials, usually make use of environmental hazardous compounds, such as organic substances. Employing such compounds leads to the need of a further processing step of removal, in order to decrease the potential toxicity of the produced materials. This step usually involves the use of high temperatures, which, on its turn may unable the incorporation of thermosensitive bioactive compounds during processing.

Supercritical carbon dioxide ($scCO_2$) foaming/mixing process (SFM) arises as a clean and environmental safe alternative towards the production of porous biomaterials for hard tissue engineering applications, allowing to incorporate bioactive compounds without degrade them, due to its easily achievable supercritical conditions and recovery feature. Also, CO_2 acts as a temporary plasticizer and as foaming agent, reducing the melting (T_m) and glass transition (T_g) temperatures of several polymers facilitating their processing.

This work is divided into four stages, with the main goal to optimize processing and obtain composite porous materials with controlled morphology, mechanical and thermal properties towards hard tissue engineering applications.

On the first stage poly(ε-caprolactone) (PCL)-based porous composite biomaterials were produced by SFM by pressure quench at constant processing conditions, namely pressure (20 MPa), temperature (45ºC), depressurization rate (1 $MPa.min^{-1}$) and contact time (2h). Three inorganic fillers were incorporated, hydroxyapatite (HA), montmorillonite (MMT) and mesoporous silica nanoparticles SBA-15 type (SBA-15), in two compositions (10 and 20 wt. %). The obtained composites were morphologically (macroscopic and water absorption analysis) and mechanically (compression tests) characterized. Composite porous biomaterials were found to be morphologically and mechanically enhanced due to the incorporation of these fillers. The obtained results were not conclusive in order to choose an inorganic type and composition as the optimum towards the development of a porous composite biomaterial for hard tissue engineering applications, since no homogeneous dispersion of the fillers was obtained. So, SBA-15 was chosen as the ideal filler due to its high surface area and mesoporous feature, ensuring to the biomaterial an extra drug carrier potential.

On the second stage PCL porous biomaterials were produced by SFM at variable processing conditions in order to obtain an optimum set of operating conditions towards the development of hard tissue engineering-grade materials, based on their morphological and mechanical properties. At constant pressure (20 MPa) and contact time (2h) a variation on $scCO_2$ density of 100 $kg.m^{-3}$ and 2 Pa.s on $scCO_2$ viscosity were tested, by varying the operating temperature, employing 35, 40, 45 and 50ºC. Two depressurization rates were also tested, of 1 $MPa.min^{-1}$ and 0.3 $MPa.min^{-1}$. It was found that operating at a temperature of 40ºC with a depressurization rate of 0.3 $MPa.min^{-1}$ and at a temperature of 45ºC with a depressurization rate of 1 $MPa.min^{-1}$ similar morphological properties were obtained (BET average pore diameter of 0.5 ± 0.0 and 0.6 ± 0.0 µm respectively) tough the first set yielded into improved mechanical properties (Young's modulus of 32.6 ± 3.0 MPa comparing to 23.9 ± 1.2 MPa). The first set of operation

conditions was found to be the optimum, so the obtained results in this work could be compared with previous works.

On the third stage, PCL/SBA-15 (20 and 30 wt. %) porous composite biomaterials were produced by SFM at the optimal operating conditions, determined in the previous stage. These composite porous biomaterials were also additivated with greener and safer liquid additives, which are expected to act as porogenic agents, plasticizers and polymer compatibilizers, such as Glycofurol (GF), a FDA approved hydrotrope and Trihexyl(tetradecyl) phosphonium bis (trifluoromethylsulfonyl)imide (TTPB), a nontoxic ionic liquid in a molar composition of 98% relative to PCL and in three relative molar proportions, in mixture, (GF:TTPB) of 2:1, 3:1 and 5:1. The effects of the inorganic filler and liquid additives were assessed by scanning electron microscopy - energy-dispersive X-ray spectroscopy (SEM-EDS), mercury intrusion, nitrogen adsorption, helium picnometry, simultaneous differential thermal analysis (SDT), X-ray diffraction (XRD) and with compression tests.

By macroscopic and microscopic (SEM) analysis a SBA-15 composition of 30 wt. % was found to be a high silica content. The results from SEM-EDS confirmed the presence of the liquid additives and the filler, as well as their improved foaming effect, if compared with samples without. From mercury intrusion the strong porogenic effect of TTPB was confirmed with an increase on porosity from 28.5 $\pm$ 1.1 to 41.2 $\pm$ 0.2 %. From nitrogen adsorption an increase on BET surface area was found when a mixture of the two additives in a molar proportion of 2:1 was incorporated, from 0.8 $\pm$ 0.1 to 2.3 $\pm$ 0.4 $m^2.g^{-1}$. Helium picnometry confirmed an overall increase on the real density of the produced porous composite biomaterials when SBA-15 (20 wt. %) was incorporated. A decrease on the melting temperature was found when the liquid additives were incorporated (from 66.1 $\pm$ 0.1 to 60.1 $\pm$ 0.6ºC for GF and to 64.9 $\pm$ 0.9ºC for TTPB). The incorporation of SBA-15 was found to have little effect on the melting temperature and on thermal degradation temperature of the produced porous composite biomaterials. Crystallinity of the produced additivated porous biomaterials was found to decrease when liquid additives were incorporated, by SDT, but by XRD it was found to slightly change when a single additive was incorporated (decreasing with GF and increasing with TTPB), but the same trend was found by both techniques when a mixture of the two liquid additives was incorporated, decreasing PCL crystallinity. By the compression test, again, an increase on the compression strength at rupture was found with the incorporation of SBA-15 (20 wt. %) from 1.9 $\pm$ 0.4 to 7.8 $\pm$ 0.3 MPa. In overall, the addition of the liquid additives led into more ductile materials, as expected.

On the fourth stage, fixation devices of pure PCL and PCL/SBA-15 (10 wt. %) composite, for hard tissue engineering applications were produced using stainless steel moulds, by SFM at constant pressure (20 MPa), temperature (40ºC), depressurization rate (2 $MPa.min^{-1}$) and contact time (2h). Those devices were morphologically characterized by SEM-EDS. It was found a reduction on average pore diameter, by image analysis, from 569.6 $\pm$ 0.5 to 209.5 $\pm$ 1.2 µm, for the pin device, when SBA-15 (10 wt. %) was incorporated. It is showed that by SFM it is possible to produce materials with the desired shape, size and with controlled properties, using large scale techniques, coupling SFM to an extruder or to an injection blower, for example.

With this work it is showed that SFM allows to obtain porous biomaterials with controlled physical properties in a safer and environmentally friendly manner when compared with conventional techniques, allowing to process polymers at low temperatures. It was shown that is, thus, possible to incorporate, in the future, a bioactive compound, in which PCL and/or SBA-15 can act as carriers for delivery and/or controlled release, what would enhance the biological activity of the produced biomaterials. Adding SBA-15 is revealed as a good approach with high

potential for hard tissue engineering applications. It stays proven that incorporating TTPB the processability of the polymer is facilitated and by adding GF the morphology of the porous biomaterials, like average pore diameter, can be controlled. Such composite porous materials can be used for these applications, through their incorporation into bone/dental defects filling materials (cements, hydrogels, etc.). With SFM it is possible to produce materials with controlled shape, size and physical properties, using moulds, which largely enhances the economic potential of such process

Resumo

Para além das propriedades químicas e biológicas o sucesso de processos de desenvolvimento de materiais adequados para engenharia de tecidos duros depende fortemente do controlo sob propriedades físicas como, porosidade, tamanho médio de poro, área de superfície, rugosidade da superfície, força de compressão e cristalinidade. Materiais poliméricos não possuem propriedades mecânicas suficientes para aplicações em engenharia de tecidos duros, a incorporação de um enchimento inorgânico, produzindo materiais compósitos porosos surge como a solução a adotar para o desenvolvimento de materiais com propriedades mecânicas melhoradas. Os métodos convencionais de processamento de polímeros em materiais porosos, normalmente fazem uso de compostos perigosos para o ambiente, como substâncias orgânicas. Utilizando este tipo de compostos leva à necessidade de acrescentar uma etapa de processamento de remoção destes compostos, de forma a reduzir a possível toxicidade dos materiais produzidos. Esta etapa de processamento, geralmente envolve a utilização de temperaturas elevadas, que podem, por sua vez, impedir a incorporação de compostos bioativos termo sensíveis durante o processamento. Este trabalho está dividido em quatro etapas, com o principal objetivo de otimizar o processamento supercrítico e obter materiais com propriedades morfológicas, mecânicas e térmicas controladas para aplicação em engenharia de tecidos ósseos.

O processo de foaming/mistura com CO_2 supercrítico (SFM) surge como uma alternativa limpa e amiga do ambiente para a produção de materiais porosos para aplicações em engenharia de tecidos duros, permitindo a incorporação de compostos bioativos sem os degradar, devido à facilidade em atingir as condições supercríticas do CO_2 e à sua possível recuperação. O CO_2 atua, também, como um plastificante temporário e como agente de *foaming*, reduzindo as temperaturas de fusão (T_m) e de transição vítrea (T_g) de vários polímeros, facilitando o seu processamento.

Este trabalho encontra-se dividido em quatro etapas, com o principal objetivo de otimizar o processamento e obter materiais compósitos porosos com morfologia, e propriedades mecânicas e térmicas controladas para aplicação em engenharia de tecidos duros.

On the first stage poly(ε-caprolactone) (PCL)-based porous composite biomaterials were produced by SFM by pressure quench at constant processing conditions, namely pressure (20 MPa), temperature (45ºC), depressurization rate (1 $MPa.min^{-1}$) and contact time (2h). Three inorganic fillers were incorporated, hydroxyapatite (HA), montmorillonite (MMT) and mesoporous silica nanoparticles SBA-15 type (SBA-15), in two compositions (10 and 20 wt. %). The obtained composites were morphologically (macroscopic and water absorption analysis) and mechanically (compression tests) characterized. Composite porous biomaterials were found to be morphologically and mechanically enhanced due to the incorporation of these fillers. The obtained results were not conclusive in order to choose an inorganic type and composition as the optimum towards the development of a porous composite biomaterial for hard tissue engineering applications, since no homogeneous dispersion of the fillers was obtained. So, SBA-15 was chosen as the ideal filler due to its high surface area and mesoporous feature, ensuring to the biomaterial an extra bioactive compound carrier potential.

Na primeira etapa foram produzidos materiais porosos compósitos à base de por SFM por *pressure quench* sob condições de operação constantes, nomeadamente pressão (20 MPa), temperatura (45ºC), taxa de despressurização (1 $MPa.min^{-1}$) e tempo de contacto (2h). Foram incorporados três enchimentos inorgânicos, hidroxiapatite (HA), montmorillonite (MMT) e nanoparticulas de sílica mesoporosa do tipo SBA-15 (SBA-15), em duas composições (10 e 20 wt. %). Os compósitos obtidos foram caracterizados quanto à sua morfologia (análise

macroscópica e teste de absorção de água) e quanto às suas propriedades mecânicas (testes de compressão). Os biomateriais compósitos apresentaram tanto propriedades morfológicas como mecânicas melhoradas com a incorporação destes enchimentos. Os resultados obtidos não foram conclusivos de forma a se poder escolher um tipo de inorgânico e composição como ótimo para o desenvolvimento de um biomaterial compósito poroso para aplicação em engenharia de tecidos duros, uma vez que foram sempre obtidas dispersões heterogéneas dos enchimentos inorgânicos. Portanto, SBA-15 foi escolhido como enchimento inorgânico ideal devido à sua elevada área de superfície e carácter mesoporoso, garantindo ao biomaterial compósito um potencial extra de transporte de substâncias bioativas.

Na segunda etapa foram produzidos biomateriais porosos de PCL por SFM sob condições de operação variáveis com o objetivo de se determinar um conjunto de condições de operação ótimo para a produção de materiais para aplicação em engenharia de tecidos duros, com base nas suas propriedades morfológicas e mecânicas. A pressão e tempo de contato constantes (20 MPa e 2h respetivamente) foi testada uma variação de 100 $kg.m^{-3}$ e 2 Pa.s na densidade e viscosidade, respetivamente, do $scCO_2$, por variação da temperatura de operação, utilizando como temperatura de operação 35, 40, 45 e 50ºC. Foram testadas, igualmente, duas taxas de despressurização, de 1 MPa e 0.3 MPa. Operando a uma temperatura de 40ºC com uma taxa de despressurização de 0.3 e a uma temperatura de 45ºC com uma taxa de despressurização de 1 MPa foram obtidos biomateriais com propriedades morfológicas semelhantes (diâmetro médio de poro BET de 0.5 ± 0.0 e 0.6 ± 0.0 µm respetivamente, no entanto o primeiro conjunto de condições de operação originaram biomateriais com propriedades mecânicas melhoradas (módulo de Young de 32.6 ± 3.0 MPa comparando com 23.9 ± 1.2 MPa). O primeiro conjunto de condições de operação revelou-se como o ótimo, de forma a que os resultados obtidos neste trabalho possam ser comparados com os resultados obtidos em trabalhos anteriores.

Na terceira etapa foram produzidos por SFM biomateriais compósitos porosos de PCL/SBA-15 (20 e 30 wt. %) sob as condições de operação ótimas definas na etapa anterior. Estes biomateriais compósitos foram também aditivados com aditivos líquidos verdes e seguros, que é esperado que atuem como agentes porogénicos, plastificantes e compatibilizantes, como glicofurol (GF), um hidrótopo aprovado pela FDA e Trihexyl(tetradecyl) phosphonium bis (trifluoromethylsulfonyl)imide (TTPB), um líquido iónico não tóxico, numa composição molar de 98 % relativa à PCL e em mistura, em três proporções molares (GF:TTPB) de 2:1, 3:1 e 5:1. Os efeitos do inorgânico e dos aditivos foram avaliados com microscopia eletrónica de varrimento (SEM-EDS), intrusão de mercúrio, adsorção de azoto, picnometria de hélio, análise térmica diferencial simultânea (SDT), difração de raio-X (XRD) e com teste de compressão.

Através da análise macroscópica e microscópica (SEM) dos biomateriais produzidos, 30 wt. % revelou-se como uma concentração de inorgânico muito elevada. Os resultados obtidos através de SEM-EDS confirmaram a presença dos aditivos líquidos e do enchimento inorgânico, bem como o seu efeito porogénico, quando comparado com amostras sem enhcimento e não aditivadas. A partir de intrusão de mercúrio confirmou-se o forte efeito porogénico do TTPB com um aumento na porosidade desde 28.5 ± 1.1 para 41.2 ± 0.2 %. A partir de adsorção de azoto verificou-se um aumento na área de superfície BET quando uma mistura dos dois aditivos numa proporção molar de 2:1 foi incorporada, desde 0.8 ± 0.1 para 2.3 ± 0.4 $m^2.g^{-1}$. Picnometria de hélio confirmou um aumento feral da densidade real dos biomateriais compósitos porosos produzidos quando SBA-15 (20 wt. %) foi incorporada. Observou-se uma diminuição na temperatura de fusão quando os aditivos foram incorporados (desde 66.1 ± 0.1 to 60.1 ± 0.6ºC para GF e para 64.9 ± 0.9ºC no caso do TTPB). A incorporação de SBA-15 revelou-se como tendo pouco efeito na temperatura de fusão e na temperatura de degradação dos biomateriais produzidos. Observou-se que a cristalinidade dos biomateriais porosos aditivados produzidos, por SDT, diminui quando os aditivos líquidos são adicionados, mas por XRD, observou-se que

a cristalinidade é ligeiramente alterada quando um simples aditivo é incorporado (diminuindo com GF e aumentado com TTPB), no entanto a mesma tendência, quando uma mistura dos dois aditivos foi incorporada, é observada pelas duas técnicas, diminuindo a cristalinidade da PCL. Com os testes de compressão, uma vez mais, um aumento na resistência à compressão foi verificado com a incorporação da SBA-15 (20 wt. %) desde 1.9 ± 0.4 para 7.8 ± 0.3 MPa. Em geral, verificou-se que a adição dos aditivos líquidos levou à formação de materiais mecanicamente mais frágeis e menos resistentes à compressão, como esperado.

Na quarta etapa, foram produzidos dispositivos de fixação, utilizando moldes de aço inoxidável, de PCL pura e compósitos de PCL/SBA-15 (10 wt. %), para aplicação em engenharia de tecidos duros, por SFM a pressão constante (20 MPa), temperatura (40ºC), taxa de despressurização (2 $MPa.min^{-1}$) e tempo de contato (2h). Estes dispositivos foram morfologicamente caracterizados utilizando SEM-EDS. Verificou-se uma redução no diâmetro médio de poro, por análise de imagem, desde 569.6 ± 0.5 para 209.5 ± 1.2 µm, para o dispositivo "*pin*" de fixação, quando se adicionou SBA-15 (10 wt. %). Mostrou-se que por SFM é possível produzir materiais com a forma desejada, tamanho e propriedades controladas, utilizando técnicas de larga escala, como por exemplo, acoplando a técnica de SFM a uma extrusora ou injetora.

Com este trabalho fica demonstrado que com a técnica de SFM é possível obterem-se biomateriais porosos com propriedades físicas controladas de uma forma segura e amiga do ambiente, quando comparada com as técnicas convencionais, permitindo processar polímeros a baixas temperaturas. É demonstrado, igualmente, que é possível, então, possível incorporar no futuro, um composto bioativo, no qual tanto a PCL e/ou a SBA-15 podem atuar como veículos de entrega/libertação, o que melhoraria a atividade biológica dos biomateriais produzidos. Adicionando SBA-15 revela-se como uma boa abordagem, com elevado potencial para aplicações em engenharia de tecidos duros. Fica provado que incorporando TTPB a processabilidade do polímero fica facilitada e adicionando GF a morfologia dos biomateriais porosos, como tamanho médio de poro podem ser controladas. Biomateriais compósitos porosos, como os produzidos neste trabalho, podem ser utilizados no tipo de aplicações proposto através da sua incorporação em materiais de enchimento de defeitos dentários/ósseos (cimentos, hidrogéis, etc.). Com a técnica de SFM é possível produzir materiais com forma, tamanho e propriedades físicas controladas, utilizando moldes, o que aumenta largamente o potencial económico deste tipo de processamento.

Table of Contents

List of Figures

List of Abbreviations and Symbols

Abbreviations

β-TCP – β-Tricalcium Phosphate

BET – Braunauer – Emmett – Teller method

BJH – Barret – Joyner - Halenda method

CAD – Computer Aided Design

CAGR – Compound Annual Growth Rate

CFA – Chemical Foaming Agent

EDS – Energy DispersiveX-Ray Spectroscopy

EMA – European Medicines Agency

et al. – *et alii*, "and others"

EU – European Union

FDA – Food and Drug Administration

GF – Glycofurol

GRAS – Generally Recognised as Safe

HA - Hydroxyapatite

HC's – Hydrocarbons

HCFC's – Hydrochloroflurocarbons

ILs – Ionic Liquids

IUPAC – International Union of Pure and Applied Chemistry

MCM-41 – Mobil Crystalline Materials type 41

Mili-Q-water – Ultra pure water type 1

MMT – Montmorillonite clay

PCL – poly(ε-caprolactone)

PDLA – poly(D,L-(lactic acid))

PDS - poly(p-dioxanone)

PFA – Physical Foaming Agent

PHB – poly(3-hydroxybutyrate)

PLGA – poly(lactic-co-glycolic acid)

PTFE – poly(tetrafluoroethylene)

RP – Rapid Prototyping

SBA-15 – Santa Barbara Amorphous type 15

SCF – Supercritical Fluid

SDT – Simultaneous Differential Thermal Analysis

SEM – Scanning Electron Microscopy

SFF – Solid Free Form Techniques

SFM – Supercritical CO_2 foaming/mixing process

SLS – Selective Laser Sintering

TIPS – Thermally Induced Phase Separation

TTPB - Trihexyl(tetradecyl) phosphonium bis (trifluoromethylsulfonyl)imide

UK – United Kingdom

USA – United States of America

USD – United States Dollar

VOC's – Volatile Organic Compounds

XRD – X-Ray Diffraction

Symbols

~ - Approximately

3 – D – Three Dimensional

A_A – Area of amorphous parts (m^2)

A_{base} – Area of the base of the foam (cm^2)

A_c – Area of crystalline parts (m^2)

A_s – Area of cross section of the sample (m^2)

D_{HA} – Hydroxyapatite particle size (mm)

$D_{part\ SBA-15}$ – SBA-15 aggregates size (µm)

$D_{part\ PCL}$ – PCL powder particle size (mm)

E – Young's Modulus (MPa)

$F_{applied}$ – Applied Force in the foam (N)

H – Height of the foam

h - Final height of the sample (mm)

h_0 – Initial height of the sample (mm)

L_{ap} – Applied load on the loading arm (kg)

L_{ef} – Effective load applied (kgf)

M_n – Number average molecular weight ($g.mol^{-1}$)

m_{aw} – Absorbed mass of water (mg)

$m_{i,foam}$ – Initial mass of the foam (mg)

$m_{f,foam}$ – Final mass of the foam (after 192h water-wet) (mg)

n – Number of pores identified

P – Operating Pressure (MPa)

P_c – Critical Pressure (MPa)

P_D – Pore density of the foam (pores.mm^{-2})

scCO$_2$ – Supercritical Carbon Dioxide

T – Operating Temperature (ºC)

T_c – Critical Temperature (ºC)

T_D – Degradation Temperature (ºC)

T_g – Glass Transition Temperature (ºC)

T_m – Melting Temperature (ºC)

V_{aw} – Volume of absorbed water (cm^3)

V_{foam} – Envelope volume of the foam (cm^3)

V_{pore} – Percentage of pore volume (%)

wt. % - Weight percentage composition (%)

wt. % $_{SBA\text{-}15}$ – SBA-15 weight percentage composition (%)

Greek Letters

ΔH_f – Enthalpy of fusion (J.g^{-1})

$\Delta H_f^0(T_m^0)$ – Enthalpy of fusion of the totally crystalline polymer at the equilibrium (J.g^{-1})

ε – Strain (mm/mm)

2θ – Variation of the exit angle of the incident beam on XRD analysis, diffraction angle (º)

$\lambda_{K\alpha 1}$ – Wave length of the emissioned energy from electron transition from the 2p orbital to the 1s orbital (nm)

ρ – Density (g.cm^{-3})

ρ_{HA} – HA Density (g.cm^{-3})

ρ_{MMT} – MMT Density (g.cm^{-3})

ρ_{SBA-15} – SBA-15 Density (g.cm^{-3})

ρ_w – Water density (g.cm^{-3})

σ – Stress (MPa)

$\bar{\sigma}$ – Standard Deviation

$\bar{\phi}$ – Average Pore diameter (µm)

χ_c – Degree of Crystallinity measured by SDT (%)

χ_i – Degree of Crystallinity measured by XRD (%)

This page was intentionally left in blank

1. Introduction

1.1. Tissue Engineering

Throughout the History, mankind has created myths concerning asexual generation of beings, regeneration of organs and body parts or miraculous cures from traumas, being the most known examples the creation of Eve, in Genesis and the myth of Prometheus, in ancient Greece. The desire of a long life with quality of living, free from physical trauma, for family and loved ones has always existed, but sickness, malformations and accidents followed the History of mankind, leading to a desire of improving the life of those suffering from these diseases. The methodical increase of the perception of Nature, trough scientific knowledge allows nowadays that this dream of humanity is achievable trough Tissue Engineering (Lanza *et al*., 2007; Meyer *et al*., 2009; Horch, 2006).

Tissue engineering is a multidisciplinary field that brings together the principles and knowledge of engineering to life sciences, such as biology, towards the knowledge of relationships functions-structures of human tissues, normal and pathological, and the development, using biomaterials, stem-cells and bioactive agents, of substitutes to restore, maintain or improve the tissue function, being identified as a branch of regenerative medicine (Duarte *et al*., 2013; de Matos *et al*., 2013; Patel *et al*., 2010). Over time regenerative medicine techniques have evolved to provide better quality of living for patients, proving to be effective and lifesaving, being organ transplant the best known case. However, the waiting lists for this type of procedure are, generally all over the world, very large, leading to death of many of the waiting patients, due to the shortage of donors and to the increasing demand and need for new organs and/or tissues. The transplantation from one individual to another, allograft, or from another species to human beings, xenografts, can result in chronic rejection from the immune system of the receptor or in transmitted diseases (Takahashi *et al*., 2012; Lanza *et al*., 2007; Bonfield, 2006; Reverchon and Cardea, 2012). Owing to this problem, research and market for tissue engineering applications have grown significantly in the past years with the goal to avoid, simultaneously, the long waiting time for the medical procedure and the rejection response by the receptor, being pointed a global market growth towards 2019 of 56.9 billion USD with a CAGR (Compound Annual Growth Rate) of 22.3% (Website1).

Currently, tissue engineering techniques are based on three main approaches: using isolated cells from the host, replacing just the cells of the tissue to recover/heal, being a minimally invasive approach, using substances inducing new tissue growth with the ability to work as markers, such as differentiation/growth factors and using matrices/materials, scaffolds, which can transport cells and/or differentiation/growth factors, or combining the aforementioned approaches two by two or all at once, as shown in Figure 1. Nanotechnology arises as a new technology to couple to tissue engineering approaches, providing morphological and topological improved approaches, for example by producing nanocomposite scaffolds with improved surface area and nanopores and/or surface engineered materials with nanoroughness (Duarte *et al*., 2013; Lanza *et al.*, 2007).

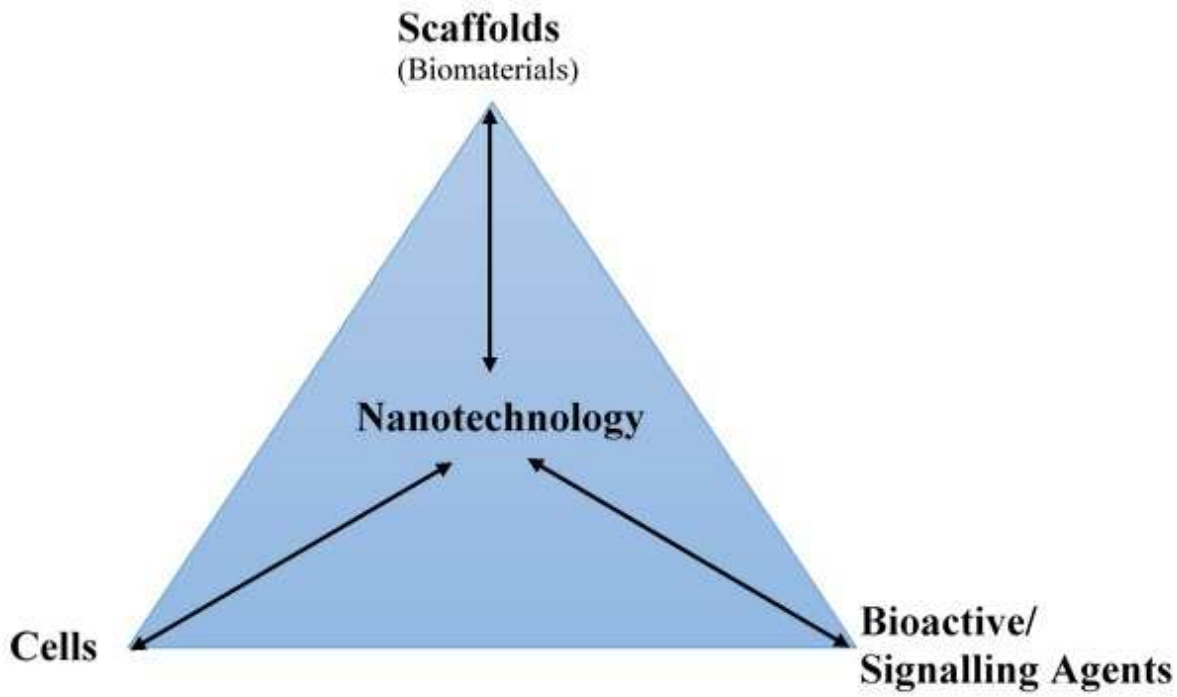

Figure 1. *Tissue Engineering Approaches.*

Off all of the approaches, the most promising towards the main goal to generate new tissue is the one using scaffolds seeded with cells in their interior/surface and/or applying jointly differentiation/growth factors. Scaffolds have as primary function to provide a temporary three dimensional (3-D) structure inducing and favouring cell growth and formation of new tissue, without losing its structural integrity (throughout the desired time) (Nishida *et a*l., 2015). It is in the design and development of this fundamental key, in tissue engineering applications, that goes to engineering and materials science. The scaffold, new tissue ingrowth matrix, can be made of one material (polymeric, metallic, ceramic, etc.) or by a mixture of these, in this case being formed by a composite material (this kind of materials will be discussed further ahead in section 1.4.). It is widely accepted, for all applications in tissue engineering using scaffolds, that these should consist of materials with a porous structure (Fanovich and Jaeger, 2012; Duarte *et al*., 2009). Porous materials are classified by the average pore diameter of their structure, accordingly to IUPAC (International Union of Pure and Applied Chemistry) standard, being classified as micropores, pores with diameter lower than 2 nm, as mesopores, pores with diameter higher than 2 nm and lower than 50 nm and macropores all with diameter higher than 50nm (Rouquerol *et al*., 2012).

In order to be fully functional and fulfil its primary function, the scaffold should be designed, produced and characterized in order to meet some specifications. It must exhibit a reproducible 3-D macrostructure similar to the tissue to repair/substitute, a high porosity (to about 90%) and with high interconnected pores (open pores with access to the neighbouring pores) enhancing the transport of nutrients and body fluids as well as cell migration and communication, with a macroporous rich structure (of 100-500 µm) in order to favour cellular adhesion and proliferation, but also with micropores and mesopores to allow the diffusion of nutrients and body fluids as well. Interconnectivity of the structure reveals to be of major concern as Uebersax and co-workers showed, that highly interconnected structures yielded into a homogenously cellular distribution and vascularization than in few interconnected structures (Reinwald *et al*., 2014; Fanovich and Jaeger, 2012; Lemon *et al*., 2012; Reverchon and Cardea, 2012; Uebersax

et al., 2006). In Table 1 are shown the obtained results from several research groups in the formation of new bone tissue as function of the porosity and average pore diameter of the produced scaffolds, for example. It must, as well, have similar mechanical properties to the tissue to repair/substitute, must be made of biodegradable, biocompatible and easily sterilizable materials with a degradation rate suitable to the new tissue formation rate, without releasing toxic sub-products to the biological medium resulted from the degradation of the material, the ideal degradation mechanisms of the scaffold material must be essentially by hydrolytic, enzymatic or ionic strength (pH of the medium) action, additionally the material(s) constituent of the scaffold must not induce inflammatory or immune response by the host, usually caused by the existence of residual amounts of solvent used in the production of the scaffold (Reverchon and Cardea, 2012; Sultana, 2012; Collins *et al.*, 2010; Rezwan *et al.*, 2006).

Table 1. *Reported effects in literature of average pore size of scaffolds in the growth of new bone tissue.*

Average pore size diameter (µm)	**Scaffold material**	**Porosity**	**Reported effects**
30-100 (80% < 100)	Calcium Aluminate	~ 47%	50 µm of formed bone tissue, growth of fibrous tissue (Klawitter and Hulbert, 1971).
60-100 (37% < 100)	Calcium Aluminate	~ 47%	600 µm of formed bone tissue, growth of fibrous tissue (Klawitter and Hulbert, 1971).
≤ 350	Poly(D,L-lactide-*co*-glycolide) (85:15)	~75%	Sample with larger amount of formed bone tissue (Whang *et al*., 1999).
90 – 120	Honeycomb-shaped Hydroxyapatite	-	Promote chondrogenesis (Karande *et al*., 2004).
50 – 400	Hydroxyapatite/β-Tricalcium phosphate	-	Optimum distribution for osteogenesis (Karande *et al*., 2004).
100 – 200	Hydroxyapatite loaded with Bone Morphogenic Protein-2	-	Substantial growth of bone tissue (Karageorgiou and Kaplan, 2005).
≥ 100 and 150	Chitosan	-	Facilitate vascularization and cellular growth, as well as migration of cells and nutrients, pores should be highly interconnected (Costa-Pinto *et al*., 2011).
300 – 350	Poly(ε-caprolactone) /Thermoplastic zein/ Hydroxyapatite	-	Enough size for cellular adhesion, proliferation and migration (Salerno *et al*., 2010 (a)).

The main methods to manufacture porous scaffolds of organic and inorganic basis (polymeric and/or ceramic) are mainly based in techniques such as fibre felt and fibre bonding, electrospinning, freeze drying, solvent casting and particulate leaching, melt moulding, solid free form techniques (SFF) and foam production techniques (Lu *et al*., 2013; Subia *et al*., 2010; Ma *et al*., 2004; Lanza *et al*., 2007). Fibre felt and fibre bonding consists in connecting polymer fibres at their crossing points using a secondary polymer that is later removed. Through electrospinning, polymer fibres are manufactured applying a very high voltage to a capillary tube filled with a solution with polymer and solvent, which is held at the tip of the capillary *via* surface tension, when the strength of the electric field overcomes the surface tension of the drop of the solution at the tip of the capillary, is initiated a polymer jet. When the jet contacts with the surrounding air, the solvent starts to evaporate forming a polymer fibre. These textile-like techniques have as main advantages the capability to produce ultra-fine fibres with spatial

orientation, high aspect ratio, and high surface area with controlled pore geometry, these features enhance a better cellular growth, however produced scaffolds by these techniques have low mechanical strength, fast degradation rate and limited variations regarding fibre diameter. Freeze drying techniques are based in sublimating the employed solvent in which the polymer was dissolved. To achieve this the solution is frozen and then the solvent is sublimated in a high vacuum, creating pores where the solvent were without the formation of a meniscus, resulting from the phase equilibrium, which would lead into the collapse of the formed pores, the pore size can be controlled with the freezing rate and the pH of the solution. This technique has the main advantage using mainly water as a solvent but the main drawbacks are concerning to the difficulty to achieve a hierarchical structure (with a good pore size distribution) and to the long processing times and small pore sizes (Ma *et al*., 2004; Subia *et al*., 2010; Lu *et al*., 2013; Lanza *et al*., 2007). Solvent casting and particulate leaching are often one of the most employed techniques in the fabrication of porous scaffolds. It consists in the casting of a low boiling point solvent, usually organic solvents are employed, and/or a salt from the mixture with polymer, followed by the evaporation of the solvent and/or dissolution of the salt particles in an aqueous medium. The pore size can be controlled with the amount of salt particles added to the polymer solution and/or by the salt type, usually porous films are manufactured by this technique. It has as main advantages that is very inexpensive and easy and simple to perform, but the major drawbacks of this technique rely on the use of organic solvents. After evaporation of the solvent it is very likely to remain some residual concentration in the scaffold and due to the toxicity of the organic solvents this will increase the toxicity of the scaffold, and the presence of such hazardous compounds in materials for biomedical/pharmaceutical applications are highly regulated. Also, in order to completely remove the organic solvents high temperature can be employed, denaturising thermal sensitive compounds, like drugs or proteins, making it impossible to add these type of bioactive compounds to the scaffolds by this technique (Ma *et al*., 2004; Lu *et al*., 2013; Subia *et al*., 2010; Lanza *et al*., 2007). By the melt moulding technique the mixture polymer/porogenic agent particles is placed into a mould and heated above the glass transition temperature (T_g) or melting temperature (T_m) of the polymer, then the mixture is removed from the mould and placed into the adequate medium for leaching the particles of the porogenic agent, yielding to the porous scaffold. This technique has the main advantage to allow the manufacturing of scaffolds with shape and size customized to the patient needs, but the major drawbacks fall once again on the use of hazardous organic solvents (Subia *et al*., 2010). SFF techniques include methods for manufacturing scaffolds such as rapid prototyping (RP), selective laser sintering (SLS) and 3-D printing (melt moulding is pointed out from several authors as a SFF technique), the process to manufacture porous scaffolds by these techniques comprises in general, the use of a computer aided design (CAD) software in which the structure of the scaffold is designed, then the material is produced by layered manufacturing techniques, starting from the bottom and moving up layer by layer of polymer conducted by the CAD software. The major advantages and drawbacks of these techniques are the very same as the ones of the melt moulding techniques, adding the advantage of a greater control over the porosity and interconnectivity and the drawback of the cost of operation of these kind of new technologies (Karande *et al*., 2004; Subia *et al*., 2010; Rezwan *et al*., 2006). Foam production techniques allow the manufacturing of a type of material with great interest in the biomedical/pharmaceutical field - foams, foams are defined as two phase materials, constituted by a solid matrix and gaseous voids resulted from the blowing agent action (Lee *et al*., 2005). The main techniques to produce foams are gas foaming, thermally induced phase separation (TIPS) and using chemical or physical foaming agents (CFA or PFA). These techniques are based on the use of a blowing agent, dissolved/incorporated into the polymeric matrix or polymeric solution with a solvent, as the blowing agent is removed the porous structure is formed (Jacobs *et al*., 2008; Rezwan *et al*., 2006). These techniques have the main advantages to produce structures with controlled pore sizes with hierarchical distribution, the main

drawbacks fall into the low interconnectivity and the low mechanical properties of the produced scaffolds (these techniques for foam manufacturing will be discussed further ahead in section 1.2.) (Karageorgiou and Kaplan, 2005; Lanza *et al*., 2007; Reverchon and Cardea, 2012; Karande *et al*., 2004; Tai *et al*., 2007; Jacobs *et al*., 2008; Rezwan *et al*., 2006).

Despite the high number of available techniques, and independently of the gains and drawbacks in the use of each one, it is particularly difficult to control simultaneously, in a precise manner, the macro, micro and nano characteristics and surface chemistry of the scaffold in order to achieve its objectives as above mentioned. To control the surface chemistry of the scaffolds one can also employ surface engineering techniques or material coating techniques, through which the surfaces of the materials are functionalized by physical adsorption or chemical modification, allowing a better imitation of extracellular matrix and protein adsorption (Lanza *et al*., 2007; Ohtsuki *et al*., 2007).

1.1.1. Hard Tissue Engineering

Tissue engineering based alternatives, are increasingly required in the field of clinical regeneration of new bone/dental tissue. Increasing need of materials to ensure a better filling of large orthopaedic/dental defects as well as of orthopaedic/dental grafts made since the 60s of the XX century, to arose more and more research groups dedicated to the development of these kind of alternatives. From the 90s of the past century, increasing knowledge of the bone/dental tissue biology and of the natural regeneration process, has led to appearance of commercial solutions towards bone/dental regeneration (Burg *et al*., 2000; Lanza *et al*., 2007; Hollinger *et al*., 2005; Zhang *et al*., 2014; Neel *et al*., 2014;).

Bone is a tissue in constant renovation, with the ability to self-regenerate. Its main function is to ensure structural support to the human body, serving as well as a mineral reservoir, supporting muscular contractions resulting from the movement as well as the body weight, protecting more sensible organs and/or tissues from the violent actions resulting from the exterior and from the movement of the human body (Hollinger *et al*., 2005; Salgado *et al*., 2004). The bone structure is a hierarchical structure constituted of two distinctive parts, trabecular or spongy bone (20% of the skeleton) and cortical or compact bone (80% of the skeleton). Trabecular bone possess a highly porous structure (50 to 90% porosity) similar to a sponge. This structure allows a greater available volume to the presence of blood vessels, as a greater surface area, allowing the growth of large numbers of plackets and blood cells (red and white blood cells) (Salgado *et al*., 2004; Website 2; Tal, 2012). Opposing, cortical bone has an almost solid structure with only 10% porosity. It is constituted by cylindrical microstructures made up of multiple layers of osteoclasts and osteocytes with metabolic function to growth and reabsorb bone tissue. Is the cortical structure of the bone tissue which allows to bear major loads and all motor activities of the human body (Salgado *et al*., 2004; Website 2).The two structures together form one of the most “intelligent” materials known to Man, allowing to support high mechanical loads and presenting high vascularization and cell transport characteristics due to its structure with high surface area, at the same time. It is reported that cortical bone can bear a compressive strength up to 130-180 MPa and trabecular bone 4-12 MPa, the elasticity of these materials, indicated by the Young’s Modulus, is reported as being of 3-30 GPa and 0.02-0.05 GPa, respectively, showing that the bone tissue is little elastic and is able to support high mechanical loads and that cortical bone is more elastic than trabecular bone (Yang *et al*., 2001).

Bone tissue is made of a truly composite material (mixture of two or more materials of different nature), of fibres of type I collagen (organic part) and hydroxyapatite crystals, $Ca_{10}(PO_4)_6OH_2$, (HA) (inorganic part), collagen fibres act as nucleation points towards the formation of HA

crystals. *In vivo*, about 10 to 20 wt. % of its composition is water, but of its dry mass, the organic part represents 30 wt. % and the inorganic 60-70 wt. %, though bone tissue is also constituted by other proteins and salts (Website 2; Hollinger *et al*., 2005). Bone is a dynamic and in constant activity tissue, its fabric, maintenance and reabsorption result from the interaction between three types of cells, osteoblasts, osteocytes and osteoclasts. Osteoblasts have as main functions to synthesize and regulate the deposition of the bone tissue extracellular matrix and the mineralization and deposition of these compounds into the organic structure of the tissue, their activity is regulated in response to the mechanical stimuli which they suffer from the human being physical activity, osteocytes have as main functions the calcification of the bone matrix and the blood-calcium homeostasis, keeping the equilibrium of the bone system between the inorganic component and its interaction with the biological medium, osteoclasts, in their turn, are the main instigators of the bone resorption, leading to the lysis of bone cells allowing renovation of the tissue (Salgado *et al*., 2004; Conaway *et al*., 2011; Sahoo *et al*., 2013).

Dental tissue, much like bone tissue is also made of a composite material constituted by enamel, dentin, cementum and dental pulp. The inorganic counterpart, hard tissue of the human teeth, is constituted by the first three, in which enamel is constituted by 96% inorganics, mainly hydroxyapatite crystals, dentin is constituted by 65-70% of inorganics and the cementum by 45-50% of inorganics. The organic counterpart of dental tissue is mainly composed by collagen fibres, much like bone, except the enamel part, in which its organic counterpart is mainly constituted by proteins like amelogenins and enamelins (Zhang *et al*., 2014; Hosoya and Nakamura, 2015). The regeneration mechanism of dental tissue is very similar to the mechanism of bone tissue, being stimulated as well, by mechanical stimuli, the type of cells responsible for dental tissue regeneration are odontoblasts and pulp cells. Although the origin of hard tissue forming cells for the regeneration of dental tissue is controversial, the most promising proposal refers that bone marrow-derived mesenchymal cells participate in osteoblast-like cell differentiation, giving to the formation of new dental tissue a similar mechanism to the new bone tissue formation (Hosoya and Nakamura, 2015; Neel *et al*., 2014).

The mechanical behaviour of dental tissue varies accordingly to the type of tooth. Tough, the most studied are the molar teeth, being reported values for compressive strength of the third molar teeth of 4.88-5.7 GPa and for Young's modulus in the range of 87.5 - 97.72 GPa (Zhang *et al*., 2014).

The increasing aging of the population, unhealthy dieting practices, and the growing number of leukaemia cases in developed countries, led to a growth in clinical procedures with the need to a bone/dental graft or bone/dental cement, making the same motivations, as referred above, leading to the appearance of commercial technologies of tissue engineering applications, as well as the increase in scientific research, the very same that motivate the appearance of commercial and scientific research in the field of hard tissue engineering. When there is clinical need to treat a bone/dental defect, an autologous bone graft is the standard practice to employ (Damien and Parsons, 1991; Salgado *et al*., 2004; Oryan *et al*., 2014; Babu and Ogle, 2015). This procedure has the advantage to minimize almost to zero the immune and/or inflammatory response, as eliminating a possible transmission of disease, however, it has major limitations related to limited availability, donor site morbidity and possibility of future complications related to the removal of tissue from healthy areas (Sahoo *et al*., 2013; Salgado *et al*., 2004; Oryan *et al*., 2014; Damien and Parsons, 1991). As alternative to the standard practices to bone/dental graft substitutes, arise the solutions pointed by the techniques of tissue engineering, motivating their appearance in the market and research, as scaffolds for bone/dental grafts substitutes as monoliths, bone/dental cements and polymeric-based fixation devices as screws and/or pins (produced by conventional extrusion/injection processes) (Kumbar and Laurencin, 2011; Babu and Ogle, 2015).

1.2. Foams Manufacturing Processes

Foams, as referred, are defined as two phase materials, constituted by a solid matrix and gaseous voids resulted from the blowing agent action, and can be classified as rigid or flexible foams depending on their composition, physical properties and cell morphology (Lee *et al*., 2005). Foams can be used in several applications from sound and heat insulation, cushion, absorbents, weight-bearing structures and tissue engineering mainly due to their high aspect ratio, strength-to-weight ratio and achievable cellular interconnectivity (Lee *et al*., 2005; Zeng *et al*., 2003; Chen L. *et al*., 2013; Salerno *et al*., 2011).

As says their definition, the gaseous voids – cells, are resulted from the action of the employed blowing agent on their manufacturing technique. Blowing agents are gases that expand when pressure is released, liquids that by heating change phase into gas, physical agents that are leached out by concentration-derived driving forces or chemical agents that decompose or react into gases by the influence of catalysts/heat (Eaves, 2004; Zeng *et al*., 2003; Chen L. *et al*., 2013). The main techniques to manufacture foams are, as stated above, thermally induced phase separation (TIPS), using chemical or physical foaming agents (CFA or PFA) and gas foaming (Jacobs *et al*., 2008; Eaves, 2004; Landrock, 1995).

Foaming *via* the TIPS process takes place by dissolving the polymer into an organic solvent, forming a single-phase solution at high temperatures. Then the phase separation is induced by temperature quench after which the solvent is removed either by freeze-drying, evaporation or supercritical extraction (Jacobs *et al*., 2008; Jacobs *et al*., 2004). Another common method of the TIPS process is through a two-step process. In the first step, polymer pellets with blowing agent are partly foamed with steam, then they are transferred into a steam exposed mould resulting in further foaming of the pellets which stick together and take shape of the mould (Jacobs *et al*., 2008). CFA is a thermally unstable compound which is added to the polymeric matrix. When the solution is heated, or a reaction between two, or more, polymeric components occurs, the CFA decomposes into gaseous components that are released from the matrix resulting in a cellular structure. Typically CFA are azo compounds, hydrazine derivatives and N-nitroso compounds (Eaves, 2004). PFA are usually water soluble salts such as NaCl or KCl. The use of a PFA is through the method of casting and leaching, in which the polymer is dissolved into a high volatile solvent and the solution is casted into a PFA containing mould. Then it is leached out into a solvent, in which the PFA is soluble and the solvent is evaporated resulting into a highly porous polymeric structure (Duarte *et al*., 2012; Jacobs *et al*., 2008). Typically PFA are halogenated hydrocarbons such as hydrofluorocarbons (HFC's) and hydrochloroflurocarbons (HCFC's) and hydrocarbons (HC's), namely low boiling point aliphatic hydrocarbons (Eaves, 2004).

All of the above mentioned methods for the manufacturing of polymeric foams (mainly polystyrene, polyurethane, poly(vinyl chloride), polyolefins, poly(lactic-*co*-glycolic acid), poly(lactic acid) and other biodegradable poly(α-hydroxy acids)) make use of toxic and/or environmentally hazardous compounds, such as volatile organic solvents (VOC's), contributing to greenhouse effect, air pollution and ozone depletion and contamination of fresh water streams (Eaves, 2004; Nalawade *et al*., 2006). Also, materials for tissue engineering applications are highly regulated by entities such as FDA ("Food and Drug Administration") in USA and EMA ("European Medicines Agency") in EU. These entities have strict standards for the use and residual amounts of hazardous/toxic compounds present in materials for biomedical application, such as tissue engineering applications, listing them with the maximum allowed residual concentration of each hazardous/toxic compound in materials for biomedical/pharmaceutical applications (Website 3; Website 4). Due to the high standards of

the required purity of the materials for tissue engineering applications, employing one of the above mentioned methods, requires the use of further purification steps that usually are very expensive (time and energy consuming) or make use of high temperatures, which can lead to the degradation of thermo sensitive compounds such as proteins, drugs and growth factors making almost impossible to apply these most needed compounds for tissue engineering applications through these methods (Nalawade *et al*., 2006; Salerno *et al*., 2011; de Matos *et al*., 2013). In order to avoid this problem, gas foaming techniques arises eliminating any residual amount of toxic/hazardous compounds or the use of any VOC or HCFC.

Gas foaming is a method in which the blowing agent is a gas or a supercritical fluid such as N_2, O_2, CO_2, supercritical carbon dioxide ($scCO_2$) and supercritical N_2. The gas or supercritical fluid is dissolved into the polymeric matrix and latter is removed leaving a porous matrix (Jacobs *et al*., 2008; Jacobs *et al*., 2004; Duarte *et al*., 2012). The most employed blowing agents through this technique are N_2, CO_2 and $scCO_2$, because they are cheaper and easier to acquire, tough CO_2 and $scCO_2$ are the most employed ones because carbon dioxide can affect several properties of the polymer enhancing its processing (Eaves, 2004; Jacobs *et al*., 2008).

1.2.1. Supercritical CO_2 Foaming/Mixing Process (SFM)

A supercritical fluid (SCF) is a dense phase of a substance which is in a state above its critical temperature (T_c) and critical pressure (P_c) (Liao *et al*., 2012; Kazarian *et al*., 2000). At the critical point there is an equilibrium of liquid and gas phase, and the SCF shows properties both typical of gas and liquid state but different from those obtained under standard conditions. This feature allows the SCF to have similar solvating power to liquid state solvents and mass transport properties better than those of conventional organic liquid solvents due to its gas-like diffusivity, liquid-like density, low viscosity, high compressibility and low surface tension (Liao *et al*., 2012; Kazarian *et al*., 2000; Bhamidipati *et al*., 2013; Karimi *et al*., 2012). All of these properties and features of SCF are easily tuned, accordingly to the desired properties to employ, by changing the temperature and/or the pressure of the SCF, approaching the properties of the SCF to the liquid or gas state (Kazarian *et al*., 2000). Is this feature, of adjustable solvent power, that makes the SCF a very attractive solvent for many applications like polymer synthesis, particle formation, lithography, coating, drying, extraction, impregnation of additives into polymeric or inorganic matrices and blowing agent for solid state foaming and for tissue engineering applications (Yuvaraj *et al*., 2007; Wang *et al*., 2008; Rogers *et al*., 2001; Choi *et al*., 2006; Ratcharak and Sane, 2014; Cooper *et al*., 2003; Kazarian *et al*., 2000; de Matos *et al*., 2013; Kiran, 2009; Sekhon, 2010; Duba and Fiori, 2015; Braga *et al*., 2008).

Supercritical carbon dioxide arises as the main advantageous blowing agent to employ in the manufacturing of foams for tissue engineering applications, due to its easily achievable supercritical conditions, $T_c = 31.1^{o}C$ and $P_c = 7.38MPa$, and because CO_2 is a gas at ambient conditions (pressure and temperature) leaving no residual amount left in the foam and can be fully recovered, without contributing to greenhouse effect (Bhamidipati *et al*., 2013; Nalawade *et al*., 2006; Liao *et al*., 2012; de Matos *et al*., 2013; White *et al*., 2012). It has also unique properties of great interest, it is non-toxic, non-flammable, chemically inert, is a GRAS (Generally Recognised as Safe) compound, abundant, inexpensive and commercially available in high purity (Liao *et al*., 2012; Nalawade *et al*., 2006; Salerno *et al*., 2011). Amongst all of the special properties and features of the $scCO_2$ it is specially its low critical temperature and pressure and total removal feature that make it very desirable for the production of materials for tissue engineering applications, allowing to process thermo sensitive compounds such as proteins, drugs and growth factors, also by being employed a supercritical fluid there is no

formation of a meniscus resulting from a phase separation, avoiding any pore collapse in the material (Liao *et al*., 2012; Nalawade *et al*., 2006; de Matos *et al*., 2013; White *et al*., 2012).

For many non-polar low molecular weight compounds $scCO_2$ is a good solvent, as well as for amorphous fluoropolymers and silicones, but for higher molecular weight compounds and polymers it is usually a very poor solvent (for achievable operating conditions, namely temperature and pressure) however the solubility of $scCO_2$ in many polymers is very high, being function of the temperature, pressure, molecular weight, crystallinity of the polymer and week interactions with functional groups of the polymer chains. For instance, $scCO_2$ is more absorbed by the amorphous chains of the polymers than by the crystalline ones and has good affinity with the carbonyl group of polymers, being the Lewis acidity of CO_2 the main contributor to its solubility since in this molecule there is a charge separation between the carbon and oxygen atoms. In this case, the polarized electron density moves towards the oxygen atoms, resulting in a carbon atom with a partial positive charge acting as a Lewis acid and the two oxygen atoms have partial negative charges acting as a Lewis base, leading to the carbon atom acting as an electron acceptor in a Lewis acid-base interaction with carbonyl groups (Nalawade *et al*., 2006; Kiran *et al*., 2008; Liao *et al*., 2012; Davies *et al*., 2008; Goodship and Ogur, 2004; Kazarian *et al*., 1996; Jacobs *et al*., 2008; Kim and Kim, 2007).

Manufacturing foams applying $scCO_2$ as the blowing agent, and temporary polymer plasticizer is a process that can be divided into three stages: (i) firstly $scCO_2$ is absorbed by the polymer until it is saturated, at constant temperature and pressure, leading to the formation of a homogeneous solution of polymer + $scCO_2$, surrounded by a pure $scCO_2$ phase; (ii) secondly and after the system reaches its equilibrium, the nucleation and formation of bubbles can be induced by a thermodynamic instability, which can be achieved either through temperature increase (temperature soak method) or pressure decrease (pressure quench method); (iii) lastly the growth, expansion and coalescence of bubbles result from a combination of mass transfer and fluid dynamics resulting from the flow of $scCO_2$. These process stages are represented schematically in Figure 2. Throughout the (i) stage $scCO_2$ is absorbed into the polymer chains resulting in their swelling lowering the T_g– plasticization of the polymer as well as the $T_m$of the polymer, the viscosity of the polymer decreases and consequently the polymer state becomes rubbery also this melting point depression allows a more uniform sorption of CO_2 into the polymer. The effect of $scCO_2$ during this stage mimics the effect of heating the polymer. This depression on the T_m of the polymer allows to "melt" polymers, like poly(ε-caprolactone) (PCL), poly(lactic acid) (PLA) and poly(3-hydroxybutyrate-co-3-hydroxyvalerate) (PHBV), which are the most used poly(α-hydroxy acids) with $scCO_2$ foaming/mixing process, at a lower temperature than in ambient conditions, allowing to use any kind of mould, producing tailor-made materials, or to incorporate an extruder and a mould following the (i) stage of the process (de Matos *et al*., 2013; Duarte *et al*., 2012; Frerich, 2015, Salerno *et al*., 2013; Nofar and Park, 2014, Kiran, 2010; Le Moigne *et al*., 2014; Sauceau *et al*., 2011). The most important process conditions influencing the solubility of the $scCO_2$ in the polymer, and thus the swelling, are the free volume between polymer chains (molecular weight of the polymer) and crystallinity of the polymer (as referred). Increasing the operating pressure will lead into an increase in the concentration of CO_2 within the polymer chains since the $scCO_2$ molecules are forced between the chains consequently increasing the polymer swelling and its plasticization effect. As a result of the increased free volume and enhanced chain mobility the diffusion of CO_2 molecules is therefore facilitated. Increasing the operating temperature, for a given pressure, there is a decrease in the density of the $scCO_2$ which is associated with lower solubility of the CO_2 into the polymer leading to a lower plasticization effect (Jacobs *et al*., 2008; White *et al*., 2012; Kazarian, 2000; Karimi *et al*., 2012; Bhamidipati *et al*., 2013; Salerno et al., 2013; Fanovich and Jaeger, 2012). At constant temperature, inducing the thermodynamic instability by

decreasing the operating pressure, stage (ii), inducing the nucleation of bubbles, the concentration of CO_2 in the polymer will decrease leading to an increase of the T_g of the polymer, and vitrification occurs with the final porous structure – foam, fixed into a glassy state (White *et al*., 2012; Jacobs *et al*., 2008; Nalawade *et al*., 2006).

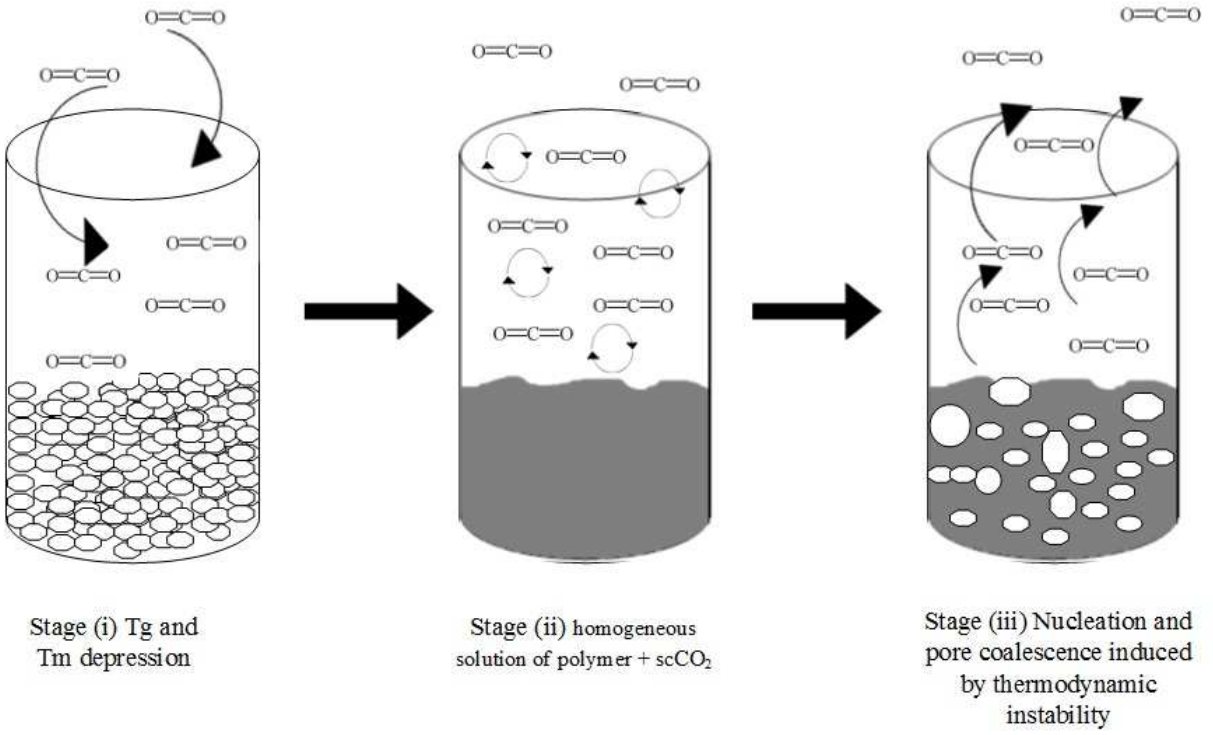

***Figure 2**. Schematic representation of the three stages of the $scCO_2$ foaming/mixing process.*

The nucleation of $scCO_2$ in viscous liquids such as polymers, resulting in the formation of pores leading to the final porous polymeric structures, is often modelled using as basis the classical nucleation theory, claiming that the Gibbs free energy required to create a void in a liquid, resulting into a bubble, is in mechanical and thermodynamic equilibrium with the surrounding fluid. However, the system, molten polymer + $scCO_2$, is not very similar to a liquid + gas system. Due to that limitation, several approaches have been made to model and describe the nucleation mechanism of bubbles, leading to the formation of pores, in molten polymer + $scCO_2$ systems. Colton and Suh, developed a model capable to describe this mechanism for this type of systems, validated with experimental results (Jacobs *et al*., 2008; Colton and Suh, 1987). Accordingly, the bubble nucleation mechanisms for the formation of pores can be either one of two types, homogeneous or heterogeneous. The first one occurs when molecules of gas or SCF dissolved in a homogeneous polymer aggregate during a long period of time, producing a stable bubble nucleus. If is added to the system a soluble additive it will affect the surface tension of the mixture, and if the mixture of polymer and additive has a lower surface tension than the pure polymer, the activation energy to occur homogeneous nucleation is reduced and the rate of nucleation increases. Heterogeneous nucleation occurs when a bubble forms at an interface between two phases such as polymer and an additive, in this case the presence of an interface will reduce the activation energy for this mechanism increasing the nucleation mechanism (Colton and Suh, 1987). Both mechanisms, in systems when they occur simultaneously, compete for available CO_2 during the depressurization of the system, but in this situations, heterogeneous nucleation occurs preferentially since its activation energy is lower than the one required for the homogeneous mechanism (Tsimpliaraki *et al*., 2011; Colton and Suh, 1987)

The final morphological properties of the produced porous materials, for example porosity and average pore size are easily tuned with proper selection of the process conditions, mainly temperature, pressure, saturation time and depressurization rate (Liao *et al*., 2012; White *et al*., 2012; Jenkins *et al*., 2006; Karimi *et al*., 2012). Increasing the operating pressure, the $scCO_2$ intake is greater leading to higher concentration of CO_2 absorbed by the polymer, this will lead to, as referred, an increase in chain mobility and polymer swelling, resulting in the formation of more nucleation sites increasing the final pore density but decreasing their average diameter, giving rise to foams with narrower pore size distribution. In its turn, increasing the operating temperature, the viscosity of the homogeneous mixture polymer + $scCO_2$ is decreased so that there is less resistance to the bubble formation and coalescence, increasing the average size of the final pores but decreasing the pore density, giving rise to foams with larger pore size distribution. Throughout the depressurization stage the nucleation of bubbles competes with diffusion of $scCO_2$in the polymer which results in pore growth, so, slower depressurization rates lead to greater average pore diameter, since there is more time for bubble to grow and coalesce, but the pore density is lower, faster depressurization rates, on the other hand, leads to smaller average pore diameter since the nucleation is fast, leaving few time for bubbles to growth, but there are more nucleation sites, once the CO_2 molecules do not have time to diffuse to larger bubbles, leading to a greater pore density. An increase in the saturation time leads to larger pores since it provides more time for the CO_2 molecules to absorb into the polymer chains (Liao *et al*., 2012; White *et al*., 2012; Fanovich and Jaeger, 2012; Karimi *et al*., 2012; Nalawade *et al*., 2006; Collins *et al*., 2010; de Matos *et al*., 2013).

1.3. Biodegradable Polymers, Green Plasticizers and Polymer Compatibilizers

Biodegradable Polymers

As a requirement for the scaffolds to employ in a hard tissue engineering application, the material from which they are constituted must be biocompatible and biodegradable or bioabsorbable, as referred in section 1.1. In order to fulfil this requirement the choice of material to employ in this type of applications falls into a biodegradable polymer.

Biodegradable polymers is a class of polymers that have been receiving great attention over the last few years due to their environmentally friendly feature for several applications, such as packaging and for biomedical/pharmaceutical applications, such as drug delivery devices, medical devices (wound dressings, dental substitutes or fixation devices as screws) and tissue engineering/regenerative medicine applications (polymeric-based scaffolds and organ replacements) (Takahashi *et al*., 2012; Vroman and Tighzert, 2009). Accordingly to their source and/or method of production biodegradable polymers, and polymers in general, can be classified as natural or synthetic, being the first ones produced from renewable sources and are usually expensive and available in large quantities (in the environment), and the latter ones are produced from non-renewable sources like petroleum and are usually non-expensive and available in limited quantities (due to the non-renewable feature of their raw materials) (Vroman and Tighzert, 2009). Naturally-derived polymers are proteins (collagen, gelatine, fibroin, etc…) and polysaccharides (cellulose, chitin and derivatives, alginate, starch, etc…), these type of polymers have great potential to be employed in tissue engineering applications since some are naturally-occurred in the human body, and are present in the extracellular matrix, thus mimicking better the natural environment minimizing the rejection of the material by the host, but these polymers also have great limitations mainly due to their difficult processability, poor mechanical behaviour, high crystallinity limiting their solubility, low degradation temperature, high batch heterogeneity, acquisition cost and that they can act as diseases carriers

(Duarte *et al*., 2012; Lacroix *et al*., 2014). In order to avoid these problems, one can employ biodegradable synthetic polymers.

The biodegradation feature of a polymer depends not only of its nature but also of its chemical structure and application medium. Biodegradation occurs by action of enzymes and/or occurring chemical reactions associated with the biological medium of application (Vroman and Tighzert, 2009; Sultana, 2013). There are other degradation mechanisms for polymers, but these are not derived from any microorganism or any other biological action, being named only as degradation paths/mechanisms for polymers, biodegradable polymers can also be degraded by these mechanisms. Such paths/mechanisms include, photoinduced degradation, thermal degradation and chemical degradation as oxidation for instance (Scott, 1990). Among biodegradable synthetic polymers, there are some with hydrolysable groups such as ester, amide and urethane or polymers with chains at which were added additives that work as chain-cleavage points (Vroman and Tighzert, 2009). Among these type of synthetic biodegradable polymers, aliphatic polyesters ((poly) α −hydroxy acids) are by far the most studied polymers in biomedical/pharmaceutical research and applications as well as for proposed tissue engineering applications. Of this polymers poly(D,L-(lactic acid)) (PDLA), poly(lactic-co-glycolic acid) (PLGA), poly(3-hydroxybutyrate) (PHB) and poly(ε-caprolactone) (PCL), derivatives and their copolymers are the most used and studied for tissue engineering applications (Nishida *et al*., 2015; Baker *et al*., 2011; Goswami *et al*., 2013; Andreas *et al*., 2011; Takahashi *et al*., 2012; Lee *et al*., 2015; Ye *et al*., 2009; de Matos *et al*., 2013; Fanovich and Jaeger, 2012; Salerno and Domingo, 2013).

Between this group of synthetic aliphatic polyesters one of the most studied for biomedical/pharmaceutical and hard tissue engineering applications is PCL. PCL is a semi-crystalline polyester, with chemical structure presented in Figure 3, with hydrophobic behaviour, is FDA approved (as used in biomedical devices and combination products), has a T_g of -60ºC and a T_m in the range of 59-64ºC and is obtained *via* ring-opening polymerization of the monomer ε-caprolactone and its source can be either natural or synthetic (Karimi *et al*., 2012; Kiran *et al*., 2008; Takahashi *et al*., 2012; Woodruff and Hutmacher, 2010).

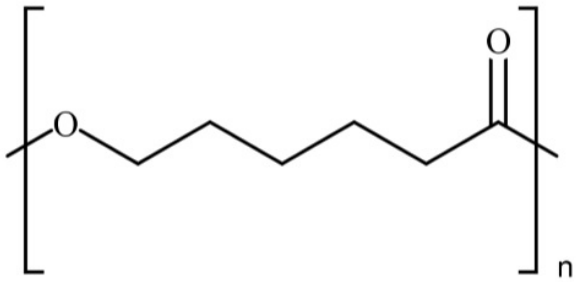

Figure 3*. Chemical structure of poly(ε-caprolactone).*

Since PCL has a non-toxic nature and was found to be cytocompatible with several body tissues, also has been shown that PCL is a bone tissue compatible material due to its compatibility to support both *in vitro* and *in vivo* bone cell and tissue growth without inducing immune and/or inflammatory response, preserving its mechanical function making it the most studied polymer for biomedical/pharmaceutical and hard tissue engineering applications (Salerno *et al*., 2012; Salerno *et al*., 2010 (a); Dash and Konkimalla, 2001). Its compatibility with several hydrophobic drugs and other bioactive compounds ensures a uniform distribution of these compounds within the PCL matrix to employ, enabling a release up to several months due, also, to its biodegradation rate. All of these features are making PCL the material of choice towards the development of scaffolds, fibres, films, micelles, hydrogels and nano and micro carriers, as

spheres and/or particles, towards drug delivery applications. It is also already used in finished medical devices such as sutures, wound dressings, fixation devices and contraceptive devices (Dash and Konkimalla, 2012; Woodruff and Hutmacher, 2010). PCL is degraded in biological medium by enzymatic action of lipases inducing hydrolytic cleavage of the polymeric chain by bulk degradation, which rate is pointed out to be 2-4 years, depending on the molecular weight, until total degradation, making it the ideal material for long-term applications, its degradation product is 6-hydroxycaproic acid which is metabolized *via* the citric acid cycle. For tissue engineering applications, PCL is advantageous since it have better rheological and viscoelastic properties over other biodegradable aliphatic polyesters, allowing it to be used in a very wide range of manufacturing methods of scaffolds, also its carbonyl group allows a good processing with $scCO_2$ as referred in the previous section. PCL in presence of pressurized CO_2 presents a depression in its T_m(40-45ºC for 14.4-27.5 MPa) which allows the process to be conducted at temperature near the body temperature without inducing any degradation on thermo sensitive compounds (Sivalingam *et al*., 2003; Woodruff and Hutmacher, 2010; Kazarian *et al*., 1996; Takahashi *et al*., 2012; Kiran *et al*., 2008).

In order to improve biological properties of polymers, namely PCL, as well as processability parameters by changing its thermoplastic properties, plasticizers and/or compatibilizers can be used The use of these type of compounds allows a reduction on polymer viscosity, allowing a better processing in extrusion/injection processes and promote miscibility with immiscible substances. Other methods rely on surface modification techniques, in order to allow protein and other biomolecules to adsorb on the surface of the polymeric matrix, improving cell adhesion.

Green plasticizers and polymer compatibilizers

In recent years ionic liquids (ILs) have received attention from both the academic and industrial research in an exponential way (Chen B-K. *et al*., 2013; Keskin *et al*., 2007). Ionic liquids are salts that are liquid at room temperature and pressure, contrasting with common salts that usually do not melt below 800ºC. A liquid salt is classified as an ionic liquid if its upper limit of melting temperature is around 100ºC, higher melting salts systems are usually referred as molten salts (Keskin *et al*., 2007; Livi *et al*., 2014; Chen B-K. *et al*., 2013 ; Silva *et al*., 2012). ILs have a large number of properties which make them a very desirable material both for academic research and industrial application, they are based on their negligible vapour pressure, non-flammability, chemical stability, solvating ability both for organic, inorganic and organometallic materials, high thermal conductivity, high electrochemical range and recycling feature, since they have negligible vapour pressure they do not evaporate allowing a full recovery of the employed IL giving them their "green" and sustainable feature (Keskin *et al*., 2007; Dias *et al*., 2012; Chen B-K. *et al*., 2013). Due to their properties ILs are seemed as greener alternatives to conventional VOC's, giving them their "green feature" (Silva *et al*., 2012; Duarte *et al*., 2012). ILs are constituted both by an anion and a cation, and their properties, such as viscosity, density, hydrophilicity, solubility and toxicity, can be easily tuned by the choice of cation and/or anion or by their alkyl chains, making them a very desirable material for several applications such as solvents, thermal fluids, lubricants and surfactants for layered silicates, antimicrobial agents, solvents for polymerization reactions, electrolytes, plasticizers, foaming agents and stabilizers for proteins (Duarte *et al*., 2012; Dias *et al*., 2012; Livi *et al*., 2014; Gilmore, 2011; Keskin *et al*., 2007; Vrikkis *et al*., 2009).

ILs have also been proven to be good plasticizers and foaming agents both for natural of synthetic-derived polymers (Dias *et al*., 2012; Wang and Hou, 2011). This feature, employing jointly with $scCO_2$, facilitates the plasticization and acts as a foaming agent of the polymer in the (i) stage of the SFM process (presented on section 1.2.1.), lowering the surface tension of

the mixture, promoting homogeneous nucleation of pores leading to foams with more homogeneous pore size distributions with larger and more interconnected pores than using only $scCO_2$ as foaming agent, but the harmful potential of some functional groups used on ILs is already known and one can assert the toxicity of the employed IL only by the functional group. (Colton and Suh, 1987; Salerno *et al*., 2013; Salerno *et al*., 2014). In order to achieve these effects, the employed IL must have good affinity with $scCO_2$, and also low or negligible toxicity, since for tissue engineering applications all of the employed materials must be non-toxic, and should be environmentally safe following the green chemistry ideology. The toxicity of ILs is a difficult and complicated issue, in the literature, mainly due to the lack of regulation by the authorities but the harmful potential of some functional groups used on ILs is already known and one can forecast the toxicity of the employed IL only by the functional group (Dias *et al*., 2012; Keskin *et al*., 2007). Phosphonium-based ILs are, by these means, the ideal choice of IL to employ in the production of $scCO_2$-assisted foams towards tissue engineering applications, since they have high thermal and chemical stability and are produced in large scales (Dias *et al*., 2012; Fraser and MacFarlane, 2009; Livi *et al*., 2014). Also, it has been proven that Trihexyl(tetradecyl) phosphonium bis (trifluoromethylsulfonyl)imide (TTPB) has low cell toxicity and has been proposed as plasticizer for biomedical-grade materials (Rosa, 2013; Dias *et al*., 2012). Phosphonium-based ILs can be functionalized by the choice of the alkyl chain of the functional group long alkyl chains are considered CO_2-phobe and perflurinated chains are considered CO_2-philic (Livi *et al*., 2014). In Figure 4 A is shown the molecular structure of the employed phosphonium-based IL. As it can be seen, the anion is functionalized with fluor atoms, which are known for their great affinity with CO_2 molecules allowing a good processability of polymers by SFM process (Jacobs *et al*., 2008).

Several ILs have already been used with $scCO_2$ as foaming agents for several applications, namely biomedical applications the most studied systems involves the use of 1-butyl-3-methylimidazolium acetate, 1-butyl-3-methylimidazolium chloride, 1-butyl-3-methylimidazolium hexafluorophosphate, alkyltriphenyk phosphnium and perfluorinated alkylpyridinium-based ILs, N, N, N-trimethylethanolammonium pentoate and Trihexyl(tetradecyl) phosphonium bis (trifluoromethylsulfonyl)imide (Duarte *et al*., 2012; Silva *et al*., 2011; Martins *et al*., 2014; Bendaoud and Chalamet, 2014; Andanson *et al*., 2009; Livi *et al*., 2012; Rosa, 2013).

In Figure 4 B is also presented another employed compound, Glycofurol (GF), which is already used as an injectable solvent in parenteral pharmaceutical formulations, is usually regarded as a nontoxic and non-irritant solvent, is a FDA approved solvent for biomedical/pharmaceutical applications and is biocompatible (Rowe *et al*., 2009; Allhenn and Lamprecht, 2011; Boongird *et al*., 2014). Also, by its chemical structure with a hydrophobic head and a hydrophilic alkyl chain, one can expect, that in the mixture with PCL and $scCO_2$, the hydrophobic end will have good affinity with the polymer, acting as a hydrotrope – surfactant-like behaviour but it is not a molecule big enough to self-aggregate. GF acts as a polymer compatibilizer promoting interfacial adhesion between the polymer (PCL) and another immiscible phase, like an inorganic phase, when manufacturing a composite. This effect is due to the fact that GF is a linear molecule with two different natures, being one compatible with the hidrophilic phase of the mixture (for example, an inorganic phase) and the other compatible with the hidrophobic one (for example, PCL). Glycofurol will concentrate at the interface and stabilize both phases allowing a better dispersion of the immiscible phase throughout the polymeric matrix, also GF can act as a foaming agent facilitating the polymer processability in SFM process (Welge and Wolf, 2001).

Employing liquid additives in SFM process, the poor solubility of CO_2 within the crystalline parts of polymers, and since PCL is a highly crystalline polymer, is increased allowing a more

homogeneous dispersion of the CO_2 molecules within all of the polymeric matrix and so obtaining a more homogeneous porous strucutre (Salerno *et al*., 2011). Other green and safe liquid additives already proposed and used combined with SFM process are ethyl-lactate and ethyl-acetate, which act as plasticizers facilitating polymer processing (Salerno *et al*., 2014). Using GF, its plasticizer effect will enhanced even more the T_g and T_m depression, by lowering the surface tension of the mixture.

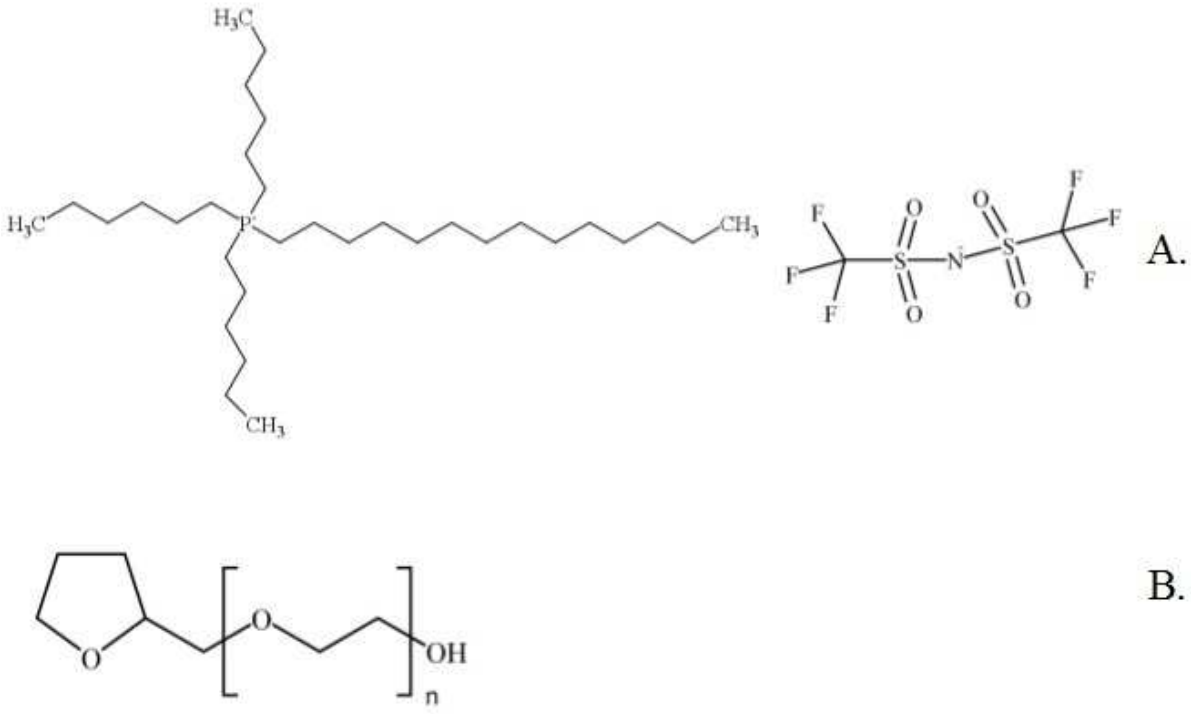

Figure 4*. Chemical structures of the employed green plasticizers and polymer compatibilizer (B), A. Trihexyl(tetradecyl) phosphonium bis (trifluoromethylsulfonyl)imide (TTPB), B. Glycofurol (GF).*

1.4. Nanocomposites and the Effects of Nanofillers in the $scCO_2$ Foaming/Mixing Process

The best approach of tissue engineering applications is trough biomimetism of the natural tissue in order to ensure a good acceptance by the host organism without inducing immune and/or inflammatory response. The imitation of the physical properties of the natural tissues, is achieved by controlling the physical properties of the employed materials in tissue engineering applications. As referred in section 1.1.1., bone tissue is a truly composite material, composed of type I collagen and hydroxyapatite. So, following the biomimetism approach, a material to employ as a substitute for bone/hard tissue must be, as well, a composite material, miming the natural tissue. Moreover a single polymeric material cannot fulfil the mechanical requirements for hard tissue substitutes, so a composite material composed by a polymer and an inorganic filler is the best approach to achieve this functional requirement (Liao *et al*., 2012).

A polymeric-based composite material is a material composed by two immiscible phases in which one is a polymer (matrix – continuous phase) and the other is a filler (disperse phase), a nanocomposite material is a material wherein the filler has at least one dimension at the nanoscale (smaller than 100 nm) (Liao *et al*., 2012; Chen B-K *et al*., 2012; Chen L. *et al*., 2013; Lee *et al*., 2005). Nanocomposites are a class of materials with enhanced properties, comparing with micro and macrocomposites, the addition of a small amount of nanoparticles, for example, can improve significantly several properties without losing the inherent properties of the polymer, polymer nanocomposites show excellent balance between strength and toughness.

Such materials provide the ideal choice for applications requiring high strength, light weight, flammability resistance and the addition of an inorganic filler, allows to control and tailor the biocompatibility and biodegradation rate of the composite material. Also, nanofillers have a high aspect ratio with high surface area ensuring a larger three dimensional interface to the composite, and a great surface area as well. (Lee *et al*., 2005; Liao *et al*., 2012; Tsimpliaraki *et al*., 2011; Tsimpliaraki *et al*., 2013; Chen L. *et al*., 2013). Several methods have been reported for incorporation of nanofillers in polymeric matrices such as physical mixture, *in-situ* polymerization, melt intercalation, solution intercalation and $scCO_2$ that could act as a plasticizer and as a carrier (in some cases) (Nalawade *et al*., 2006; Shieh *et al*., 2009; Bonilla *et al*., 2014; Tsimpliaraki *et al*., 2011; Lee *et al*., 2005; de Matos *et al*., 2013).

In the SFM process nanofillers act as heterogeneous nucleation sites due to the interface created by them, lowering the activation energy for nucleation, favouring the heterogeneous mechanism. High number of fillers, high nucleant density, result in high nucleation rate and therefore high pore density, but with small size since there is a high number of nucleation sites leading to a smaller amount of available blowing agent for bubble to grow. The presence of nanoparticles, for example, can provide a greater interconnectivity of the porous structure. The greater the surface area of the fillers the greater the interface favouring nucleation. This ability, allows to control the pore size distribution and pore density controlling the concentration of fillers and their size/surface area (Nalawade *et al*., 2006; Jacobs *et al*., 2008; Lee *et al*., 2005; Collins *et al*., 2010; Chen L. *et al*., 2013). The shape, size and distribution of the fillers throughout the polymeric matrix as well as the pore nucleation efficiency can be tailored by changing the surface chemistry of the nanofillers, lowering even more the activation energy for nucleation and allowing a better dispersion of the fillers within the matrix, this can be achieve, for example, through chemical modification of the fillers surface by adding a surfactant (Chen L. *et al*., 2013; Tsimpliaraki *et al*., 2011).

For hard tissue engineering applications several fillers have been proposed, with the objective either to improve mechanical properties, biocompatibility and osteoinducity. The most commonly used fillers proposed for this type of applications are micro and nano particles of hydroxyapatite (HA), β-tricalcium phosphate (β-TCP), carbon nanotubes, montmorillonite clay (MMT), layered silicates and micro and nano particles of silica (Delabarde *et al*., 2012; Mou *et al*., 2011; Erisken *et al*., 2008; Mattioli-Belmonte *et al*., 2012; Wu *et al*., 2010; Collins *et al*., 2010; de Matos *et al*., 2013; Bonilla *et al*., 2014).

Mesoporous silicates, have been widely studied and proposed for several applications, due to their unique chemical and physical properties, namely food industry, biomedical/pharmaceutical, for drug delivery, drug targeting and tissue engineering applications. Of the mesoporous silicates, by far, the most used is Santa Barbara Amorphous type 15 (SBA-15). This material exhibits high surface area and pore volume, also, possess ordered cylindrical pores structures with tunable pore diameters and easily functionalizable surfaces. These features provide very large internal surface area and pore volume, which allows a high adsorption of drugs and proteins into their structures (Heikkilä et al., 2010; Hudson *et al*., 2008; Izquierdo-Barba *et al*., 2011; Jaganathan and Godin, 2012; Xu *et al*., 2012). It is known that crystalline forms of silicates are toxic to human and that particle size, surface, shape and chemistry play a major role determining the behaviour of cells in contact with these materials, however, SBA-15 has been reported as biocompatible and bioabsorbale by some authors, being pointed applications in the biomedical/pharmaceutical and tissue engineering field, still there are a lack of regulation regarding the use of nanoparticles for these type of applications besides all the efforts made recently by FDA, namely (Hudson *et al*., 2008; Jaganathan and Godin, 2012; Heikkilä *et al*., 2010). Comparing SBA-15 to other commonly used mesoporous silicates like Mobil Crystalline Materials type 41 (MCM-41), it is clearly that

MCM-41 have higher surface area (1050 $m^2.g^{-1}$ comparing to 718 $m^2.g^{-1}$), improving surface properties of composites produced with this filler, however, pore diameter of SBA-15 is larger than pore diameter of MCM-41 (8.5 nm comparing to 2.4 nm) allowing a greater adsorption of compounds, like drugs or growth factors into the composite material (Appendix J).

1.5. Objectives

The main goal of this work is to develop, produce PCL-based porous biomaterials, with drug carrier potential, by $scCO_2$ foaming/mixing process (SFM), a green and sustainable process, and characterize them morphologically, thermally and mechanically for hard tissue engineering applications. To improve mechanical properties SBA-15 is incorporated (20 and 30 wt. %), producing PCL/SBA-15 porous biomaterials with enhanced drug carrier potential, by SFM. To achieve control over morphological properties, filler distribution, as well as to facilitate polymer processing, glycofurol (GF), a FDA approved solvent, and trihexyl(tetradecyl) phosphonium bis (trifluoromethylsulfonyl)imide (TTPB), a non-cytotoxic ionic liquid, are incorporated, acting as green and non-toxic blowing agents, plasticizers and compatibility agents.

The operating conditions, such as temperature, pressure and depressurization rate were optimized and selected accordingly to morphological and mechanical properties of the obtained porous biomaterials, and contact time was selected, allowing the solution to become homogeneous (reaching stage (ii) of the foaming process) and then adding the appropriate time to claim, without doubt, that the solution is saturated.

2. Materials and Methods

2.1. Materials

Poly (ε-caprolactone) (PCL) (CAS [24980-41-4]), in pellet form, with a number average molecular weight (M_n) of 45000 $g.mol^{-1}$, glycofurol (tetraglycol CAS [31692-85-0]), methanol HPLC (CAS [67-56-1], purity≥99.9%) and acetone G.C. (CAS [67-64-1] purity≥99.5%) were purchased from Sigma-Aldrich. Mesoporous silica 1D-Hexagonal SBA-15 type (SBA-15) (average BJH framework pore size 8.5 nm, BET surface area 718 $m^2.g^{-1}$, total pore volume 0.93 $cm^3.g^{-1}$) was supplied by Claytec (USA), Hydroxyapatite (HA) (average BJH framework pore size 26.4 nm, BET surface area 10.6 $m^2.g^{-1}$, total pore volume 54.3 $cm^3.g^{-1}$) was acquired at ÁgoraMat, Portugal, Montmorillonite (MMT) was acquired in Algeria, of natural source and suffered acidic activation (MMT H^+). Trihexyl(tetradecyl) phosphonium bis (trifluoromethylsulfonyl)imide (TTPB) (purity>98%) was purchased from Cytec Industries (France). Carbon dioxide (purity of 99.998% (v/v)) was supplied by Praxair (Spain). All chemicals were used as received except PCL, PCL was processed from pellet into powder form in order to allow a greater superficial area facilitating the physical mixture and enhancing the interaction with $scCO_2$, reducing the needed processing time.

2.2. Experimental Methods

2.2.1. Preparation of PCL into Powder Form

Approximately 12g of PCL pellets were dissolved into 200 mL of acetone at ambient temperature and pressure under magnetic stirring. After complete solubilisation of the PCL, 20 mL of methanol were added slowly drop by drop and 20 mL of water after following the same method, until precipitation of PCL occurred. After precipitation of the PCL, it was allowed to fully settle. Afterwards the supernatant was removed and the precipitate was poured into Petri

dishes where it was allowed to dry at room temperature and pressure until complete removal of any residual solvent or anti-solvent employed by evaporation. The supernatant was centrifuge at 5000 rpm for 10 minutes and then removed, allowing to the remaining powders to dry at room conditions. After complete drying of the PCL powder, it was mechanically sieved, in test sieve trays of several diameters (0.6 and 0.35 mm Retsch 5657 Haan. W., Germany) and stored in flasks accordingly to their diameter. For the performed tests only PCL powders with diameters equal or lower than 0.35mm were used.

2.2.2. Batch Solid-State Foaming/mixing Process with Supercritical Carbon Dioxide Technology

Previously to the foaming process 1g of PCL, MMT (10 wt. % and 20 wt. %), HA (10 wt. % and 20 wt. %) and SBA-15 (10 wt. %, 20 wt. % and 30 wt. %) were physically mixed, manually, in a 7 mL glass flask or in a 5 mL PTFE (polytetrafluoroethylene) beaker (Sigma-Aldrich) both with cylindrical shape, until homogenization of the mixture. Then the porogenic/plasticizer agents, GF and TTPB, were added in three molar proportions 2:1, 3:1 and 5:1 (for 98% molar of the employed amount of polymer) respectively, keeping constant the molar fraction of GF and varying the molar fraction of TTPB. The preformed assays of pure, composite and addtivated PCL samples, were conducted in a batch solid-state foaming/mixing process, as shown in Figure 5. The presented apparatus consists in a compressor, high pressure vessel (approximately 23 cm^3), a temperature controlled water bath (Thermoscientific, Haake AC 150), a manometer (Lab DMM, REP transducer), a magnetic stirrer plate, high pressure valves and fittings used to connect the system (High Pressure Equipment Company, Erie, USA).

The glass vial or PTFE beaker was placed inside the high pressure vessel, leaving approximately 20% of free volume allowing a better diffusion of the $scCO_2$ throughout the entire sample, then the vessel was closed and inserted inline, immersed in the water bath at the desired operating temperature. Later the vessel was filled with CO_2 until the operating pressure was reached, the filling time was the same for every processed material, and was approximately 10 minutes. The system was maintained at constant temperature and pressure over a period of time, established by visual observation of the process allowing the solution to become homogeneous and then adding the appropriate time to claim, without doubt, that the solution is saturated, being of 2 hours for every processed sample. After this stage, the high pressure vessel was then depressurized until ambient pressure was reached at a constant depressurization rate, in constant temperature.

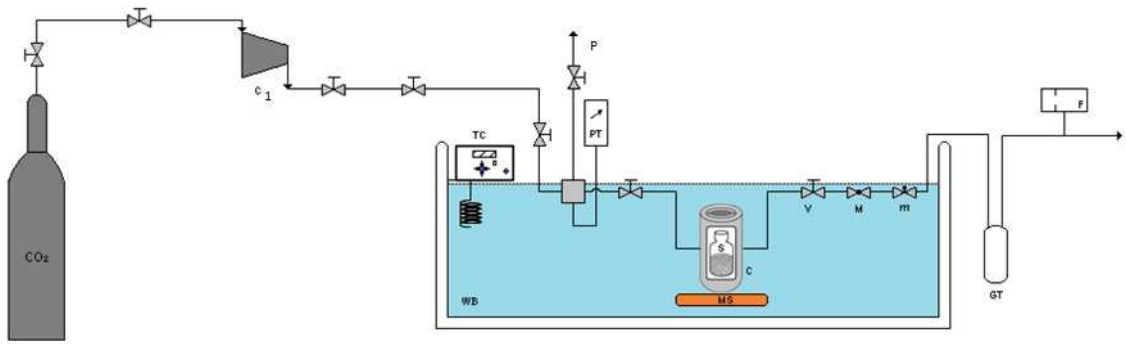

Figure 5. *Experimental apparatus for the solid-state foaming/mixing with supercritical carbon dioxide. CO_2 – Carbon dioxide vessel; C_1 – Compressor; TC – Temperature controller; WB – Water bath; P – Purge; PT – Pressure transducer; S – Sample; MS – Magnetic stirrer; C – High pressure vessel; V – Screw down valve; M - macrometric valve; m - micrometric valve; GT - glass trap; F - mass flow meter.*

In this work the operating temperature, pressure and depressurization rate were optimized and selected accordingly to the morphological and mechanical properties of the obtained porous biomaterials of pure PCL, selecting the most suitable for a material for hard tissue engineering applications. In order to do so, the tested operating conditions were chosen concerning a variation on the density and viscosity of $scCO_2$ of 100 $kg.m^{-3}$ and 2 Pa.s, respectively, at constant pressure of 20 MPa, operating with temperatures of 35, 40, 45, 50 and 55ºC. All tested conditions and $scCO_2$ physical properties are shown in Table 2. Two depressurization rates ($\Delta P/\Delta t$) were tested, one fast of 1 $MPa.min^{-1}$ and another one slow of 0.3 $MPa.min^{-1}$, allowing a depressurization time in the order of one hour, which according to the literature is the appropriate amount of time to obtain pores with optimum size for hard tissue engineering applications (Bhamidipati *et al*., 2013).

Table 2*. Tested physical properties of $scCO_2$ for optimization of the operating conditions towards porous biomaterials for hard tissue engineering applications (Website5).*

Pressure (MPa)	**Temperature (ºC)**	**Saturation time (h)**	**Density ($kg.m^{-3}$)**	**Viscosity (Pa.s)×10^5**	**Depressurization rate ($MPa.min^{-1}$)**
20	35	2	865.7	8.5	1 and 0.3
20	40	2	839.8	7.8	1 and 0.3
20	45	2	812.7	7.3	1 and 0.3
20	50	2	784.3	6.9	1 and 0.3
20	55	2	754.6	6.4	1 and 0.3

A screw and a pin mould were also employed, and placed inside the high pressure vessel, producing screws and pins of pure PCL and PCL/SBA-15 (10 wt.%) composites, at a pressure of 20 MPa, a temperature of 40ºC, a saturation time of 2h and a depressurization rate of 2 $MPa.min^{-1}$ [1] . All the samples were produced in triplicate, including filler selection assays.

For a better understanding, all of the manufactured porous biomaterials and devices for this work are shown in Table 3, and classified as the type of the corresponding assay.

[1] All of these operating conditions were established after a second set of preliminary assays.

***Table 3**. Manufactured porous biomaterials during this work with corresponding operating conditions, type and amount of filler and plasticizers and compatibility agents distributed by type of assay.*

Polymeric Matrix	Operating Conditions				Filler (wt. %)			Green Plasticizers and Compatibility Agents (molar % and molar proportion)		Type of Assay
	P (MPa)	T (ºC)	CO_2 Density ($kg.m^{-3}$)	$\Delta P/\Delta t$ ($MPa.min^{-1}$)	MMT	SBA-15	HA	GF	TTPB	
PCL	20	45	812.7	1	10	-	-	-	-	Filler Selection
					-	10	-	-	-	
					-	-	10	-	-	
					20	-	-	-	-	
					-	20	-	-	-	
					-	-	20	-	-	
	20	35	865.7	0.3	-	-	-	-	-	Optimization
				1	-	-	-	-	-	
		40	839.8	0.3	-	-	-	-	-	
				1	-	-	-	-	-	
		45	812.7	0.3	-	-	-	-	-	
				1	-	-	-	-	-	
		50	784.3	0.3	-	-	-	-	-	
				1	-	-	-	-	-	
		55	754.6	0.3	-	-	-	-	-	
				1	-	-	-	-	-	
	20	40	839.8	0.3	-	20	-	-	98	Additivated and Composite Porous Biomaterials
					-		-	98	-	
					-	30	-	98	-	
					-	20	-	2:1		
					-	30	-			
					-	20	-	3:1		
					-		-	5:1		
					-	20	-	-	-	
					-	-	-	-	-	
	20	40	839.8	2	-	-	-	-	-	Fixation Devices
					-	10	-	-	-	

2.3. Characterization Methods

2.3.1. Morphological Analysis

Macroscopic Analysis

Macroscopic analysis was achieved through digital photographs of pure PCL porous biomaterials, PCL/SBA-15 (30 and 20 wt. %) composites and pure and composite PCL porous biomaterials additivated with the liquid additives. The employed resolution was of 5184x3456 pixels.

Scanning Electron Microscopy (SEM) and Energy-Dispersive X-Ray Spectroscopy (EDS)

The morphology of porous biomaterials of pure PCL, PCL/SBA-15, PCL addtivated with either GF and TTPB and with three mixtures of these additives, as the prepared devices, were evaluated by scanning electron microscopy (SEM) using a microscope (Jeol JSM-5310, Japan) coupled with an EDS analysis system Oxford X-Max, with an operating voltage of 10kV and using AZtec software for image treatment and EDS analysis. Mean pore size was determined using ImageJ software, based on the horizontal Feret diameter of the pores. The samples were sputter-coated with a gold film for 20 seconds (~ 6nm thickness).

Mercury Intrusion

Pore size distribution, porosity, total pore area, skeletal density and bulk density of the produced porous biomaterials were determined by mercury intrusion (Autopore IV 9500 Micromeritics). For this method all the samples were cut in pieces with a height approximately of 1cm and a thickness between 5-8 mm. Bulk density can be defined as the density corresponding to the volume occupied by the solid material and by all the empty spaces that it composes. Skeletal density is correspondent only to the material, excluding all of empty spaces in the porous material. Pore size distribution and total pore area were obtained by application of Washburn's equation, in which all the pores are assumed as cylindrical with a circular opening (Webb, 2001). The presented results are the average and standard deviation of two samples.

Nitrogen Adsorption

Surface area, pore volume and average pore diameter of the produced porous biomaterials were determined by nitrogen adsorption (ASAP 2000 Micromeritics, model 20Q-34001-01). For this method all the samples were cut in pieces with a height approximately of 1cm and a thickness between 5-8 mm. Surface area and average pore diameter were calculated by the Brunauer, Emmet and Teller (BET) method and pore volume by Barret, Joyner and Halenda (BJH) method. Nitrogen adsorption occurs by physical adsorption, condensation of the gas on the free surface of the material, by van der Walls interactions. Adsorption isotherms follow, usually one of six forms: Type I isotherms, characteristic of microporous materials, Type II, characteristic of non-porous materials and/or mesoporous materials, Type IV and V, characteristic of mesoporous materials (showing a characteristic hysteresis cycle in the process adsorption-desorption) and Type VI, characteristic of nonporous materials with an almost completely uniform surface (Webb and Orr, 1997; Gregg and Sing, 1982).The results presented are the average and standard deviation of two samples.

Helium Picnometry

The real density (skeletal density) and volume of samples were evaluated with helium picnometry (Quanta-Chrome, MPY-2). For this method all the samples were cut in pieces with a height approximately of 1cm and a thickness between 5-8 mm. The real density, or skeletal density, is defined as the density corresponding only to the volume of material, excluding all of the empty spaces, in a porous materials. The presented results are the average and standard deviation of two samples.

2.3.2. Thermal and Crystallinity Analysis

Simultaneous Differential Thermal Analysis (SDT)

The thermal behaviour and crystallinity of PCL pellets, powder, pure PCL porous biomaterials, PCL/SBA-15 composites and plasticized with GF and TTPB were evaluated on a Simultaneous Differential Thermal equipment (TA Q600) using standard alumina pans. Measurements were made on samples of 7-10 mg, from the centre of each produced biomaterials, so homogeneous dispersion of fillers and plasticizers could be confirmed, in a temperature range between 25ºC and 700ºC at a heating rate of 10ºC.min^{-1}. With this method were measured the amount and rate of change in weight, weight loss, degradation temperature (T_D), melting temperature (T_m), enthalpy of fusion ($\Delta H_f(\mathrm{T_m})$) and crystallinity ($\chi_c(\%)$).The degree of crystallinity of pure composite porous biomaterials and plasticized with GF and TTPB is defined by equation (1) (Kong and Hay, 2002; Fukushima *et al*., 2009).

$$\chi_c(\%) = \frac{\Delta H_f(\mathrm{T_m})}{\Delta H_f^0(\mathrm{T_m^0}) \times (1 - \frac{wt.\%_{SBA-15}}{100})} \times 100 \quad (1)$$

In which $\Delta H_f(\mathrm{T_m})$ represents the enthalpy of fusion, at the melting point, obtained from the SDT analysis, $\Delta H_f^0(\mathrm{T_m^0})$ represents the enthalpy of fusion of the totally crystalline polymer at the equilibrium point, $\mathrm{T_m^0}$ and $wt.\%_{SBA-15}$ represents the percentage of weight of SBA-15 in the prepared composites. For totally crystalline PCL (100% crystalline), the value of $\Delta H_f^0(\mathrm{T_m^0})$ is reported in the literature as 139.3 J.g^{-1} (Jenkins *et al*., 2006; Chasin and Langer, 1990). All of the presented results are concerning to the average and standard deviation of two prepared samples.

X-Ray Diffraction (XRD)

Crystallinity of pure and additivated PCL porous biomaterials was evaluated by X-ray Diffraction (XRD) (Philips, X'Pert). Samples were cut in pieces with a height approximately of 1cm and a thickness between 5-8 mm and then powdered so the beam of light could capture material of the sample and not the sample holder, since all the samples have voids resulting from their pores. Samples were analysed with Co radiation ($\lambda_{K\alpha 1} = 0.178896\ nm$ and $\lambda_{K\alpha 2} = 0.179285\ nm$), varying the diffraction angle (2θ) from 6º up to 60º, an acquisition step of 0.004º and an acquisition time of 1s/step (40 kV and 35 mA). The degree of crystallinity, can be calculated by the following equation (2),

$$\chi_i(\%) = \frac{\sum A_C}{\sum A_c + \sum A_A} \times 100 \quad (2)$$

Where χ_i represents the degree of crystallinity calculated accordingly to the results obtained by XRD, A_C represents the area of the crystalline parts of each sample (m^2) and A_A represents the

area of the amorphous parts of each samples (m^2). The results presented are the average and standard deviation of two samples.

2.3.3. Mechanical Analysis

Mechanical properties of all of the prepared porous biomaterials, such as compressive strength and Young's Modulus, were determined using an oedometer (Wykeham Farrance, model no. 24251) at room temperature. The tests were performed applying increasing loads, of 0.25, 0.5, 1, 2, 4 and 5 kg into the samples, with 1 minute interval between each load, measuring the vertical deformation of the sample at every 3 seconds with a deformation transducer (strain gauge) coupled to a computer in which the deformation was read with TRIAX software (Durham University). The oedometer was adapted to apply the force only in the superficial area of the cylindrical shaped biomaterial, as shown in Figure 6. All the samples were cut in the top, until a cross-section was obtained, ensuring a homogeneous bearing of each load perpendicular to the vertical axis. The heights and diameters of each sample used for determination of the mechanical properties of the prepared biomaterials are shown in Appendix C, Table C 1. Compressive strength of each sample was determined plotting stress (MPa) *versus* strain (mm/mm). The maximum stress was defined as ultimate stress (break of the porous structure). The load applied at the top of each biomaterial structure is multiplied by a load ratio of 11.04 corresponding to the further point of application of load in the loading arm. Finally stress was determined by equations (3), (4) and (5) (Salerno *et al*., 2010 (b); Baker *et al*., 2011; White *et al*., 2012),

$$L_{ef} = L_{ap} \times 11.04 \quad (3)$$

In which L_{ef} represents the effective load applied in the samples (kgf) and L_{ap} represents the applied load on the loading arm (kg), and knowing that 1 kgf = 9.81 N, since the only acceleration involved in the system is the acceleration of gravity. So stress, σ, is determined by

$$\sigma = \frac{L_{ef}}{A_s} \quad (4)$$

In which σ represents the applied stress on the sample (MPa), and A_s the cross section of the sample in which the load is applied (m^2). The strain, ε, of each sample was calculated with equation (6),

$$\varepsilon = 1 - \frac{h_0 - h}{h_0} \quad (5)$$

Where $h_0 - h$ represents the difference between the initial height, h_0 (mm), and the final height, h (mm), of the sample. Young's Modulus (linear elastic modulus, E) was determined applying linear regression on the elastic region of the plotted stress *versus* strain curve, at 5% deformation of each sample.

Figure 6. *Employed oedometer for mechanical characterization of the produced biomaterials. D -deformation transducer; S – sample; CW – counterweight; L – applied load.*

The results presented are the average and standard deviation of two samples.

For better understanding of the developed work in this thesis, in Figure 7 is shown a scheme consisting in the "flowsheet" of this work, towards the development of porous biomaterials towards hard tissue engineering applications by solid-state supercritical CO_2 foaming/mixing technology.

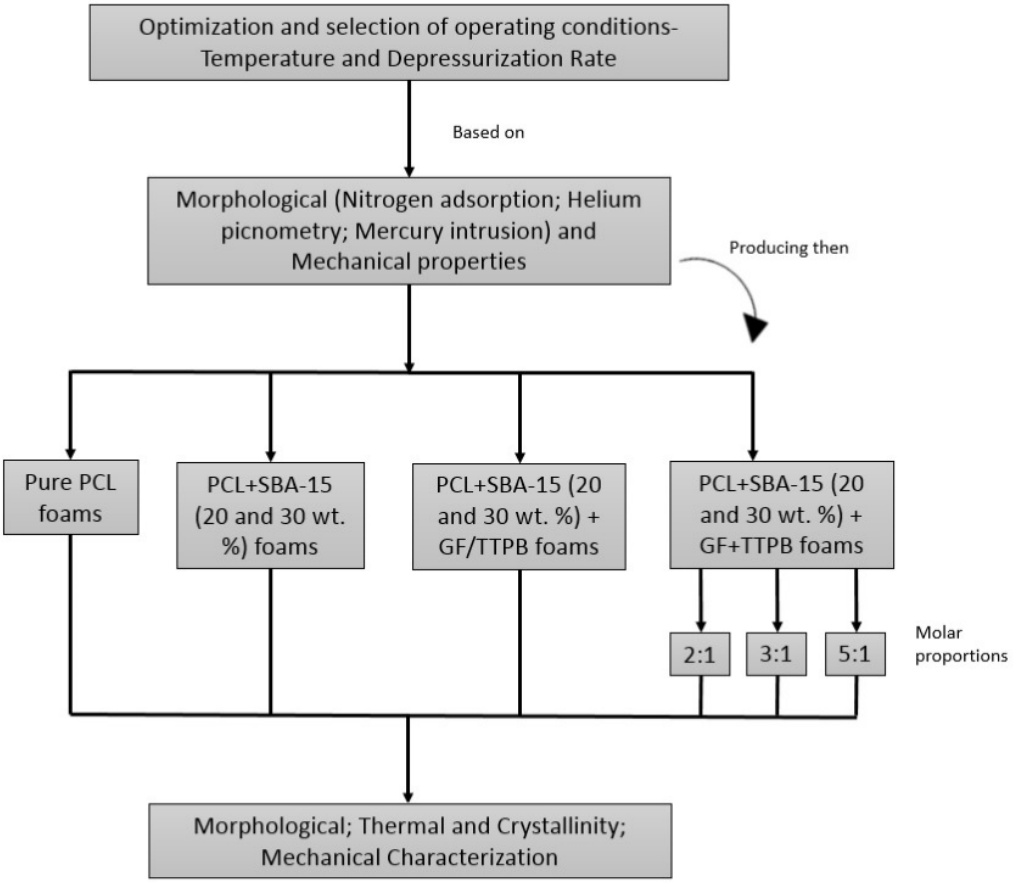

Figure 7. *"Flowsheet" of the developed work towards the development and characterization of porous biomaterials by solid-state supercritical CO_2 foaming/mixing technology for hard tissue engineering applications.*

3. Results and Discussion

3.1. Filler Selection - Description and Conclusions

Filler selection assays were performed producing PCL-based composites biomaterials, with 10 wt. % and 20 wt. % of three different inorganics, MMT, HA and SBA-15, in order to, based on their mechanical properties and porosity select the most suitable composite and composition for hard tissue engineering applications. The assays were performed under processing conditions such as P = 20 MPa, T = 45ºC and $\Delta P/\Delta t$ = 1 MPa.min^{-1}. The used diameter of the PCL powder was $\geq$ 0.6 mm and $\leq$ 0.85 mm for composite porous biomaterials with 10 wt. % of HA and MMT (due to visual observations). The obtained biomaterials as well as the characterization methods employed and obtained results are showed and discussed in Appendix A.

The obtained results are not presented and discussed, in a more detailed way, in the main body of this work because they were not conclusive in order to select one inorganic filler and one composition to use further in the development of PCL-based composite porous biomaterials for hard tissue engineering applications.

The difficulty in obtaining conclusive results from these assays was mainly due to the difference between the particle size of the polymer and inorganic powder, making almost impossible the physical mixture to be homogeneous. All the obtained composite porous biomaterials had, visible at the naked eye, the two phases almost completely separated. This happened, despite all the efforts to achieve a good physical mixtures, due to the difference between the density of the employed inorganics and of PCL (ρ_{PCL} = 1.1 g.cm^{-3}, ρ_{MMT} = 2.0 g.cm^{-3}, ρ_{HA} = 3.3 g.cm^{-3} and ρ_{SBA-15} = 1.8 g.cm^{-3})[2] inducing phase separation, during stage (ii) of the scCO$_2$ process, by force of gravity. The surface chemistry of the employed inorganics could also affect their dispersion, and affinity, with the polymer particles, preventing a homogeneous dispersion throughout the polymeric matrix to be achieved. In the specific case of MMT, its hydrophilic character could make it to carry water molecules and so preventing its homogeneous dispersion in the hydrophobic particles of PCL, since the employed MMT and other inorganics were never dried.

Even do this approach was not further explored it stays clear that some of the difficulties could be avoided, requiring some future work, by drying inorganic particles, by surface chemistry modification of the employed inorganic particles and/or employing surfactants which would help in the dispersion of the inorganics throughout the polymeric matrix (Tsimpliaraki *et al*., 2013; Tsimpliaraki *et al*., 2011; Bonilla *et al*., 2014). From these assays it remained clear that the most fined powder of PCL must be employed in order to achieve good physical mixture with fine inorganic particles and that using SBA-15 as inorganic filler is a good approach to produce mechanical improved biomaterials with good porosity. However further work should be done to fully understand and compare the three inorganic fillers in order to conclude which one is most suitable for organic-inorganic composites for hard tissue engineering applications.

3.2. Optimization and Selection of the Operating Conditions

As shown in Figure 7, this work started by optimization of the operating conditions, such as foaming temperature and depressurization rate, from a variation of approximately 100 kg.m^{-3}

[2] These values are obtained from the information provided by the suppliers.

in $scCO_2$ density and a depressurization time from a magnitude of minutes to hours, as shown in Table 2 as well, on pure PCL biomaterials. Knowing that the critical parameters in order to control the morphology and/or mechanical properties of the biomaterials are the concentration of CO_2 within the polymeric matrix and the rate of CO_2 leaving the matrix. These parameters are linked to the solubility of CO_2 in the polymer which depend on the foaming pressure, temperature and intrinsic properties of the polymer like molecular weight and chemical structure. The selection criteria was based on morphological and mechanical analysis, based on the required properties for a suitable scaffold for hard tissue engineering applications.

3.2.1. Morphological Analysis

Macroscopic Analysis

The effect of $scCO_2$ density, viscosity and depressurization rate were evaluated on the macroscopic morphology of the prepared biomaterials. In Figure 8 are shown the digital images of the obtained biomaterials.

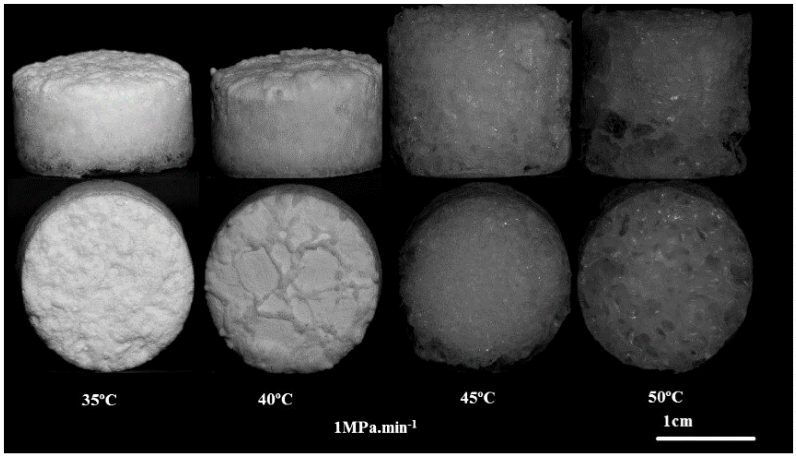

A.

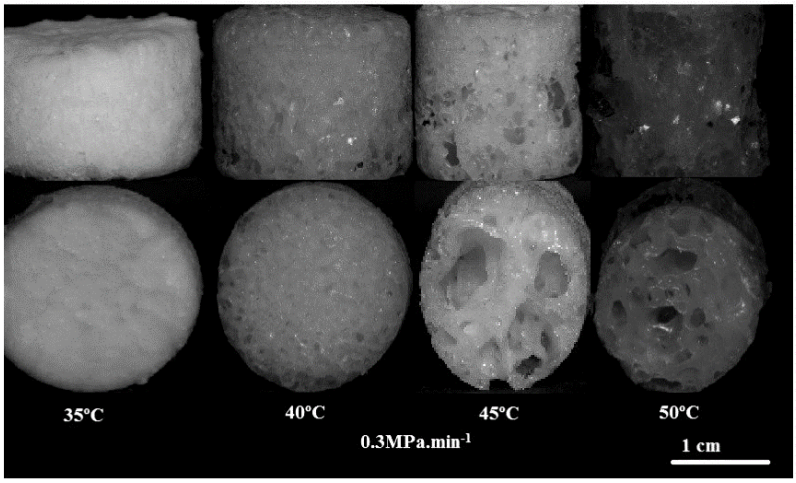

B.

Figure 8. *Digital images of the obtained porous biomaterials for the tested $scCO_2$ physical properties, varying temperature and depressurization rate. A. - Obtained porous biomaterials for a depressurization rate of 1MPa.min^{-1}; B. - Obtained porous biomaterials for a depressurization rate of 0.3MPa.min^{-1}. Top images – lateral view, Bottom images – top view. Scale bar 1cm.*

The temperature of 55ºC was also tested, but was discarded since when the sample was removed from the high pressure vessel it was still in a semi-molten state, which can be explained by the fact that this temperature is too close to the melting temperature of PCL at ambient conditions, preventing the full vitrification of the porous material, also no reproducible porous structure was obtained operating at this temperature for both depressurization rates.

As can be seen, in all of the prepared samples was formed a non-porous skin surrounding each one. This is due to the rapid diffusion of CO_2 from the surface of the sample during depressurization (White *et al*., 2012; Jacobs *et al*., 2008; Tsimpliaraki *et al*., 2011; Fanovich and Jaeger, 2012; Markočič *et al*., 2013; Rosa, 2013). This effect was tested and optimized as shown in Appendix B, since firstly a glass vial was employed in which the polymer powder was placed for supercritical foaming/mixing processing, and in these cases the resulted non-porous skin was very thick. Then a PTFE beaker was employed and the thickness of the non-porous skin was found to be reduced, adding the advantage that the porous material did not stuck to the walls of the beaker allowing it to be reutilized for every produced sample unlike in the case of the glass vial which had to be broken for each produced porous material. This PTFE feature has already been explored by some authors (Reinwald *et a*l., 2013) but the effect on thickness reduction has never been reported.

From visual observation of the produced biomaterals, it is clearly that increasing foaming temperature, decreasing $scCO_2$ density and viscosity, the obtained structures have larger pores, and the same is evident when the depressurization rate decreases, a slower rate leads to structures with larger pores. A clearly change in height of the samples is also evident, when temperature increases and when depressurization rate decreases, which is due to the presence of larger pores, samples with smaller pores (lower foaming temperature) are also smaller since pores occupy volume increasing the samples height, when larger. And, when combining a higher temperature with slower depressurization rate the obtained structure presents even larger pores.

In Figure 9 is represented a digital photograph of an axial cross-section of a produced porous biomaterial.

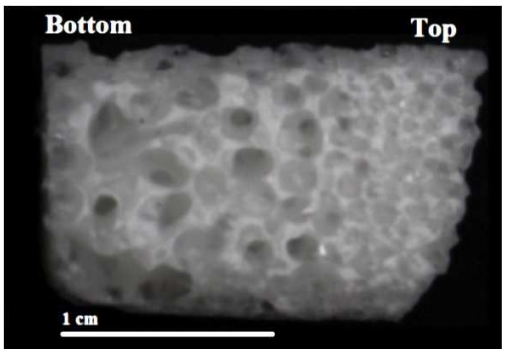

Figure 9. *Axial, top-to-bottom, cross-section of a prepared porous biomaterial at P = 20MPa, T = 40º C and a depressurization rate of 0.3 MPa.min^{-1}. Scale bar 1cm.*

As can be seen, throughout the height of the produced biomaterial, the distribution of pore size appears to be different, yielding larger pores in the bottom of the sample and smaller ones on top of the sample. This effect was clearly visible in all the performed porous structures, for the optimization and selection of operating conditions assays of this work. This aspect can be pointed out as a drawback of the SFM process, but for tissue engineering applications it can be seen as an important feature, since for these type of applications a wide range of pore size is required, but it should be obtained homogeneously throughout the material and not separated as is visible, in order to obtain so and to avoid these heterogeneity, a double step

depressurization stage is pointed as the solution (Salerno *et al*., 2014; Huang *et al*., 2015; Bao *et al*., 2011). What could explain this effect is the diffusivity of the CO_2 molecules during the depressurization step. Initially bubble start to nucleate in the bottom on the molten polymer and as the CO_2 molecules start to leave the bubbles and out of the polymeric matrix, they find greater physical resistance resulting from the vitrifying layers of polymer in the bottom leading to larger pores, where the diffusivity of CO_2 towards out of the polymer is lower and in the top they find less resistance and so the diffusivity is higher leading to smaller pores, since CO_2 molecules spend more time in the bottom of the sample and less in the top due to their diffusivity. It can also be seen that pores appear to grow more preferentially on the height direction (foaming direction), from top to bottom, because bubbles cannot grow freely on the radius direction due to space limitation of the employed mould, these effect have already been reported by some authors (Xu *et al*., 2004; Mathieu *et al*., 2006).

Mercury Intrusion

Mercury intrusion was employed to determine the average pore diameter, total porosity, total pore area, skeletal density and bulk density, of the produced porous biomaterials varying with foaming temperature and depressurization rate. In Figure 9 are shown the obtained results for average pore diameter, porosity and total pore area for the two depressurization rates employed as function of foaming temperature. The porous structures produced at 50ºC and with a depressurization rate of 0.3MPa.min^{-1} were not analysed with this technique since it was not possible to obtain reproducible results, being removed from the solution set.

As can be observed in Figure 10 A., both profiles reach a maximum in average pore diameter when foaming temperature is increased (0.6 $\pm$ 0.0 µm for a depressurization rate of 0.3 MPa.min^{-1} and 0.4 $\pm$.0.1 µm for a depressurization rate of 1 MPa.min^{-1}) In part this effect can be explained by the detection limits of the employed technique (0.04-150 µm) in which larger pores – of few hundred µm, or even in mm scale, cannot be detected, also all the samples were cut with a thickness between 5-8 mm so larger pores could have been cut as well and not being recognized by this technique as so, the only way to assess correctly the average pore diameter of the prepared porous biomaterials would be by analysing the entire sample as one piece, what could not be possible.

The effect of temperature on the average pore diameter is clearly visible when temperature is increased and depressurization rate is kept constant. This effect can be explained because at high temperatures the dilatation capacity of the polymer increases, its chains have increasing free movement, facilitating the CO_2 intake into the polymer structure and therefore its swelling. By increasing the operating temperature the viscosity of the system is lower, as shown in Table 2, reducing the resistance to pore bubble nucleation and coalescence resulting into an increase on their size (Jacobs et al., 2008; Fanovich and Jaeger, 2012). Also, when density of scCO_2 decreases, increasing operating temperature the solubility of CO_2 in PCL increases, providing a greater intake of CO_2 within the polymeric matrix (Leeke *et al*., 2006; Fanovich and Jaeger, 2012). When depressurization rate is decreased, there is more time for bubble to growth *via* diffusion of CO_2, since during this stage diffusion competes with bubble nucleation, leading to larger bubbles and therefore to larger pores. So, it is expected that when depressurization rate decreases, larger pores can be found but in smaller number, and when depressurization rate increases, nucleation is rapid and a larger number of pores is formed, but with lower diameter (White *et al*., 2012; Fanovich and Jaeger, 2012; Jenkins *et al*., 2006; Salerno *et al*., 2014).

By observation of Figure 10 B., it is clearly that the processing conditions corresponding to a temperature of 40ºC and a depressurization rate of 0.3 MPa.min^{-1}, are the processing conditions which allow to produce porous structures with greater porosity, approximately 50% porosity.

It is also evident that when temperature is increased, porosity tends to decrease, this is due to the fact that when temperature increases, average pore diameter also increases, but the number of pores decrease, since there are less nucleation points, because in the competition between diffusion and nucleation, diffusion is enhanced, which will lead to a reduced porosity of the porous structure (White *et al*., 2012; Fanovich and Jaeger, 2012). When depressurization rate decreases from 1 MPa.min^{-1} to 0.3 MPa.min^{-1} porosity increases slightly for operating temperatures of 35 and 40ºC, at higher temperatures porosity decreases with a decrease in depressurization rate which is explained by the presence of larger pores, but in smaller number (lower pore density).

When smaller pores are obtained, employing a foaming temperature of 35ºC and a depressurization rate of 1 MPa.min^{-1}, for example and as shown is Figure 9 C., a greater total pore area is obtained. When pores are smaller, their surface area is larger and so the total pore area increases (also related to the number of pores, high pore density is related to a high total pore area) which is obtained when nucleation is enhanced, operating at lower temperatures and/or at faster depressurization rates. Observing Figures A., B. and C., it can be seen the potential to employ two sets of processing conditions, at a pressure of 20 MPa, which are at a temperature of 40ºC and a depressurization rate of 0.3 MPa.min^{-1} and at a temperature of 45ºC and a depressurization rate of 1 MPa.min^{-1}, since they are the operating conditions that present larger average pore diameters, better porosity and better total pore area towards producing biomaterials fitted to hard tissue engineering applications requirements, presented in section 1.1 and 1.1.1 of this work.

Same results were obtained by Fanovich and Jaeger, when increasing foaming temperature from 30 to 40ºC, observing an increase in average pore diameter from 130-180 μm to 290 μm -1.5 mm. The same trend was found by the same authors as well as by White *et al*. and by de Matos *et al*., when decreasing depressurization rate an increase on average pore diameter was found (Fanovich and Jaeger, 2012; Salerno *et al*., 2012; White *et al*., 2012; de Matos *et al*., 2013).

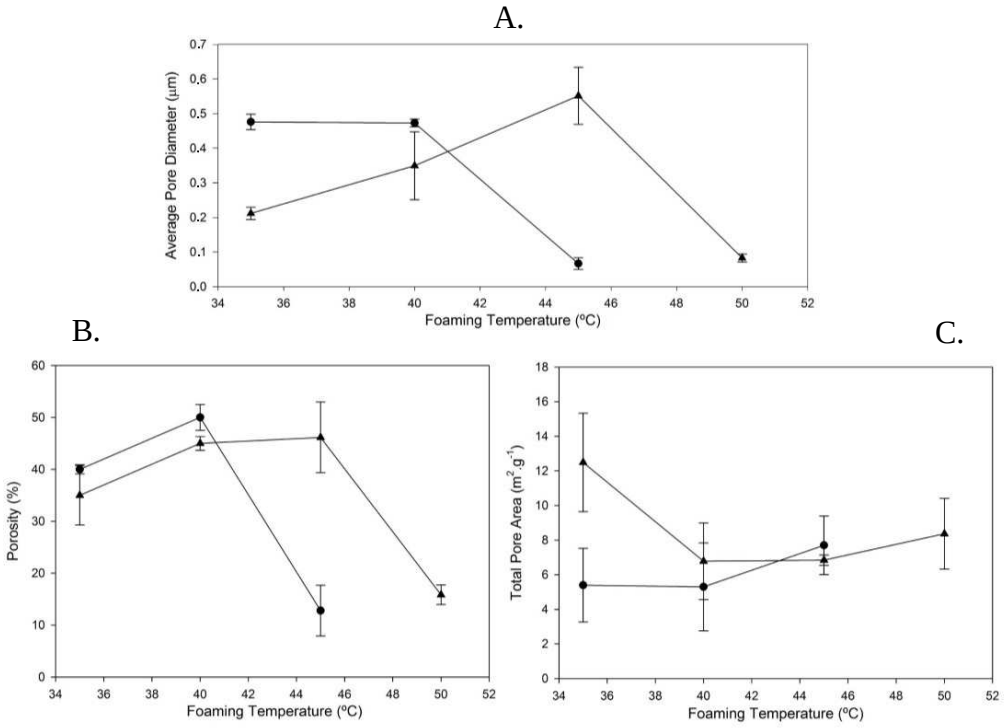

Figure 10. *Obtained results from mercury intrusion for average pore diameter (A.), porosity (B.) and total pore area (C.) for the two depressurization rates employed as function of foaming temperature at constant Pressure = 20 MPa, ● - 0.3MPa.min^{-1}, ▲ - 1 MPa.min^{-1}.*

Nitrogen Adsorption

The obtained isotherms for adsorption and desorption, shown in Appendix D, Figure D 3 are of type II and IV for every produced porous biomaterial and processing conditions, revelling that the produced materials have either very small pores (like in the case of using 35ºC and 1 MPa.min^{-1} as foaming temperature and depressurization rate respectively) or mesoporous, since all the obtained isotherms showed hysteresis, being characteristic of porous materials and non-porous materials show no hysteresis.

In Figure 11 are shown the obtained results from nitrogen adsorption, for surface area (BET) and for pore volume of each produced porous biomaterial at each depressurization rate as function of foaming temperature.

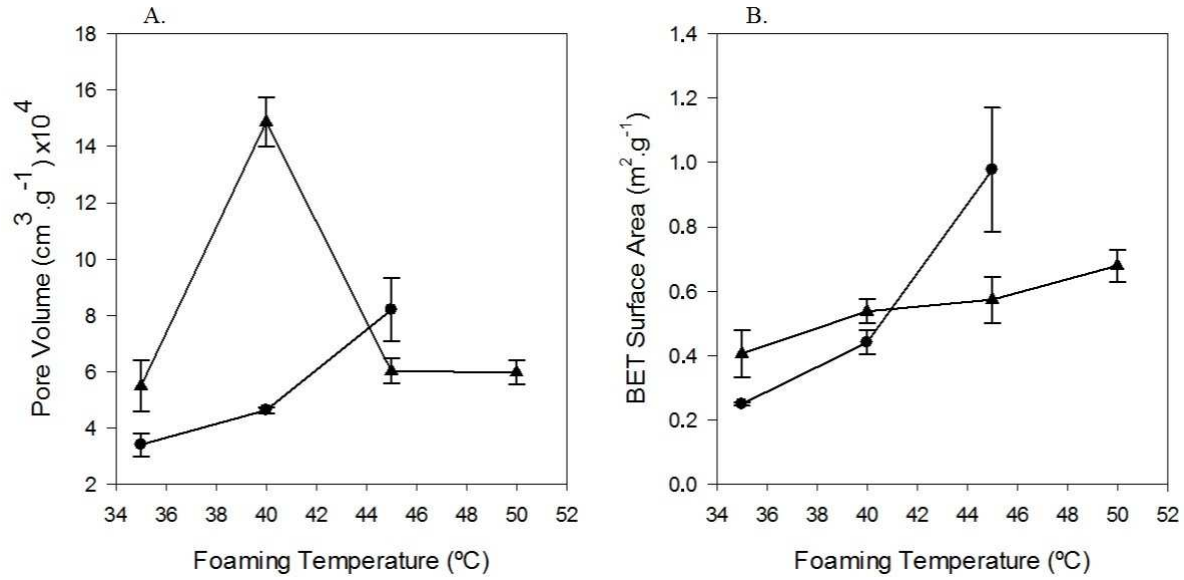

Figure 11. *Obtained results for pore volume (A.) and Surface area (BET) (B.) from nitrogen adsorption, as function of foaming temperature, for the two tested depressurization rates ● - 0.3MPa.min^{-1}, ▲ - 1 MPa.min^{-1} at constant pressure P = 20MPa.*

By observation of Figure 11 A., porous structures produced at 40º C and 1 MPa.min^{-1} have larger pore volume of $1.5 \times 10^{-3} \pm 8.8\times10^{-4}$ cm^3.g^{-1}, comparing with the ones obtained employing other processing conditions, this is justified by the fact that the produced porous structure under these processing conditions has, as shown in Figure 10 B and C., high porosity and total pore area, so the pore volume will also be larger which might be indicative of a material with a large number of pores. When increasing temperature, the pore volume increases, since pores are larger when foaming temperature is increased, when depressurization rate is kept constant and equal to 0.3 MPa.min^{-1}. As depressurization rate is decreased the pore volume is almost always lower, except for a foaming temperature of 45ºC when is higher.

Figure 11 B., indicates that the BET surface area increases whit foaming temperature for both employed depressurization rates. When foaming temperature is equal to 40ºC the obtained values for BET surface area are very close for the two depressurization rates, 0.5 ± 0.0 m^{2}g^{-1} for 1 MPa.min^{-1} and 0.4 ± 0.0 m^{2}g^{-1} for 0.3 MPa.min^{-1}, being lower than the ones obtained in previous works for similar operating conditions (40ºC and a depressurization rate of 0.3 MPa.min^{-1} at P = 20 MPa) (0.9 ± 0.2 m^{2}g^{-1}) (Rosa, 2013). The increase of surface area with foaming temperature might be due to the fact that the samples needed to be cut for analysis, and since the largest pores were not assessed by these techniques (mercury intrusion and nitrogen adsorption), so, the obtained values for surface area and pore volume might induce in error,

since when pores are smaller, like when porous structures are produced with lower foaming temperatures and with fast depressurization rate, one can expect that the surface area and pore volume would be greater than when porous biomaterials are produced with higher temperatures or with slower depressurization rates.

These trend, of approximated morphological features of the produced porous structures at 40ºC and depressurization rates of 1 and 0.3 MPa.min^{-1} and at 45ºC and a depressurization rate of 1 MPa.min^{-1}, is observed for all the morphological properties assessed with mercury intrusion, shown in Figure 10, and by nitrogen adsorption, shown in Figure 11, except for the pore volume. This effect might indicate that similar morphological properties are achieved when using these three combinations of processing conditions, which are presented, morphologically, as the possible solutions sets for optimization of processing conditions for the intended application of the produced porous biomaterials in hard tissue engineering.

In Figure 12 are shown the obtained results of average pore diameter of each sample, as function of foaming temperature, obtained from nitrogen adsorption.

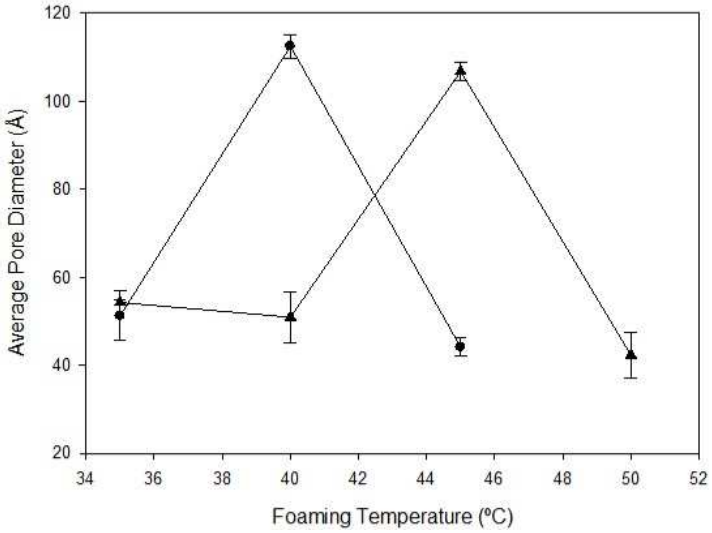

Figure 12. *Obtained results for average pore diameter as function of foaming temperature from nitrogen adsorption for the two tested depressurization rates ● - 0.3MPa.min^{-1}, ▲ - 1 MPa.min^{-1} at constant pressure P = 20MPa.*

Figure 12 shows the same trend for both depressurization rates but with a difference in temperature of about 5ºC, *i.e.*, approximately the same values for average pore diameter are obtained for both depressurization rates but 5ºC lower for a slower depressurization rate and 5ºC higher for a faster depressurization rate. By nitrogen adsorption only a range of pores from 0.2 to 300 nm can be determined, this limitation is evident when foaming temperature is increased and pore size increases, and in Figure 12 is evident that average pore diameter decreases with foaming temperature after reaching a maximum at 40ºC, for a depressurization of 0.3 MPa.min^{-1} and at 45ºC for a depressurization rate of 1 MPa.min^{-1} (Allen, 1997). The larger average pore diameter obtained was for the operating conditions of T = 40ºC and a depressurization rate of 0.3 MPa.min^{-1}, of 112.5 $\pm$ 2.7 Å, but similar results were obtained when a foaming temperature and a depressurization rate of 45ºC and 1 MPa.min^{-1} were employed respectively, of 106.8 $\pm$ 2.2 Å.

The needed morphological properties for a material suitable for hard tissue engineering applications are, as presented in Table 1 in section 1.1. and in section 1.1.1., of a material with a distribution in pore size, from micropores to macropores up to 300-350 µm, and a porosity

from 50 to 90%. So, observing Figures 10 and 11, the solutions sets for optimization of SFM operatingconditions, are operating either at 40ºC and 0.3 MPa.min^{-1} or at 45ºC and 1 MPa.min^{-1}, since these are the conditions that allowed to obtain porous biomaterials with larger average pore diameters, higher porosity, suitable total pore area and BET surface area.

All the obtained results from mercury and nitrogen adsorption were plotted as function of $scCO_2$ density. The same trend in every property was observed as well as the same shift of 5ºC, since foaming temperature is directly obtained from this $scCO_2$ physical property.

Helium Picnometry

The real density of the produced porous biomaterials was evaluated with helium picnometry, in order to understand if the density of the employed $scCO_2$ has any effect on this physical property of the polymeric matrix, as well as the foaming temperature and depressurization rate. In Figure 13 are shown the obtained results for the real density of the produced porous biomaterials, varying with the employed foaming temperature and for both used depressurization rates at constant pressure. The supplier information concerning the density of the employed PCL is 1.1 g.cm^{-3}.

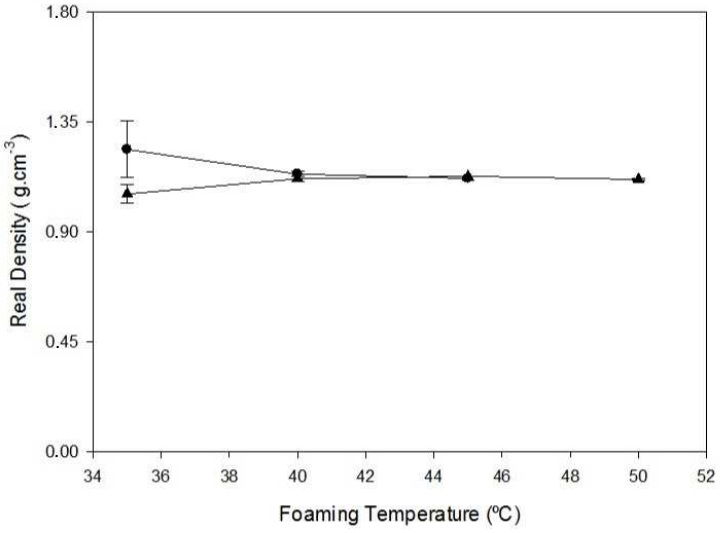

Figure 13. *Real density of the produced porous biomaterials, as function of foaming temperature, obtained from helium picnometry, for the two tested depressurization rates ● - 0.3MPa.min^{-1}, ▲ - 1 MPa.min^{-1} at constant pressure P = 20MPa.*

Accordingly to the obtained results, neither the density of $scCO_2$ nor the depressurization rate have any change in the real density of the pure PCL porous biomaterials. The only observed variation is when a foaming temperature of 35ºC is employed, for both depressurization rates, being smaller for the fast rate and higher for the slower one.

As expected, since no other substance was added to PCL, like an inorganic or a plasticizer, when producing the porous biomaterials, the real density of the biomaterials is not changed by the operating conditions such as temperature and depressurization rate, being kept constant and equal to 1.1 $\pm$ 0.0 g.cm^{-3}. Other authors have also reported that depressurization rate have no effect on the density of pure PCL porous biomaterials (de Matos *et al*., 2013).

All of the obtained results for average pore diameter, bulk density, skeletal density, porosity, total pore area, pore volume, BET surface area and real density for each sample, from mercury intrusion, nitrogen adsorption and helium picnometry are shown in Appendix D, Table D 1.

3.2.2. Mechanical Analysis

Mechanical properties, such as compressive strength and Young's modulus were assessed with an oedometer applying several loads into the samples.

In Figure 14 are shown the obtained values for Young's modulus (at 5% strain) and compressive strength (ultimate stress) for the two employed depressurization rates as function of the foaming temperature.

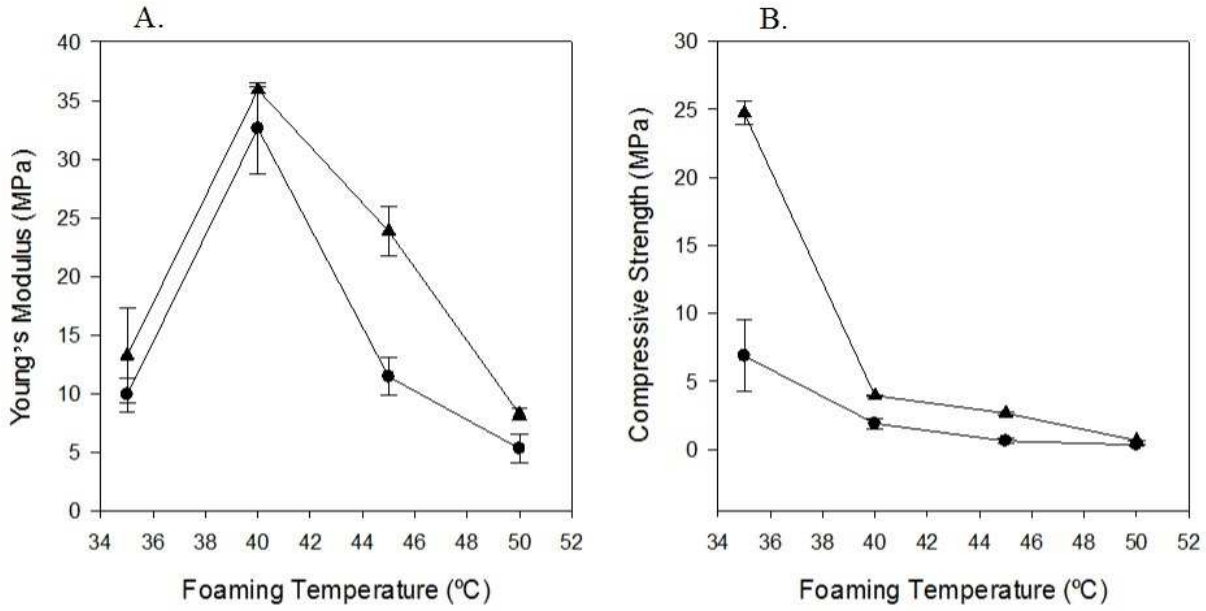

Figure 14. *Mechanical properties, Young's modulus (A.) and Compressive Strength (B.) of the produced porous biomaterials as function of foaming temperature, for the two employed depressurization rates ● - 0.3MPa.min^{-1}, ▲ - 1 MPa.min^{-1} at constant pressure P = 20MPa.*

An example of a stress *versus* strain curve obtained by this analysis, and used in order to obtain the presented values is shown in Appendix G, Figure G 1. Table G 1 in Appendix G also shows the obtained results from mechanical analysis of the produced porous biomaterials for the optimization assays. All the samples presented a typical stress *versus* strain curve of polymeric materials, with a linear elastic zone, which is controlled by the bending of the walls (strut) of the pores, until 5% strain, for all the produced porous biomaterials, a plateau was reached, due to the instability of pore walls and collapse of pores and then a densification zone could be identified, resulting when almost all the pores have collapsed and opposing pore walls touch each other (White *et al*., 2012; Kweon *et al*., 2003; Lebourg *et al*., 2008; Salerno *et al*., 2012).

Observing Figure 14 A., the Young's modulus appears to increase when temperature is increased from 35 to 40ºC (reaching a maximum of 35.9 $\pm$ 0.3 MPa and 32.6 $\pm$ 3.9 MPa at 40º C for a depressurization rate of 1 and 0.3 MPa.min^{-1}, respectively, and for higher temperatures it decreases, when depressurization rate is kept constant. When depressurization rate is slower the obtained values for Young's modulus of the porous biomaterials are slightly lower for temperatures from 35 to 40ºC and for 50ºC, for 45ºC the difference is larger. Observing Figure 14 B, the compressive strength of the porous biomaterials is greater when foaming temperature decreases, being achieved a maximum compressive strength (24.7 $\pm$ 0.8 MPa), when a foaming temperature of 35ºC is employed with a depressurization rate of 1 MPa.min^{-1}. When depressurization rate decreases, is observed a decrease in compressive strength for all of the tested foaming temperatures. However, and analysing Figure 14, the samples produced at 35ºC

for both depressurization rates, despite presenting the greater compressive strength of all the produced porous biomaterials, once these are the biomaterials with smaller pores, they present the lower Young's modulus of all the produced porous biomaterials. These indicates that despite the materials are very hard and can support high loads, they are between the most elastic biomaterials produced.

The mechanical properties of porous materials, depend essentially on the geometric structure of the biomaterial, comprising the number of pores, their size, distribution and their interconnectivity, and on the intrinsic properties of the polymeric material (White *et al*., 2012; Salerno *et al*., 2012). So, when porous materials have larger pores, the supported stress will be lower than when pores are smaller, since larger pores have more empty volume, and the thickness of their walls is generally smaller, leading to less mechanical resistance, *i.e.*, increasing porosity and/or average pore diameter the mechanical properties will decrease. Observing Figure 8, on section 3.2.1., it can be seen that when temperature is increased, and when depressurization rate is slower, the biomaterials presented gradually larger pores as well as more fragile structures, which validates the obtained results presented in Figure 14. Other authors have already reached the same conclusions regarding the influence of porosity on the mechanical properties of materials (White *et al*., 2012; Salerno *et al*., 2012; Mathieu *et al*., 2006; Yoshimura *et al*., 2012; Kweon *et al*., 2003; Estellés *et al*., 2006).

All the obtained values for the mechanical properties of the produced porous biomaterials were inferior to the ones required for bone tissue engineering, except for trabecular bone substitution/replacement. Since in an application of hard tissue engineering, and as referred, the materials to employ must have similar properties to the natural tissue, namely mechanical properties, so bone compressive strength is about 130-180 MPa for cortical bone and 4-12 MPa for trabecular bone and Young's modulus of 3-30 GPa and 0.02-0.05 GPa respectively. So, and analysing Figure 14, the produced porous biomaterials of pure PCL, at both depressurization rates either at 40ºC and 45ºC are suitable for trabecular bone tissue engineering applications since they present values of Young's Modulus, within the range of trabecular bone, of 35.91 ± 0.25 (at 40ºC and a depressurization rate of 1 $MPa.min^{-1}$), 32.6 ± 3.9(at 40ºC and a depressurization rate of 0.3 $MPa.min^{-1}$), 23.9 ± 2.1 (at 45ºC and a depressurization rate of 1 $MPa.min^{-1}$) and 11.5 ± 1.6 (at 45ºC and a depressurization rate of 0.3 $MPa.min^{-1}$).

3.2.3. Selection of the optimum operating conditions

Observing Figures 10 and 12 it is very clearly that the morphological properties of pure PCL biomaterials are approximately the same for both depressurization rates, but with a disparity in temperature of about 5ºC, being reached approximately the same values at lowers temperatures with a slower depressurization rate and at higher temperatures with a faster depressurization rate. This is explained by the effect of both these processing variables on the morphological properties of the porous biomaterials. As referred, when foaming temperature increases, bubble nucleation decreases and there is a formation of larger bubbles leading to larger pores, and when depressurization rate increases, CO_2 bubbles have less time to grow *via* diffusion, but nucleation rate increases. So when increasing temperature and depressurization rate, there is a balance between bubble nucleation and bubble growth similar to the one obtained operating at lower temperatures and slower depressurization rates. So, when optimizing the SFM process applied to produce PCL porous biomaterials, based on the morphological and mechanical properties it should be taken into account the needed energy to achieve higher temperatures, if a thermosensitive compound will be added further on (and if it is stable at that temperature) and the needed time to obtain similar porous structures at lower temperatures and slower depressurization rates. The most suitable processing conditions, towards achieving porous biomaterials for hard tissue engineering applications, based on the morphological and

mechanical properties of the produced biomaterials are employing either a foaming temperature of 40ºC with a depressurization rate of 0.3 MPa.min^{-1} or a foaming temperature of 45ºC with a depressurization rate of 1 MPa.min^{-1}, both at constant pressure of 20 MPa.

In Figure 15 is presented a Gantt chart comparing the batch foaming process for both the most promising solution sets as the two optimum solutions towards producing porous biomaterials for hard tissue engineering applications.

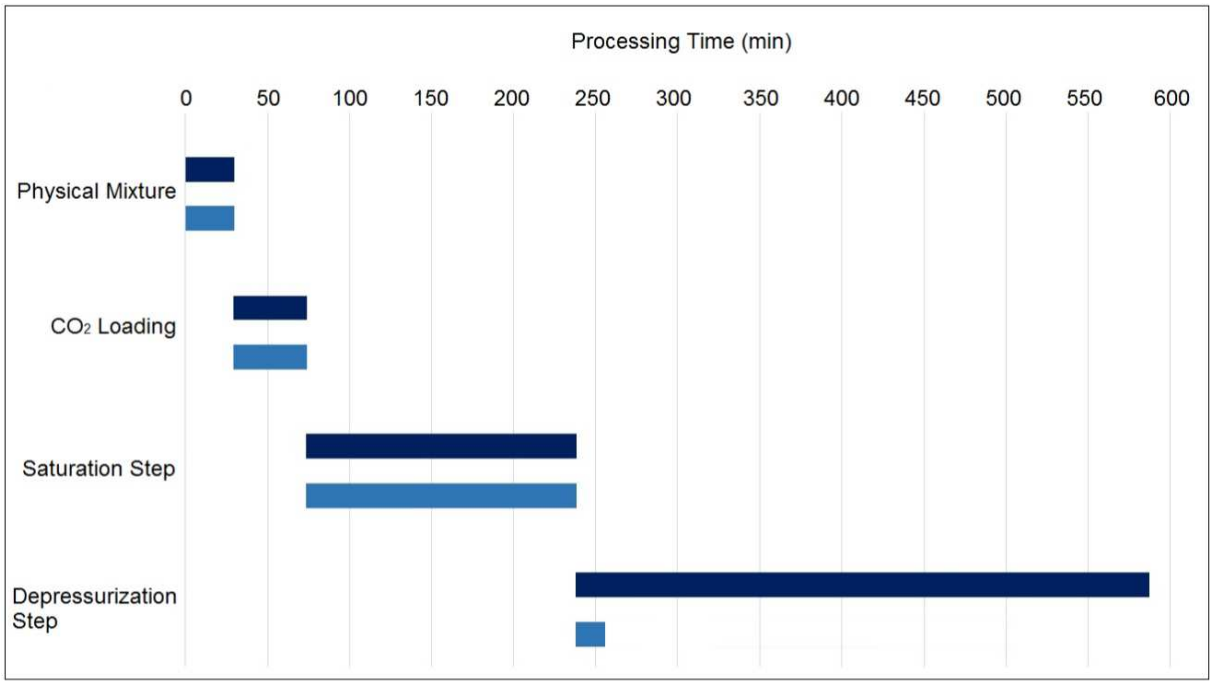

Figure 15. *Gantt chart of the tasks/operations of the employed solid-state batch-scCO$_2$ foaming/mixing process for two parallel batch processes* ■ *- processing at P = 20MPa, T = 40ºC and ΔP/Δt=0.3 MPa.min^{-1},* ■ *- processing at P = 20 MPa, T = 45ºC and ΔP/Δt=1 MPa.min^{-1}.*

In Figure 15 are shown the main four operations of the employed solid-state batch-scCO$_2$ foaming/mixing process, comparing the needed time to achieve porous structures with approximately similar morphological properties, as shown in Figures 8, 10, 11 and 12. The step of physical mixture comprises the mixture of 1g of PCL with inorganic towards the production of composites and/or with a bioactive compound and and/or an additive and approximately takes 30 min for each mixture to be homogeneous (in the case of optimization assays this step takes about 10 min for each batch). The step of CO$_2$ loading comprises the loading of the high pressure vessel with CO$_2$ already at the desired foaming temperature (the time needed for the water bath to reach the desired temperature is in parallel with the first step and takes about the same time (not showed)) and takes about 15 min for each sample, to reach and stabilize at the pressure of 20 MPa. The saturation step comprises the time during which the sample is left in contact with scCO$_2$, until saturation is reached, this step takes about 2h (120 min). The depressurization step, comprises all the time needed for the vessel to reach a pressure equal to the ambient pressure. This step takes about 110 min, when a depressurization rate of 0.3 MPa.min^{-1} is employed and 20 min for a depressurization rate of 1 MPa.min^{-1}. Observing Figure 14 is clearly that operating at 40ºC and 0.3 MPa.min^{-1} is more time-consuming than operating at 45ºC and 1 MPa.min^{-1}, since the time to reach the 5ºC difference is ignored (too small when compared with the time needed for the depressurization step). However, and as referred it is needed to understand and evaluate if the energy consumption to reach and maintain the water bath 5ºC higher compensates the time consumption and the productivity (number of batches/day). This evaluation was not performed, and could be done in future work, as well as

evaluate further the morphological properties obtained in porous structuress produced at this two processing conditions, with other techniques, since the ones employed, as shown, reveal large limitations, since these are techniques most suitable for characterizing porous fine particles, and not very large constructs like the produced porous biomaterials.

Based on the mechanical analysis of all of the produced porous biomaterials, these solutions sets are presented as the most suitable to explore further ahead, since they present the greater Young's modulus and a good and suitable compressive strength (considering their porosity and average pore diameter) for bone tissue engineering. Despite, these mechanical properties are not close to the mechanical properties of the natural trabecular bone, by adding an inorganic phase, and as referred in section 1.4, they can be enhanced. Once again, on mechanical properties, these two sets of operating conditions, present very close values, which validates what was stated before regarding morphological properties, and since mechanical properties are very dependent on morphological properties, if the morphological properties of these two sets of processing conditions are very similar, then their mechanical properties will also be very similar, as verified. Taking into account Figure 15 and what was discussed, employing a foaming temperature of 45ºC and a depressurization rate of 1 $MPa.min^{-1}$ will be time-saving as well as enhance the productivity of these porous biomaterials, but the energetic aspect was not evaluated, even do one can speculate that despite having to increase 5ºC on the water bath, the time to keep them will be less than when employing 40ºC and a depressurization rate of 0.3 $MPa.min^{-1}$ and so the energy to reach 5ºC higher will be almost the same, or less, than to keep 40ºC for much more time, as showed in Figure 15.

Despite all the stated advantages in using a foaming temperature of 45ºC and a depressurization rate of 1 $MPa.min^{-1}$, the selected optimum solution set, is by operating at 40ºC and at a depressurization rate of 0.3 $MPa.min^{-1}$, because, and as referred on section 1.5, this work has as main objective to further investigate the obtained results in a previous work (Rosa, 2013), and in order to compare safely the obtained results, this optimum solution is the one that goes against the operating conditions employed on the previous work. Still, this optimization step, must be further investigate, using morphological characterization methods more suitable to the produced materials, since a way to produce porous strucutres with similar properties in a more time-saving way appears to be found.

3.3. Additivated and Composite Porous Biomaterials

Based on the optimum solution set found for the operating conditions (P = 20 MPa, T = 40ºC, $\Delta P/\Delta t$ = 0.3 MPa.min^{-1}, PCL/SBA-15 (20 and 30 wt. %) composite porous biomaterials and pure and composite additivated biomaterials with GF and TTPB (98% molar) as well as additivated biomaterials with a mixture in three molar proportions of the mixture GF+TTPB (2:1, 3:1, 5:1) were performed, comprising always 98% molar of the total mixture.

3.3.1. Morphological Analysis

Macroscopic Analysis

In Figure 16 are shown the digital images of the obtained porous biomaterials for the additivated and composite assays, at the optimized operating conditions.

All the produced samples of additivated PCL, showed in Figure 16 A., were cut in the same proportion, ~10% of the sample height, so the figure is very well elucidative regarding the difference in the obtained heights of the produced porous structures, shown in Appendix C, Table C 1. The samples shown in Figure 16 B. and C., were not cut for the digital photographs, so it is also possible to verify in these figures the obtained differences in height of the produced porous biomaterials. The biomaterials produced with a mixture of GF and TTPB (2:1) and (5:1) were produced using a glass vial, so, and as referred, a non-porous skin was observed surrounding these biomaterials with greater thickness than the one observed on the other biomaterials, which were produced using a PTFE-based beaker. This non-porous skin is only visible on the base of the biomaterials due do the effect of the additives on their surface, which led to a reduction on the thickness of the non-porous skin throughout their height. The obtained difference in heights is due to the presence of larger pores, which occupy larger volume leading to higher porous structures.

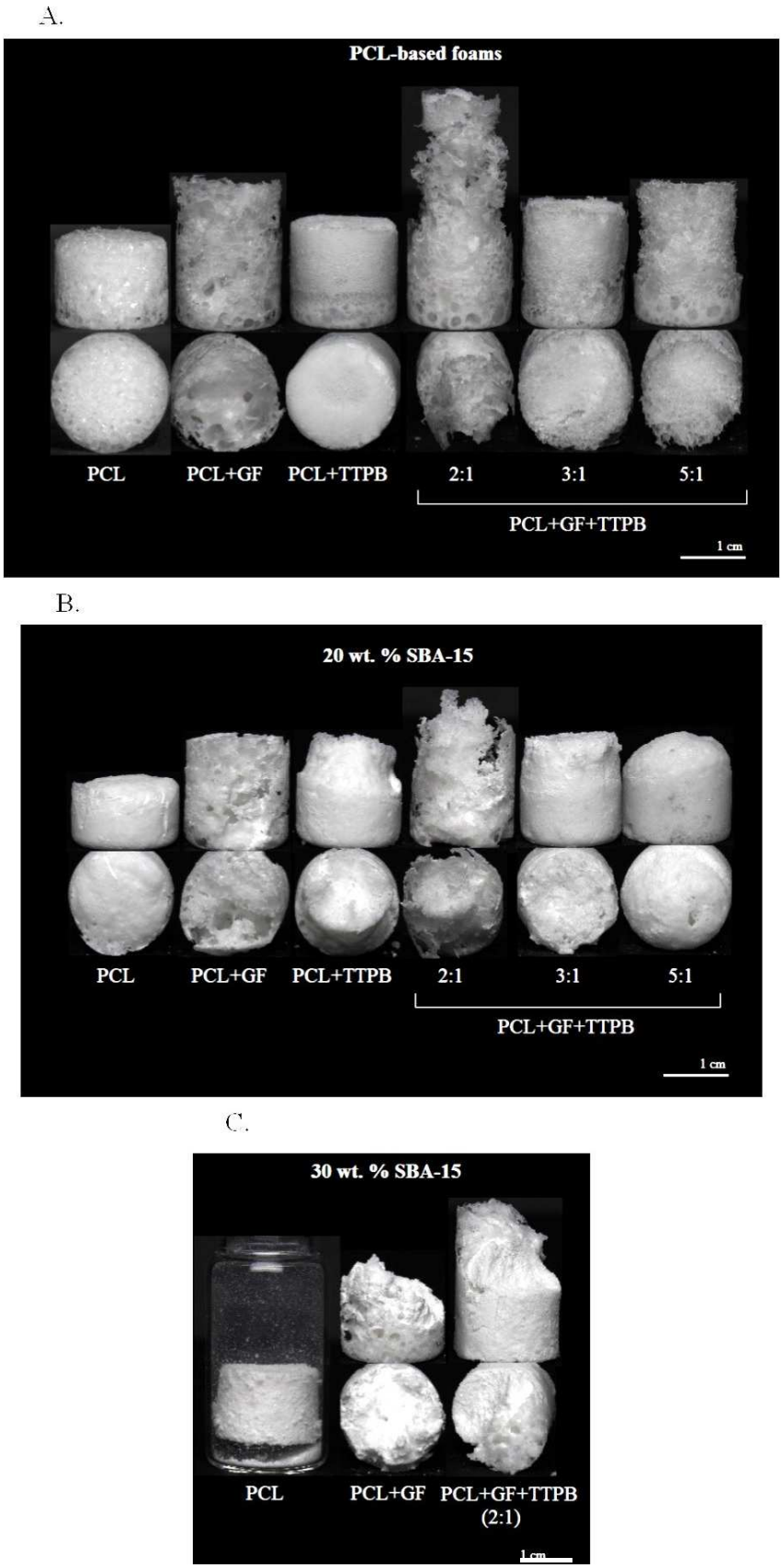

Figure 16. *Digital images of the obtained porous biomaterials for the additivated and composite assays, prepared at P = 20MPa, T = 40ºC and $\Delta P/\Delta t$ = 0.3 MPa.min^{-1}.A – obtained pure and additivated PCL biomaterials (0 wt. % SBA-15); B – obtained PCL/SBA-15 pure and additivated composites biomaterials (20 wt. %); C – obtained PCL/SBA-15 pure and additivated composites biomaterials (30 wt. %). Top images – lateral view, Bottom images – top view. Scale bar 1cm.*

As can be seen in all the produced biomaterials, a non-porous skin was always formed surrounding each one, the same effect was verified for the filler selection assays and for the optimization assays, however, and as referred on section 3.2.1, employing a PTFE mould this non-porous skin thickness is considerably reduced, as can be seen on Figure 16 for all the produced porous structures, except in the ones additivated with a mixture of the liquid additives in a molar proportion of 2:1 and 5:1, since for these biomaterials a glass vial was used.

Observing Figure 16 A., when GF is incorporated, pore size appears to increase and when TTPB is incorporated, pore size appears to decrease, but the pore density appears to increase, comparing with pure PCL and GF-additivated porous biomaterials.

When a mixture of the two additives (2:1) is employed the obtained structure presents to be the highest of all the produced porous structures. This biomaterial has increased volume mainly by its centre, where the additives were added in the physical mixture step. This same effect can be seen in the biomaterial with TTPB added, in the middle of the porous structure (top view), it is visible a sudden change in pore size, of circular shape in its centre, in which is visible an increase in pore size on that area, so it can be concluded that the distribution of additives throughout the polymeric matrix is not completely homogeneous. However, when the two additives are employed together the distribution of the effect of both of them throughout the matrix appears to be more homogeneous, as the amount of ionic liquid is decreased.

Once again, and as referred in section 3.2.1, it is observed a variation on the distribution of pore size throughout the height of the produced samples, being possible to observe, in Figure 16 A., in the base of each porous strucutre, larger pores on the base and smaller ones through the height of the biomaterials. In Figure 17 is shown a digital photograph of an axial cross-section of a produced biomaterial additivated with TTPB.

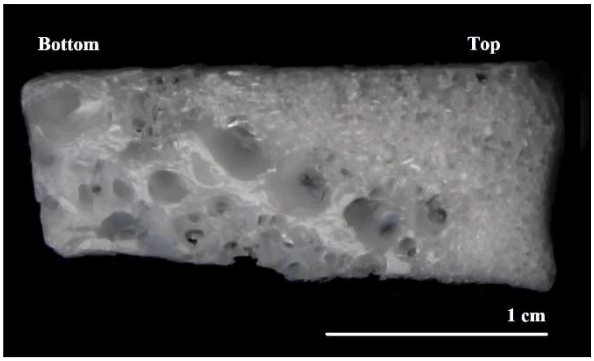

Figure 17. *Axial, top-to-bottom, cross-section of a PCL+TTPB biomaterial at P = 20MPa, T = 40º C and a depressurization rate of 0.3 MPa.min-1. Scale bar 1cm.*

As can be seen, in Figure 17, in the base of the porous biomaterial, pores are much larger than in the top section. As referred, this effect might be due to the diffusion of CO_2 molecules out of the polymer, which is lower in the base of the structure, during the depressurization step, possibly because in the bottom the physical resistance of the vitrifying polymer is greater and when CO_2 molecules leave the bubbles nucleated in the bottom they find less resistance and leave the polymeric matrix in a faster way, having a higher diffusivity out of the polymer in the top layers. In Figure 17 it is also possible to observe that the dispersion of TTPB throughout the polymeric matrix is not homogeneous, since towards the centre of the biomaterial the number of pores appears to increase, due to the effect of this additive.

When 20 wt. % of SBA-15 is added, Figure 16 B., the height of all the produced composite porous biomaterials appears to decrease, and no particles are found to be released from the strucutres. This can be indicative that SBA-15 particles are all incorporated within the

polymeric matrix. The decrease in height might be due to the existence of smaller pores in the composites. When GF is added to the composite biomaterial, the same effect as in non-composite biomaterials is observed, this additive leads to the formation of very large pores, heterogeneously dispersed throughout the polymeric matrix. When TTPB is added, the biomaterial height increases, showing that either it has larger pores or has pores in high number, revealing, again, that these additives increase the solubility of CO_2 in the polymer, mainly TTPB, as so appears.

When a mixture of the additives is employed it is visible, Figure 16 B., for a molar proportion of 2:1 the obtained structure is not neither homogeneous nor compact, since a very disordered structure was obtained. As the amount of GF is increased, the porous strucutres appears to be more homogeneous, as well as the dispersion of the fillers throughout the polymeric matrix, since GF acts as a polymer compatibilizer, as expected. The effect of TTPB is also visible, since smaller pores and in large number appear to be formed, due to the increase in height of the additivated composite biomaterials (visible in the composite biomaterial produced with a mixture of 3:1), and when the amount of GF increases and the amount of TTPB decreases (5:1), larger pores appear to be formed. Observing Figure 16 B., it is clearly that the interaction between these two additives is very important relating to the main objective comprising the production of composite biomaterials with homogeneous dispersion of the filler, with high porosity.

Composites with 30 wt. % of SBA-15 were obtained with a very heterogeneous dispersion of the fillers. First, observing Figure 16 C. (PCL), using only PCL the polymer did not had the capability to plasticize, and incorporate completely the SBA-15 nanoparticles within its structure. As can be seen large amounts of SBA-15 particles were not incorporated at all remaining in the bottom of the flask (a glass flask was employed in order to allow the visual effect). Adding GF to the mixture, more SBA-15 appeared to be incorporated by the polymeric structure, what was expected since GF acts as a polymer compatibilizer with the inorganic particles, allowing a better incorporation, however, and the obtained porous structure was not homogeneous. As can be seen in Figure 16 C. (PCL+GF), zones on the porous structure with inorganic agglomerates and areas with only polymer were obtained, what was indicative of a poor mixture of the SBA-15 with PCL. Several attempts were performed achieving always the same results (a very poor distribution of the inorganic particles within the polymeric matrix). When a mixture of GF and TTPB (2:1 molar) was incorporated, again it was not achievable a composite biomaterial with a macroscopic homogeneous distribution of the inorganic particles in the polymeric matrix, Figure 16 C. (PCL+GF+TTPB (2:1)). With this mixture an even better incorporation was achieved, comparing when only GF was added, still, and once again, a phase separation was observed, as can be seen there is a section of the porous structure rich in polymer, in which the structure has grown (with large pores due to the action of TTPB), and another section which has not grown as much as the other one, due to the presence of large amounts of SBA-15 particles, originating smaller pores. Again, several attempts were made with this mixture and SBA-15 proportion, and the same results were always achieved (a separation of phases). Analysing the obtained results, macroscopically, it can be said that the maximum amount of SBA-15, which can be incorporated by PCL, foamed with $scCO_2$, is within the interval [20, 30[wt. %.

Due to the obtained results, the incorporation of 30 wt. % of SBA-15 particles within the PCL polymeric structure was discarded, since composites with homogeneous dispersion of the filler could not be obtained, and biomaterials with other composition, of the mixture PCL+GF+TTPB, were not performed. Still, the produced porous structure with 30 wt. % of SBA-15, presented in Figure 16 C., were characterized regarding its microscopic, mechanical and thermal properties.

Scanning Electron Microscopy (SEM)

SEM imaging was employed in order to analyse the morphology of powdered PCL and of SBA-15 nanoparticles, in Figure 18 A is showed the obtained SEM photographs from PCL powder and in Figure 18 B is showed the obtained SEM photographs from SBA-15 nanoparticles. These materials were used as showed and physically mixed previously to the SFM processing of each sample.

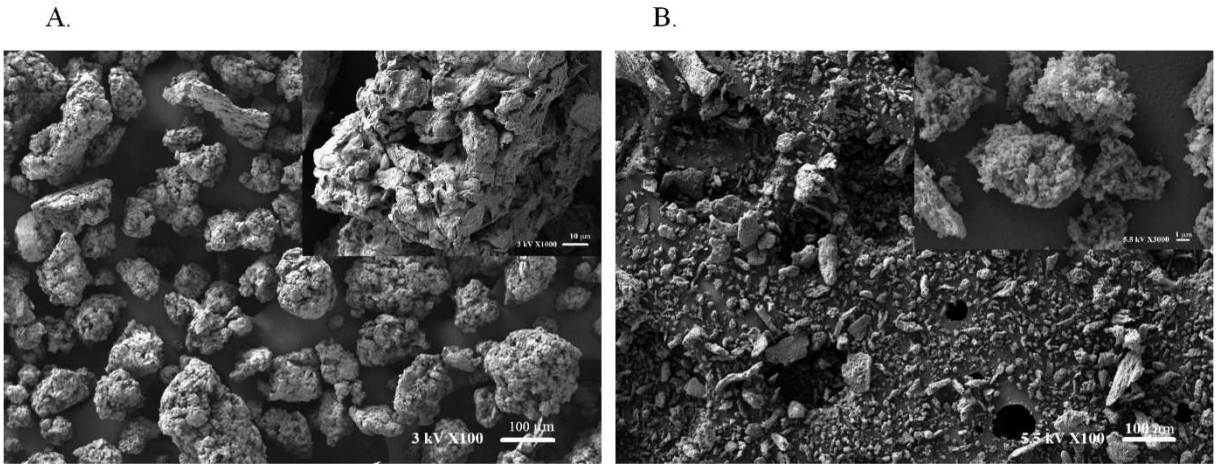

***Figure 18**.SEM photographs of PCL powder (A.) and SBA-15 nanoparticles (B.) both with a magnification of X100. On the right top corner is showed a detail of each photograph at a magnification o X1000 for PCL powder (A.) and at a magnification of X3000 for SBA-15 nanoparticles (B.). Scale bar represents 100 µm for photographs at a magnification of X100, 10 µm for photographs at a magnification of X1000 and 1 µm for photographs at X3000.*

Figure 18 A is very elucidative about the benefits of preparing PCL from pellet into powder form. As can be seen PCL grains have a very large superficial area, since these particles appears to be formed by smaller particles "glued" one to another, forming larger agglomerates. Due to the irregular shape of these smaller particles, these agglomerates (PCL powder particles) show a very large surface roughness which increases the powders surface area and aspect ratio (although no suitable technique was employed to measure PCL powder surface area). This increase in surface area enhances the mass transfer of CO_2 molecules into polymer chains, allowing a faster solubilisation of CO_2 into the polymer, throughout the SFM process. Figure 18 B., shows that the large majority of SBA-15 nanoparticles agglomerates into larger particles. This tendency difficult largely the physical mixture step in order to achieve homogeneous distribution of these particles throughout the polymeric matrix, making it very hard to achieve composite biomaterials with homogeneous dispersion of the filler. In order to avoid this, and achieve composites with homogeneous dispersion of the filler (with good spacial distribution of SBA-15 nanoparticles in the porous structure), it is expected that GF, acting as a polymer compatibilizer between PCL and SBA-15, will enhance the distribution of the filler in the composite biomaterial. It is also noticeable that SBA-15 particles and agglomerates present a very high surface roughness, yielding into large surface area, which will promote the production of composite porous biomaterials with increased surface area and aspect ratio.

The effect of the employed additives as well as the SBA-15 nanoparticles on the morphological properties of the produced composite biomaterials was assessed with SEM. The obtained photographs are shown in Figure 18 for pure and additivated PCL biomaterials, in Figure 19 for pure and additivated PCL/SBA-15 composite (20 wt. %) biomaterials and in Figure 20 for pure and additivated PCL/SBA-15 composite (30 wt. %) biomaterials for three magnifications

(X35, X100 and X5000, the latest is a magnification of a pore surface from the porous structure of the biomaterial).

As can be observed in Figure 19, the changes in the morphology of the porous structures are very clearly when additives are employed, as well as structures with heterogeneous pore size diameters. When GF is added, the plasticizer effect can be verified, since larger pores are obtained, comparing with pure PCL biomaterial, favouring the homogeneous nucleation mechanism which by decreasing the surface tension of the mixture molten PCL+scCO_2, leads to the formation of larger pores. The surface tension of the mixture is even further decreased, and the plasticizer effect enhanced, when TTPB is employed, favouring even more the homogeneous nucleation, leading to an increase in rate of nucleation which is translated into a larger number of pores. This effect of both additives is even more elucidative when a mixture of both is employed. By reducing the surface tension of the mixture, these additives increase the solubility of CO_2 in the polymer, leading to the formation of larger pores (more CO_2 intake by the polymeric chains) and in larger number, this effect appears to be enhanced by TTPB, since smaller pores and in larger number are resulted from more CO_2 dissolved in the polymer. When these additives are incorporated either alone or in a mixture of both, the surface roughness of the pore walls of the produced biomaterials appears to increase, which might be due to the increase of solubility of CO_2 in the polymer, which during the depressurization step will drag the vitrifying polymer, increasing the surface roughness, which is better evidenced in Figure 18 on the porous biomaterial produced with a mixture of the two additives in a molar proportion of 2:1 (Karimi *et al*., 2012; Salerno *et al*., 2013; Salerno *et al*., 2014).

When a mixture of these two additives is employed, in a molar proportion of 2:1, even larger pores are formed. As the amount of GF is increased and of TTPB decreased, the morphology of the porous structures appears to approach the morphology observed when only GF is incorporated, since the morphology of the biomaterial produced with a GF+TTPB mixture of molar proportion of 5:1, is the closest one to the morphology presented by the biomaterial additivated with only GF, which is understandable since this is the mixture in which a larger amount of GF was added. The ionic liquid appears to have a role in the mixture which leads to an increase in the interconnectivity of the pores (sample with a mixture with a molar proportion of 3:1) as well as an increase in pore size (sample with a mixture with a molar proportion of 2:1), although no other technique was used to determine effectively the interconnectivity of the produced porous materials. When PCL is additivated with a mixture of GF and TTPB in a molar proportion of 2:1, the structure presents a more uniform distribution, of very large pore sizes, when comparing with the other incorporated mixtures. The obtained biomaterial additivated with a mixture in the proportion of 3:1, appears to be the material with higher interconnectivity, presenting a very number of open pores with connections to other pores, as can be seen in the photograph with a magnification of X100 (middle image of the sample PCL+GF+TTPB (3:1)), which shows an open pore with pores in its surface connecting it to other pores creating a "communication" network. This effect can be due to the porogenic action of TTPB, which decreases the surface tension of the mixture (molten polymer+scCO_2) allowing an increase in the intake of CO_2 molecules within the polymeric structures and thereafter increasing the solubility of CO_2 in the polymer which leads to a formation of more bubbles of CO_2 enhancing the formation of larger and more interconnected pores, as referred. Same results were achieved in a previous work, in which adding these additives, porous materials with larger average pore diameters and with an increase in surface roughness were obtained (Rosa, 2013). Thus, Figure 19 is very well elucidative of the effects of the employed additives, as well as their mixtures towards the development of hard tissue engineering materials.

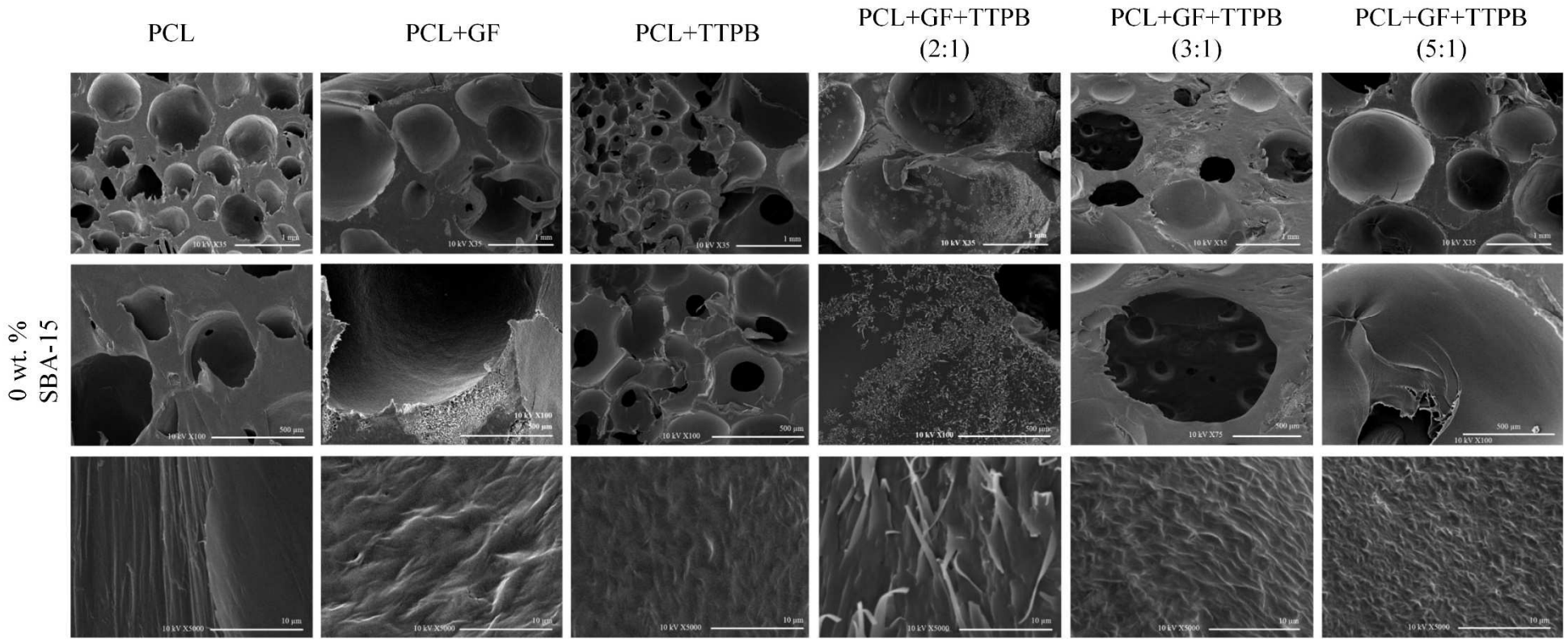

Figure 19. *SEM cross-section photographs of the produced porous biomaterials of pure and additivated PCL at P = 20 MPa, T = 40ºC and $\Delta P/\Delta t$= 0.3 MPa.min-1. The presented magnifications from top to down are X35, X100 and X5000, respectively. Scale bar for X35 – 1mm, for X100 - 500µm and for X5000 - 10µm.*

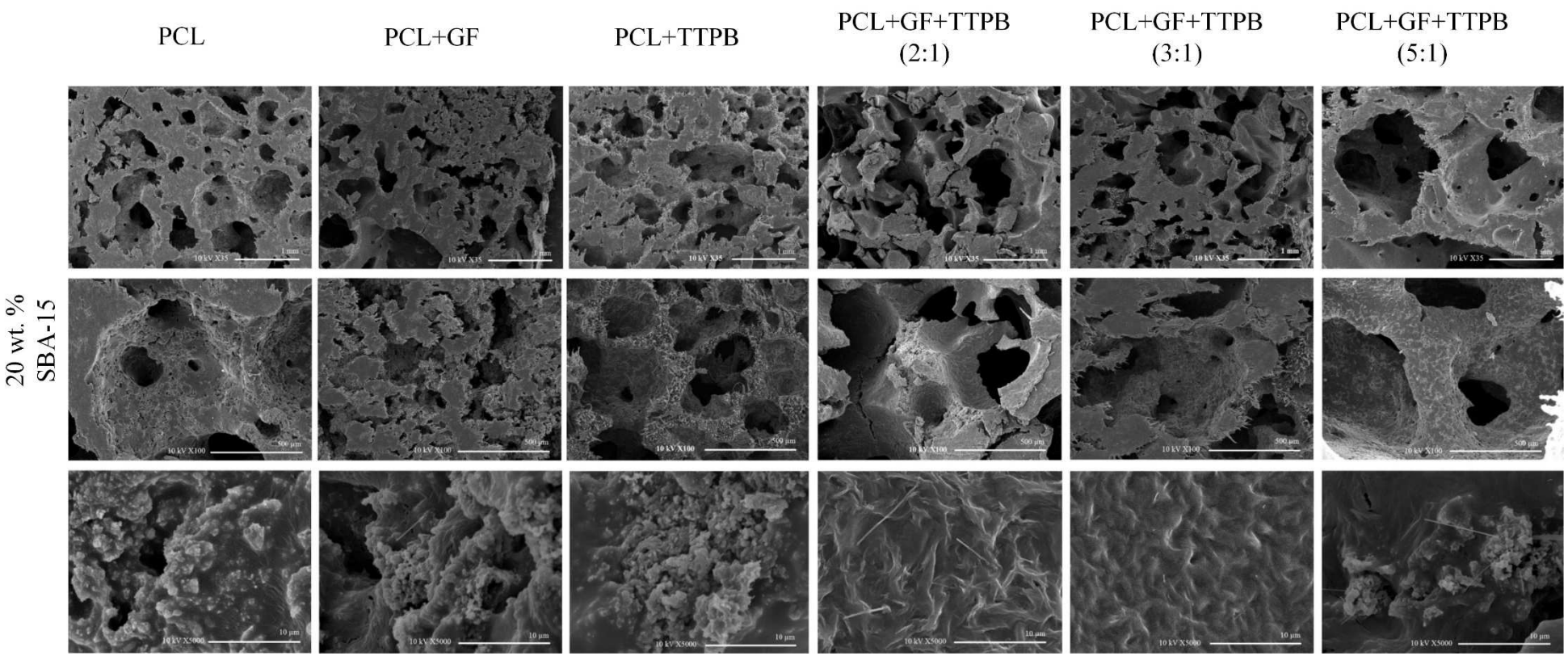

Figure 20. *SEM cross-section photographs of the produced composite porous biomaterials of PCL and SBA-15 (20 wt. %) at P = 20 MPa, T = 40ºC and $\Delta P/\Delta t$ = 0.3 MPa.min-1. The presented magnifications from top to down are X35, X100 and X5000, respectively. Scale bar for X35 – 1mm, for X100 - 500µm and for X5000 - 10µm.*

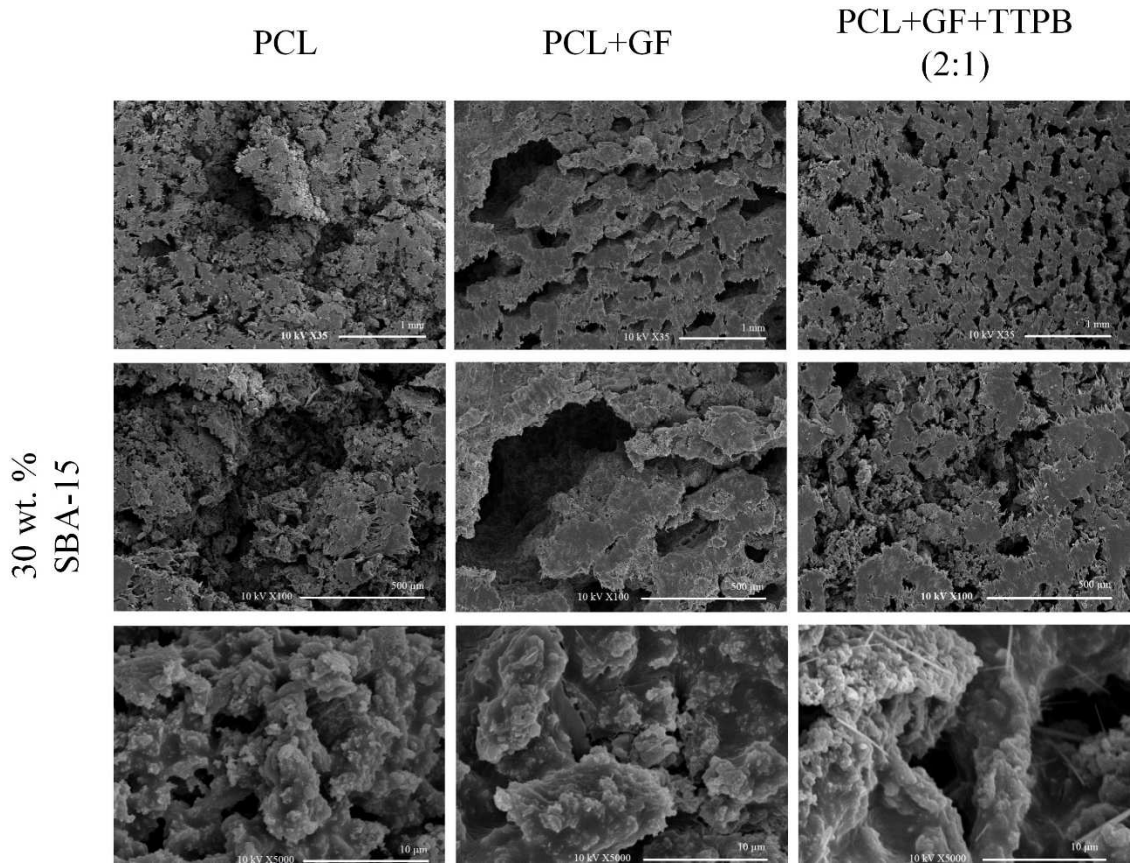

Figure 21. *SEM cross-section photographs of the produced composite porous biomaterials of PCL and SBA-15 (20 wt. %) at P = 20 MPa, T = 40ºC and $\Delta P/\Delta t$ = 0.3 MPa.min-1. The presented magnifications from top to down are X35, X100 and X5000, respectively. Scale bar for X35 – 1mm, for X100 - 500µm and for X5000 - 10µm.*

When SBA-15 nanoparticles (20 wt. %), as can be seen in Figure 20, are incorporated in PCL, or in mixtures of PCL+GF/TTPB, organic/inorganic composites are produced, changing radically the morphology of all the produced composite porous bioamterials. The nanoparticles have great effect on the number of pores obtained in the porous structures, as can be seen, comparing pure PCL biomaterial with PCL/SBA-15 (20 wt. %) composite biomaterial, one can see the formation of a greater number of pores, but apparently in smaller size. The obtained pores appear to be much more interconnected, being almost every one open. The surface of each one, as seen in Figure 20 (PCL X5000), presents much more roughness and thus an enhanced superficial area. Observing the surface of the composite it is clearly that SBA-15 nanoparticles have a tendency to agglomerate and form areas of the biomaterial very rich in this filler and others with almost none, not being achieved a perfect distribution of the particles (Jacobs *et al.*, 2008). These nanoparticles act as heterogeneous nucleation points, favouring heterogeneous nucleation, that by being more energetically favourable than homogeneous nucleation occurs preferentially, yielding porous biomaterials with smaller pores, but in larger number than on non-composite biomaterials, where homogeneous nucleation is favoured, since there is no interface (ensured by the presence of the nanoparticles) to favour heterogeneous nucleation mechanism. This effect is very well perceptive in all the additivated and non-additivated composite porous biomaterials, as presented in Figure 19, and was showed by other authors. (Jacobs *et al*., 2008; Rosa, 2013; Collins *et al*., 2010; White *et al*., 2012; Fanovich and Jaeger, 2012).

Incorporating GF to the composite, larger pores are obtained with walls presenting very small pores within, resulted from the action of the nanoparticles throughout the SFM process. The effect of this polymer compatibilizer is well perceptive, comparing the non-additivated

composite with the GF additivated composite, in which agglomerates of SBA-15 tend to be more displaced between them revealing an enhanced dispersion of this filler throughout the polymeric matrix, however these agglomerates are still formed. Adding TTPB instead, leads to a formation of even larger pores and to an even highly interconnected structure (as it seems) with more open pores, leading to a very rich inter-pore communication network, which is justified once again through the effects promoted by the incorporation of this ionic liquid, which has great affinity with CO_2.

As the GF amount is increased, adding to the composites a mixture of this polymer compatibilizer with the ionic liquid, larger pores appear to be formed on the biomaterials. When a mixture in a molar proportion of 2:1 is employed, the sample appears to present a very high density of pores, with heterogeneous pore size distribution (as seems analysing Figure 20, (PCL+GF+TTPB (2:1))) however, and possible due to the presence of a high number of small pores and very large pores as well, the sample was very brittle, and as can be seen, pores walls collapsed, despite this, it is still visible that the morphology of this biomaterial presents a structure with open pores. Adding to the composite biomaterials a mixture in a molar proportion of 3:1, an intermediary morphology was obtained between the one obtained when mixtures in a molar proportion of 3:1 and 5:1 are added, with, once again, a heterogeneous pore size distribution, but with a very high density of pores. The morphology of the additivated biomaterial with a mixture in a molar proportion of 5:1 is the one which presents the largest pores. Due to that, it is possible to see, observing the photograph of the magnification of X100, that the porous structure presents a highly interconnected network, with smaller pores within the walls of the largest pores.

Concerning to the distribution and existence of agglomerates of SBA-15 nanoparticles within the porous structure, biomaterials additivated with a mixture of the additives present an improved distribution of these agglomerates/particles throughout the polymeric matrix, which was expected since GF acts as a polymer compatibilizer, promoting affinity and distribution of SBA-15 nanoparticles throughout the polymeric matrix, and TTPB which acts as both a plasticizer and as an agent promoting the distribution of GF, and consequently the SBA-15 nanoparticles, due to its good affinity, ensured by its phosphonium group, with the CO_2 molecules, which when diffusing within the polymeric structure, carry the ionic liquid and GF, enhancing a good distribution of the filler yielding an homogeneous dispersion of it in the composite (Dias *et al*., 2012; Livi *et al*., 2014). Of all the produced additivated composites with a mixture of the two additives, and presented in Figure 19, the one which presents better dispersion of the filler throughout the polymeric matrix is the one additivated with a mixture in a molar proportion of 2:1. The other proportions of mixture, ensured good distribution of the filler, analysing the obtained SEM photographs, but still with agglomerates in the inner surface of pores from the biomaterial, yet smaller and better spatially distributed than when only an additive was incorporated.

Increasing the amount of the filler from 20 wt. % to 30 wt. %, the same effects are obtained, concerning the morphology of the biomaterials, but in a much more evident fashion, as can be seen in Figure 21. The non-additivated composite with 30 wt. % of SBA-15 particles presents a structure rich in very small pores, which as referred is due to the heterogeneous nucleation points ensured by the nanoparticles of the filler, as well as pores surfaces with a very high roughness. In this porous structure the agglomerates of the filler are very well perceptive and some SBA-15 aggregates can be seen to not be plasticized by the polymeric matrix and are not part of the composite, as shown as well in Figure 16. As additives are added to the composite, such as GF, the distribution of these particles is improved, as more particles appear to be

incorporated by the polymeric matrix. The incorporation of GF to this composites also induces the formation of larger pores, due to its porogenic effect. Producing a PCL/SBA-15 composite biomaterial additivated with a mixture of GF and TTPB in a molar proportion, led to the formation of small pores but in larger number, than when non-additivated composite was produced. This mixture also induced a better distribution of the filler throughout the polymeric matrix, promoting a better dispersion of the filler throughout the polymeric matrix, when comparing with composite non-additivated and GF-additivated biomaterials.

From the morphological analysis ensured by SEM, it stays clearly that when SBA-15 is incorporated, producing an organic/inorganic composite, essential morphological properties, for hard tissue engineering application, are achieved. Firstly, hard tissues, namely bone, as referred, is an organic/inorganic composite, the produced PCL/SBA-15 composite biomaterials are of same nature and secondly, interconnectivity of the porous structure appears to be enhanced by the presence of this nanoparticles, as well as the presence of a great overall porosity and heterogeneous pore size distributions. Also, adding additives such as GF and TTPB, helps improving crucial properties such as surface roughness, open pore structure and distribution of the fillers through the polymeric matrix, which allows a better cellular adhesion (Reverchon and Cardea, 2012; Reverchon *et al*., 2008). From the SEM analysis, it was possible to conclude that incorporating a mixture of the two additives to the composite biomaterials (20 wt. %) is the best approach to achieve the desired morphological properties towards the development of materials for hard tissue engineering applications.

In every sample prepared with GF and SBA-15 nanoparticles in both filler compositions, the appearance of "fibre"-like structures was always noticed, as shown in Figure 22. When TTPB was added to this mixture this effect was observed to be more dispersed throughout the sample. The visible amount of these "fibre"-like structures increased with the composition of SBA-15 and GF in the composites. In non-composite biomaterials, prepared with PCL and GF no such structure was visible, despite all the efforts. In composite and non-composite biomaterials additivated only with TTPB, again no such structure was visible. In Appendix H, are shown all the photographs of the samples in which those structures were found as well as all the efforts made in order to understand their nature and mechanism of formation.

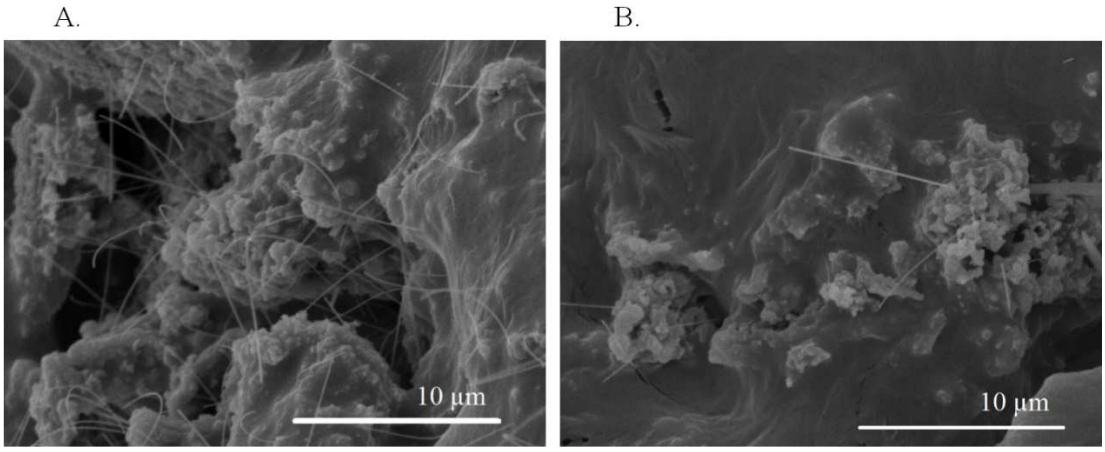

Figure 22*.SEM photographs of the observed tube-like structures found, at a magnification of X5000, on biomaterials produced at P = 20 MPa, T = 40 ºC, $\Delta P/\Delta t$ = 0.3 MPa.min^{-1}. A. Composite biomaterial with 20 wt. % SBA-15 and additivated with a mixture of GF and TTPB (3:1); B. Composite biomaterial with 20 wt. % SBA-15 and additivated with a mixture of GF and TTPB (5:1).*

As seen on Figure 22, these “fibre”-like structures appear to be formed only where SBA-15 agglomerates are found. A possible explanation for this finding is that SBA-15 is partially soluble on GF, due to its affinity with the hydrophilic end of GF, and upon depressurization, GF is dragged by CO_2 molecules leaving the polymer, guiding the formation of these structures in height. A possible mechanism of formation of these structures is found in Appendix H.

Average Pore Diameter

The horizontal Feret diameter was determined and the average pore diameter calculated, based on the SEM photographs for each sample. An example of the obtained results is shown in Appendix E, Figure E 1. The used method to determine the average pore diameter is explained in Appendix E in further detail.

In Table 4, are displayed the average pore diameter for each produced porous biomaterial, based on the obtained photographs by SEM imaging.

Table 4. *Average pore diameter for each produced biomaterial at P = 20 MPa, T = 40ºC and $\Delta P/\Delta t$ = 0.3 MPa.min^{-1}, based on morphological analysis by SEM imaging.*

SBA-15 content (wt. %)	Biomaterials Composition	Average pore diameter (µm)
0	PCL	585.7 ± 153.7
	PCL+GF	1136.4 ± 435.8
	PCL+TTPB	390.2 ± 109.6
	PCL+GF+TTPB (2:1)	1851.8 ± 918.3
	PCL+GF+TTPB (3:1)	432.8 ± 147.3
	PCL+GF+TTPB (5:1)	700.0 ± 165.0
20	PCL	195.2 ± 104.9
	PCL+GF	224.2 ± 106.4
	PCL+TTPB	171.7 ± 59.5
	PCL+GF+TTPB (2:1)	318.9 ± 131.9
	PCL+GF+TTPB (3:1)	258.9 ± 75.4
	PCL+GF+TTPB (5:1)	246.5 ± 79.1
30	PCL	89.1 ± 34.3
	PCL+GF	114.6 ± 32.5
	PCL+GF+TTPB (2:1)	89.8 ± 12.0

The calculated values for average pore diameter, confirm the observation made on the analysis of the SEM photographs. Adding GF to PCL, leads to an increase on average pore diameter, from 585.7 ± 153.7 µm to 1136.4 ± 435.8 µm, and a slightly decrease is observed when TTPB is incorporated, but as seen previously the incorporation of this additive leads to an increase in pore density and interconnectivity. When a mixture of the two additives is employed, very large pores (1851.8 ± 918.3 µm) are obtained using a molar proportion of 2:1, despite the very large deviation obtained. Increasing the amount of GF, average pore diameter decreases for a molar proportion of 3:1 and increases for a molar proportion of 5:1, which is in accordance with the observation made previously. This effect, as referred, can be due to the porogenic effect of GF on the SFM process, combined with the effect of TTPB on the formation of pores.

In Table 4 it is also clearly that when nanoparticles of SBA-15 are incorporated, producing composites biomaterials (20 wt. %), average pore diameter decreases, from 585.7 ± 153.7 µm to 195.2 ± 104.9 µm, which as referred is due to the heterogeneities originated by the nanoparticles, leading to a nucleation of more CO_2 bubbles yielding porous structures with high pore density and with decreased average pore diameter. In the composite biomaterials the incorporation of GF and TTPB has the same effect as in non-composite ones, leading to an increase on average pore diameter, due to their porogenic effect promoting as well a higher incorporation of SBA-15 nanoparticles within the vitrified polymer, as seen on Figure 20. Adding to the composite biomaterials a mixture of the two additives leads to the same effect verified for non-additivated and non-composite biomaterials except when a mixture in a molar proportion of 5:1 is used. With a mixture of 3:1 and 5:1 approximately the same values for average pore diameter were obtained, which could show that the optimum amount of GF, for better dispersion of the nanoparticles, in the mixture is probably within this interval. Increasing the amount of SBA-15 nanoparticles incorporated, is verified, in the composite biomaterials from 20 to 30 wt. %, a decrease in average pore diameter, what was expected and confirms the visual observation by SEM imaging. When a filler is introduced in the SFM process, they act as heterogeneities promoting the formation of large amount of bubbles which leads to biomaterials with smaller pore sizes but with very large porosity and surface area. In these composite, the effect of GF is also noticeable increasing the average pore diameter, as well as the effect of TTPB in the mixture with molar proportion of 2:1, leading to a decrease on the diameter of pores.

Observing Table 4, composite biomaterials (20 wt. %) are presented as the main suitable candidates towards the development of materials for hard tissue engineering applications, regarding their average pore diameter, since they are in the suitable range for these type of applications with macropores in the range of 300-350 µm, as presented in Table 1, being these interval the most suitable to tissue ingrowth. By observing Figure 20, they also present mesopores, which induces degradation of the material, efficient loading and release of bioactive compounds and good diffusion of body fluids throughout the matrix. The high deviation values obtained, confirms the presence of a very heterogeneous distribution of pore sizes, which for the proposed hard tissue engineering applications, as referred on section 1, is a desirable feature. Among these composite biomaterials, the ones additivated with a mixture of the two additives are presented as even more suitable materials for hard tissue engineering, they present pores within the optimum range for tissue ingrowth, their interconnectivity appears to be enhanced and their surface area appears to be greater, with good roughness, allowing better cellular adhesion and proliferation, as well as efficient nutrient diffusion (due to the presence of more open pores, which appear to communicate) (Salerno *et al*., 2010 (a); Reverchon and Cardea, 2012; Reinwald *et al*., 2014; Fanovich and Jaeger, 2012; de Matos *et al*., 2013)

The very same trend was observed in previous works, as Rosa, shows that incorporating GF in the SFM process leads to a formation of porous structures with larger pores and when TTPB is added smaller pores are obtained in those structures. In this work, however, when a mixture of the additives (2:1) is employed a slightly increase on average pore diameter is observed, despite Rosa showed a slightly decrease, from pure PCL porous structure. This difference can be explained since for this analysing only a small area of the porous material was analysed, as well as for SEM sampling the materials had to be cut what could have led to the destruction of the larger pores leading to non-representative areas of the material. In this work, at least four samples of each porous material were analysed towards determination of average pore diameter. Adding nanoparticles of SBA-15, producing composite biomaterials, it has also been shown

that leads to a formation of smaller pores, as referred, an increase on pore density and overall porosity of the biomaterials, the same trend, increasing the amount of fillers was observed. de Matos and co-workers, also showed that adding nanofillers lead to a decrease on average pore diameter. Salerno and co-workers also verified an increase in average pore diameter when incorporating plasticizers in the SFM process of PCL co-polymers, verifying what was expected towards the effect of these additives in the SFM process, lowering the surface tension of the mixture molten polymer+scCO$_2$ leading to an increase on the solubility of CO$_2$ within the polymer (Rosa, 2013; de Matos *et al*., 2013; Salerno *et al*., 2013). Observing the obtained high deviation values it can be concluded that all the produced porous biomaterials are highly heterogeneous, presenting a wide distribution of pore sizes, as seen in Appendix E. This feature is advantageous concerning a hard tissue engineering application, since a wide distribution of pore sizes are required for cell adhesion, growth and proliferation.

Pore density was also measured for all the produced porous biomaterials except the produced composite biomaterials with a filler composition of 30 wt. %, using Image J software, considering the obtained images from SEM imaging. This measurement serves only as an estimation of the pore density of the produced biomaterials, since for some samples the measured photographs were not representative of the entire porous structure (since for others, more samples were analysed). The calculation of pore density was performed based on the equation proposed by Salerno and co-workers (Salerno *et al*., and presented on Appendix E, equation E 3. The obtained results are also presented and discussed in Appendix E.

Energy-Dispersive X-Ray Spectroscopy (EDS)

The presence of the fillers and both additives in the produced porous biomaterials were confirmed using EDS, coupled to the SEM apparatus, through the identification of the distinctive chemical elements of each compound of the produced additivated and non-additivated composite porous biomaterials. In Figure 22 is showed an EDS punctual spectra of all the identified chemical elements within the non-additivated composite biomaterial (20 wt. %).

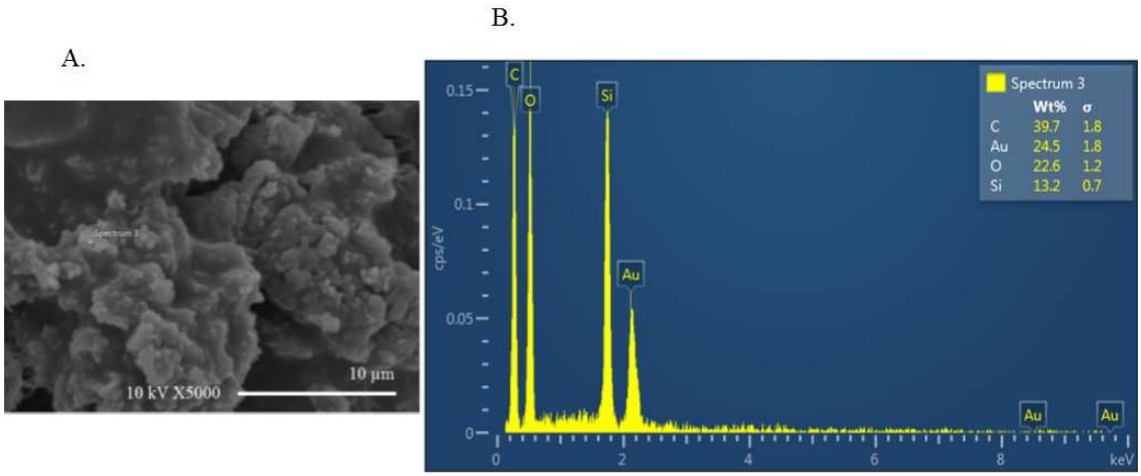

Figure 23. *EDS spectrum of the produced non-additivated composite biomaterial PCL/SBA-15 (20 wt. %). A – SEM image, obtained from a pore surface with a magnification of X5000, scale bar – 10 µm. B. – EDS spectra of the identified chemical elements.*

The obtained spectra, presented in Figure 23, confirms the presence of SBA-15 (SiO$_2$) particles by the identification of the chemical element Si. The chemical elements C and O were also

identified, resulting from the polymeric matrix, and in the case of O, also from the SBA-15 nanoparticles. The high intensity on the Si peak, reveals that there are agglomerates of SBA-15 nanoparticles, resulting from their tendency to form such structures. Chemical element Au is resulted from the coating of the sample previous to the analysis.

In Figure 24, is showed a mapping of the chemical elements detected by EDS, as well as the obtained spectra, from an additivated composite biomaterial with a mixture of the two employed additives in a molar proportion of 2:1 (20 wt. %).

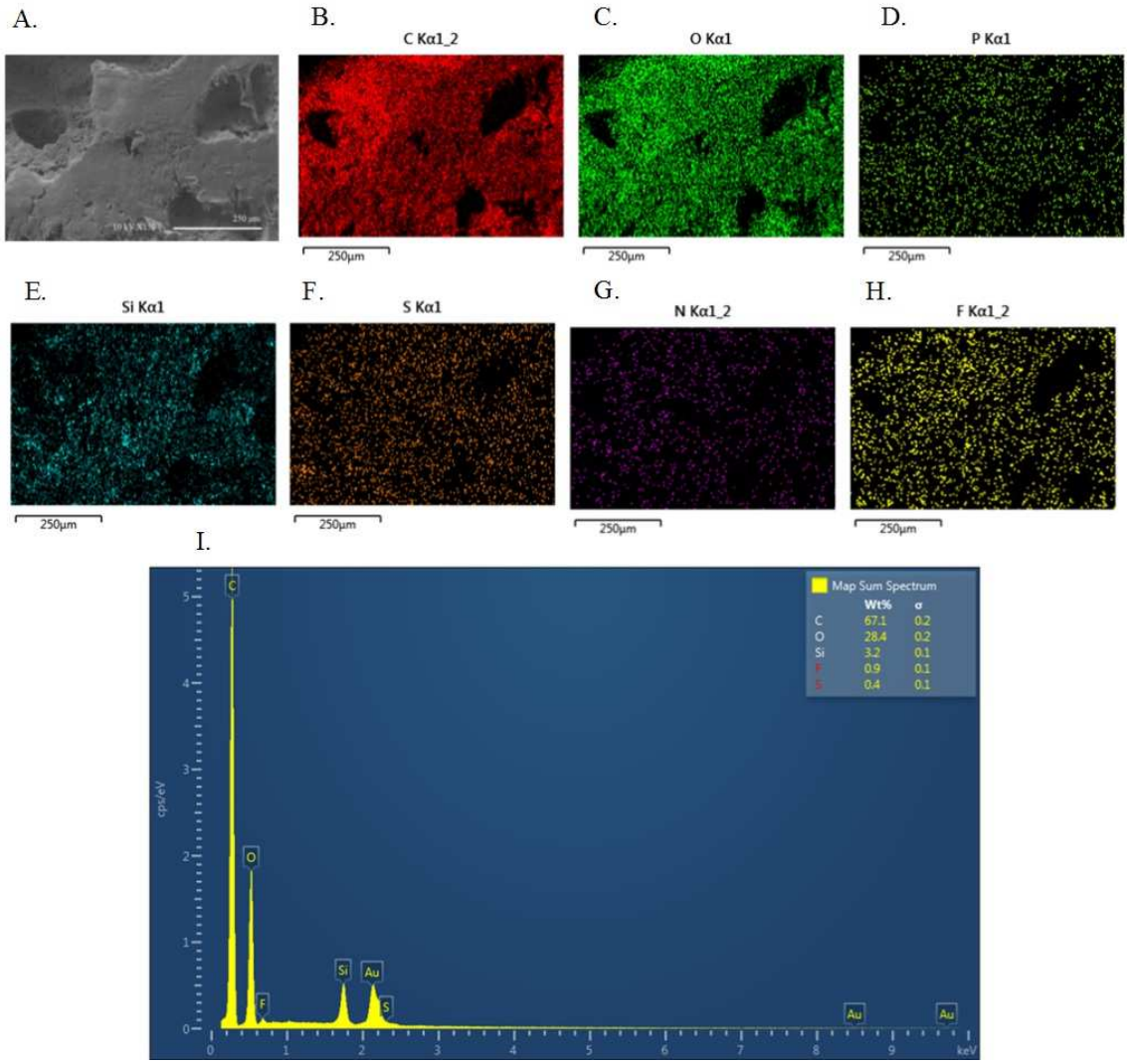

Figure 24. *EDS mapping image of the produced additivated composite biomaterial (20 wt. %) with a mixture of the two additives in a molar proportion of 2:1. A. – Obtained SEM image of the additivated composite biomaterial at a magnification of X150, scale bar – 250 µm; B. – mapping image of the chemical element C; C. – mapping image of the chemical element O; D. – mapping image of the chemical element P; E. – mapping image of the chemical element Si; F. – mapping image of the chemical element S; G. – mapping image of the chemical element N; H. – mapping image of the chemical element F; I. – EDS spectra of the identified chemical elements.*

Analysing Figure 24, it is possible to see that SBA-15 nanoparticles are very well distributed throughout the polymeric matrix, since in Figure 24 E., the EDS mapping shows very few agglomerates of the nanoparticles, and they are clearly dispersed in all the taken sample. In this Figure 24 it also visible the presence of the ionic liquid, since is the only additive which has distinctive chemical elements in its structure from the polymer, such as P, S, N and F, as

previous seen in Figure 4. These chemical elements were also detected by EDS but in not a much accentuated way when comparing with Carbon and Oxygen because these elements are present in a very large amount that the elements characteristic from the ionic liquid, which is also noticeable in the obtained EDS spectra (Figure 24 I.). In the EDS spectrum, gold (Au) was detected, but this detection is neglected since the samples was sputter-coated with gold.

Mercury Intrusion

Porosity, average pore diameter, skeletal and bulk density and total pore area were determined using mercury intrusion. The obtained results are shown in Appendix D, Table D 3, the results of skeletal and bulk density are only shown in this Table and are not discussed in the main body of this work, since helium picnometry provides information concerning the real density of the produced biomaterials and therefor only the obtained results of density, from this technique are discussed here. As referred, due to the inability to obtain a reproducible feature on the composite biomaterials prepared with 30 wt. %, these were not further morphologically characterized.

In Figure 25 is shown the porosity of the produced biomaterials as function of the incorporation of the two additives, alone and in mixture (three molar proportions) and of the incorporation of SBA-15, an inorganic filler.

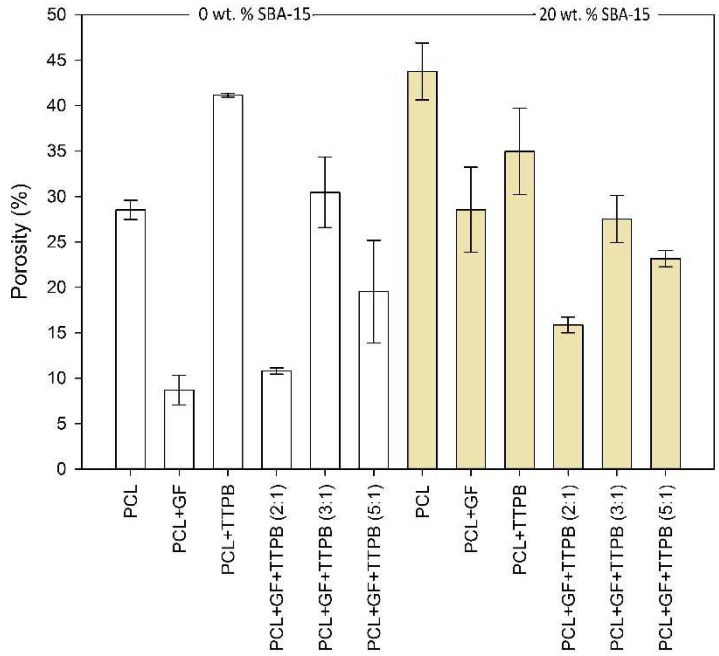

Figure 25. *Porosity, determined by mercury intrusion, of the prepared biomaterials at P = 20 MPa, T = 40 ºC and $\Delta P/\Delta t$ = 0.3 MPa.min^{-1}for 2h for the additivated and composite assays. □ - 0 wt. % SBA-15, □ - 20 wt. % SBA-15.*

As seen previously in Figure 19 and confirmed by Figure 25, the incorporation of TTPB yields into porous biomaterials with high porosity. As seen, from the employed additives, the ionic liquid is the one which yields into a porous structure with higher porosity (41.2 $\pm$ 0.2 %), when SBA-15 is not incorporated. This is result from the plasticizer effect of TTPB, which enhances

the absorption of more CO_2 molecules within the polymeric chains, by increasing the solubility of CO_2 in the polymer due to its phosphonium group with affinity to CO_2. TTPB lowers the surface tension of the mixture molten polymer + $scCO_2$, consequently lowering the activation energy for homogeneous nucleation to occur, increasing the nucleation rate of stable nucleus of CO_2, yielding into porous biomaterials with increased porosity. By these means, and observing Figure 25, it is shown that TTPB has greater plasticizer effect than GF, since more CO_2 is dissolved into the polymer by its action (Tsimpliaraki *et al*., 2012; Karimi *et al*., 2012; Salerno *et al*., 2013; Salerno *et al*., 2014). As seen previously in Figure 19, as well, incorporating GF yielded into the formation of very large pores on the prepared biomaterial. The existence of very large pores, but in low density (low number of pores per volume of material), yields into materials with lower porosity.

Incorporating in the PCL-based biomaterials a mixture of the two additives yielded into materials with lower porosity than the pure PCL biomaterial, except when a mixture in the molar proportion of 3:1 was employed (30.5 $\pm$ 3.9 %). Since, as seen previously, the action of GF leads to a decrease in porosity, since it yields into structures with very large pores, and TTPB yields into structures with higher porosity, an optimum, concerning the porosity of the material, appears to be found in this molar proportion of the mixture of the two additives. Although, the biomaterial prepared with a mixture in a molar proportion of 2:1 (the richest in TTPB) should present larger porosity of the three, yet, as seen previously in this section, the incorporation of this mixture yielded into biomaterials with a very heterogeneous structure with the presence of very large pores. And the biomaterial prepared with a mixture in a molar proportion of 5:1 (the poorest in TTPB) should present a lower porosity, however it does not happen. This is indicative that the influence on porosity of both additives when added in mixture is not linear.

The incorporation of SBA-15 nanoparticles in a composition of 20 wt. %, on a non-additivated porous biomaterial, led into an increase on the porosity of the porous structure. The presence of these inorganic particles within the SFM process, ensures an interface with the organic phase. They act as heterogeneous nucleation points, favouring heterogeneous nucleation mechanism (energetically more favour than the homogeneous mechanism), yielding into the formation of a large number of pores, but in smaller size. The formation of a very high density of pores leads to biomaterials with increased porosity. The same trend was also found and reported by several authors in literature (Jacobs *et al*., 2008; de Matos *et al*., 2013; Rosa, 2013; Collins *et al*., 2010; Tsimpliaraki *et al*., 2011).

Once an additive is added to the composite biomaterial, porosity decreases, as seen in Figure 25. This can be due to presence of larger pores, formed by action of the additives, which favour, in their turn, homogeneous nucleation. In the case of additivated composite biomaterials, heterogeneous nucleation competes with homogeneous mechanism for available CO_2. Since the first is more energetically favourable an increase in porosity, from the non-composite additivated to the composite additivated biomaterials is visible (Jacobs *et al*., 2008; White *et al*., 2012). Incorporating GF, a clearly increase in porosity is visible, from the non-composite biomaterial, from 8.7 $\pm$ 1.6 % to 28.6 $\pm$ 4.7 %. The high deviation obtained, can be indicative of a poor distribution of the SBA-15 nanoparticles. However, in order to perform this analysis the sample had to be cut into small pieces, which could have led to the loss of inorganic content and/or destruction of the formed pores, since, and as observed in Figure 20, large and highly interconnected pores appear to be formed, and by reduction of the sample size, these large pores could have been destroyed. Adding TTPB to the composite biomaterial, led to a reduction in

porosity, which could be due to the poor spatial distribution of the inorganic particles throughout the polymeric matrix.

Again, incorporating to the composite biomaterial a mixture of the two additives an optimum is found when this mixture is in a molar proportion of 3:1, concerning the porosity of the material. Tough, only an increase in porosity, by addition of the SBA-15 nanoparticles, is visible when mixtures in molar proportions of 2:1 and 5:1 are incorporated. In the case of the mixture in a molar proportion of 3:1 a reduction in porosity is visible, incorporating the filler. This can be indicative, that the mixtures in molar proportions of 2:1 and 5:1 ensure a better dispersion of the filler, tough, the obtained porosity is lower than the one obtained with a mixture in a molar proportion of 3:1.

As seen, highly porous PCL-based biomaterials can be produced with SFM process suitable for hard tissue engineering applications, although, and as presented in Table 1 on section 1, even more porous materials are required. As shown in this work, incorporating a plasticizer like TTPB and an inorganic filler like SBA-15 the porosity of the porous biomaterials can be highly enhanced and increased.

In Figure 26 are shown the obtained values of total pore area and average pore diameter from mercury intrusion of the prepared biomaterials for the additivated and composite assays.

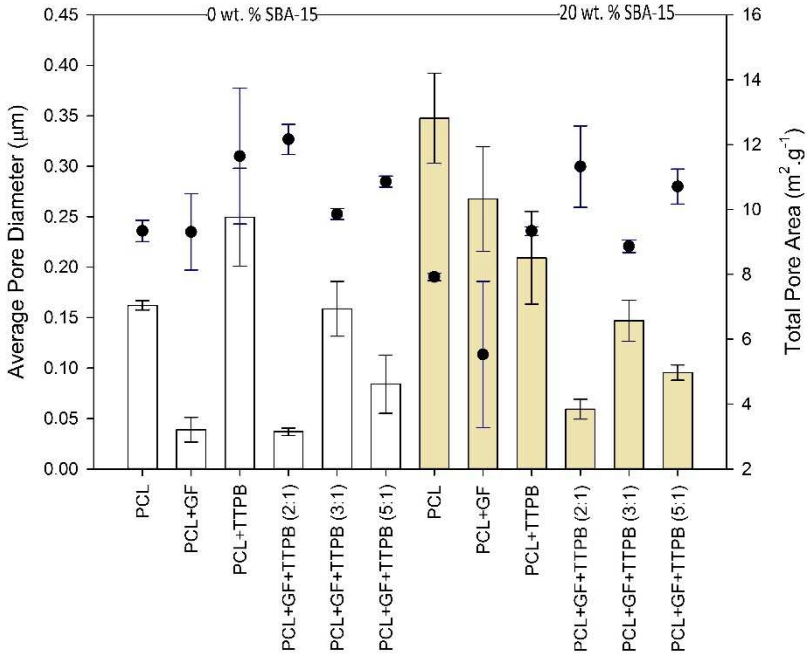

Figure 26. *Average pore diameter and total pore area, determined by mercury intrusion (●) of the prepared biomaterials, at P = 20 MPa, T = 40 ºC and $\Delta P/\Delta t$ = 0.3 MPa.min^{-1}for 2h, for the additivated and composite assays, obtained from mercury intrusion. □ - 0 wt. % SBA-15, ▭ - 20 wt. % SBA-15.*

The employed technique can measure pores within the range of 0.04-150 µm, so, only macropores were identified and measured.

The average pore diameter of pure PCL biomaterial, for the additivated and composite assays, was found to be 0.2 ± 0.0 µm. This finding is different from the one obtained for the

optimization assays (0.5 ± 0.0 µm), tough, for the discussion of the additivated and composite assays results the first one was used, since for the optimization assays, all the samples were measured in one batch and for the additivated and composite assays all the samples were measured in another batch. So, that the obtained results are comparable within each assay, each result was used in its own type of assay, not being possible to be compared between them, despite the composition and processing conditions of this biomaterial were the same. The obtained high deviations for total pore area are due to the fact that this parameter is not a direct measure of the technique and so these high deviations are obtained, even so it is possible to analyze and discuss this property.

Observing Figure 26, generally, total pore area increases with decreasing of average pore diameter. This is due to the high surface area ensured by smaller pores (which are present in much larger number). This is an important feature of materials for hard tissue engineering, as explained, materials with increased surface area ensures a better cellular adhesion.

Again, by observation of Figure 26, the porogenic effect of TTPB is observed. In this porous structure, larger pores are obtained as well as total pore area. That is indicative of the presence of large pores in larger number, which are formed due to more absorption of CO_2 within the polymer. Although, as seen by SEM imaging, adding GF yielded into biomaterials with very large pores, by mercury intrusion this biomaterial appears with smaller average pore size. This can be due to the limitations of the employed technique, the samples had to be cut into small pieces which, in the case of porous structures with very large pores, led to the destruction of the pores inducing in error the analysis. Adding to the PCL-based biomaterials a mixture of the two additives, larger average pore diameter is obtained with a mixture with a molar proportion of 3:1, with consequently lower total pore area. Adding a mixture with a molar proportion of 2:1 yields into biomaterials with lower average pore size and consequently greater total pore area. Once again, the effect of the individual additives in mixture is not linear on the morphological behavior of the porous biomaterials.

The size of the obtained macropores increased with the incorporation of SBA-15 nanoparticles (as determined by mercury intrusion), as seen in Figure 26. This is due to the effect of the filler in the nucleation mechanism of CO_2 within the polymeric matrix. Similar results were found in the literature, employing the same technique, as the amount of inorganic filler increased, also the average pore diameter increased, despite the expected effect of decreasing the average pore diameter (as seen by SEM imaging analysis) (de Matos et al., 2013).

Adding GF to the composite biomaterial, a better dispersion of the filler appears to occur, since smaller average pore diameter are obtained. Incorporating the inorganic filler in the additivated biomaterial with TTPB, a decrease on average pore diameter is observed, which is due to the induced interface between organic and inorganic phases acting as heterogeneous nucleation points, although total pore area was found to decrease (may be due to the formation of larger pores by action of TTPB).

Incorporating in the composite biomaterials a mixture of GF and TTPB an even better dispersion of the filler appears to be enhanced. The mixture of both additives, generally, led to biomaterials with smaller average pore size. Again, the effect of a single additive in mixture is not evident, the mixture richer in TTPB (5:1) did not led into a porous strucutre with larger average pore size diameter being the biomaterial additivated with a mixture in a molar proportion of 3:1 the one reaching the larger average pore diameter and consequently lower total pore area, 0.2 ± 0.0 µm and 8.9 ± 0.2 $m^2.g^{-1}$ respectively.

Nitrogen Adsorption

Surface area (BET and BJH), pore volume and average pore diameter (BET) (in the range of 0.2 to 300 nm) were determined using nitrogen adsorption. The obtained isotherms, for all the prepared additivated and composite biomaterials were of type II and type IV, which are indicative of mesoporous materials, and an example of an obtained isotherm is showed in Appendix D, Figure D 4. The obtained values are listed in Appendix D, Table D 3. In Figure 27 is shown the obtained surface area and average pore diameter of the prepared biomaterials for the additivated and composite assays, determined by nitrogen adsorption.

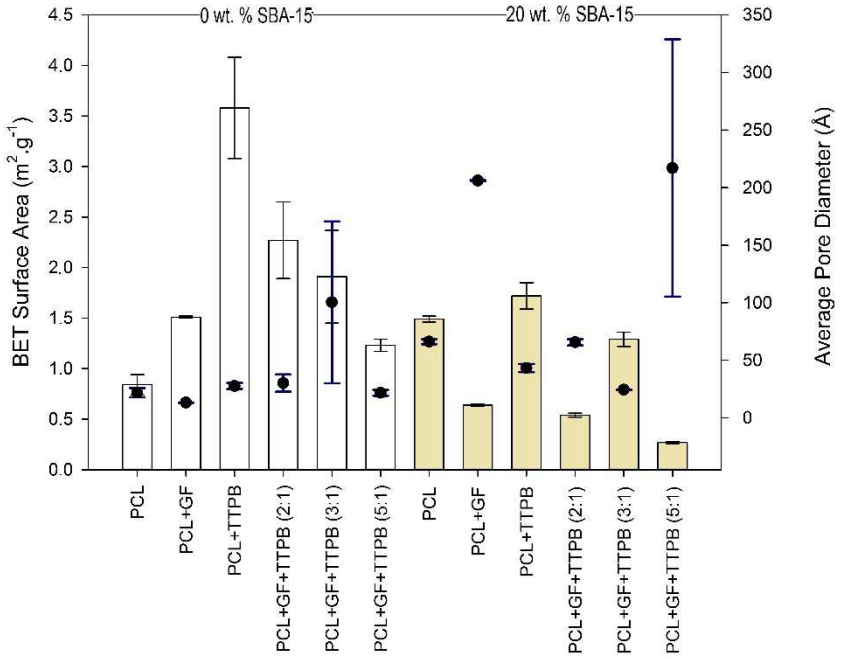

Figure 27. *BET surface area and average pore diameter, determined by nitrogen adsorption (●) determined by nitrogen adsorption of the biomaterials, prepared at P = 20 MPa, T = 40 ºC and $\Delta P/\Delta t$ = 0.3 MPa.min^{-1}for 2h, for the additivated and composite assays.* □ *- 0 wt. % SBA-15,* □ *- 20 wt. % SBA-15.*

As can be seen in Figure 27, since surface area is a direct measure of this technique the obtained deviations are not very high contrasting to average pore diameter, which is an indirect measure, presenting very high deviations, in some cases.

Concerning to surface area it stands almost immediately that incorporating with TTPB non-composite biomaterials leads to the formation of materials with enhanced surface area (3.6 ± 0.5 m^2.g^{-1} comparing to 0.8 ± 0.1 m^2.g^{-1} of pure PCL biomaterial). Also, adding additives to the PCL-based biomaterials always increases the surface area of the material. This effect can be due to the favouring of the homogeneous nucleation mechanism induced by the liquid additives (lowering the surface tension of the mixture) allowing more CO2 to be absorbed and yielding into the formation of more pore (mainly in the case of TTPB as previously seen). Concerning to the effect of addition of TTPB on the surface area of PCL biomaterials similar results were found in literature (Rosa, 2013), although the effect, of incorporation of GF on the surface area of the same type of biomaterials, reported in literature is contrary to the one found in this work. Rosa, reported a decrease on surface area once GF was incorporated. Contrary to

the findings of this work, this results is in accordance to the obtained SEM images as seen in Figure 19, since larger pores yields into smaller surface area of the material. Although, in this work, the number of pores obtained once GF was incorporated, should have been much more than for pure PCL biomaterial, which translates into larger surface area (Rosa, 2013). Tough the obtained average pore diameter, from nitrogen adsorption, are almost constant for all the non-composite biomaterials except when a mixture of the two additives is added in a molar proportion of 3:1, yet in this case the obtained deviation is very high (100.3 $\pm$ 70.4 Å) so no conclusion can be withdrawn from this result.

Incorporating SBA-15 nanoparticles (20 wt. %), producing composite porous biomaterials, the surface area of non-additivated biomaterials increases from 0.8 $\pm$ 0.1 $m^2.g^{-1}$ to 1.5 $\pm$ 0.0 $m^2.g^{-1}$. This effect is due to the presence of a larger number of pores and to the surface roughness ensured by the agglomerates of the inorganic filler. Also, the porous feature of the SBA-15 nanoparticles ensures an enhanced surface area. This aspect is very important concerning the application of such materials in hard tissue engineering applications, since high surface area enhances cellular adhesion as well as promotes the degradation of the material promoting mass transfer between the biological medium and the material (Reinwald *et al*., 2014; Fanovich and Jaeger, 2012).

Once the composite porous biomaterials are additivated with GF the surface area decreases, which can be indicative of the heterogeneity of the analysed sample, since as seen by macro and microscopic analysis this sample had a clear change on morphology from the centre of the sample to the border (varying accordingly to the zone in which the additive was incorporated). The obtained high average pore diameter is also an evidence of such heterogeneity, perhaps the analysed sample is not representative of the prepared biomaterial, despite the efforts made to be so. Adding TTPB to the composite biomaterial, higher surface area is achieved with decreased average pore diameter, comparing to pure PCL biomaterial. This effect is resulted from both the action of TTPB (inducing the formation of a large number of pores) and the action of the inorganic particles (ensuring higher surface area). The surface area reported in the literature, of additivated PCL/SBA-15 composite biomaterials, decreases comparing the non-composite biomaterials to the composite ones with lower amount of filler. It only increases significantly when a higher amount of filler is incorporated (Rosa, 2013).

The additivated composite biomaterials with a mixture of the two additives present reduced surface area comparing to the non-additivated composite biomaterial and to the additivated with TTPB composite biomaterial, although, all are larger than the additivated composite biomaterial with GF. Of the three employed mixtures, adding a mixture in a molar proportion of 3:1 reveals, once again, as the material with better morphologic properties for hard tissue engineering applications, of the three tested mixtures. This result can be elucidative that this mixture is the one which yields into composite biomaterials with better distribution of the filler throughout the polymeric matrix.

Figure 28 shows the pore volume of the prepared biomaterials for the additivated and composite assays, determined by nitrogen adsorption.

As seen, pure PCL biomaterial presents a total pore volume of 4.7 $\pm$ 1.4 $\times$ 10^{-4} $cm^3.g^{-1}$ and when is additivated with GF this property suffers almost no noticeable change. Although once TTPB is incorporated, total pore volume increases to 17.8 $\pm$ 7.1 $\times$ 10^{-4} $cm^3.g^{-1}$. This is, once again, indicative of the porogenic effect of TTPB. Due to its high affinity to CO_2, more CO_2 was absorbed by the polymer, yielding into the formation of more pores, as referred. Similar

results were reported in literature, when GF is incorporated a decrease in pore volume is observed, tough when TTPB is added pore volume increases (Rosa, 2013).

When a mixture of both additives is added to the PCL biomaterial, comparing to the biomaterial additivated with GF, pore volume slightly increases, reaching a maximum with a mixture in a molar proportion of 3:1, although this sample presents a very high deviation ($56.0 \pm 45.2 \times 10^{-4}$ $cm^3.g^{-1}$) and no right conclusion can be made.

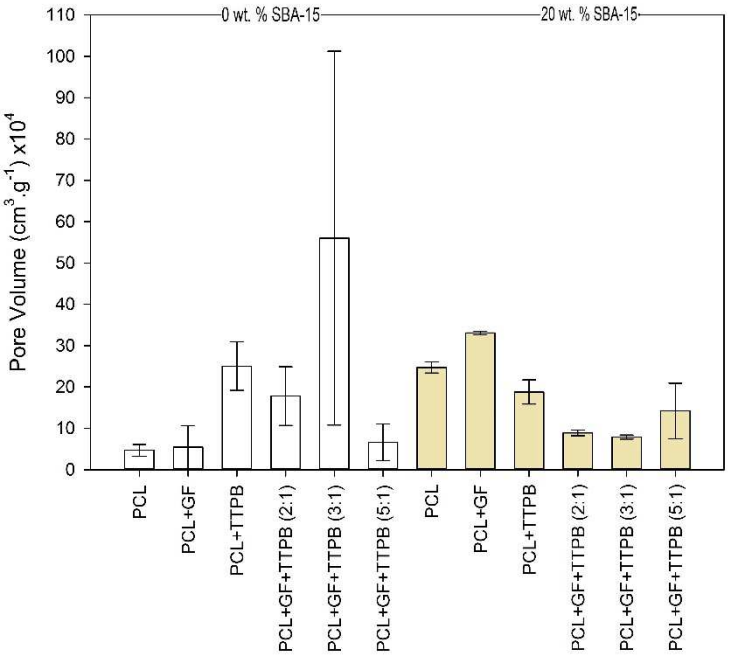

Figure 28. *Pore volume determined by nitrogen adsorption of the prepared biomaterials, at P = 20 MPa, T = 40 ºC and $\Delta P/\Delta t$ = 0.3 MPa.min^{-1}for 2h, for the additivated and composite assays.*

Incorporating SBA-15 nanoparticles and producing composite biomaterials highly increases the total pore volume of the materials, as seen in Figure 28. The inorganic particles acting as heterogeneous nucleation sites, promote the nucleation of a high number of cells, yielding into highly porous materials (Collins *et al*., 2010; de Matos *et al*., 2013; Jacobs *et al*., 2008). Same results were found in literature, when an inorganic is incorporated, pore volume increases with the amount of filler (Rosa, 2013; de Matos *et al*., 2013; Tsimpliaraki *et al*., 2011). Once GF is added to the composite biomaterial, greater pore volume is obtained, this result can be indicative of a good distribution of the filler throughout the polymeric matrix. GF acts as polymer compatibilizer (has a hydrotrope feature) between the SBA-15 nanoparticles and PCL, presenting and end on its molecule with affinity to PCL and another with affinity to SBA-15, so distributing the inorganic throughout the matrix (Welge and Wolf, 2001).

After a mixture of both additives is added pore volume decreases, which can be indicative that the competition between the formation of large pores (due to action of the additives) and the formation of smaller pores (due to action of the fillers) is balanced in the way for the first one. Similar results were found in literature, when a mixture in a molar proportion of 2:1 of GF and TTPB was added to PCL/SBA-15 composites, the pore volume decreased (Rosa, 2013). In this

case, the mixture in a molar proportion of 5:1 appears to be the one with enhanced dispersion of the filler, since a greater pore volume was obtained.

Concerning to the effect of GF on the dispersion of the filler, promoting the production of composites with more homogeneous dispersion of the inorganic, no conclusion can be drawn. Of the performed morphologic analysis several discordant results were obtained, namely from mercury intrusion and nitrogen adsorption. Future work on the development of composites additivated with GF and on their morphologic analysis should be performed, preferentially analysing the entire sample.

Helium Picnometry

The effect of the liquid additives and of the filler on the real density of the prepared biomaterials was assessed using helium picnometry. In Appendix D, Table D 3, are listed the obtained results so they can be compared with the determined bulk and skeletal density (with mercury intrusion). In Figure 29 are shown the obtained results of real density of the prepared biomaterials.

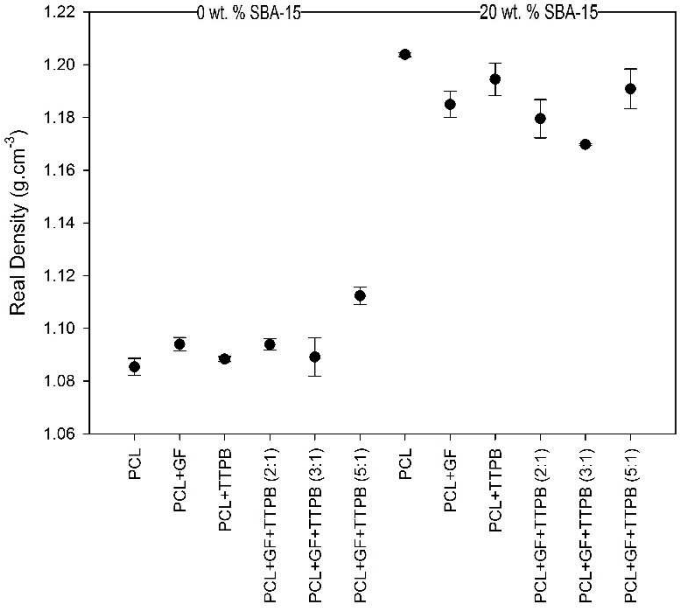

Figure 29. *Real density obtained from helium picnometry of the prepared biomaterials at P = 20 MPa, T = 40 ºC and $\Delta P/\Delta t$ = 0.3 MPa.min^{-1}for 2h.*

Pure PCL porous biomaterial real density was found to be 1.1 $\pm$ 0.0 g.cm^{-3}, which is slightly lower than the value reported in literature (1.1 $\pm$ 0.0 g.cm^{-3} by Rosa (Rosa, 2013)) and in the optimization assays (1.1 $\pm$ 0.0 g.cm^{-3}). The obtained value is also lower than the value indicated by the supplier (1.2 0.0 g.cm^{-3}), although the difference between the several obtained results is not very high. Since the pure compounds density is not very different from the obtained density of the biomaterial of pure PCL, when either GF or TTPB are added to the porous biomaterial or with a mixture of both (except when a mixture in a molar proportion of 5:1 is incorporated) the density of the additivated biomaterial varies little, slightly increasing (ρ_{GF} = 1.09 g.cm^{-3}, ρ_{TTPB} = 1.07 g.cm^{-3}).

The porous biomaterial density is mainly influenced by the incorporation of the inorganic particles, due to the high density of SBA-15 (ρ_{SBA-15} = 1.82 g.cm^{-3}). As seen in Figure 29, the density of the biomaterials highly increased with the addition of SBA-15 (20 wt. %). In the composite biomaterials as there are additivated the density decreases, which is due to the presence of another compound with lower density than SBA-15. In literature the same effects are reported, when inorganics are added the real density of the porous biomaterials increases and when additives with lower density are incorporated the density of the composite biomaterials decreases (Tsimpliaraki *et al*., 2011; de Matos *et al*., 2013; Rosa, 2013).

3.3.2. Thermal and Crystallinity Analysis

Simultaneous Differential Thermal Analysis (SDT)

SDT was used to determine if the method to powder PCL pellets, SFM process, plasticizer/polymer compatibilizer, filler and composite composition had any effect on thermal and crystallinity properties of PCL. In Figure 30 are showed the obtained degradation temperatures and melting temperatures for the produced porous biomaterials of pure and additivated PCL and of composite PCL/SBA-15 additivated and non-additivated. The degradation and melting temperatures of pure (pellet) PCL and powdered PCL are also shown.

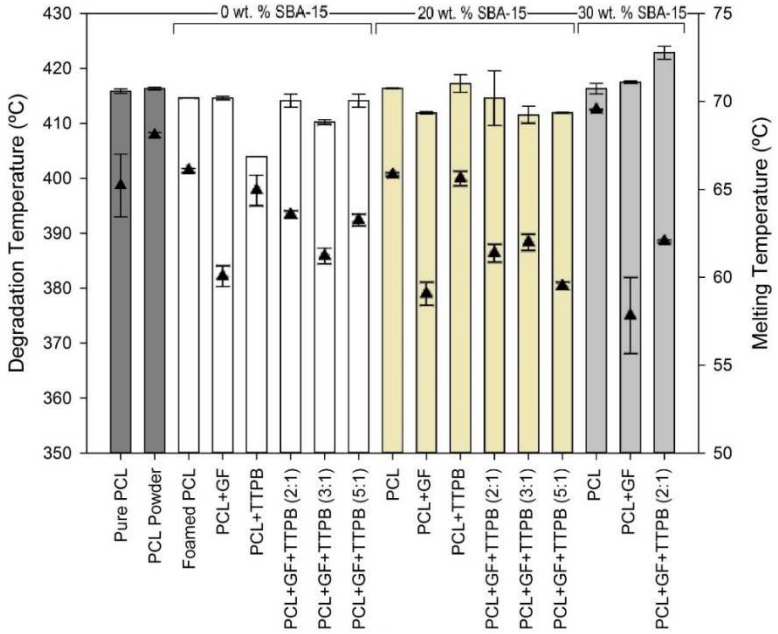

Figure 30. *Degradation temperatures (■ - Pure PCL (pellet) and PCL powder, □ -0 wt. % SBA-15, □ - 20 wt. % SBA-15, □ - 30 wt. % SBA-15) and melting temperatures (▲) of the produced biomaterials at P = 20 MPa, T = 40 ºC and $\Delta P/\Delta t$ = 0.3 MPa.min^{-1}for 2h, along with pure PCL (pellet) and powdered PCL.*

It stays undoubtedly, by observation of Figure 30 and Table F 1 in Appendix F, that the used method to obtain PCL powder from pellet had no influence on the degradation temperature (Td) of the polymer, since for pure PCL (pellet) the obtained Td was of 415.9 ± 0.4 ºC and of 416.3 ± 0.3 ºC for the powder PCL. Processing PCL with $scCO_2$, had, as well, no significant influence on the

thermal stability of the polymer, having been obtained a Td value of 414.7 ± 0.0 ºC. A similar trend was observed by other authors, leading to the conclusion that PCL thermal stability is kept constant before and after exposure to $scCO_2$ (Kiran *et al*., 2008; de Matos *et al.*, 2013; Rosa, 2013).

The obtained degradations temperatures for the employed pure liquid additives, was of 208.2 ± 2.4 ºC and 403.3 ± 7.4 ºC for GF and TTPB respectively. The degradation temperature of the produced biomaterials is almost unchangeable, when SBA-15 nanoparticles are incorporated in both compositions, yet a slightly increase on the degradation temperature is reached when 30 wt. % and a mixture of GF and TTPB (2:1) is incorporated, which could be explained by a better dispersion of the filler in the polymeric matrix, leading to an increase on the thermal stability, what was found by other authors as well (Chen *et al*., 2012; Rosa, 2013). This thermal stability achieved with the incorporation of the filler, might be due to the formation of polymer networks and inorganic moieties, which appears to increase when the amount of inorganic is increased (Chen *et al*., 2012; Rosa, 2013; Bonilla *et al*., 2014). This shows that the used method to mix the polymer with the filler, was used employing suitable particle size of the polymer, since if they were too big, the filler would act as an impurity, due to the large voids between the two phases during physical mixture that would have formed, decreasing the thermal stability of the composites (Lee *et al*., 2005).

The liquid additives have negligible significant effect on the degradation temperature of the prepared biomaterials. The only exception is when TTPB is added, in the sample PCL+TTPB, reaching a lower degradation temperature of 404.0 ± 0.0 ºC, which is in disagreement with what was found in previous works, in which the effect of this ionic liquid on the thermal behaviour of the PCL porous structures was negligible (Rosa, 2013). When a mixture of the two additives is used, the degradation temperature slightly decreases. This effect is indicative that the two liquid additives marginally decrease the thermal stability of the prepared PCL-based biomaterials. However this decreasing is not very expressive, and in overall the thermal stability of the biomaterials is kept, when SBA-15 nanoparticles and the two liquid additives (pure and in mixture) are incorporated.

The measured melting temperature for pure PCL (pellet) was determined to be of 65.2 ± 1.8 ºC which despite being marginally out of the interval reported by the supplier (59-64 ºC) is in agreement with the values obtained and reported in literature (Fanovich et al., 2013; de Matos *et al*., 2013; Rosa, 2013). After exposure to $scCO_2$, at P = 20 MPa and T = 40 ºC, the obtained calorimetric behaviour of PCL, is similar to the one obtained for pure unprocessed PCL, as shown on the obtained SDT profiles presented on Figures F 3 and F 4 on Appendix F, since the melting temperature of PCL is kept almost unchanged, 66.1 ±0.1 ºC. This behaviour clarifies that the polymer underwent complete melting, due to the effect of $scCO_2$ (Kiran *et al*., 2008). Increasing the SBA-15 composition within the prepared biomaterials, an increase in the melting temperature is verified, as seen in Figure 30, being more accentuated when 30 wt. % is incorporated. This effect on the $T_m$of polymeric matrixes in organic/inorganic composites was also reported in literature (Chen *et al*., 2012; Bonilla *et al*., 2014; Rosa, 2013; de Matos *et al*., 2013).

The ionic liquid and the polymer compatibilizer, both have major influence on the T_m of the produced composite and non-composite biomaterials, as is noticeable in Figure 30. Incorporating GF alone, the decrease on T_m is more accentuated even when SBA-15 nanoparticles are added, appearing to decrease even more when the composition of the filler increases. TTPB has a similar effect but not in a so much accentuated way. When a mixture of

the two additives is employed, are obtained intermediary values, considering the effect of both the additives alone. Again, when SBA-15 composition is increased T_m values slightly decrease. This effect clearly shows that PCL was effectively modified by the presence of both these additives, which by decreasing T_m of the biomaterials, both composite and non-composite, confirming their plasticizer/foaming effect on the polymer during SFM processing.

The obtained results allow to conclude that the produced composite and non-composite biomaterials do not melt and/or degrade under body temperature (~37 ºC) which allows them to be used in hard tissue engineering applications as solid biomaterials.

SDT was used, as well, to determine the residual amount of inorganic after exposure the PCL/SBA-15 composite biomaterials at 700ºC. By observation of Figure 30, it is clearly that PCL degrades at approximately 414.7 ± 0.0 ºC, so after exposure to that temperature all the organic component of the composite biomaterials is lost and the remaining mass is concerned to the inorganic phase which does not degrade. By these means it is possible to assess in a qualitative way, if the produced composites are homogeneous or not In Table 5 is presented the mass loss, and the real SBA-15 composition of all the produced additivated and non-additivated composite biomaterials.

***Table 5**. Mass loss and real SBA-15 content of the produced additivated and non-additivated composite biomaterials at P = 20 MPa, T = 40 ºC,$\Delta P/\Delta t$ = 0.3 MPa.min^{-1} for 2h.*

SBA-15 content (wt. %)	Biomaterials composition	Mass Loss (%)	Real SBA-15 Content (wt. %)
20	PCL	80.7 ± 0.9	19.3 ± 0.9
	PCL+GF	86.5 ± 0.2	13.5 ± 0.2
	PCL+TTPB	85.3 ± 0.1	14.7 ± 0.1
	PCL+GF+TTPB (2:1)	89.4 ± 0.9	10.6 ± 0.9
	PCL+GF+TTPB (3:1)	84.7 ± 1.7	15.3 ± 1.7
	PCL+GF+TTPB (5:1)	87.7 ± 1.2	12.4 ± 1.2
30	PCL	79.7 ± 0.9	20.4 ± 0.9
	PCL+GF	80.4 ± 1.0	19.6 ± 1.0
	PCL+GF+TTPB (2:1)	81.1 ± 0.2	18.9 ± 0.2

All the produced non-composite biomaterials had mass losses approximately of ~98-99%, which is indicative that all the organic phase was degraded and there was no inorganic phase on those biomaterials, as expected, these values are shown in Table F2 on Appendix F.

As presented in Table 5, when 20 wt. % of SBA-15 nanoparticles were incorporated, the obtained mass losses are within the range of 80–89 %, and therefore the real silica content in the range of 19–10%. The biomaterial which presents a real silica content nearest to the initial amount added to the PCL powder during the physical mixture step is the non-additivated biomaterial with a composition of 20 wt. %. This means that the filler was homogeneously dispersed throughout the polymeric matrix in this biomaterial. When the liquid additives are incorporated, a decrease in the real silica content is observed, contrary to what was expected, since GF should act as a polymer compatibilizer, enhancing the distribution of SBA-15 nanoparticles within the polymeric matrix, and TTPB increasing the solubility of $scCO_2$ in the polymer should increase even further the distribution of GF, when incorporated in mixture, and

therefore of the filler. However, and considering that SDT analysis was performed with fractions from the centre of each biomaterial, these additives, as seen on section 3.3.1., had large impact on the morphology of the biomaterials, yielding into porous structures with increased average pore diameter. By cutting the biomaterials those very large pores were fractured and some of the plasticized SBA-15 could have been loose, leading these results into error. Still, observing Table 5, it is clearly that additivated composites present a more homogeneous distribution of the filler. These results shows that the mixture of molten polymer + SBA-15 + additive(s) should be stirred, since SBA-15 has a density greater than PCL, which by gravity action will sediment on the mixture, accumulating on the bottom of the biomaterials, yet to stirrer this mixture will be very difficult, since the viscosity of the mixture is very high due to the molten polymer.

Once a mixture of the two additives was incorporated, the one which yielded into composite biomaterials with more homogeneous filler spatial distribution for a composition of 20 wt. % of SBA-15, was using a molar proportion of 3:1 (although 5:1 yielded into a very similar result). These result might be due to the effect of the ionic liquid which allows a better distribution of GF and SBA-15 throughout the polymer, by enhancing the intake of CO_2 molecules within the polymeric chains, due to the good affinity between the phosphonium group (due to the fluorine atoms) and CO_2 molecules (Jacobs *et al*., 2008).

As seen in Table 5, for the composite porous biomaterials prepared with 30 wt. % of SBA-15 it is confirmed what was observed and stated based on the morphological analysis for these composites, PCL does not have the capability to incorporate the total amount of the filler in this composition, since all the produced biomaterials present a real silica content equal and lower than 20 wt. %, even when additives are employed such as GF, a polymer compatibilizer between the inorganic and the organic phase. Based on the morphological analysis (macroscopic analysis) and in the mass loss results, it is possible to conclude that the optimum amount of filler that is possible to incorporate is within the interval [20, 30[(wt. %), and this study should be conducted in future work, in order to determine the maximum incorporation capacity of SBA-15 particles by PCL of this molecular weight.

The effect of the SFM process, the used plasticizer/porogenic agents and polymer compatibilizer and the SBA-15 nanoparticles on the crystallinity of the obtained porous biomaterials was evaluated concerning the obtained results for melting enthalpy from SDT analysis, shown in Table F1 on Appendix F. In Figure 31 are presented the obtained crystallinity results from SDT analysis. The crystallinity of polymers is an important characteristic since it has major role determining its mechanical properties, such as Young's modulus and impact resistance, as well as it degradation rate, since higher melting enthalpies and higher degradation temperatures (which lead into higher degree of crystallinity) yield into longer degradation times for biodegradable polymers such as PCL, hindering water diffusion within the polymeric chains, as well as in drug permeability (Kong and Hay, 2002; de Matos *et al.*, 2013; Natu *et al*., 2008).

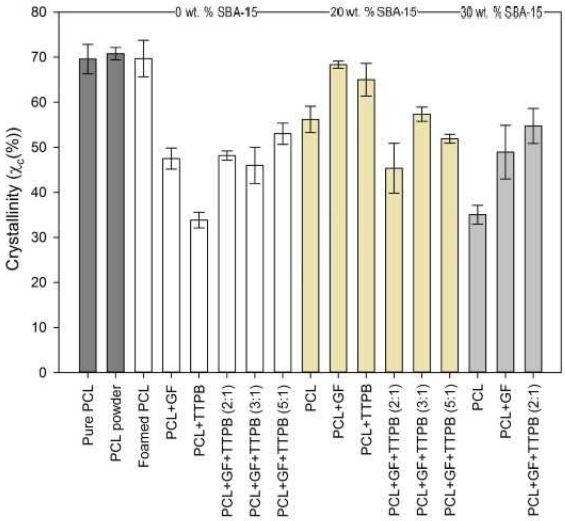

***Figure 31**. Crystallinity of the produced biomaterials at P = 20 MPa, T = 40 ºC,$\Delta P/\Delta t$ = 0.3 MPa.min-1 and t = 2h., obtained with SDT analysis. Legend: ■ - Pure PCL (pellet) and PCL powder, □ -0 wt. % SBA-15, ■ - 20 wt. % SBA-15, ■ - 30 wt. % SBA-15.*

SDT analysis allowed to determine the crystallinity of pure PCL to be 69.6 $\pm$ 3.3 %. The method used to obtain PCL powder from pellet, revelled to have negligible influence on the crystallinity of the polymer, as seen on Figure 31, showing the advantage of using this method, since it has no effect on thermal and crystallinity properties of the polymer, increasing its surface area, enhancing mass transfer during the SFM process. Processing the polymer with $scCO_2$ at P = 20 MPa, T = 40ºC and $\Delta P/\Delta t$ = 0.3 MPa.min^{-1} had, as well, little influence on the crystallinity of the polymer, contrary to the results obtained in the literature which reported a decrease on the crystallinity of PCL after $scCO_2$ processing (Rosa, 2013; Jenkins *et al*., 2006; Kiran *et al*., 2008; Shieh *et al*., 2009). The incorporated additives highly influenced the crystallinity of the produced biomaterials, decreasing it. This decrease is more accentuated when only TTPB is added. Once a mixture of the two additives is employed, intermediate values for crystallinity are obtained, increasing with the GF proportion. Similar results were found by Rosa, when incorporating these additives a decrease on crystallinity, determined by DSC, was found to occur comparing with pure PCL porous material (Rosa, 2013).

The incorporation of SBA-15 nanoparticles lead into a decrease in the crystallinity of the biomaterials, which is more accentuated when a composition of 30 wt. % is incorporated. This composition, as presented above, corresponds to an excess of filler, which greatly slows and hinders the crystallization of the polymer (Shieh *et al*., 2009). The presence of the nanoparticles within the polymeric structure creates obstacles for the polymeric chains to rearrange, inhibiting the free movement of the chains due to the presence of the micropores, and create crystallites, this happens due to the lack of intercalation between the organic and inorganic phase (Rosa, 2013; de Matos *et al*., 2013; Shieh *et al*., 2009; Jiang *et al*., 2001). When a polymer compatibilizer and a plasticizer are added, the crystallinity observed is higher, due to the action of this additives, creating more intercalation between the filler and the polymer (mainly due to the action of GF, which is the one that leads into higher crystallinity index) since SBA-15 nanoparticles are more dispersed throughout the matrix creating less resistance for polymer chains to rearrange during depressurization (Shieh *et al*., 2009). In the literature several authors reported a decrease on crystallinity after incorporation of inorganic fillers, such as SBA-15 and

MCM-41 nanoparticles, and other authors reported increase on crystallinity after the incorporation of inorganics within polymeric matrices (Rosa, 2013; de Matos *et al*., 2013; Shieh *et al*., 2009).

Producing PCL/SBA-15 porous composite biomaterials, , allows not only to obtain highly porous structures with high surface area and roughness, as previous seen on section 3.3.1., but allows as well to produce thermally stable composite biomaterials with controlled and speeded up degradation rate (lower crystallinity), which are key-points on the development of biomaterials towards hard tissue engineering applications. The incorporation of additives such as GF and TTPB allows to produce composite biomaterials with better incorporation of filler particles within the polymeric structure allowing a better dispersion of the enhanced properties by the filler throughout the entire composite biomaterial, as well as controlled thermal properties.

X-Ray Diffraction (XRD)

Molecular weight and crystallinity have been showed as the main properties of polymers affecting their biodegradability. In order to understand the biodegradability of the produced biomaterials, crystallinity is an important aspect to assess and to control, since it is known that amorphous regions degrades prior to crystalline regions, so tailor-made biomaterials can be produced for the desired specific biomedical/pharmaceutical application (Yu and Dean, 2005; Berens *et al*., 1992). The obtained results of the effect of the used additives, GF and TTPB, on the crystallinity of pure and processed non-composite PCL-based biomaterials, was evaluated and confirmed using XRD. Figure 32 shows the XRD patterns of the prepared non-additivated biomaterial and additivated biomaterials with only GF and TTPB. Figure 33 shows the XRD patterns of the prepared non-composite additivated biomaterials with a mixture of both the employed additives in three molar proportions (2:1, 3:1 and 5:1).

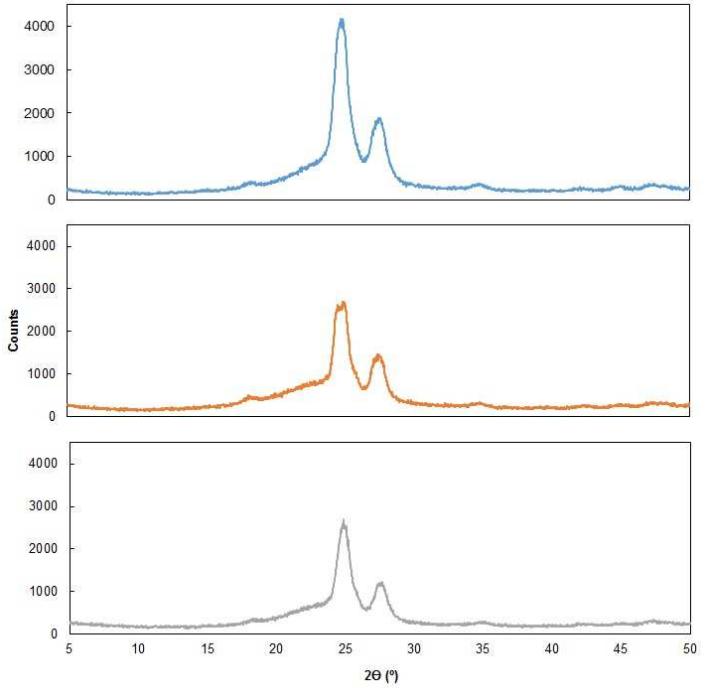

***Figure 32**. XRD diffractograms of non-additivated PCL porous biomaterial (—), PCL additivated porous biomaterial with GF (—) and PCL additivated porous biomaterial with TTPB (—).*

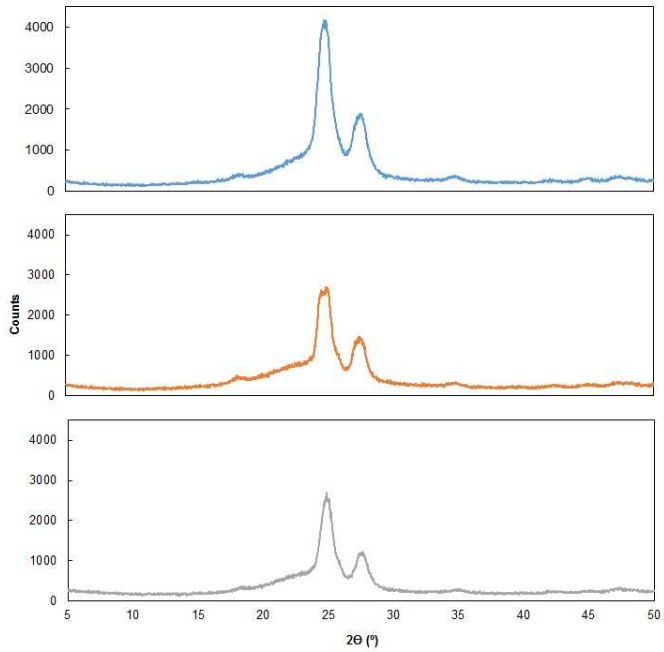

***Figure 33**. XRD diffractograms of additivated PCL porous biomaterials with a mixture of the two additives in three molar proportions, 2:1 (—), 3:1 (—) and 5:1 (—).*

Observing the diffractograms presented in Figures 32 and 33, the typical PCL crystalline behaviour is observed. PCL diffractograms, as seen, usually present broad peaks at approximately 18º and 23º for amorphous regions and other peaks at approximately 25º and 27º for crystalline regions (diffractions planes (110) and (200) respectively). A crystalline peak was also identified at 34º, however, has an almost negligible area when comparing to the crystalline peaks at 25º and 27º (de Matos *et al*., 2013; Yu and Dean, 2005; Zhang *et al*., 2005). The identification of the crystalline and amorphous areas is presented on Appendix F, Figure F 6.

The obtained peaks for the additivated biomaterials with GF, as seen in Figure 32, are slightly broader than for pure PCL biomaterial, which translates into a reduction of crystallinity, since the amorphous region is larger, from 67.8 $\pm$ 0.2 % to 62.6 $\pm$ 0.6 %. When TTPB is incorporated a slightly increase in crystallinity to 68.1 $\pm$ 0.5 %, is observed. The presence of the additives decrease the intensity of the crystalline peaks, as seen for the biomaterial of pure PCL, higher intensity peaks are obtained.

The molecular structure of the polymer and initial crystallinity (previous to SFM process) affect the $scCO_2$ solubility within the polymer, since $scCO_2$ is adsorbed preferentially into amorphous regions. The processing conditions, such as pressure, temperature and processing time also affect the amount of $scCO_2$ dissolved in the polymer (Kiran *et al*., 2008; Fanovich *et al*., 2012). Incorporating GF and TTPB in the mixture, the plasticizer effect of CO_2 is enhanced and more CO_2 molecules are adsorbed into the amorphous regions of the polymer chains increasing their free mobility. This increased free movement enables to the polymeric chains to rearrange inducing crystallization, enabling the crystallization process to continue beyond the limits of a melt crystallization, and the related, observed changes in morphology (section 3.3.1) (Jenkins *et al*., 2006; Fanovich *et al*., 2012; Kiran *et al*., 2008). The incorporation of plasticizers allows a greater mobility of the amorphous chains causing the spacing between crystalline planes (d spacing) to slightly increase, and is controlled by the molecular weight of the employed plasticizer/additive (Donhowe and Fennema, 1993; Panda *et al*., 2014; Berens *et al*., 1992). The

increase in crystallinity index, as measured by XRD, by action of TTPB, shows that this compound is, from the two employed, the one with greater plasticizer effect since it allows a greater intake of CO_2 by the polymer than GF, in the SFM process.

The observed effect of both additives is in disagreement with what was found by SDT analysis despite, and as referred in literature a similar trend should be found when comparing both techniques (de Matos *et al*., 2013; Yu and Dean, 2005). In Appendix F, Table F 2, are presented the obtained results of crystallinity index from XRD comparing to the ones obtained with SDT.

Once a mixture of the two additives is incorporated, as seen in Figure 33, crystalline peaks present the same intensity as the biomaterials additivated with only one additive. The biomaterial additivated with a mixture in a molar proportion of 5:1 presents a broader amorphous area, although the Gaussian fit of this area was very hard to obtain, and a higher crystallinity was obtained (65.7 ± 0.3 %) than the other additivated biomaterials with a mixture of the additives. Nonetheless this biomaterial presents the peaks with more intensity. The biomaterial additivated with a mixture with a molar proportion of 2:1 presents the narrower amorphous region, but less intense peaks, presenting an intermediate crystallinity index of the three employed mixtures. The visible trend on the effect of the three different mixtures on the crystallinity of the prepared biomaterials, measured by XRD, is also visible by SDT despite values of different magnitude were obtained, as seen in Appendix F, Table F 2. The reported decrease on crystallinity of the prepared materials, by incorporation of a mixture of both additives, leads to the conclusion that more amorphous regions are formed during vitrification of the polymer throughout the depressurization step.

This feature enables to produce biomaterials with lower biodegradation rate, since their crystallinity is reduced, which is presented as another advantage, despite the morphologic effects, of using a mixture of both the additives in producing porous materials towards hard tissue engineering applications. Also, by controlling the degradation rate, through the crystallinity of the material, the release of a bioactive compound, which could be incorporated, would be enhanced and accelerated if so would be desired.

3.3.3. Mechanical Analysis

Mechanical properties, such as compressive strength and Young's modulus were assessed with an oedometer applying several loads into the samples.

The effect of the additives and the filler composition on the mechanical properties of the produced biomaterials was evaluated. Compressive strength (ultimate stress) and Young's Modulus (at 5% strain) are shown in Figure 34 A and B respectively. These results are summarized in Appendix G, Table G 2.

Hard tissue engineering materials must present suitable mechanical properties allowing the biomaterial to withstand the *in vivo* stress and load bearing, protecting the newly-formed tissue from excessive loads (Salerno *et al*., 2012; White *et al*., 2012). The prepared biomaterials presented the typical stress versus strain profile found in porous materials as well as in PCL-based materials, as shown in Appendix G Figure G 2, presenting an elastic linear zone, controlled by the bending of the pore walls, then a plateau is reached due to instability of pore walls and their collapse and then a densification zone corresponding to when the pores are all deformed and collapsed and their walls touch each other, as identified in the biomaterials

prepared for the optimization assays (White *et al*., 2012; Kweon *et al*., 2003; Lebourg *et al*., 2008; Salerno *et al*., 2012).

The mechanical properties of porous materials much like the prepared biomaterials, are very dependent on their morphologic properties, such as pore architecture, size distribution and density (Lebourg *et al*., 2008). As seen in Figure 34 A, for the non-composite biomaterials (0 wt. %) as the porous structures are additivated, the compressive strength decreases when comparing with pure PCL biomaterial, the same trend is observed in Young's modulus, in Figure 34 B. Incorporating only TTPB in the porous biomaterials led into materials with increased mechanical strength to compression (1.2 ± 0.1 MPa), than when only GF was incorporated (0.7 ± 0.1 MPa), the same trend is observed for the Young's modulus, in Figure 34 B, which led to the conclusion that of the two employed additives TTPB is the one which least decreases the mechanical properties of PCL. Also, and as expected, after observing the SEM photographs, as shown in Figure 19 on section 3.2.1, when these additives are incorporated, larger pores are obtained, which is even more evident when incorporating GF, and the presence of larger pores leads into more fragile structures, since they occupy a larger volume reducing the thickness of the pore walls. This effect of pore size and porosity on the mechanical properties of porous materials, was also found and reported in literature (White *et al*., 2012; Salerno *et al*., 2012; Mathieu *et al*., 2006; Yoshimura *et al*., 2012; Kweon *et al*., 2003; Estellés *et al*., 2006).

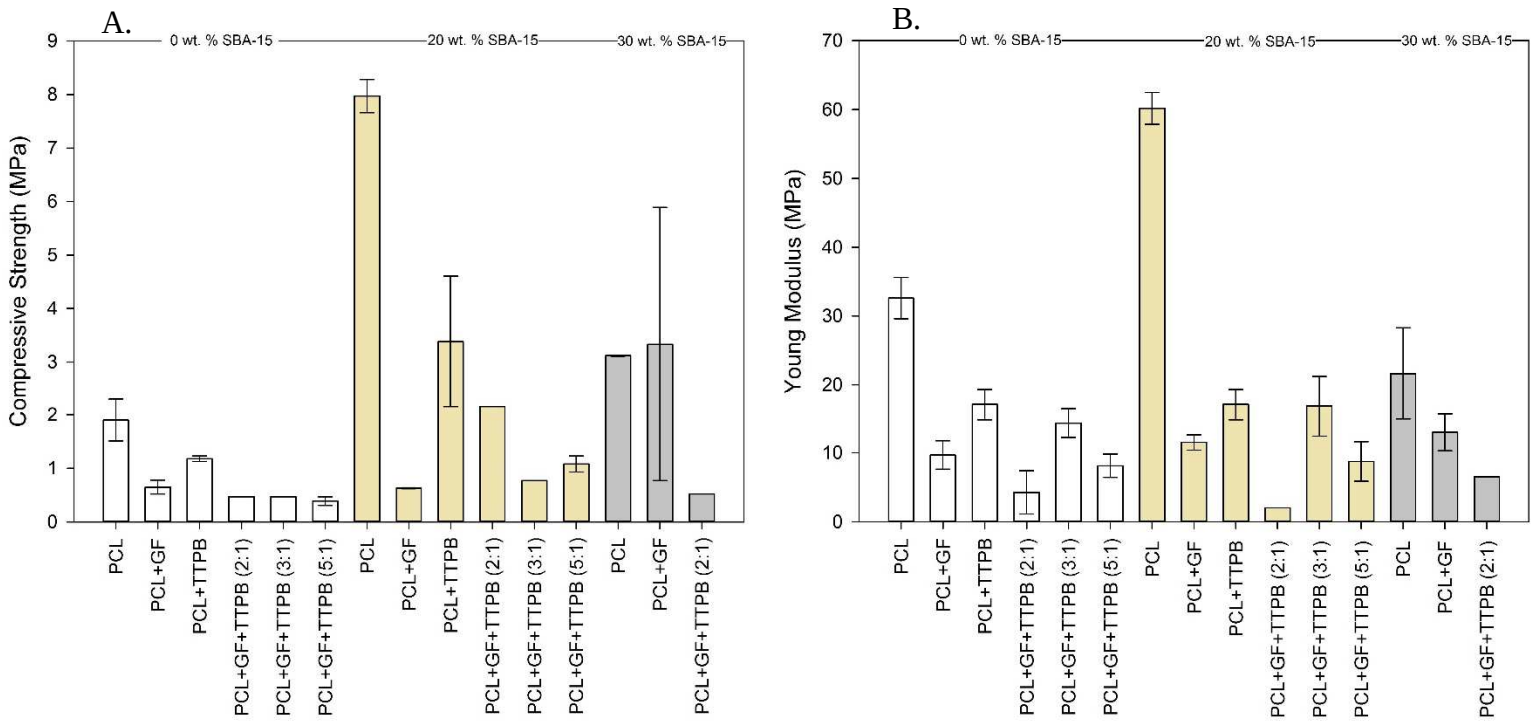

***Figure 34**. Compressive strength (A) and Young's modulus (B) of the prepared additivated composite porous biomaterials at P = 20 MPa, T = 40°C, $\Delta P/\Delta t$ = 0.3 MPa.min^{-1} for 2h. Legend, □ -0 wt. % SBA-15, □ - 20 wt. % SBA-15, □ - 30 wt. % SBA-15.*

Incorporating mixtures of the two additives in the molar proportions of 2:1, 3:1 and 5:1 respectively led into biomaterials with similar compressive strength and smaller than when incorporating only a single additive. This could be due to the effect of GF on the polymeric structure and on pore size of the biomaterials, reducing the mechanical strength to compression of the prepared porous materials, as seen in Figure 34 A. The effect on Young's Modulus, of the incorporation of these mixtures of the two additives, does not follow the same trend as the compressive strength does. Incorporating a mixture in a molar proportion of 2:1 led into more elastic biomaterials, followed by when incorporating a mixture in a molar proportion of 5:1. However, when a mixture in a molar proportion of 3:1 is employed, greater value of Young's modulus is reached (17.1 $\pm$ 2.3 MPa) (more rigid biomaterial). This effect can be elucidative that when a mixture of GF and TTPB is incorporated, in this molar proportion, the obtained morphologic structure allows to achieve more rigid biomaterials, being indicative that, concerning to a maximum on Young's modulus of additivated biomaterials, an optimum is reached.

Nevertheless adding GF, TTPB and a mixture of the two to the biomaterials, is not advantageous concerning the improvement of mechanical properties of pure PCL biomaterials, what is indicative that producing non-additivated organic/inorganic composite is the best approach to produce mechanically improved materials, as can be seen in Figures 34 A and B.

When SBA-15 nanoparticles are incorporated in both compositions (20 and 30 wt. %) the mechanical properties such as compressive strength and Young's modulus are improved, as seen both in Figure 34 A and B. This improvement is more accentuated when the filler is incorporated in a composition of 20 wt. %, since compressive strength is increased from 1.9 $\pm$ 0.4 MPa to 8.0 $\pm$ 0.4 MPa and Young's modulus from 32.6 $\pm$ 3.0 MPa to 60.2 $\pm$ 2.3 MPa, which can be elucidative that 30 wt. % is a too high amount of filler, yielding into highly heterogeneous structures of the biomaterials, since the performed mechanical test was difficult with the heterogeneity of the porous structures of the biomaterials (it was necessary to achieve a truly homogeneous cross section) what is justified by the lower mechanical properties of those biomaterials. The mechanical properties of this non-additivated composite biomaterial are in the range of trabecular bone (4-12 MPa for compressive strength and 20-50 MPa for Young's modulus).

Adding the additives to the biomaterials one could expect an improvement on the mechanical properties, since it is expected that the incorporation of the additives will homogeneously disperse the filler throughout the polymeric matrix, however, as seen in the non-composite biomaterials, the incorporation of both the additives and in mixture, yielded into a decrease on the mechanical properties of the biomaterials, as seen in Figures 34 A and B, yet the obtained values are higher than the obtained for the non-composite biomaterials due to the effect of the inorganic.

Once more, when GF is incorporated, both compressive strength and Young's modulus of the biomaterial are highly reduced. Since, as seen before, for non-composite biomaterials, this additive weakens the porous material due to its induced formation of larger pores. Although it was expected a better filler dispersion adding GF, this effect is not visible on an improvement of the mechanical properties of the biomaterials since the effect of GF on the mechanical properties overlaps the reinforcement effect of SBA-15. Incorporating TTPB in the PCL/SBA-15 porous composite biomaterial (20 wt. %) led into an increase on the compressive strength, as well as on the Young's modulus, as seen on Figures 34 A and B. This can be indicative of a good dispersion of the filler into a more homogeneous porous structure with smaller pores.

When a mixture of the two additives was incorporated, in all the three molar proportions, greater compressive strength is obtained with a molar proportion of 2:1, despite its highly

heterogeneous macroscopic morphology, yet it is the more elastic PCL/SBA-15 porous composite biomaterial. As the amount of GF is increased so the mechanical properties of the additivated and composite biomaterials (20 wt. %) decrease. Of these three mixtures, an optimum, concerning the resistance to compression and stiffness, is reached employing a molar proportion of 3:1, which might be indicative that this proportion is the one that induces a better dispersion of the filler, yielding into porous biomaterials with a good distribution of pore sizes, as seen on section 3.3.1, and (apparently) highly interconnected. Yet, the best values obtained concerning hard tissue engineering applications, using the entire material, as it was tested, are achieved with a non-additivated composite biomaterial (20 wt. %).

Similar results are found in the literature, when silicate-based inorganic fillers are incorporated into polymeric matrices for biomedical applications the mechanical properties are enhanced (Rosa, 2013; de Matos *et al*., 2013; Lee *et al*., 2003). However, opposite results were reported concerning the incorporation of additives like a polymer compatibilizer and ionic liquids (Rosa, 2013).

When the inorganic content is increased from 20 to 30 wt. %, the obtained biomaterials become more brittle and even more heterogeneous when additives were incorporated, resulting in lower compressive strength and Young's modulus. This can be indicative that 30 wt. % is an excess of inorganic content for PCL as polymeric matrix. Increasing the inorganic content the interface separation between the polymer and the filler is enhanced, leading to even more agglomerates of filler, privileging proliferation pathways for cracks to propagate (Mathieu *et al*., 2005). Similar results were found in previous works, when increasing the inorganic content to 30 wt. %, lower mechanical performance was achieved producing PCL-based biomaterials (de Matos *et al*., 2013). Incorporating GF the highly heterogeneous porous structure obtained with a visible phase separation, as seen in Figure 16 on section 3.3.1, lead into very variable mechanical behaviour, since non-reproducible morphologic structures were achieved within the replicas of the composition of this biomaterial, as seen by the deviation bars showed in Figure 34 A. The high inorganic content led, in this case to an increase of the compressive strength, comparing to the composite biomaterials prepared with lower filler composition. Adding a mixture of GF and TTPB in a molar proportion of 2:1 to a composite biomaterial (30 wt. %), originated biomaterials with phase separation, with a heterogeneous dispersion of the fillers. This morphologic feature led into a very fragile and elastic biomaterial as seen in Figure 34 A and B. This reveals that even with a mixture of both the additives, the filler distribution throughout the polymeric matrix is very poor, for this composition. Possibly, incorporating larger amounts of ionic liquid and/or GF in mixture would help to achieve a better dispersion of the fillers, in order to do so and to be more conclusive, the other tested compositions of the mixture of additives had to be tested for this filler composition as well.

All the obtained biomaterials in this work clearly presented heterogeneous pore size distributions, vertically orientated, inducing locally higher stress and deformation, resulting in a lower global stiffness of the porous material. Due to the pore growth orientation, in the vertical direction, induced by the guided diffusion path of CO_2 molecules, leaving the polymer during depressurization, the produced biomaterials have an anisotropic mechanical behaviour, just like natural hard tissue (Mathieu *et al*., 2005; White *et al*., 2012; Salerno *et al*., 2012; Lebourg *et al*., 2008; Zhang *et al*., 2014).

The performed compression tested was highly dependent of a truly homogeneous cross section, which was very difficult to achieve for some materials, in order to perform a reliable test. Some

of the produced and tested replicas did not undergo a homogeneous compression which could have led to misled mechanical properties.

3.4. Fixation Devices

The use of moulds in materials processing, allow to produce materials in a very easy and fast way, with highly reproducible dimensions and shapes. This feature is of great importance for materials manufacturers at an industrial scale. Using moulds in $scCO_2$ processing is possible, as referred, some authors and some industrial manufacturers already have proposed and used extrusion processes coupled to $scCO_2$ polymer processing (Sauceau *et al*., 2011; Kiran, 2010; Le Moigne *et al*., 2014; Website 6). This is due to the effect of $scCO_2$ on polymers, lowering their melting and glass transition temperature, allowing to achieve a polymer melt, which when incorporated in a mould, takes the shape of the mould producing polymeric materials with the desired morphological features.

In this work a stainless steel mould of a pin and of a screw were employed, in order to produce polymeric-based fixation devices with the required shapes for medical application in hard tissue grafts. In those clinical procedures, using a polymeric fixation device, which obviously does not have the same mechanical performance of a metallic device, the surgeon has to create the plug assist on the healthy tissue in which the polymeric fixation device is placed, fixating the graft. The use of polymeric fixation devices is advantageous concerning their biodegradable feature, reducing the need of a second surgery to remove the metallic devices, as referred on section 1.1.1.

3.4.1. Morphological Analysis

Macroscopic Analysis

In Figure 35 are showed the macroscopic photographs of the obtained fixation devices of pure PCL (A) and PCL/SBA-15 composite (10 wt. %) (B).

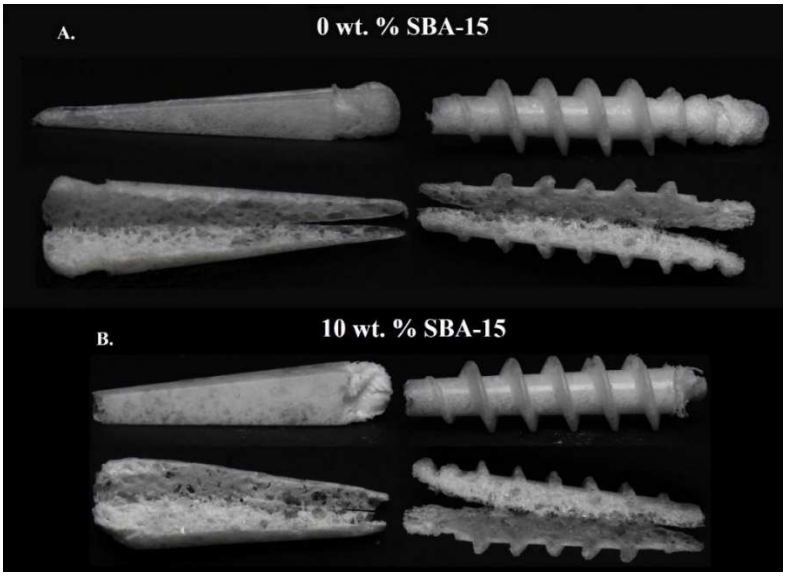

Figure 35. *Digital images of the prepared fixation devices of pure PCL (A.) and PCL/SBA-15 composite (B.). Produced at P = 20 MPa, T = 40ºC, $\Delta P/\Delta t$ = 2 MPa.min^{-1} for 2h.*

As seen in Figure 35 the polymer took exactly the shape and dimensions of the moulds originating fixation devices in the shape of pins and screws respectively. Figure 35 proves that processing polymers with $scCO_2$ in moulds, yields into highly porous fixation devices. Once again, it is clearly the heterogeneous pore size distribution, as seen mainly in Figure 35 A on the cut devices, throughout the foaming direction, having been obtained larger pores on the bottom of the device and smaller on the top, as seen for the prepared biomaterials in every performed assay. This porous feature of such materials, allows to achieve, as referred in section 1.1, good cellular adhesion, proliferation and growth allowing the ingrowth of hard tissue, also to control the degradation rate of such materials, highly porous materials present larger interfacial area yielding into faster degradation rates.

A non-porous skin was formed around each device, as previously seen for other mould materials, such as glass and PTFE. In this case, and since the mould material was stainless steel, the formed non-porous skin appears to be much thicker than the one observed employing the glass and the PTFE vial. This non-porous skin is, as referred, due to the rapid diffusion of CO_2 molecules from the surface of the vitrifying polymer during depressurization (White *et al*., 2012; Jacobs *et al*., 2008; Tsimpliaraki *et al*., 2011; Fanovich and Jaeger, 2012; Markočič *et al*., 2013; Rosa, 2013). This processing effect is undesirable, since a totally porous device would be the best approach, however the non-porous skin allows a more solid structure of the device. If a reduction of thickness of the non-porous skin, would be desirable, a PTFE mould should be the best solution to employ, since, as found in this work and presented on Appendix B, using a PTFE surface in contact with the vitrifying polymer a reduction of thickness of the non-porous skin is observed.

Observing Figure 35 B, when SBA-15 is incorporated (10 wt. %) pore size appears to decrease and pore density appears to increase for both prepared devices, but this claims can be confirmed by observation of the SEM images, since no other technique was performed towards analysing the porosity and average pore diameter of the produced devices in these assays.

The used pin and screw moulds had in their shapes, the “head” of this devices, which was filled with PCL particles. Though, the formation of such part of the devices was not verified, despite the attempts to do so. This shows that the surface tension of the molten polymer is very high, and due to the shape constraint of the mould, the tendency of the molten polymer on the top of the mould was towards the same shape of the constraint. Another explanation concerns to the diffusion path of the CO_2 molecules, during depressurization, dragging the vitrifying polymer on the foaming direction.

Scanning Electron Microscopy (SEM)

In Figure 36 are shown the obtained SEM photographs of the produced fixation devices of pure PCL, in order to observe the effects of processing PCL with $scCO_2$ on the microscopic morphology of the devices. In Figure 37 are shown the obtained SEM photographs of the produced PCL/SBA-15 (10 wt. %) composite fixation devices, so the effect of the filler on the microscopic morphology of the devices could be assessed.

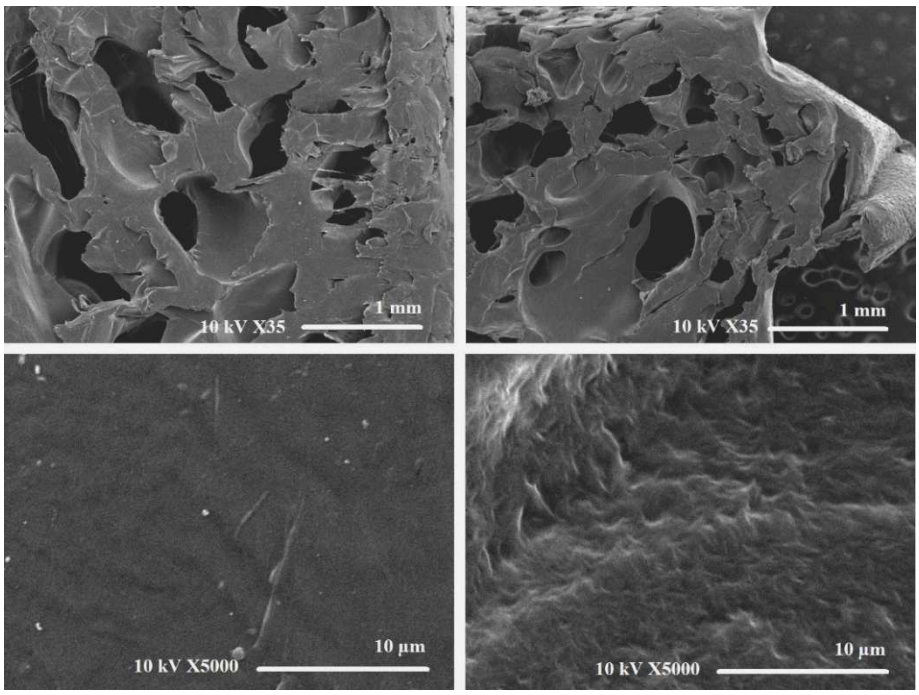

***Figure 36**. SEM cross-section photographs of the produced fixation devices of pure PCL at P = 20 MPa, T = 40ºC, $\Delta P/\Delta t$ = 2 MPa.min^{-1} for 2h. On top are showed the SEM images with a magnification of X35, on the left is showed the obtained device from the pin mould, on the right the obtained device from the screw mould, and on the bottom SEM images with a magnification of X5000 from a pore surface.*

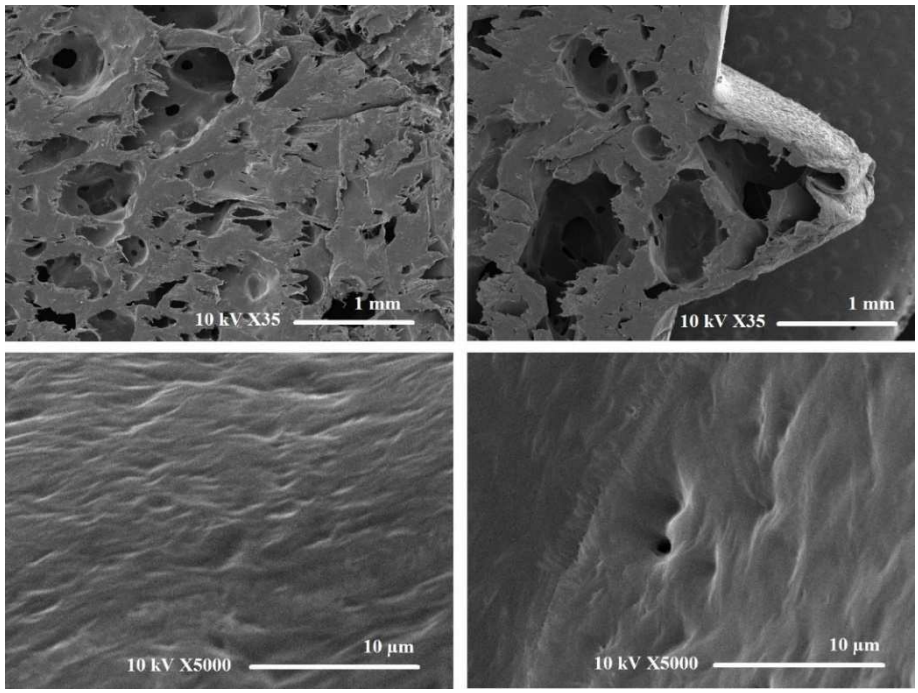

***Figure 37.** SEM cross-section photographs of the produced composite fixation devices of PCL/SBA-15 (10 wt. %) at P = 20 MPa, T = 40ºC, $\Delta P/\Delta t$ = 2 MPa.min^{-1} for 2h. On top are showed the SEM images with a magnification of X35, on the left is showed the obtained device from the pin mould, on the right the obtained device from the screw mould and on the bottom SEM images with a magnification of X5000 from a pore surface.*

Observing both Figures 36 and 37 it stays clear that the non-porous skin, visible on the border of the samples at a magnification of X35 (top images), is very thick (0.2 ± 0.0 mm) which is result of the mould material, and as previously stated, using a PTFE mould would help to achieve a reduction on thickness of the non-porous skin.

As seen in Figure 36, a highly porous structure is obtained, with pores of different sizes and the larger pores appears to be interconnected. Pore surfaces appears to be very smooth, this feature is not desirable since cells preferentially adhere to rough surfaces (Lanza *et al*., 2007).

When SBA-15 nanoparticles are incorporated on the devices (10 wt. %), Figure 31 top images, the appearance of smaller pores and in larger number is observed. Also, the porous structure appears to be much more interconnected. This is due to the effect of the nanoparticles on the SFM process, which act as heterogeneous nucleation points, inducing an interface between polymer and inorganic, favouring heterogeneous nucleation mechanism yielding into smaller pores and in larger number (greater pore density), as seen previously on section 3.3.1. Observing the pore surface of the composite devices, a slightly increase in roughness appears to be observed, and as seen on the pore surface of the screw device, very small pores appears to be formed (0.70 µm), which is indicative of the effect of the filler on the processing, yielding into the formation of very small pores throughout the polymer matrix. Though the incorporated amount of filler was not sufficient to achieve a very rough surface, as seen when 20 wt. % of SBA-15 was incorporated into the produced biomaterials, showed on section 3.3.1. This is due to the fact that all the filler was plasticized by the polymer, and no aggregate was visible on the cut surface of the devices. In Figure 38 is showed a fracture of the polymeric structure in which the particles of filler are clearly visible.

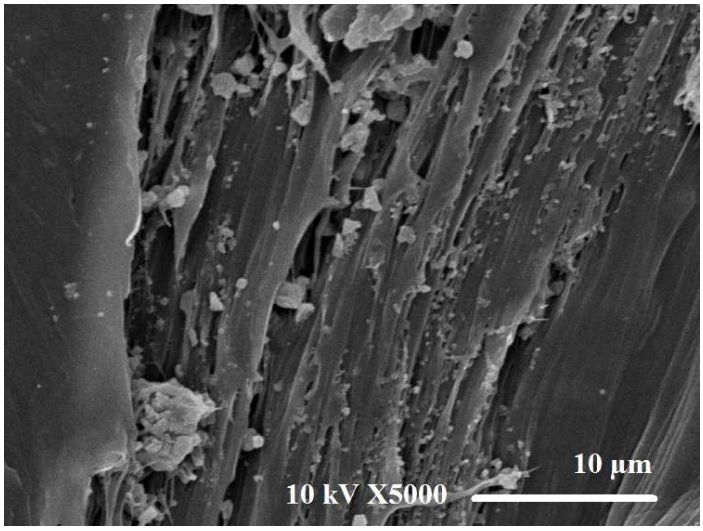

***Figure 38**. Fracture of the PCL/SBA-15 (10 wt. %) composite screw device prepared at P = 20 MPa, T = 40ºC, $\Delta P/\Delta t$ = 2 MPa.min^{-1} for 2h.*

As seen in Figure 38, the inorganic particles were all incorporated inside the vitrified polymer, since only a small amount was incorporated (10 wt. %). This clearly states that in order to obtain PCL/SBA-15 composites with a rough surface, and with an enhanced effect on pore size and porosity a higher amount than 10 wt. % must be incorporated. Since all the SBA-15 nanoparticles were incorporated inside polymeric pore walls and surface their effect on the pore surface roughness and subsequently on surface area is not very obvious.

Average Pore Diameter

The horizontal Feret's diameter was determined and the average pore diameter calculated, based on the SEM photographs for each sample. The employed method was the same for the additivated and composite assays, as showed in Appendix E. In Table 6 are presented the obtained results for the prepared fixation devices of pure PCL and PCL/SBA-15 (10 wt. %) composite.

Table 6. *Average pore diameter of the prepared fixation devices from SEM imaging.*

SBA-15 content (wt. %)	Type of Device	Average Pore diameter (μm)
0	Pin	569.6 ± 0.5
	Screw	385.1 ± 0.8
10	Pin	209.5 ± 1.2
	Screw	243.7 ± 1.4

Table 6 confirms the visual observations made based on both the macroscopic digital images and on the SEM images. When SBA-15 nanoparticles are incorporated a reduction on average pore diameter is observed, for the same type of device, which confirms their effect as heterogeneous nucleation points, favouring this nucleation mechanism.

These assays showed that using SFM process is possible to obtain tailor-made porous materials with controlled macro and microscopic morphology. Using a suitable mould it is possible to produce, in a non-toxic and environmentally friendly way, at easily achievable operating conditions, the desired shape of a polymeric and/or composite device for biomedical/pharmaceutical applications. Due to the low employed operating temperature, a bioactive compound can be incorporated in the devices enhancing its application on these fields of application. Producing composite devices, their mechanical strength is expected to be enhanced, tough not tested, as it was for the composite biomaterials, as seen on section 3.3.3, as well as the pore size decreases, yielding devices with larger surface area and consequently with faster and controlled degradation rate. Also, by controlling the average pore size the release of a bioactive compound would be controlled accordingly to the desired release rate.

Energy Dispersive X-Ray Spectroscopy (EDS)

The presence of the filler and its dispersion within the polymeric matrix of the prepared devices was evaluated and confirmed using EDS. This observation was made detecting the presence of the chemical element Si, since O is common both to the silica particles and to the polymer. In Figure 39 are shown a mapping of the chemical elements detected by EDS and the obtained spectra, from the composite screw device (10 wt. %).

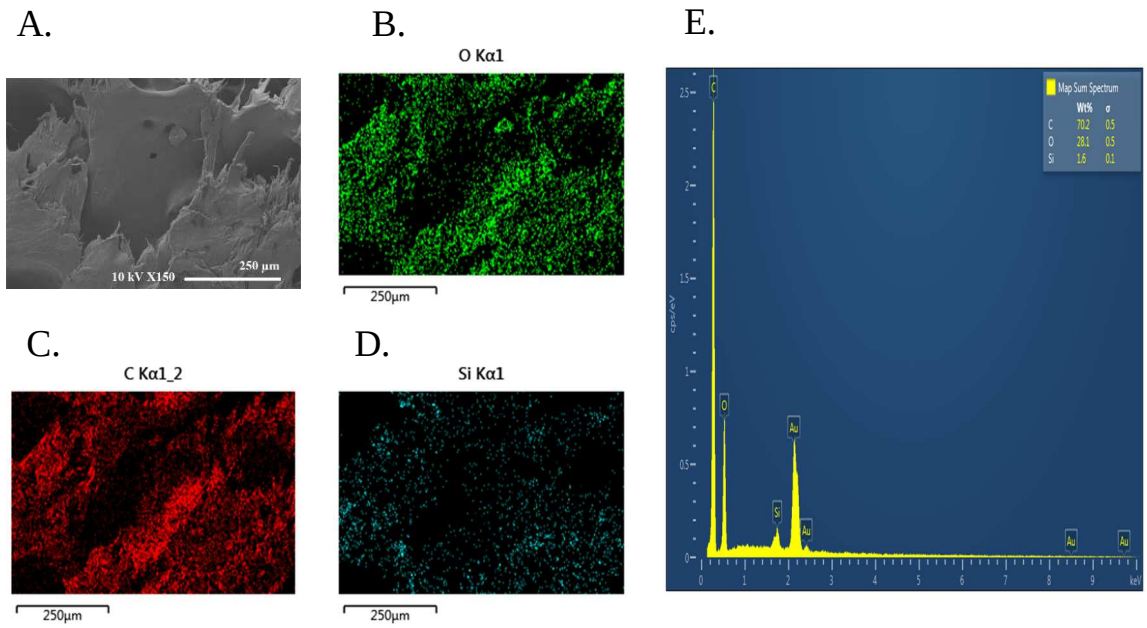

***Figure 39**. EDS mapping of the composite screw device (10 wt. % of SBA-15). A. – Obtained SEM image of the composite screw device at a magnification of X150, scale bar – 250 µm; B. – mapping image of the chemical element O; C. – mapping image of the chemical element C; D. – mapping image of the chemical element Si; E - EDS spectra of the identified chemical elements.*

By observation of Figure 39, it is possible to confirm the presence and distribution of SBA-15 nanoparticles in the composite screw device, since in Figure 39 D., the EDS mapping shows very few agglomerates of the nanoparticles, and they are clearly dispersed in all the taken sample. In the EDS spectrum, gold (Au) was detected, but this detection is neglected since the samples was sputter-coated with gold.

4. Conclusions and Future Remarks

4.1. Applications of the Produced Biomaterials in Hard Tissue Engineering

The produced porous materials in this work are proposed for applications in the field of hard tissue engineering, inducing bone/dental tissue regeneration.

The application of such porous materials in this field could be performed in several different approaches, one using the materials as a monolith, another using the obtained materials in a bone/dental cement/gel and another using the materials as a surface coating of a membrane and/or bone/dental cement.

In the first approach, the monolith is placed inside a bioreactor and osteoblasts and/or undifferentiated cells, collected from the host, are placed inside the porous materials. Then the system is submitted to mechanical and/or another stimuli (electrical/chemical) in order to induce cellular differentiation into the desired type of cells (if undifferentiated cells are used). At that moment, when a proto-tissue is formed the material supporting the proto-tissue is grafted into the bone/dental tissue of the host, under surgery. Then throughout the recovery time, the new tissue is formed around the biomaterial (which ensures structural and mechanical support during recovery time) as it starts to degrade. In this approach the prepared porous materials acts

as a monolith scaffold, and it is expected to maintain its morphological and mechanical properties throughout the needed time to form new tissue. In this type of application, the monolith has to be made of standard dimensions and shapes, employing moulds. Using SFM process it was proven to be possible, however at a commercial scale the economic valorisation of such process would only be possible by coupling an extrusion/injection blow step.

In the second approach, the obtained porous biomaterial, either composite or non-composite additivated or non-additivated, could be incorporated into a commercially available bone/dental cement and/or into a seringable gel. For this approach the obtained materials have to be reduced into fine particles, by mechanical action for example, afterwards the fine particles would be physically mixed with the bone/dental cement mixture (before application) and/or with the gel. For this specific application, the performed mechanical analysis are not very indicative how the produced porous material would perform under compression strength, since the test was performed using the biomaterials as monoliths, analysing the entire structure. So for this case, the mechanical analysis has to be reconsidered, and analyse how the produced biomaterials as fine particles would act under compression strength, with and without incorporation into the bone/dental cement/gel. Also, for this application, the existence of very large pores (millimetre range) is not needed since by reduction of the biomaterials into fine particles they would be destroyed, so concerning to the morphology of the biomaterials, in this case, the focus should be in obtaining highly porous structures (porosity) with meso and micropores with a good dispersion of inorganic fillers, like SBA-15 throughout the polymeric matrix with suitable surface area and controlled degradation rate.

For this application a bioactive compound, like a drug for example, could be incorporated into the porous material by supercritical assisted impregnation/deposition method, since it stays proven that is possible to incorporate thermal sensitive compounds in the used SFM process. By incorporation of the polymer and/or composite, carrying a bioactive compound, into the bone/dental cement/gel, this compound would be homogeneously dispersed in the matrix ensuring another mass transfer barrier, helping to achieve a more controlled release rate, depending on the specific type of application. In Figure 40 is showed the scheme of this type of proposed application of the produced biomaterials in this work, for a bone tissue engineering application.

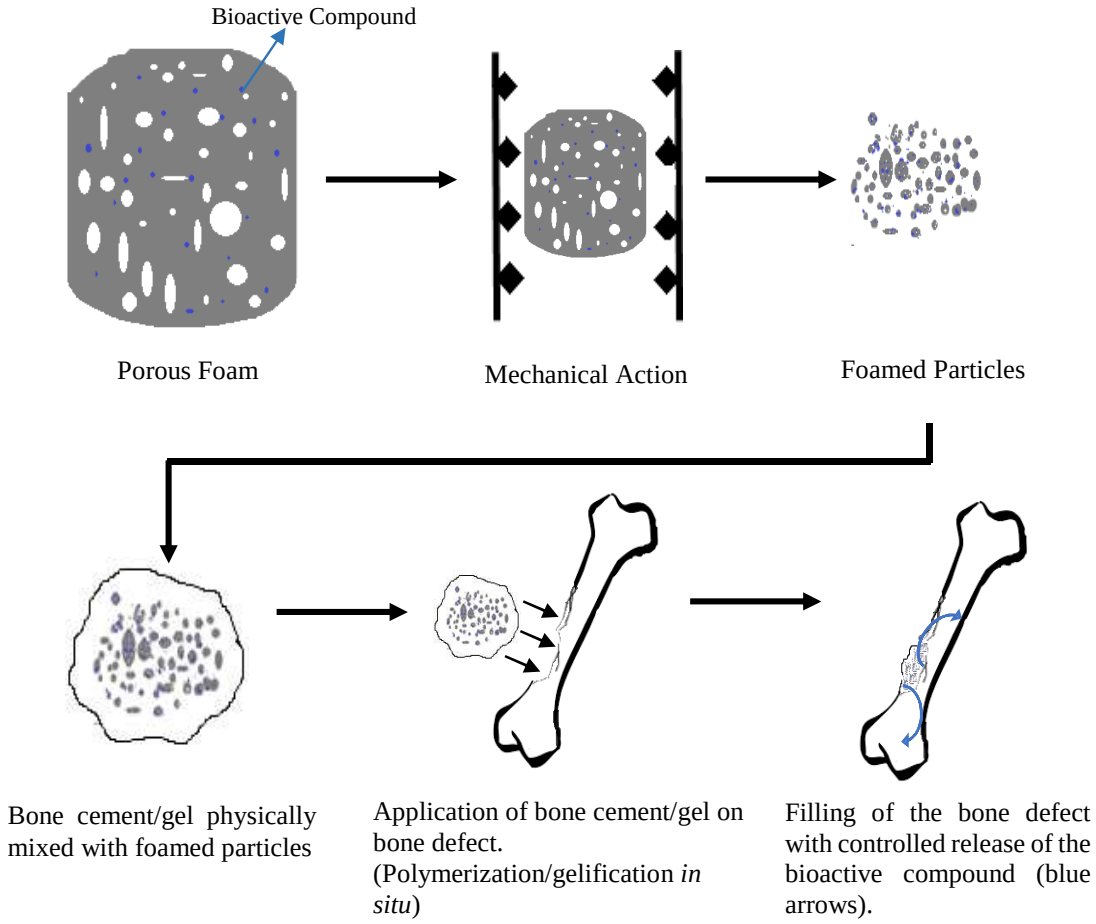

Figure 40. *Schematic representation of a proposed application of the produced biomaterialss in this work, in the field of bone tissue engineering.*

After incorporation of the fine particles of the biomaterials (with or without incorporation of a bioactive compound), the bone cement would be placed and hardened (polymerized) *in situ* physically incorporating the porous particles. Using a seringable gel with the fine particles of the biomaterials, the gel would be seringable directly into the bone defect, in which, due to the nature of gel, the matrix would totally fulfil the defect carrying the foamed particles (with or without the bioactive compound), this approach is less evasive than the previous but the gel does not ensure a suitable mechanical strength for bone tissue application, however, introducing composite foamed particles in the gel and/or the bone cement their mechanical properties are expected to be enhanced, as showed in this work.

The third proposed approach, concerns again the reduction of the prepared biomaterials into fine particles, by mechanical action for example. Then the produced porous particles would be used in order to coat a bone/dental implant. The coating of an implant with this foamed highly porous particles is very advantageous, since they provide mechanical reinforcement, greater surface area to proteins and cells to adhere and, in the case when a bioactive compound is incorporated, the controlled release of such compounds almost immediately after application (if so is desired for a specific type of application and need).

4.2. Materials with Controlled Morphologic and Mechanical Properties

In this work it was proven that is possible to produce biodegradable porous biomaterials with controlled physical properties in a green and sustainable way, using SFM technology. Such properties can be controlled by adjusting the operating conditions, the presence and composition of liquid additives such as hydrotropes (GF) and ionic liquids (TTPB) and the incorporation of inorganic particles such as SBA-15. Controlling the morphologic properties, such as porosity, pore size and surface area other properties like degradation rate can be controlled as well (despite it was not evaluated in this work).

Operating at a pressure of 20 MPa, a temperature of 40ºC, with a depressurization rate of 0.3 $MPa.min^{-1}$ for 2h it was shown to be the best operating conditions for hard tissue engineering applications with pure PCL biomaterials, obtaining suitable properties such as porosity (33.0 ± 2.5 %), BET surface area (0.4 ± 0.04 $m^2.g^{-1}$) and compression strength (1.9 ± 0.4 MPa). However operating at the same pressure and with the same saturation time but at a temperature of 45ºC and a depressurization rate of $1MPa.min^{-1}$ similar morphologic and mechanical properties appear to be found to when operating at 40ºC and 0.3 $MPa.min^{-1}$, with the advantage of a smaller global operating time. Despite it, in this work the chosen operating conditions relied on the same that were used in previous works (Rosa, 2013) since it had been proven, in this work, that they are suitable to achieve hard tissue engineering grade materials. However, and for future work to develop, this similarity on morphological and mechanical properties obtained in PCL biomaterials, operating at both operating conditions sets, must be confirmed. Also, it must be found if those similarities are maintained when other blowing agents, like GF and TTPB, are incorporated as well as when SBA-15 is incorporated in the same proportions and compositions used in this work. If similar properties are achieved, what was found in this work can be confirmed and the used SFM process can be optimized.

The blowing effect of GF and TTPB was confirmed, as well as their plasticizer effect. Revelling to be two green and safe suitable blowing agents, besides $scCO_2$. It was clear, by morphologic and crystallinity analysis, that TTPB has the greater plasticizer effect of both employed additives, since and due to its phosphonium group which has good affinity with CO_2 molecules, larger amounts of $scCO_2$ are absorbed and diffuse into the polymeric chains increasing their free movement. GF is incorporated in order to achieve better dispersion of the inorganic acting as a polymer compatibilizer between PCL and SBA-15.

Of the three used mixtures of both additives, the morphological, thermal and mechanical properties of the biomaterials appear to be improved as the amount of GF increased in the mixture. However it was always needed to incorporate the ionic liquid otherwise the biomaterials would be too brittle to handle, presenting a highly heterogeneous morphology. This approach must be further studied in future work, by reduction of the relative molar proportion to PCL, and by optimization of the amount of GF and TTPB to achieve the best morphologic and mechanical features for hard tissue engineering applications.

Incorporating an inorganic, such as SBA-15 nanoparticles, both morphologic and mechanical properties can be controlled by adjusting its composition, producing organic/inorganic composites (similar to the natural composition of hard tissue). Pore area is decreased, but surface roughness, pore number and consequently superficial area are increased, making it, therefore, possible to control the degradability rate of the material. Mechanical properties are largely improved by the addition of SBA-15 on the biomaterials, although the incorporation of

the liquid additives led into a decrease on these properties. The optimum composition of SBA-15 to incorporate in PCL-based biomaterials, additivated and non-additivated was between 20 and 30 wt. %, since with 30 wt. % it was found to be an excess of inorganic, leading among other effects to a reduction on the mechanical properties and to biomaterials with a high heterogeneous dispersion of the filler.

Other inorganics could be used in order to obtain composites for hard tissue engineering applications, as showed on the filler choice assays. HA, MMT and β-TCP, for example, could be incorporated. However, SBA-15 is more advantageous to incorporate towards the development of hard tissue engineering materials, since it has a mesoporous structure with highly orientated pores. This feature allows to incorporate a drug and/or other bioactive compound, by $scCO_2$ impregnation/deposition, on the inorganic particles, which in turn, due to its high surface area, will enhance and allow to achieve a more controlled release of such compounds suitable for the specific application (de Matos *et al*., 2013).

All the produced porous materials presented high thermal stability, showed by SDT, indicating that they are suitable to be manipulated until high temperatures as well as to employ directly into the biological medium without any change on the materials. The incorporation of TTPB and SBA-15 yielded into even more thermally stable materials due to the ionic liquids inherent thermal stability even when added in mixture with GF.

The employed SFM process, can be used to produce porous polymeric and composite devices for several applications, namely biomedical/pharmaceutical. Since, just by using a suitable mould, the desired device for a specific application, with controlled shape and sizes and with controlled morphologic, thermal and mechanical properties can be easily produced. The production of materials using moulds has numerous advantages, namely economic advantages and can increase the industrial interest in such type of manufacturing process, consequently increase the economic value of the SFM process.

4.3. Experimental Apparatus Limitations and Possible Modifications

As the diffusion path of CO_2 molecules, during depressurization, is conducted, in the used experimental apparatus, throughout the height of the biomaterials, pores with considerably different sizes are obtained. On the bottom of the biomaterials it was verified that the formed pores are much larger than in the top, due to the geometric conformation of the used apparatus. The heterogeneity on distribution of pore sizes is a desirable feature but not in this geometrical separated way. To better understand this effect, the diffusion path was changed and the mass transfer area for CO_2 during depressurization was increased. The obtained porous structure and its vertical cross section are showed in Figure 41 A and B respectively.

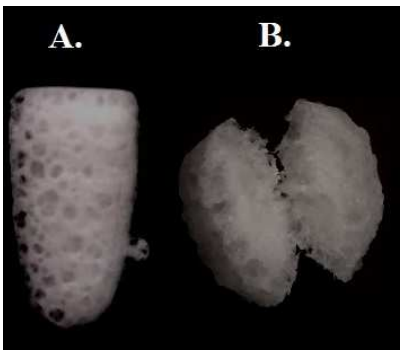

Figure 41. *Obtained porous structure with increased mass transfer area for CO_2 during depressurization prepared at P = 20 MPa, T = 40ºC, $\Delta P/\Delta t$ = 1 MPa.min^{-1} for 2h. (A) - Top view of the produced porous structure; (B) - Vertical cross section.*

As can be seen a more homogeneous pore size distribution appears to be found along the horizontal direction of the porous structure, when increasing the mass transfer area. On the base of the porous structure the existence of larger pores is not verified, since those are almost all located at the top of the porous structure. This could have happened, also, due to the increased mass transfer area and more CO_2 molecules were absorbed on the top of the sample.

From this effect, of the geometrical conformation of the used experimental apparatus, with the objective to obtain porous materials presenting heterogeneous pore size distribution, with a homogeneous spacial distribution, several geometrical conformations, concerning a changing of the diffusion path of CO_2 molecules during depressurization are proposed:

- Using a high pressure vessel with more exit points for CO_2 spatially distributed along the vertical axis;
- Using a microporous mould, ensuring a CO_2 exit more spatially distributed along the vertical and horizontal axis of the sample;
- Using a combination of these two proposes, employing several exit points coupled with a microporous mould.

Employing the first proposal, the diffusion path could still be limited, since it will only be through the top cross section of the sample, what could still yield into a heterogeneity in spatial distribution of pore sizes. With only one exit point of CO_2 molecules, even employing the second proposal, the path would be limited and favoured in the vertical direction. The last proposal seems to be the most promising, since it would not favour any diffusion path and could yield into more homogeneous spatially distributed pore sizes. In Figure 43 is showed the proposed experimental apparatus.

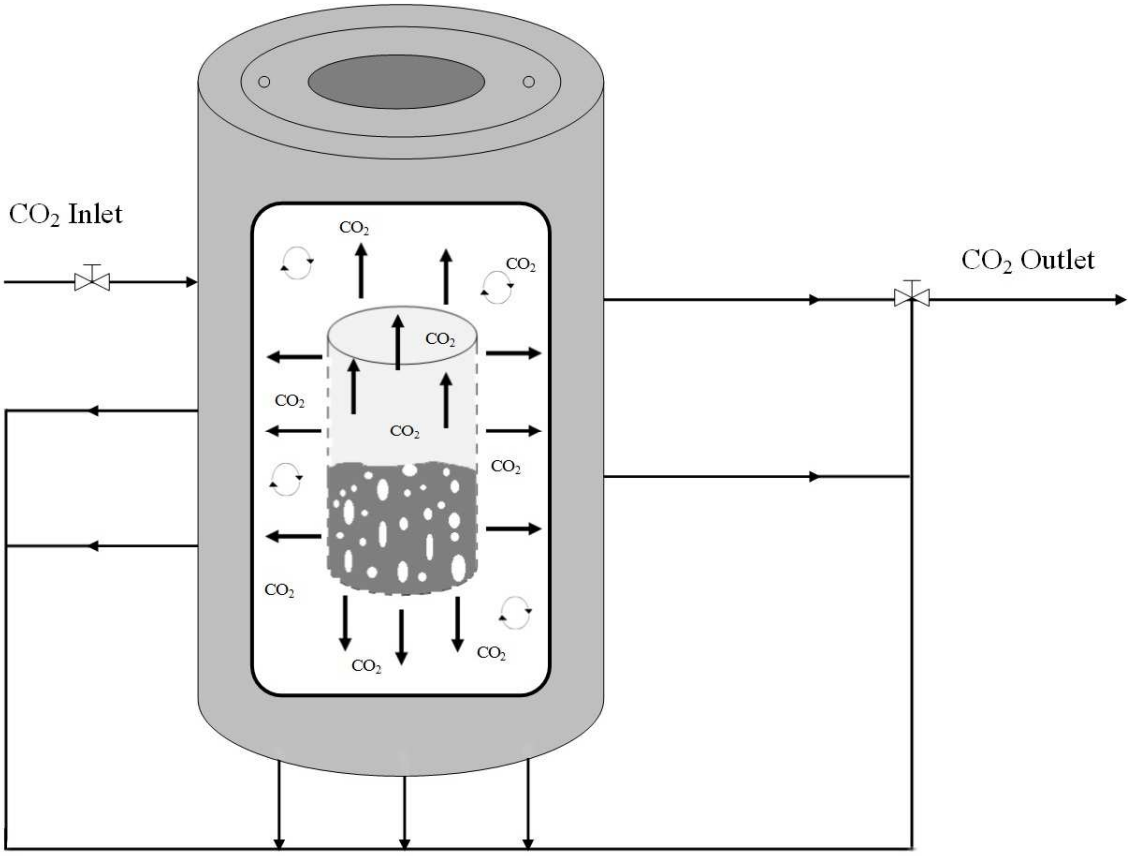

Figure 42. *Proposed new configuration of the high pressure vessel used on the experimental apparatus.*

Despite the exposed potential drawbacks of the first two proposals, in order to fully understand if they could work or not they would have to be experimented and the pore morphology spatial orientation of the produced materials analysed. The third approach is the one which is pointed to be the most promising because, on paper, it seems like so.

4.4. Future Work

Considering the results found in this work, several approaches for future work to be performed are presented, since in the available time it was not possible to test every variable and to continue the manipulation of the produced materials towards the development of a ready-to-apply material for hard tissue engineering.

Future work, should concern the production of additivated and composite biomaterials in identical compositions by the SFM process, but employing a different operating conditions set, such as P = 20 MPa, T = 45ºC, $\Delta P/\Delta t$ = 1 MPa.min^{-1} for 2h. With the objective to confirm what was reported by the optimization assays in this work. Operating at these conditions, for the same composition of GF and TTPB, the amount of SBA-15 should be increased to 30 wt. % and the experimental set started in this work, with this inorganic content, should be completed, if composite biomaterials with homogeneous dispersion of the filler are obtained, if not the findings of this work are validated.

Considering the compositions of pure and mixture of additives, used in this work, future work can be performed by varying the used compositions, with the objective to decrease the amount

of ionic liquid, since this is the most expensive additive/blowing agent. Although one should always consider that the utilization of TTPB, was verified as very advantageous, with the objective to produce morphological-controlled biomaterials with homogeneous spatial pore size distribution, as seen by the SEM analysis. Other ILs can be used, and compared to TTPB, by changing their anions and/or cations, taking into account that phosphonium groups have good affinity with CO_2 absorbing more CO_2 molecules yielding into a greater plasticizer effect.

Continuing the work line, initiated and reported by Rosa, future work could also be done, firstly by performing a cytotoxic and/or biocompatibility test of the produced materials, since no such test was done in this work, although Rosa reported the production of non-toxic materials this property should be confirmed, in order to understand the behaviour of cells and/or bacteria when in contact with the produced materials (Rosa, 2013). Secondly by incorporating a bioactive compound, dexamethasone for example due to its osteoinductive effect by $scCO_2$-assited impregnation/deposition, then proceeding as indicated in Figure 41, reducing the produced biomaterials into smaller particles and then mixing them with a bone/dental cement/seringable gel, in order to produce materials suitable to the most promising application approach, as referred. Then, the characterization methods to employ will ensure physical properties more similar to the ones found on the final material for the proposed applications (de Matos *et al*., 2013).

The formulation of the produced additivated-biomaterials, can also be changed. It can be mixed, with PCL, a biopolymer, like gelatine for example, in order to obtain porous materials with a controlled and faster degradation rate without changing the biocompatibility. The mixture with other polymers, like poly(p-dioxanone) (PDS), a room-temperature liquid polymer with high anti-bacterial action and suitable for drug delivery applications, already used in sutures, which besides its biological properties can act as a plasticizer in the SFM process (Jenkins, 2007; Website 7; Lee *et al*., 2011; Boland *et al*., 2005). Other polymers, that also revel high interest towards the production of materials for hard tissue engineering applications, are poloxamines. These polymers already revealed to have osteoinductive effect (until a certain concentration is reached) and can highly enhance the formation of new hard tissue (Rey-Rico *et al*., 2011; Puga *et al*., 2012; de Matos *et al*., 2015).

5. References

Allen T., Particle size measurement - Surface area and pore size determination, Vol.2, 5th Edition, London, Chapman and Hall, 1997.

Allhenn D., Lamprecht A., Microsphere Preparation using the untoxic solvent glycofurol, *Pharmaceutical Research*, 28 (2011) 563-571.

Andanson J-M., jutz F., Baiker A., Supercritical CO_2/Ionic liquid systems: What can we extract from infrared and Raman spectra?, *Journal of Physical Chemistry B*, 113 (2009) 10249-10254.

Andreas K., Zehbe R., Kazubek, M., Grzeschik K., Sternberg, N., Bäumler H., Schubert H., Sittinger M., Ringe J., Biodegradable insulin-loaded PLGA microspheres fabricated by three different emulsification techniques: Investigation for cartilage tissue engineering, *Acta Biomaterialia*, 7 (2011) 1485-1495.

Babu A.B., Ogle O., Tissue response: Biomaterials, dental implants and compromised osseous tissue, *Dental Clinics of North America*, 59 (2015) 305-315.

Baker K.C., Manitiu M., Bellair R., Gratopp C.A., Herkowitz H.N., Kannan R.M., Supercritical carbon dioxide processed resorbable polymer nanocomposite bone graft substitutes, *Acta Biomaterialia*, 7 (2011) 3383-3389.

Bao J-B., Liu T., Zhao L., Hu G-H., A two-step depressurization batch process for the formation of bi-modal cell structure polystyrene foams using $scCO_2$, *Journal of Supercritical Fluids*, 55 (2011) 1104-1114.

Berens A.R., Huvard G.S., Korsmeyer R.W., Kunig F.W., Application of compressed carbon dioxide in the incorporation of additives into polymers, *Journal of Applied Polymer Science*, 46 (1992) 231-242.

Bendaoud A., Chalamet Y., Effect of a supercritical fluid on starch-based polymer processed with ionic liquid, *European Polymer Journal*, 63 (2015) 237-246.

Boland E.D., Coleman B.D., Barnes C.P., Simpson D.G., Wnek G.E., Bowlin G.L., Electrospinning polydioxanone for biomedical applications, *Acta Biomaterialia*, 1(2005) 115-123.

Bonfield W., Designing porous scaffolds for tissue engineering, *Philosophical Transactions of the Royal Society A*, 364 (2006) 227-232.

Bonilla C.E.P., Trujillo S., Demirdögen B., Perilla J.E., Elcin Y.M., Ribelles J.L.G., New porous polycaprolactone-silica composites for bone regeneration, *Materials and Engineering C*, 40 (2014) 418-426.

Boongird A., Nasongkla N., Hongeng S., Sukdawong N., Sa-Nguanruang W., Larbcharoensub N., Biocompatibility study of glycofurol in rat brains, *Experimental Biology and Medicine*, 236 (2011) 77-83.

Braga M.E.M., Pato M.T.V., Silva H.S.R.C., Ferreira E.I., Gil M.H., Duarte C.M.M., de Sousa H.C., Supercritical solvent impregnation of ophthalmic drugs on chitosan derivatives, *Journal of Supercritical Fluids*, 44 (2008) 245-257.

Burg K.J.L., Porter S., Kellam J.F., Biomaterial developments for bone tissue engineering, *Biomaterials* 21 (2000) 2347-2359.

Bhamidipati M., Scurto A.M., Detamore M.S., The future of carbon dioxide for polymer processing in tissue engineering, *Tissue Engineering: Part B*, 19 (2013) 221-232.

Chen B-K., Shih C-C., Chen A.F., Ductile PLA nanocomposites with improved thermal stability, *Composites: Part A*, 43(2012) 2289-2295.

Chen B-K., Wu T-Y., Chang Y-M., Chen A.F., Ductile polylactic acid prepared with ionic liquids, *Chemical Engineering Journal*, 215-216 (2013) 886-893.

Chen L., Rende D., Schadler L.S., Ozisik R., Polymer nanocomposite foams, *Journal of Materials Chemistry A*, 1 (2013) 3837-3850.

Choi W.M., Song M.Y., Park O.O., Compressed-carbon dioxide (CO_2) assisted nanoimprint lithography using polymeric mold, *Microelectronic Engineering* 83 (2006) 1957-1960.

Collins N.J., Bridson R.H., Leeke G.A., Grover, L.M., Particle seeding enhances interconnectivity in polymeric scaffolds foamed using supercritical CO_2, *Acta Biomaterialia*, 6 (2010) 1055-1060.

Colton J.S., Suh N.P., Nucleation of microcellular foam: Theory and Practice, *Polymer Engineering and Science*, 27 (1987) 500-503.

Conaway H.H., Pirhayati A., Persson E., Pettersson U., Svensson O., Lindholm C., Henning, P., Tuckermann J., Lerner U.H., Retinoids stimulate periosteal bone resorption by enhancing the protein RANKL, a response inhibited by monomeric glucocorticoid receptor, *Journal of Biological Chemistry*, 286 (2011) 31425-31436.

Cooper A.I., Porous materials and supercritical fluids, *Advanced Materials*, 15 (2003) 1049-1059.

Costa-Pinto A.R., Reis R.L., Neves N.M., Scaffolds based bone tissue engineering: The role of chitosan, *Tissue Engineering: Part B*, 17 (2011) 1-17.

Damien C. J., Parsons J.R., Bone graft and bone graft substitutes: A review of current technology and applications, *Journal of Applied Biomaterials*, 2 (1991) 187-208.

Dash T.K., Konkimalla V.B., Poly- -caprolactone based formulations for drug delivery and tissue engineering: A review, *Journal of Controlled Release*, 158 (2012) 15-33.

Davies O.R., Lewis A.L., Whitaker M.J., Tai H., Shakesheff K.M., Howdle S.M., Applications of supercritical CO_2 in the fabrication of polymer systems for drug delivery and tissue engineering, *Advanced Drug Delivery Reviews*, 60 (2008) 373-387.

Delabarde C., Plummer C.J.G., Bourban P-E., Manson J-A.E., Biodegradable polylactide/hydroxyapatite nanocomposite foam scaffolds for bone tissue engineering applications, *Journal of Materials Science: Materials in Medicine*, 223 (2012) 1371-1385.

de Matos M.B.C., Piedade A.P., Alvarez-Lorenzo C., Concheiro A., Braga M.E.M., de Sousa H.C., Dexamethasone-loaded poly(ε-caprolactone)/silica nanoparticles composites prepared by supercritical CO_2 foaming/mixing and deposition, *International Journal of Pharmaceutics*, 456 (2013) 269-281.

de Matos M.B.C., Puga A.M., Alvarez-Lorenzo C., Concheiro A., Braga M.E.M, de Sousa H.C., Osteogenic poly(ε-caprolactone)/poloxamine homogeneous blends prepared by supercritical foaming, *International Journal of Pharmaceutics*, 479 (2015) 11-22.

Dias A.M.A., Marceneiro S., Braga M.E.M., Coelho J.F.J., Ferreira A.G.M., Simões P.N., Veiga H.I.M., Tomé L.C., Marrucho I.M., Esperança J.M.S.S., Matias A.A., Duarte C.M.M., Rebelo L.P.N., de Sousa H.C., Phosphonium-based ionic liquids as modifiers for biomedical grade poly(vinyl chloride), *Acta Biomaterialia*, 8 (2012) 1366-1379.

Donhowe I.G., Fennema O., The effects of plasticizers on crystallinity, permeability and mechanical properties of methylcellulose films, *Journal of Food Processing and Preservation* 17 (1993) 247-257.

Duarte A.R.C., Mano J.F., Reis R.L., Supercritical fluids in biomedical and tissue engineering applications: a review, *International Materials Reviews*, 54 (2009) 214-222.

Duarte A.R.C., Silva S.S., Mano J.F., Reis R.L., Ionic liquids as foaming agents of semi-crystalline natural-based polymers, *Green Chemistry*, 14 (2012) 1949-1955.

Duarte A.R.C., Santo V.E., Alves A., Silva S.S., Moreira-Silva J., Silva T.H., Marques A.P., Sousa R.A., Gomes M.E., Mano J.F., Reis R.L, Unleashing the potential of supercritical fluids for polymer processing in tissue engineering and regenerative medicine, *Journal of Supercritical Fluids*, 79 (2013) 177-185.

Duba K.S., Fiori L., Supercritical CO_2 extraction of grape seed oil: Effect of process parameters on the extraction kinetics, *Journal of Supercritical Fluids*, 98 (2015) 33-43.

Eaves D. (Ed.), Handbook of polymer foams, Crewe, U.K., Rapra Technology Limited, 2004.

Erisken C., Kalyon D.M., Wang H., Functionally graded electrospun polycaprolactone and β-tricalcium phosphate nanocomposites for tissue engineering applications, *Biomaterials*, 29 (2008) 4065-4073.

Estellés J.M., Vidaurre A., Dueñas J.M.M., Cortázar I.C., Physical characterization of polycaprolactone scaffolds, *Journal of Materials Science: Materials in Medicine*, 19 (2008) 189-195.

Fanovich M.A., Jaeger P., Sorption and diffusion of compressed carbon dioxide in polycaprolactone for the development of porous scaffolds, *Materials Science and Engineering C*, 32 (2012) 961-968.

Fanovich M.A., Ivanovic J., Misic D., Alvarez M.V., Jaeger P., Zizovic I., Eggers R., Development of polycaprolactone scaffold with antibacterial activity by an integrated supercritical extraction and impregnation process, *Journal of Supercritical Fluids*, 78 (2013) 42-43.

Fraser K.J., MacFarlane D.R., Phosphonium-based ionic liquids: An overview, *Australian Journal of Chemistry*, 62 (2009) 309-321.

Frerich S., Biopolymer foaming with supercritical CO_2-thermodynamics, foaming behaviour and mechanical characteristics, *Journal of Supercritical Fluids*, 96 (2015) 349-358.

Gilmore B.F., Antimicrobial ionic liquids, in, Kokorin, A., (Ed.), Ionic Liquids applications and perspectives, InTech, 2011.

Goodship V., Ogur E.O., Polymer Processing with Supercritical Fluids (Vol.15), Rapra Review Reports, 2004.

Goswami J., Bhatnagar N., Mohanty S., Ghosh A.K., Processing and characterization of poly(lactic acid) based bioactive composites for biomedical scaffold application, *eXPRESS Polymer Letters*, 7 (2013) 767-777.

Heikkilä T., Santos H.A., Kumar N., Murzin D.Y., Salonen J., Laaksonen T., Peltonen L., Hirvonen J., Lehto V-P., Cytotoxicity study of ordered mesoporous silica MCM-41 and SBA-15 microparticles on Caco-2-cells, *European Journal of Pharmaceutics and Biopharmaceutics*, 74 (2010) 483-494.

Hollinger J.O., Einhorn T.A., Doll B.A., Sfeir C. (Eds.), Bone tissue engineering, CRC Press, Boca Raton, 2005.

Horch R.E., Future perspectives in tissue engineering, *Journal of Cellular and Molecular Medicine*, 10 (2006) 4-6.

Hosoya A., Nakamura H., Ability of stem and progenitor cells in the dental pulp to form hard tissue, *Japanese Dental Science Review*, 51 (2015) 75-83.

Huang J-N., Jing X., Geng L-H., Chen B-Y., Mi H-Y., Peng X-F., A novel multiple soaking temperature (MST) method to prepare polylactic acid foams with bi-modal open-pore structure and their potential in tissue engineering applications, *Journal of Supercritical Fluids*, 103 (2015) 28-37.

Hudson S.P., Padera R.F., Langer R., Kohane D.S., The biocompatibility of mesoporous silicates, *Biomaterials*, 29 (2008) 4045-4055.

Izquierdo-Barba I., Sánchez-Salcedo S., Colilla M., Feito M.J., Ramírez-Santillán C., Portolés M.T., Vallet-Regí M., Inhibition of bacterial adhesion on biocompatible zwitterionic SBA-15 mesoporous material, *Acta Biomaterialia*, 7 (2011) 2977-2985.

Jaganathan H., Godin B., Biocompatibility assessment of Si-based nano- and micro-particles, *Advanced Drug Delivery Reviews*, 64 (2012) 1800-1819.

Jacobs M.A., Kemmere F., Keurentjes J.T.F., Foam processing of poly(ethylene-*co*-vinyl acetate) rubber using supercritical carbon dioxide, *Polymer*, 45 (2004) 7539-7547.

Jacobs L.J.M., Kemmere M.F., Keurentjes J.T.F., Sustainable polymer foaming using high pressure carbon dioxide: a review on fundamentals, processes and applications, *Green Chemistry*, 10 (2008) 731-738.

Jenkins M.J., Harrison K.L., Silva M.M.C.G., Whitaker M.J., Shakesheff K.M., Howdle S.M., Characterisation of microcellular foams produced from semi-crystalline PCL using supercritical carbon dioxide, *European Polymer Journal*, 42 (2006) 3145-3151.

Jiang S., Ji X., An L., Jiang B., Crystallization behaviour of PCL in hybrid confined environment, *Polymer*, 42 (2001) 3901-3907.

Karageorgiou V., Kaplan D., Porosity of 3D biomaterial scaffolds and osteogenesis, *Biomaterials*, 26 (2005) 5474-5491.

Karande T.S., Ong J.L., Agrawal C.M., Diffusion in musculoskeletal tissue engineering scaffolds: Design issues related to porosity, permeability, architecture and nutrient mixing, *Annals of Biomedical Engineering*, 32 (2004) 1728-1743.

Karimi M., Heuchel M., Weigel T., Schossig M., Hofmann D., Lendlein A., Formation and size distribution of pores in poly(ε-caprolactone) foams prepared by pressure quenching using supercritical CO_2, *Journal of Supercritical Fluids*, 61 (2012) 175-190.

Kazarian S.G., Vincent M.F., Bright F.V., Liotta C.L., Eckert C.A., Specific intermolecular interaction of carbon dioxide with polymers, *Journal of the American Chemical Society*, 118 (1996) 1729-1736.

Kazarian S.G., Polymer processing with supercritical fluids, *Polymer Science C*, 42 (2000) 78-101.

Keskin S., Kayrak-Talay D., Akman U., Hortaçsu Ö., A review of ionic liquids towards supercritical fluid application, *Journal of Supercritical Fluids*, 43 (2007) 150-180.

Kim K.H., Kim Y., Theoretical studies for the supercritical CO_2 solubility of organophosphorous molecules: Lewis acid-base interactions and C-H···O weak hydrogen bonding, *Bulletin of Korean Chemical Society*, 28 (2007) 2454-2458.

Kiran E., Liu K., Ramsdell K., Morphological changes in poly(ε-caprolactone) in dense carbon dioxide, *Polymer*, 49 (2008) 1853-1859.

Kiran E., Polymer miscibility, phase separation, morphological modifications and polymorphic transformations in dense fluids, *Journal of Supercritical Fluids*, 47 (2009) 466-483.

Kiran E., Foaming strategies for bioabsorbable polymers in supercritical fluid mixtures. Part II. Foaming poly(ε-caprolactone-co-lactide) in carbon dioxide and carbon dioxide + acetone fluid mixtures and formation of tubular foams via solution extrusion, *Journal of Supercritical Fluids*, 54 (2010) 308-319.

Klawitter J.J., Hulbert S.F., Application of porous ceramics for the attachment of load bearing internal orthopedic applications, *Journal of Biomedical Materials Research Symposium*, 2 (1971) 161-229.

Kong Y., Hay J.N., The measurement of the crystallinity of polymers by DSC, *Polymer*, 43 (2002) 3873-3878.

Kumbar S.G., Laurencin C.T, US Pat., 2011008190 A1, 2011.

Kweon H.Y., Yoo M.K., Park I.K., Kim T.H., Lee H.C., Lee H-S., Oh J-S., Akaike T., Cho C-S., A novel degradable polycaprolactone networks for tissue engineering, *Biomaterials*, 24 (2003) 801-808.

Lacroix J., Jallot E., Lao J., Gelatin-bioactive glass composites scaffolds with controlled macroporosity, *Chemical Engineering Journal*, 256 (2014) 9-13.

Lanza R., Langer R., Vacanti, J. (Eds.), Principles of Tissue Engineering, 3rd Edition, London, Elsevier Inc, 2007.

Landrock A.H. (Ed.), Handbook of plastic foams Types, properties, manufacture and applications, Noyes Publications, New Jersey, 1995.

Le Moigne N., Sauceau M., Benyakhlef M., Jemai R., Benezet J-C., Rodier E., Lopez-Cuesta J-M., Fages J., Foaming of poly(3-hydroxybutyrate-co-3-hydroxyvalerate)/organo-clays nano-biocomposites by a continuous supercritical CO_2 assisted extrusion process, *European Polymer Journal*, 61 (2014) 157-171.

Lebourg M., Antón J.S., Ribelles J.L.G., Porous membranes of PLLA-PCL blend for tissue engineering applications, *European Polymer Journal*, 44 (2008) 2207-2218.

Lee L.J., Zeng C., Cao X., Han X., Shen J., Xu G., Polymer nanocomposite foams, *Composites Science and Technology*, 65 (2005) 2344-2363.

Lee J-H., Kim J-H., Oh S-H., Kim S-J., Hah Y-S., Park B-W., Kim D.R., Rho G-J., Maeng G-H., Jeon R-H., Lee H-C., Kim J-R., Kim G-C., Kim U-K., Byun J-H., Tissue-engineered bone formation using periosteal-derived cells and polydioxanone/pluronic F127 scaffold with pre-seeded adipose tissue-derived CD146 positive endothelial-like cells, *Biomaterials*, 32 (2011) 5033-5045.

Lee C.W., Horiike M., Masutani K., Kimura Y., Characteristic cell adhesion behaviors on various derivatives of poly(3-hydroxybutyrate) (PHB) and a block copolymer of poly(3-[RS]-hydroxybutyrate) and poly(oxyethylene), *Polymer Degradation and Stability*, 111 (2015) 194-202.

Leeke G.A., Cai J., Jenkins M., Solubility of supercritical carbon dioxide in polycaprolactone (CAPA 6800) at 313 and 333 K, *Journal of Chemical and Engineering Data*, 51 (2006) 1877-1879.

Lemon G., Reinwald Y., White L.J., Howdle S.M., Shakesheff K.M., King J.R., Interconnectivity analysis of supercritical CO_2-foamed scaffolds, *Computer Methods and Programs in Biomedicine*, 106 (2012) 139-149.

Liao X., Zhang H., He T., Preparation of porous biodegradable polymer and its nanocomposites by supercritical CO_2 foaming for tissue engineering, *Journal of Nanomaterials*, 2012 (2012) 1-12.

Livi S., Pham T.N., Gérard J-F., Duchet-Rumeau J., Supercritical CO_2-ionic liquids: Green combination for preparing foams, *Chemical Engineering Journal*, 240 (2014) 534-540.

Livi S., Duchet-Rumeau J., Gérard J-F., Application of supercritical CO_2 and ionic liquids for the preparation of fluorinated nanocomposites, Journal of Colloid and Interface Science 369 (2012) 111-116.

Lu T., Li Y., Chen T., Techniques for fabrication and construction of three-dimensional scaffolds for tissue engineering, *International Journal of Nanomedicine*, 8 (2013) 337-350.

Ma P.X., Scaffolds for tissue fabrication, *Materials Today*, (2004) ISSN: 1369 7021.

Markočič E., Škerget M., Knez Ž., Effect of temperature and pressure on the behaviour of poly(ε-caprolactone) in the presence of supercritical carbon dioxide, Industrial and Engineering Chemistry Research, 2013 (52) 15594-15601.

Martins M., Craveiro R., Paiva A., Duarte A.R.C., Reis R.L., Supercritical fluid processing of natural based polymers doped with ionic liquids, *Chemical Engineering Journal*, 241 (2014) 122-130.

Mathieu L.M., Mueller T.L., Bourban P-E., Pioletti D.P., Müller R., Månson J-A. E., Architecture and properties of anisotropic polymer composite scaffolds for bone tissue engineering, *Biomaterials*, 27 (2006) 905-916.

Mattioli-Belmonte M., Vozzi G., Whulanza Y., Seggiani M., Fantauzzi V., Orsini G., Ahluwalia A., Tuning polycaprolactone-carbon nanotube composites for tissue engineering scaffolds, *Materials Science and Engineering C,* 32 (2012) 152-159.

Meyer U., The history of tissue engineering and regenerative medicine in perspective *in*: Meyer U., Meyer Th., Handschel J., Wiesmann H.P. (Eds.), Fundamentals of tissue engineering and regenerative medicine, Springer, 2009.

Mou Z-L., Zhao L-J., Zhang Q-A., Zhang J., Zhang Z-Q., Preparation of porous PLGA/HA/collagen scaffolds with supercritical CO_2 and application in osteoblast cell culture, *Journal of Supercritical Fluids*, 58 (2011) 398-406.

Nalawade S.P., Picchioni F., Janssen L.P.B.M., Supercritical carbon dioxide as a green solvent for processing polymer melts: Processing aspects and applications, *Progress in Polymer Science*, 31 (2006) 19-43.

Natu M.V., Gil M.H., de Sousa H.C., Supercritical solvent impregnation of poly(*ε*-caprolactone)/poly(oxyethylene-*b*-oxypropylene-*b*-oxyethylene) and poly(*ε* -caprolactone)/poly(ethylene-vinyl acetate) blends for controlled release applications, *Journal of Supercritical Fluids,* 47 (2008) 93-102.

Neel E.A.A., Chrzanowski W., Salih V.M., Kim H-W., Knowles J.C., Tissue engineering in dentistry, *Journal of Dentistry*, 42 (2014) 915-928.

Nishida Y., Domura R., Sakai R., Okamoto M., Arakawa S., Ishiki R., Salick M.R., Turng L-S., Fabrication of PLLA/HA composite scaffolds modified by DNA, *Polymer,* 56 (2015) 73-81.

Nofar M., Park N.C.B., Poly(lactic acid) foaming: A review, *Progress in Polymer Science*, 39 (2014) 1721-1741.

Ohtsuki C., Kamitakahara M., Miyazaki T., Coating bone-like apatite onto organic substrates using solutions mimicking body fluid, Journal of Tissue Engineering and *Regenerative Medicine,* 1 (2007) 33-38.

Oryan A., Alidadi S., Moshiri A., Maffulli N., Bone regenerative medicine: classic options, novel strategies, and future directions, *Journal of Orthopaedic Surgery and Research*, 9 (2014) 1-27.

Panda B., Parihar A.D., Mallick S., Effect of plasticizer on drug crystallinity of hydroxypropyl mehylcellulose matrix film, *International Journal of Biological Macromelecules*, 67 (2014) 295-302.

Patel H., Bonde M., Srinivasan G., Biodegradable polymer scaffold for tissue engineering, *Trends in Biomaterials and Artificial Organs,* 25 (2011) 20-29.

Puga A.M., Rey-Rico A., Magariños B., Alvarez-Lorenzo C., Concheiro A., Hot melt poly-*ε*-caprolactone/poloxamine implantable matrices for sustained delivery of ciprofloxacin, Acta Biomaterialia, 8 (2012) 1507-1518.

Ratcharak O., Sane A., Surface coating with poly(trifluoroethyl methacrylate) through rapid expansion of supercritical CO_2 solutions, *Journal of Supercritical Fluids*, 89 (2014) 106-112.

Reinwald Y., Johal R.K., Ghaemmaghami A.M., Rose F.R.A.J., Howdle S.M., Shakesheff K.M., Interconnectivity and permeability of supercritical fluid-foamed scaffolds and the effect on their structural properties on cell distribution, *Polymer*, 55 (2014) 435-444.

Reverchon E., Cardea S., Supercritical fluids in 3-D tissue engineering, *Journal of Supercritical Fluids*, 69 (2012) 97-107.

Rey-Rico A., Silva M., Couceiro J., Concheiro A., Alvarez-Lorenzo C., Osteogenic efficiency of in situ gelling poloxamine systems with and without bone morphogenetic protein-2, European Cells and Materials, 21 (2011) 317-340.

Rezwan K., Chen Q.Z., Blaker J.J., Boccaccini A.R., Biodegradable and bioactive porous polymer/inorganic composite scaffolds for bone tissue engineering, *Biomaterials*, 27 (2006) 3413-3431.

Rogers T.L., Johnston K.P., Williams III R.O., Solution-based particle formation of pharmaceutical powders by supercritical or compressed fluid CO_2 and cryogenic spray-freezing technologies, *Drug Development and Industrial Pharmacy*, 27 (2001) 1003-1015.

Rosa A.B.S., Poly (ε-caprolactone)/SBA-15 composite biomaterials plasticized with greener additives, MSc Thesis, Universidade de Coimbra, Portugal, 2013.

Rouquerol J., Baron G., Denoyel R., Giesche H., Groen J., Klobes P., Levitz P., Neimarl A.V., Rigby S., Skudas R., Sing K., Thommes M., Unger K., Liquid intrusion and alternative methods for the characterization of macroporous materials (IUPAC Technical Report), *Pure and Applied Chemistry*, 84 (2012) 107-136.

Rowe R.C., Sheskey P.J., E Quinn M. (Eds.), Handbook of pharmaceutical excipients, 6th Edition, Pharmaceutical Press, London, 2009.

Sahoo N.G., Pan Y.Z.P., He C.B., Nanocomposites for bone tissue regeneration, *Nanomedicine*, 8 (2013) 639-353.

Salerno A., Oliviero M., Di Maio E., Netti P.A., Rofani C., Colosimo A., Guida V., Dallapiccola B., Palma P., Procaccini E., Berardi A.C., Velardi F., Teti A., Iannace S., Desing of novel three-phase PCL/TZ-HA biomaterials for use in bone regeneration applications, *Journal of Materials Science: Materials in Medicine*, 21 (2010) (a) 2569-2581.

Salerno A., Zeppetelli S., Di Maio E., Iannace S., Netti P.A., Novel 3D porous multi-phase composite scaffolds based on PCL, thermoplastic zein and ha prepared via supercritical CO_2 foaming for bone regeneration, Composites Science and Technology, 70 (2010) (b) 1838-1846.

Salerno A., Di Maio E., Iannace S., Netti P.A., Solid-state supercritical CO_2 foaming of PCL and PCL-HA nano-composite: Effect of composition, thermal history and foaming process on foam pore structure, *Journal of Supercritical Fluids*, 58 (2011) 158-167.

Salerno A., Zeppetelli S., Di Maio E., Iannace S., Netti P.A., Architecture and properties of bi-modal porous scaffolds for bone regeneration prepared *via* supercritical CO_2 foaming and porogen leaching combined process, *Journal of Supercritical Fluids*, 67 (2012) 114-122.

Salerno A., Domingo C., Effect of blowing agent composition and processing parameters on the low temperature foaming of poly(L-lactide/caprolactone) co-polymer by means of supercritical CO_2/ethyl lactate binary mixtures, *Journal of Supercritical Fluids*, 84 (2013) 195-204.

Salerno A., Fanovich M.A., Pascual C.D., The effect of ethyl-lactate and ethyl-acetate plasticizers on PCL and PCL-HA composites foamed with supercritical CO_2, *Journal of Supercritical Fluids*, 95 (2014) 394-406.

Salgado A., Coutinho O.P., Reis R.L., Bone tissue engineering: State of the art and future trends, *Macromolecular Bioscience*, 4 (2004) 743-765.

Sauceau M., Fages J., Common A., Nikitine C., Rodier E., New challenges in polymer foaming: A review of extrusion processes assisted by supercritical carbon dioxide, *Progress in Polymer Science*, 36 (2011) 749-766.

Scott G. (Ed.), Mechanisms of polymer degradation and stabilisation, Elsevier, London 1990.

Sekhon B.S., Supercritical fluids technology: An overview of pharmaceutical applications, *International Journal of PharmTech Research*, 2 (2010) 810-826.

Sivalingam G., Chattopadhyay S., Madras G., Enzymatic degradation of poly(ε-caprolactone), poly(vinyl acetate) and their blends by lipases, *Chemical Engineering Science*, 58 (2003) 2911-2919.

Silva S.S., Santos T.C., Cerqueira M.T., Marques A.P., Reys L.L., Silva T.H., Caridade S.G., Mano J.F., Reis R.L., The use of ionic liquids in the processing of chitosan/silk hydrogels for biomedical applications, *Green Chemistry*, 14 (2012) 1463-1470.

Silva S.S., Duarte A.R.C., Carvalho A.P., Mano J.F., Reis R.L., Green processing of porous chitin structures for biomedical applications combining ionic liquids and supercritical fluid technology, *Acta Biomaterialia*, 7 (2011) 1166-1172.

Sultana N., Biodegradable polymer based scaffolds for bone tissue engineering, Springer, 2013.

Tai H., Mather M.L., Howard D., Wang W., White L.J., Crowe J.A., Morgan S.P., Chandra A., Williams D.J., Howdle S.M., Shakesheff K.M., Control of pore size and structure of tissue engineering scaffolds produced by supercritical fluid processing, *European Cells and Materials*, 14 (2007) 64-77.

Takahashi S., Hassler J.C., Kiran E., Melting behaviour of biodegradable polyesters in carbon dioxide at high pressures, *Journal of Supercritical Fluids*, 72 (2012) 278-287.

Tal H. (Ed.), Bone regeneration, InTech, Rijeka, 2012.

Tsimpliaraki A., Tsinvintzelis I., Marras S.I., Zuburtikudis I., Panayiotou C., The effect of surface chemistry and nanoclay loading on the microcellular structure of porous poly(D,L lactic acid) nanocomposites, *Journal of Supercritical Fluids*, 57 (2011) 278-287.

Tsimpliaraki A., Tsivintzelis I., Marras S.I., Zuburtikudis I., Panayiotou C., Foaming of PCL/clay nanocomposites with supercritical CO_2 mixtures: The effect of nanocomposite fabrication route on the clay dispersion and the final porous structure, *Journal of Supercritical Fluids*, 81 (2013) 86-91.

Uebersax L., Hagenmüller H., Hofmann S., Gruenblatt E., Müller R., Vunjak-Novakovic G., Kaplan D.L., Merkle H.P., Meinel L., Effect of scaffold design on bone morphology *in vitro*, *Tissue Engineering*, 12 (2006) 3417-3429.

Vroman I., Tighzert L., Biodegradable polymers, *Materials*, 2 (2009) 307-344.

Vrikkis R.M., Fraser K.J., Fujita K., MacFarlane D.R., Elliot G.D., Biocompatible ionic liquids: A new approach for stabilizing proteins in liquid formulation, *Journal of Biomechanical Engineering*, 131 (2009) 1-4.

Wang Y-M., Pan Y., Wang Y-L., Wu G-P., Wang Y-J., Nikitin L.N., Lu X-B., Bulk graft modification of polyolefin membranes by combining pre-irradiation-induced graft and supercritical CO_2-swelling polymerization, *Journal of Supercritical Fluids*, 44 (2008) 62-70.

Wang S., Hou L., Application of four ionic liquids as plasticizers for PVC paste resin, *Iranian Polymer Journal*, 20 (2011) 989-997.

Website1: PR Newswire, http://www.prnewswire.com/news-releases/tissue-engineering-and-regeneration-technologies-and-global-markets-300001191.html (Accessed March 11th, 2015).

Website 2: Dissemination of IT for the promotion of materials science, University of Cambridge, http://www.doitpoms.ac.uk/tlplib/bones/structure.php (Accessed March 23rd 2015).

Website 3: FDA, U.S. Food and Drug Administration, USA, *Manual of policies and procedures*, available online in http://www.fda.gov/downloads/aboutfda/centersoffices/officeofmedicalproductsandtobacco/cder/manualofpoliciesprocedures/ucm124407.pdf (Accessed April 28th 2015).

Website 4: FDA, U.S. Food and Drug Administration, USA, *Guidance for industry Q3C Impurities: Residual Solvents*, available online in http://www.fda.gov/downloads/drugs/guidancecomplianceregulatoryinformation/guidances/ucm073394.pdf (Accessed April 28th 2015).

Website 5: National Institute of Standards and Technology, USA, *Chemistry WebBook - Thermophysical Properties of Fluid Systems* available online in: http://webbook.nist.gov/cgi/fluid.cgi?Action=Load&ID=C124389&Type=IsoBar&Digits=5&P=200&THigh=60&TLow=30&TInc=5&RefState=DEF&TUnit=C&PUnit=bar&DUnit=kg%2Fm3&HUnit=kJ%2Fmol&WUnit=m%2Fs&VisUnit=Pa*s&STUnit=N%2Fm (Accessed June 24th 2015).

Website 6: Micell Technologies, Durham, USA, available online in: http://www.micell.com/technology/intellectualproperty.asp (Accessed June 27th 2015).

Website 7: Ethicon, USA, available online in: http://www.ethicon.com/healthcare-professionals/products/wound-closure/absorbable-sutures/pds-two-polydioxanone#!overview (Accessed August 2nd 2015).

Welge I., Wolf B.A., Reduction of the interfacial tension between 'immiscible' polymers: to which phase one should add a compatibilizer, Polymer, 42 (2001) 3467-3473.

Whang K., Healy K.E., Elenz D.R., Nam E.K., Tsai D.C., Thomas C.H., Nuber G.W., Glorieux F.H., Travers R., Sprague S.M., Engieering bone regeneration with bioabsorbable scaffolds with novel microarchitecture, *Tissue Engineering*, 5 (1999) 35-51.

White L.J., Hutter V., Tai H., Howdle S.M., Shakesheff K.M., The effect of processing variables on morphological and mechanical properties of supercritical CO_2 foamed scaffolds for tissue engineering, *Acta Biomaterialia*, 8 (2012) 61-71.

Woodruff M.A., Hutmacher D.W., The return of a forgotten polymer-Polycaprolactone in the 21st century, *Progress in Polymer Science*, 35 (2010) 1217-1256.

Wu C-J., Gaharwar A.K., Schexnailder P.J., Schmidt G., Development of biomedical polymer-silicate nanocomposites: A materials science perspective, *Materials*, 3 (2010) 2986-3005.

Xu Q., Ren X., Chang Y., Wang J., Yu L., Dean K., Generation of microcellular biodegradable polycaprolactone foams in supercritical carbon dioxide, Journal of Applied Polymer Science, 94 (2004) 593-597.

Xu Y., Wang C., Zhou G., Wu Y., Chen J., Improving the controlled release of water-insoluble emodin from amino functionalized mesoporous silica, *Applied Surface Science*, 258 (2012) 6366-6372.

Yang S., Leong K-F., Du Z., Chua C-K., The design of scaffolds for use in tissue engineering. Part I. Traditional factors, *Tissue Engineering*, 7 (2001) 679-689.

Ye C., Hu P., Ma M-X., Xiang Y., Liu R-G., Shang X-W., PHB/PHBHHx scaffolds and human adipose-derived stem cells for cartilage tissue engineering, *Biomaterials*, 30 (2009) 4401-4406.

Yoshimura K., Nakano K., Okamoto K., Miyake T., Mechanical and electrical properties in porous structure of Ketjenblack/silicone-rubber composites, *Sensors and Actuators A: Physical*, 180 (2012) 55-62.

Yu L., Dean K., Generation of biodegradable polycaprolactone foams in supercritical carbon dioxide, in, Smith R. (Ed.), Biodegradable polymers for industrial applications, Cambridge, CRC Press, 2005.

Yuvaraj H., Hwang H.S., Jung Y.S., Kim J-H., Hong S-S., Lim K.T., Dispersion polymerization of styrene in supercritical CO_2 in the presence of non-fluorous random copolymeric stabilizers, *Journal of Supercritical Fluids*, 42 (2007) 351-358.

Zhang Y., Leblanc-Boily V., Zhao Y., Prud'homme R.E., Wide angle X-ray diffraction investigation of crystal orientation in miscible blend of poly(-caprolactone)/poly(vinyl chloride) crystallized under strain, *Polymer*, 46 (2005) 8141-8150.

Zhang Y-R., Du W., Zhou X-D., Yu H-Y., Review of research on the mechanical properties of the human tooth, *International Journal of Oral Science*, 6 (2014) 61-69.

Zeng C., Han X., Lee L.J., Koelling K.W., Tomasko D.L., Polymer-clay nanocomposite foams prepared using carbon dioxide, *Advanced Materials*, 15 (2003) 1743-1747.

6. Supplementary Data

Note: All the presented values on supplementary data are showed with two decimal places for better understanding of the presented deviations. All the presented values of the main body of this thesis are rounded to the first decimal place from the presented values on this section.

Appendix A –Filler Selection Assays

A.1. Framework and Objectives

The main objective of these assays relies on the choice of inorganic filler towards the production of composite biomaterials, *via* supercritical carbon dioxide foaming technology, a green and sustainable method towards the production of polymeric biomaterials, for hard tissue engineering applications. The choice of optimum filler will be based on the composite biomaterial final morphological and mechanical properties, such as porosity, compressive strength and Young's Modulus, respectively.

These assays were based on:

- Production of poly(*ε*-caprolactone)-based organic/inorganic composites;
- Test hydroxyapatite (HA), mesoporous silicate SBA-15 type (SBA-15) and acidly oxidized montmorillonite (MMT) in two different compositions of 10 and 20 wt. %;
- Study and discuss the effects of adding these fillers and of their composition on the morphological and mechanical properties of the composite biomaterials;
- Detection of any limitations or any other variables which may influence the supercritical carbon dioxide foaming process.

A.2. Materials and Methods

A.2.1. Materials

The used materials towards the development of these assays are referred on section 2.1. of this thesis.

A.2.2. Methods

A.2.2.1. Preparation of PCL into powder form

PCL was prepared into powder form, accordingly to the method explained on section 2.2.1. of this thesis.

A.2.2.2. Batch solid-state foaming process with supercritical carbon dioxide technology

Composite and non-composite biomaterials were performed using the same supercritical carbon dioxide foaming process explained on section 2.2.2. The experimental process conditions are shown in Table 3, on section 2.2.2., concerning to the Filler Selection assays.

A.2.2.3. Water Absorption

The prepared composite biomaterials with both inorganic compositions were placed inside falcon tubes of approximately 50 mL, and filled until complete filling of the tube with Mili-Q water. The tubes were vortexed and repeatedly filled with Mili-Q water until complete filling

in order to completely remove all the air trapped inside the biomaterials. Subsequently the tubes were saved and allowed to stand. After 3, 6, 8 and 24 hours samples were removed from the tubes and weighed, without removing the water absorbed by these. After weighing the biomaterials were placed again inside the falcon tubes and the removing air process was repeated. Following the 24h test the samples were weighed again after 96, 120, 144, 168 and 192h, between each measurement the air removing process was repeated. The pore volume was determined based on the volume of water absorbed by the biomaterials. This property can only be determined assuming that all the pores of the biomaterial were entirely filled with water and they are all interconnected, being possible to claim that the absorbed volume of water is equal to the pore volume. The absorbed water volume is determined by the following equations,

$$m_{aw} = m_{i,foam} - m_{f,foam} \quad \text{(A1)}$$

Where m_{aw} represents the absorbed mass of water by the biomaterial (mg), $m_{i,foam}$ the initial dry mass of the biomaterial (mg), $m_{f,foam}$ the final wet mass of the biomaterial after 192h (mg).

$$V_{aw} = \frac{m_{aw}}{\rho_w(T)} \quad \text{(A2)}$$

In which V_{aw} represents the volume of absorbed water (cm^3) and $\rho_w(T)$ the water density as function of temperature, determined at the temperature in which the test was conducted ($mg.cm^{-3}$). Knowing the volume of which biomaterial, determined by equation A3, it is possible to determine the percentage of pores by volume of each biomaterial,

$$V_{foam} = A_{base} \times H \quad \text{(A3)}$$

$$V_{pore}(\%) = \frac{V_{aw} \times 100}{V_{foam}} \quad \text{(A4)}$$

Where V_{foam} represents the envelope volume of the dry biomaterial (cm^3), A_{base} represents the area of the base of each cylindrical-shaped biomaterial (cm^2), H the height of the biomaterial (cm) and V_{pore} the percentage of pores in the biomaterial volume.

A.2.2.4. Mechanical Analysis

The mechanical properties of the produced composite and non-composite biomaterials dry and after 24h and 192h submerged in Mili-Q water, namely compressive strength and Young's modulus, were assessed using a TA TX Express Enhanced texture analyser (Stable Micro systems Company) equipped with 5 kg of load cell capacity. The biomaterials were cut until a height of approximately 1.40 cm was reached and compressed to a total of 25 % with a compression rate of $1mm.s^{-1}$. The load was applied vertically down through the centre of each biomaterial. Dry measurements and water-wet measurements were performed once. The water-wet measurements were performed removing the biomaterials from the water and drying the surface without removing the absorbed water.

The compressive strength of each biomaterial is dictated by the maximum supported force at a strain of 25 %, and is determined by the following equation,

$$\sigma = \frac{F_{applied}}{A_{base}} \quad \text{(A5)}$$

In which σ represents the stress (Pa), $F_{applied}$ represents the applied force in the biomaterial (N) and A_{base} the cross-section area in which the force is applied (m^2). The strain can be defined by the ratio of total deformation and its initial height, determined by the following equation,

$$\varepsilon = 1 - \frac{h_0 - h}{h_0} \tag{A6}$$

Where ε represents the strain (mm/mm), h_0 the initial height of the biomaterial (mm) and h the final height after compression of the biomaterial (mm).

Young's modulus is determined by linear regression in the zone of plastic deformation, determined at 5 % deformation, of the curve strain *versus* stress (White *et al*., 2012).

A.3. Results and Discussion

All the produced composite and non-composite biomaterials are listed on Table A1, with the respective code and description.

Table A 1. *List of abbreviation of the produced biomaterials, and their description, at P = 20 MPa, T = 45ºC, $\Delta P/\Delta t$ = 1 MPa.min^{-1}for 2h.*

Sample	Description
Blank	poly(ε-caprolactone), $D_{part} \geq 1mm$
P10HA	poly(ε-caprolactone), $D_{part} \geq 1mm$, 10 wt. % HA
P20HA	poly(ε-caprolactone), $D_{part} \geq 1mm$, / 20 wt. % HA
P10C	poly(ε-caprolactone), $D_{part} \geq 1mm$, / 10 wt.% MMT
P20C	poly(ε-caprolactone), $D_{part} \geq 1mm$, / 20 wt.% MMT
P10S	poly(ε-caprolactone), $D_{part} \geq 1mm$, / 10 wt. % SBA-15
P20S	poly(ε-caprolactone), $D_{part} \geq 1mm$, / 20 wt. % SBA-15
P85HA10	poly(ε-caprolactone), $D_{part} \leq 0.85mm$, / 10 wt. % HA
P85C10	poly(ε-caprolactone), $D_{part} \leq 0.85mm$, / 10 wt.% MMT

A.3.1. Macroscopic Analysis

In Figure A.1 and A2 are showed the digital photographs of the produced composite biomaterials with a composition of inorganic content of 10 wt. % and 20 wt. % respectively.

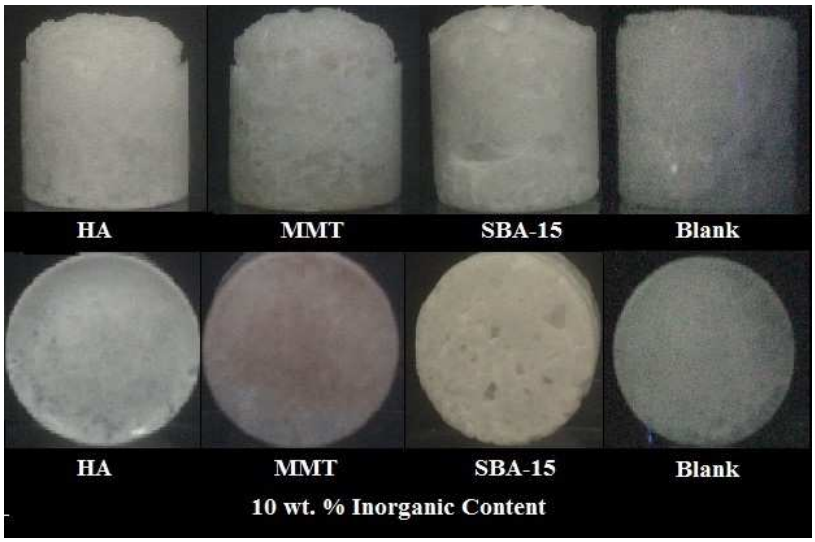

***Figure A 1**. Digital photographs of the obtained composite biomaterials with 10 wt. % of inorganic content, produced at P = 20 MPa, T = 45 ºC, $\Delta P/\Delta t$ = 1 MPa.min^{-1} for 2h. Top images lateral view. Bottom images, base view*

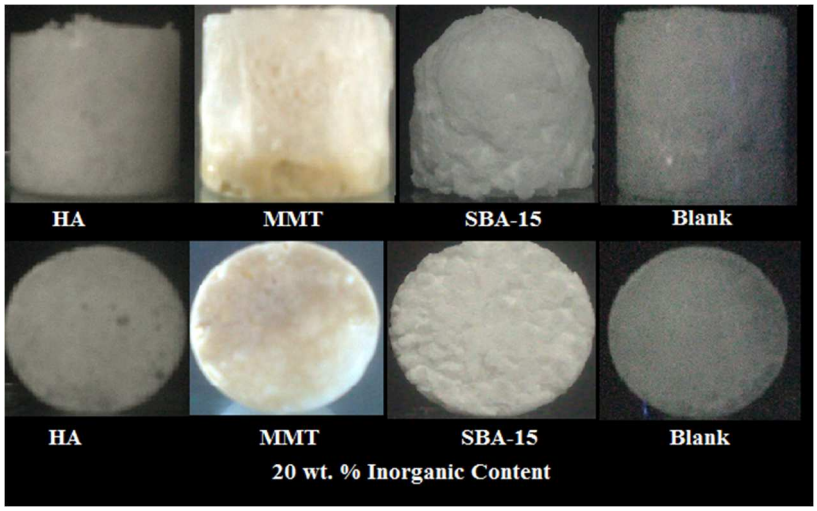

***Figure A 2**. Digital photographs of the obtained composite biomaterials with 20 wt. % of inorganic content, produced at P = 20 MPa, T = 45 ºC, $\Delta P/\Delta t$ = 1 MPa.min^{-1} for 2h.Top images lateral view. Bottom images, base view.*

As can be verified in Figures A.1 and A.2 either for both inorganic content on composites or for the non-composite biomaterial (pure PCL biomaterial), a non-porous skin around each biomaterial, was always formed. This non-porous skin is also reported in literature and is due

to the rapid diffusion of dissolved CO_2 from the borders of the material into the mould surface in contact with the molten polymer (White *et al*., 2012; Jacobs *et al*., 2008; Tsimpliaraki *et al*., 2011; Fanovich and Jaeger, 2012; Markočič *et al*., 2013; Rosa, 2013). Only on the composite biomaterial P20S, this non-porous skin was not verified. This can be explained due to the high amount of inorganic content, which due to the large difference between the diameter of PCL particles and SBA-15 nanoparticles was not possible to achieve a good physical mixture, and this might be have acted as an impurity.

Observing Figures A 1 and A 2 simultaneously it is possible to see that the produced composite are not homogeneous, being found difficult to achieve a satisfactory physical mixture between the organic and inorganic particles. That could be explained due to the enormous difference between PCL and inorganic particles diameter ($D_{part.\ PCL} \geq 1mm$, $D_{part.\ SBA\text{-}15} \approx 1\text{-}2\ \mu m$ and $D_{part.\ HA} \approx 0.17mm$) and to the difference between organic and inorganic densities ($\rho_{PCL} = 1.11\ g/cm^3$, $\rho_{MMT} = 2.01\ g/cm^3$, $\rho_{SBA-15} = 1.82\ g/cm^3$, $\rho_{HA} = 3.26\ g/cm^3$), in which the inorganics, by gravity, have the tendency to sediment on the bottom of the biomaterials. This leads to the finding of another important processing variable - stirring speed. The employed stirring during $scCO_2$ processing, was only promoting the diffusion of CO_2 molecules within the polymeric chains. Some attempts were performed using stirring promoting diffusion and stirring the mixture molten polymer + $scCO_2$ + inorganic particles, varying the stirring speed in order to obtain composites with more homogeneous spatial dispersion of the filler. The biomaterials produced by this method, had to be much larger, since after the polymer vitrifying during depressurization the magnetic stirrer was trapped inside the biomaterials which had to be later removed, ending up removing a large amount of material. Also, stirring a molten polymer is very difficult to perform due to the high viscosity of such systems. This method, besides having helped to achieve composites with more homogeneous dispersion of the filler, by visual observation, was more wasteful concerning the used material to obtain one biomaterial, and it was stated that using increasingly smaller particle diameter of PCL helped to achieve the same results, since physical mixture was enhanced.

Comparing the employed fillers, MMT appears to lead to larger pores followed by SBA-15. Increasing the amount of inorganic content from 10 to 20 wt. %, in the composite biomaterials with HA and MMT the pore size appears to be almost unchangeable. In the composite biomaterials with SBA-15 a much more visible morphological change is verified. Due to the big difference between the particles sizes PCL could not plasticized completely the inorganic particles. Also in this biomaterial is the shortest which can be indicative of the presence of very small pores and in large number. This can be due to the very large surface area of SBA-15 comparing to the other fillers ((500 $m^2.g^{-1}$ for MMT, 10.6 ± 0.1 $m2.g^{-1}$ for HA and 718 $m^2.g^{-1}$ for SBA-15) leading to an increase on contact area and interface in the $scCO_2$ processing, enhancing the heterogeneous nucleation mechanism (Wypych *et al*., 2004; Rosa, 2013).

In Figure A 3, are presented the digital photographs of the samples with smaller PCL particle size and inorganic content of HA and MMT of 10 wt. % comparing to pure PCL biomaterial.

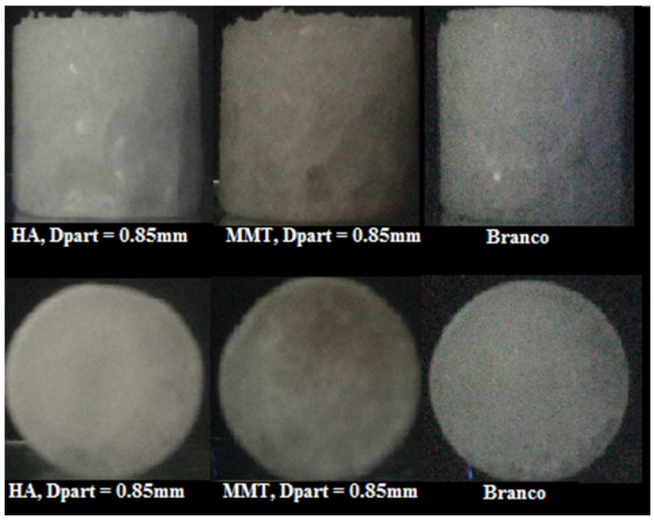

Figure A 3. *Digital photographs of the obtained composite biomaterials employing smaller PCL particle size with 10 wt. % of inorganic content, produced at P = 20 MPa, T = 45 ºC, ΔP/Δt = 1 MPa.min-1 for 2h.Top images lateral view. Bottom images, base view.*

As verified in Figure A 3 reducing the particle size of PCL powder, it was achieved a better physical mixture between the organic and inorganic particles leading to composites biomaterials with more homogeneous dispersion of the fillers (by visual observation). This result shows that just by reducing the particle size of the polymer, composites with homogeneous spatial distribution of the filler are achieved without the need to waste material, like when stirring directly the mixture.

A.3.2. Water Absorption

The water absorption test allows to determine approximately the porosity of each produced biomaterial. By diffusion, the water will enter the porous structure and fully occupy the empty space, it is assumed therefore that all the pores of the biomaterials are interconnected, allowing water to completely fill every one.

The water temperature was measured to be T = 23.30 ºC, and so the used value for water density was of ρ_{water}(23.30 ºC) = 998.20 kg.m^{-3}.

It has been found in this test the samples P20C, P20S and P10S samples have lost some of their structural integrity, beginning to lose to the aqueous medium inorganic particles from the polymeric matrix leaving these into suspension. This phenomena can be explained by the fact that the composite were not homogeneous, and in the case of the composites with SBA-15, the amount of this inorganic that was not plasticized inside the polymeric matrix was very large which lead to its rapid separation when placed in water medium. Also, the high affinity between this inorganics and water, promoted their migration from the biomaterials towards the aqueous medium.

All the presented results are normalized, concerning the initial mass of the biomaterials.

In Figure A 4. are shown the mass intake of water by the produced composites with 10 (A) and 20 B wt. % of inorganic content.

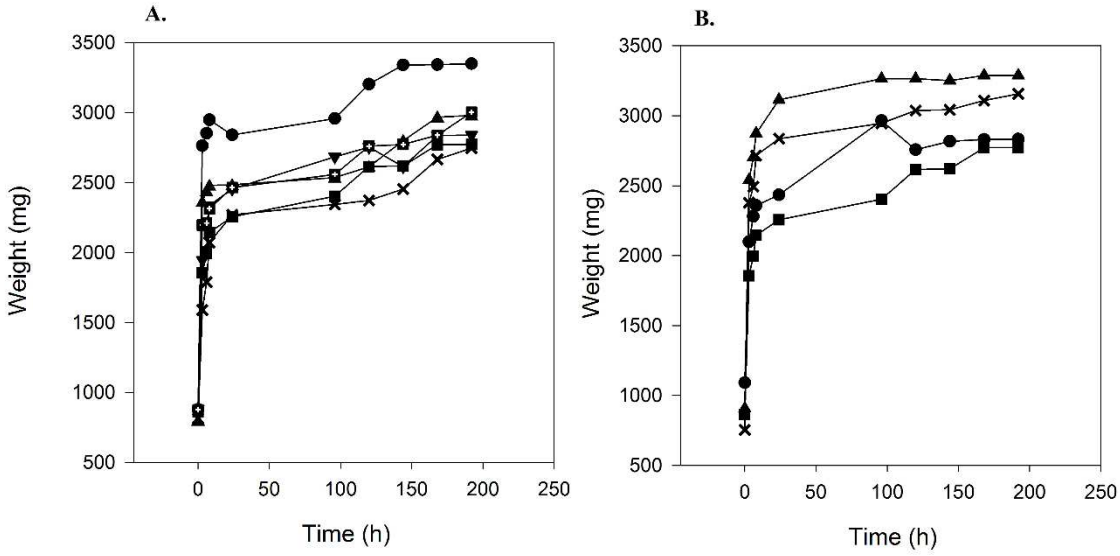

***Figure A 4**. Water intake by the composite biomaterials with 10 (A) and 20 (B) wt. % inorganic content, produced at P = 20 MPa, T = 45 C, $\Delta P/\Delta t$ = 1 MPa.min-1 and for 2h, comparing to pure PCL biomaterial. Legend: ✕ - PCL+HA, ▲ - PCL+MMT, ● - PCL+SBA-15, ■ - PCL, ▼ - P85C10, ◘ - P85HA10.*

Observing Figure A 4. A, the composite with SBA-15 is the one which can absorbe more water, which may be indicative that this composite is the one with the most porous structure. Incorporating HA, lead to a lesser intake of water, even lesser than the pure PCL biomaterial and incorporating MMT intermediate values were obtained. This can be explained not only by the porosity of the biomaterials, but also by the affinity of the inorganics with water, since PCL is hydrophobic, if the inorganic have high affinity with water, the water intake by the porous structure will be enhanced. When the PCL powder particle size is reduced, for both inorganics, similar values are obtained which might be indicative that these composites are more homogeneous, still these biomaterials present a larger intake of water, then the composites prepared with larger PCL powder particle size with the same inorganics. This is well indicative that the polymer particle size is an important processing variable which must be taken into consideration in order to achieve composites with homogeneous distribution of the filler.

When increasing the composition of inorganic in the biomaterials, as seen in Figure A 4 B, the biomaterial in which MMT was incorporated (P20C) is the one presenting larger intake of water followed by P20HA. The biomaterial in which was incorporated 20 wt. % of SBA-15 (P20S) presents smaller values of water intake, mainly due to its mass loss of inorganic particles towards the aqueous medium. In this biomaterial it was very difficult to plasticize all the inorganic particles, what could be indicative that operating at this conditions, 20 wt. % of SBA-15 can represent an excess of inorganic content for PCL. If it were not due to loss of mass in this biomaterial, it can be seen that the trend of water uptake was to obtain values higher than those of the remaining samples, which might be indicative that this biomaterial is very porous.

As mentioned, knowing the mass of water absorbed by the biomaterials, and assuming that all the pores are interconnected and filled with water it is possible to determine the pore volume and thus the volumetric percentage of pores of the biomaterials. Figure A 5 shows the percentage by volume of pores of each produced biomaterial taking into consideration the stated assumption.

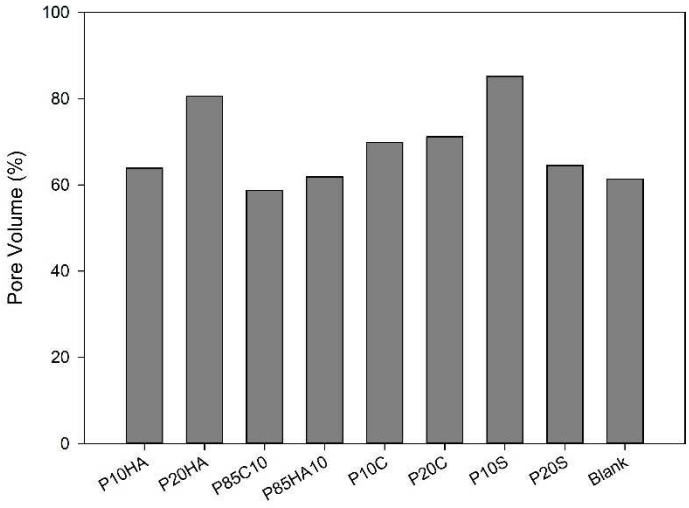

***Figure A 5**. Percentage of pore volume of the produced composite biomaterials at P = 20 MPa, T = 45 ºC,$\Delta P/\Delta t$ = 1 MPa.min-1 for 2h, based on the water absorption test for 192h.*

Through analysis of Figure A 5., it is possible to assess that SBA-15 filler is the one that ensures a greater pore volume when incorporated in a composition of 10 wt. %. This can be explained by the small size of SBA-15 nanoparticles, when comparing to HA and MMT particles, as well by its greater surface area, ensuring during depressurization greater number of nucleated bubbles then the other fillers. It would be expected, and analysing the trend that pore volume increases with the amount of filler incorporated in the composites, that the composite with 20 wt. % of SBA-15 to present larger pore volume, however this analysis was made based on the biomaterials mass gain, due to water absorption. Though, as seen previously the sample P20S had a mass loss during this test, so the obtained value for pore volume might not be accurate. Concerning to pore volume, and analysing Figure A 5, the fillers which lead to more suitable values for hard tissue engineering are HA and SBA-15, since for MMT lower values are obtained.

It stays clearly that incorporating inorganic fillers on the PCL-based biomaterials, pore volume is always increased, improving their morphologic properties towards hard tissue engineering applications.

A.3.3. Mechanical Analysis

The mechanical behaviour of the produced biomaterials is of great importance, since in their end-use application, the biomaterial should perfectly mimic in all possible features the natural tissue to substitute, in this study - hard tissue. Hard tissue is constantly undergoing mechanical stimuli of either the human body or from outside, therefore an analysis of the response to compression is relevant in order to decide which filler ensures mechanical properties closest to the natural tissue. In Figure A 6 and A 7 are shown the obtained values of compressive strength and Young's modulus, respectively as dry biomaterials A and after the water absorption test (192h contact time), wet biomaterials B.

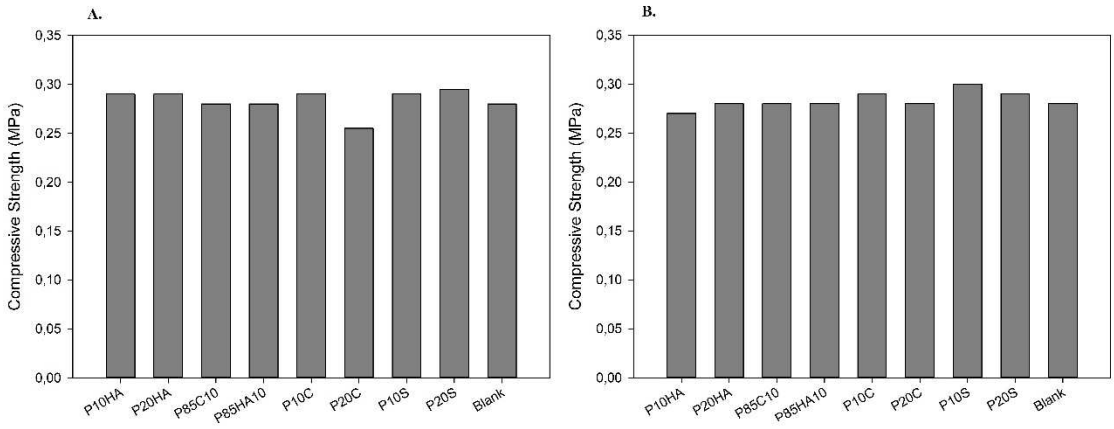

Figure A 6. *Compressive Strength of the produced composite biomaterials. A - Dry biomaterials, B - 192h water wet biomaterials.*

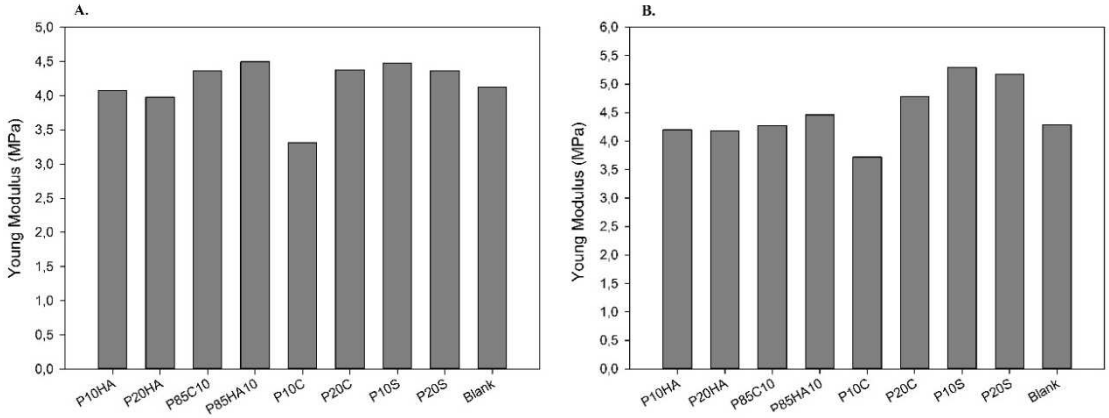

Figure A 7. *Young's modulus of the produced composite biomaterials. A - Dry biomaterials, B - 192h water-wet biomaterials.*

Analysing the compressive strength of the produced composite biomaterials, in Figure A 6 A, it can be concluded that the obtained values are very similar, but greater for composite biomaterials. It is noted that the composite with 20wt. % SBA-15 is the one with greater compression strength (0.3 MPa), however, the obtained values for the composites are all very close to each other, allowing only conclude that increasing the MMT content of the composite from 10 to 20 wt. % there is a decrease in compressive strength., which might be due to the presence of larger pores on the base of the biomaterial, originated by a phase separation between the polymer and the inorganic, as seen previously. When varying the size of PCL powder particles from >1 mm to 0.85 mm there is a slight decrease in compressive strength of the biomaterials to 0.28 MPa, for both used inorganics. This can be elucidative of composites with a more homogeneous dispersion of the filler, since no separation of phase was formed.

Same results were reported in literature, incorporating inorganics in the porous materials, producing composite materials, the mechanical properties were enhanced achieving greater values of compressive strength and Young's modulus than in non-composite polymeric-based porous materials (Salerno *et al*., 2012; Lebourg *et al*., 2008; Chang *et al*., 2006; Rosa, 2013; de Matos *et al*.,2013).

After 192h submersion of the composite biomaterials in water, observing Figure A 6 B the compressive strength slightly decreases, for example P10HA decreases from 0.29 to 0.27 MPa. This observed decreasing of compressive strength is, in general terms, negligible. It could be expected that water would decrease the mechanical properties of the biomaterials, mainly compressive strength, since PCL degrades by bulk hydrolysis, and the inorganic content could start to be released into the aqueous medium. Though, the degradation rate of PCL is very slow and a test only after 192h cannot allow to see any difference on the average pore size. Also the amount lost in some cases such as P20S was not sufficient to lead into a significant change on this mechanical property. This composite biomaterial, was also the one which yielded into greater values for compressive strength, dry and 192h water wet, which might be indicative to be a good choice for hard tissue engineering applications.

Observing Figure A 7 A, Young's modulus of the composite biomaterials, decreases when increasing the inorganic content, showing that the biomaterials became more elastic, this result is not concordant with the results found in literature, in which when the amount of inorganic content increases Young's modulus increases (Rosa, 2013; de Matos *et al*., 2013; Chang *et al*., 2006; Lebourg *et al*., 2008). P10C, obtained the lower values for Young's modulus, this could be due to an error performing the analysis. The composite biomaterials produced with lower PCL powder particle size, achieved the greater Young's modulus (4.50 and 4.36 MPa for P85HA10 and P85C10 respectively), what can be due to a more homogeneous distribution of the inorganic throughout the polymeric matrix, yet the composites with SBA-15 present closer values to these (4.48 and 4.36 MPa for P10C and P20S respectively), which can be indicative that SBA-15 is the inorganic which lead into greater Young's modulus values, considering the heterogeneity observed in these composites.

After 192h submersion of the biomaterials in water, observing Figure A 7 B, the Young's modulus increases for all the performed biomaterials. Despite the inorganic content loss observed during the water absorption test, the composite biomaterials with SBA-15 are the ones which lead into greater Young's modulus values of 5.29 and 5.27 MPa for P10S and P20S respectively. Once again this could indicative that SBA-15 can be the ideal choice for improved mechanical composite biomaterials, for hard tissue engineering applications.

A.4. Conclusions

The prepared composite biomaterials, showed by macroscopic analysis that the PCL powder particle size is a very important process parameter in order to achieve good physical mixture with all the employed inorganics, thus composite biomaterials with a homogeneous dispersion of the filler, without phase separation.

The formation of the non-porous skin layer surrounding the biomaterials is an undesired effect of the SFM process, and should be optimized in order to reduce the thickness or completely eliminate this non-porous skin. This effect affects directly the mechanical performance of the biomaterials, inducing in error, as well as it is needed to be removed adding an extra step on the batch foaming of porous structures.

All the employed inorganics have high affinity with water, and the polymeric matrix have no affinity with water since it is highly hydrophobic. This aspect, regarding surface chemistry of the inorganics also limits a homogeneous dispersion of the fillers throughout the polymeric matrix, since there is a low affinity between them. In order to avoid this and achieve better dispersion of the fillers on the hydrophobic polymer, the inorganics could be dried before mixed with the polymer, what was not performed. Also, surface chemistry modifications could be

performed and/or employing surfactant-like additives (polymer compatibilizers, for example) which would help to achieve composite biomaterials with homogeneous dispersion of the inorganics (Tsimpliaraki *et al*., 2013; Tsimpliaraki *et al*., 2011; Bonilla *et al*., 2014).

Composite biomaterials presented, for both compositions, higher porosity than pure PCL biomaterial, what is indicative that by incorporating inorganics porosity is enhanced and is a good solution towards the development of highly porous materials for hard tissue engineering applications. Incorporating 20 and 10 wt. % of HA and SBA-15 respectively yielded into the most porous materials, while incorporating MMT in both compositions similar results were found but less porous then incorporating the other inorganics.

The mechanical analysis both at dry and wet conditions revealed that under dry conditions SBA-15 is the filler which yield into mechanical improved biomaterials. However the obtained results, in general terms, were very close for all the performed composite biomaterials. This is due to the limitations of the employed test, since only a 5 kg loading cell was available, and it was not sufficient to know the true compression behaviour of the porous materials because no material was completely deformed, so the presented values for compressive strength are not corresponding to the compression at brake. This mechanical test must be questioned and a different test must be found, one which allows to apply higher loads on the materials.

From analysis of all the obtained results, the most consensual conclusion is that an organic/inorganic composite biomaterial must be manufactured towards the development of biomaterials for hard tissue engineering applications. The choice of inorganic to employ as well as its composition is not so consensual. SBA-15 yielded into biomaterials with good pore volume (in a composition of 10 wt. %) and good mechanical properties (in both compositions). However, the obtained results for porosity of HA (20 wt. %) and mechanical properties were also considerably good, MMT is the inorganic which yielded into intermediary pore volume values (for both compositions) and mechanical properties (except for a composition of 10 wt. %).

So, the obtained results are not very conclusive and future work should be done, firstly by knowing the average pore diameter of each produced biomaterial, then by changing the employed mechanical test, allowing to compress the biomaterials until brake of the material and pore collapse. The mechanical performance of the materials under wet conditions is an interesting analysis and should be performed under conditions mimicking the natural body environment in which the materials will be applied. The PCL powder particle size to employ should be the smaller possible allowing a more homogeneous physical mixture, as well as the surface chemistry of the inorganics could be modified and/or added to the mixture polymer compatibilizers and/or surfactants.

Appendix B – Optimization of Mould Surface

Using a glass vial, a non-porous skin layer was found on every produced biomaterial. This effect had already been reported in literature and is due to rapid diffusion of CO_2 molecules from the surface of the sample during depressurization (White *et al*., 2012; Jacobs *et al*., 2008; Tsimpliaraki *et al*., 2011; Fanovich and Jaeger, 2012; Markočič *et al*., 2013; Rosa, 2013; de Matos *et al*., 2013). This non-porous skin had to be removed after processing, and since cells adhere only on porous surfaces, since are ones which can provide a constant flow of nutrients, as referred on section 1 of this thesis. It also affected the mechanical performance of the biomaterials, inducing in error. These undesired effects were enhanced by the thickness of this non-porous skin.

In order to eliminate the formation of this non-porous skin or reduce its thickness, and so avoid the problems created by it, several authors refer approaches like combining to $scCO_2$ processing a porogen leaching step, adding a salt, for example, to the mixture which is later removed reporting a porous feature of the non-porous skin (Salerno *et al*., 2012). This approach brings extra concerns to the toxicity of the produced biomaterials, since for removal of the porogen an organic solvent usually is employed and/or residual amounts of porogen can be left on the biomaterial increasing its toxicity. Since for biomedical/pharmaceutical applications, and on this specific work, for hard tissue engineering applications, a non-toxic biomaterial must be employed, and in this work following the green chemistry ideology the use of this technique would be contrary to the main goal of this work. So, towards elimination or reducing the thickness of the non-porous skin, several approaches were made concerning the mould surface and type of mould.

Since no other type of mould was available, with suitable dimensions to fit inside the high pressure vessel, the glass vial was used, but lined with other film materials, in order to change the mould surface chemistry. Three attempts were made, with three different materials lining the glass vial, glass (without lining), PTFE film and acetate film. This test was performed processing pure PCL (1g) biomaterials, at P = 20 MPa, T = 45 ºC, $\Delta P/\Delta t$ = 1 MPa.min^{-1} for 2h.

In Figure B 1 are showed the digital photographs of the obtained porous materials with the three different films on the surface of the mould.

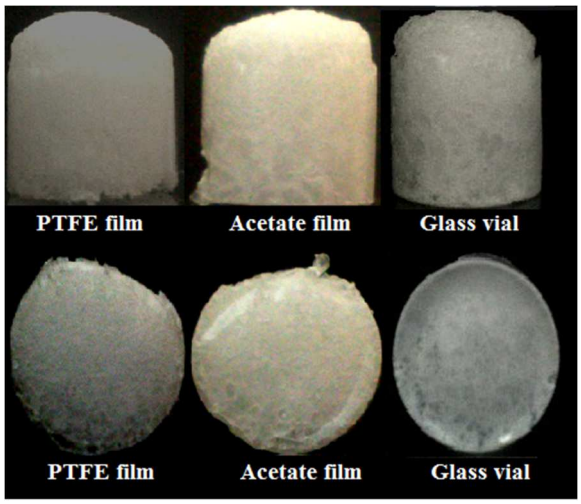

Figure B 1. *Obtained porous materials with three different materials on the surface of the mould, processed at P = 20 MPa, T = 45 ºC,* $\Delta P/\Delta t$ *= 1 MPa.min*$^{-1}$ *for 2h.*

As observed on Figure B 1, when using a glass vial the non-porous skin presents a considerable thickness, although not measured so all the affirmations are made based on visual observations. In this case the porous material was stuck on the glass, and so the vial had to be destroyed so the material could be removed.

Lining the vial with an acetate film the obtained non-porous skin was even thicker and brighter when exposed to light, than with the glass surface. In this case, the porous material did not stuck into the surface of the mould, being able to be removed without sacrificing the mould. Due to the increased thickness of the non-porous skin, in this case, its removal was even more difficult.

When processing PCL with a film of PTFE on the mould surface, the thickness of the non-porous skin was significantly reduced, being much lower than when processing with other surfaces. However there was still a formation of a non-porous skin, as reported in literature, when using PTFE moulds, but a thickness reduction of this layer was never reported, in the best knowledge (Reinwald *et al.*, 2013). Using PTFE film, the porous material did not stuck to the mould, and it has been possible to be removed easily without sacrificing it. This can be due to the high hydrophobicity feature of PTFE, even higher than PCL, which repeals the molten polymer, and when vitrifying during depressurization it does not stick to the surface of the mould/vial. This effect could be confirmed analysing the contact angle between molten PCL and PTFE, but was not performed during this work.

Observing Figure B 1, and based on the visual observations the ideal material for the mould is PTFE. With this material, the non-porous skin thickness is largely decreased and the mould becomes reusable for every processed biomaterial. Also, employing a different material on the mould, making it reusable, improving a drawback of $scCO_2$ processing, without increasing toxicity of the final biomaterials is an excellent alternative for the proposed techniques for removal of the non-porous skin.

Based on the obtained results, all the produced biomaterials will be performed with a PTFE mould, as shown in Figure B 2.

Appendix C – Heights and Diameters of the Produced Biomaterials

For determination of mechanical properties of the biomaterials, their heights and diameters must be known.

The diameter of the produced biomaterials varied little due to radial constraints ensured by the shape of the mould, since in this direction there is little or no available space for the biomaterial to grow during depressurization. So, the diameter of the biomaterials is almost equal to the diameter of the employed mould.

The height of the biomaterials varied greatly according to the employed operating conditions and to the inorganic content and/or incorporated additives (and their proportion when incorporated in mixture). This happened because in the vertical direction there was more available space for the biomaterial to grow. Under conditions that provide the formation of larger pores a greater increase in height was verified, due to the more occupied space by those pores and in contrary conditions a reduction in height was verified since smaller pores were formed.

For the mechanical analysis, as referred on section 2.3.3, the biomaterials were cut, in order to achieve a cross-section on the top.

In Table C 1 are presented the heights and diameters of the produced biomaterials for the optimization assays.

Table C 1. *Foaming heights and mechanical analysis heights used for determination of the mechanical properties of the produced biomaterials for the optimization assays.*

Temperature (ºC)	$\Delta P/\Delta t$ **(MPa.min^{-1})**	**Foaming height (cm)**	**Mechanical analysis height (cm)**
35	0.3	0.83 ± 0.08	0.83 ± 0.08
	1	0.89 ± 0.01	0.89 ± 0.01
40	0.3	1.65 ± 0.06	1.36 ± 0.02
	1	0.73 ± 0.03	0.73 ± 0.03
45	0.3	2.04 ± 0.29	2.04 ± 0.29
	1	2.00 ± 0.32	1.56 ± 0.08
50	0.3	2.27 ± 0.07	1.69 ± 0.04
	1	1.91 ± 0.19	1.78 ± 0.06

In Table C 2 are presented the heights and diameters of the produced biomaterials for the additivated and composite assays.

***Table C 2**. Foaming heights and mechanical analysis heights used for determination of the mechanical properties of the produced biomaterials for the additivated and composite assays.*

SBA-15 content (wt. %)	Biomaterials Composition	Foaming Height (cm)	Mechanical height (cm)
0	PCL	1.65 ± 0.06	1.36 ± 0.02
	PCL+GF	2.01 ± 0.11	1.90 ± 0.23
	PCL+TTPB	1.69 ± 0.03	1.53 ± 0.01
	PCL+GF+TTPB (2:1)	3.21 ± 0.45	3.21 ± 0.45
	PCL+GF+TTPB (3:1)	2.25 ± 0.12	1.85 ± 0.07
	PCL+GF+TTPB (5:1)	2.50 ± 0.15	2.20 ± 0.01
20	PCL	1.08 ± 0.06	1.08 ± 0.06
	PCL+GF	2.07 ± 0.17	1.84 ± 0.16
	PCL+TTPB	1.75 ± 0.02	1.42 ± 0.20
	PCL+GF+TTPB (2:1)	2.33 ± 0.38	1.73 ± 0.59
	PCL+GF+TTPB (3:1)	2.10 ± 0.17	1.74 ± 0.37
	PCL+GF+TTPB (5:1)	1.79 ± 0.07	1.40 ± 0.04
30	PCL	1.17 ±0.05	1.17 ± 0.05
	PCL+GF	1.48 ± 0.29	1.45 ± 0.26
	PCL+GF+TTPB (2:1)	2.51	1.11

The produced replicas of the composite biomaterial (30 wt. %) additivated with a mixture of the two additives in a molar proportion of 2:1, presented always very non-reproducible structures, with a very heterogeneous distribution of large pores mainly on the top section of the biomaterials as previously seen on Figure 16. Since only one biomaterial, produced with this composition present a slightly ordered structure, the one seen in Figure 16, its height was measured and presented on Table C 2

Appendix D – Obtained Results from Mercury Intrusion, Nitrogen Adsorption and Helium Picnometry

Table D 1. *Obtained values from Helium picnometry, Mercury intrusion and Nitrogen adsorption of the produced biomaterials for the optimization assays.*

Temperature (ºC)	**$\Delta P/\Delta t$ (MPa.min^{-1})**	**Helium Picnometry**	**Mercury Intrusion**				**Nitrogen Adsorption**		
		Real Density (g.cm^{-3})	Average Pore Diameter (µm)	Porosity (%)	Skeletal Density (g.cm^{-3})	Bulk Density (g.cm^{-3})	BET Surface Area (m^2.g^{-1})	Pore Volume (cm^3.g) ×10^4	Average Pore Diameter (Å)
35	0.3	1.24 ± 0.12	0.48 ± 0.02	33.63 ± 0.90	1.07 ± 0.01	0.71 ± 0.01	0.25 ± 0.01	3.41 ± 0.42	51.21 ± 5.58
	1	1.05 ± 0.04	0.21 ± 0.02	39.80 ± 5.73	1.03 ± 0.02	0.61 ± 0.06	0.41 ± 0.07	5.50 ± 0.92	54.25 ± 0.68
40	0.3	1.14 ± 0.01	0.47 ± 0.01	32.98 ± 2.50	1.09 ± 0.03	0.73 ± 0.04	0.44 ± 0.04	4.64 ± 0.10	112.52 ± 2.65
	1	1.12 ± 0.01	0.35 ± 0.10	36.55 ± 1.33	1.07 ± 0.01	0.68 ± 0.01	0.54 ± 0.04	1.48 ± 0.88	50.88 ± 5.73
45	0.3	1.12 ± 0.01	0.07 ± 0.02	12.79 ± 4.88	1.13 ±0.03	0.99 ± 0.07	0.98 ± 0.19	8.20 ± 1.11	44.10 ± 2.09
	1	1.13 ± 0.01	0.55 ± 0.01	46.15 ± 6.81	1.06 ± 0.02	0.57 ± 0.07	0.57 ± 0.07	6.03 ± 0.45	106.82 ± 2.17
50	1	1.11 ± 0.01	0.08 ± 0.01	15.85 ± 1.89	1.12 ± 0.03	0.94 ± 0.04	0.68 ± 0.05	5.98 ± 0.42	42.25 ± 5.11

In Table D 2, are presented the obtained values from mercury intrusion, of porosity and total pore area, for every defined pore size range in order to understand the heterogeneity of pore size distribution of the produced biomaterials from the optimization assays as well as the distribution of porosity for each pore size interval.

Table D 2. *Total pore area and porosity for each pore size interval, obtained from mercury intrusion for the produced biomaterials from the optimization assays. TPA – Total Pore Area.*

Pore Size Range (µm)	Temperature (ºC)	35		40		45		50
	$\Delta P/\Delta t$ (MPa.min^{-1})	0.3	1	0.3	1	0.3	1	0.3
0.0055 – 0.05	TPA (m^2.g^{-1})	6.04 ± 0.64	7.95 ± 1.28	5.12 ± 2.65	5.91 ± 2.25	7.64 ± 1.69	6.69 ± 0.48	8.17 ± 2.00
	Porosity (%)	1.04 ± 0.11	1.57 ± 0.11	0.85 ± 0.41	1.02 ± 0.27	1.61 ± 0.33	0.85 ± 0.04	1.68 ± 0.37
0.05 – 0.1	TPA (m^2.g^{-1})	0.09 ± 0.03	1.55 ± 0.36	0.01 ± 0.00	0.30 ± 0.10	0.02 ± 0.01	0.09 ± 0.03	0.04 ± 0.00
	Porosity (%)	0.13 ± 0.04	1.71 ± 0.31	0.02 ± 0.00	0.36 ± 0.12	0.04 ± 0.01	0.09 ± 0.03	0.08 ± 0.01
0.1 – 0.5	TPA (m^2.g^{-1})	0.21 ± 0.07	2.34 ± 1.12	0.04 ± 0.03	0.01 ± 0.00	0.01 ± 0.01	0.14 ± 0.08	0.01 ± 0.01
	Porosity (%)	0.85 ± 0.31	6.57 ± 2.58	0.22 ± 0.19	1.13 ± 0.45	0.24 ± 0.03	1.00 ± 0.08	0.19 ± 0.06
0.5 – 1	TPA (m^2.g^{-1})	0.08 ± 0.03	0.30 ± 0.13	0.05 ± 0.01	0.07 ± 0.02	0.01 ± 0.00	0.08 ± 0.03	0.01 ± 0.00
	Porosity (%)	1.06 ± 0.34	3.24 ± 1.12	0.27 ± 0.03	0.90 ± 0.25	0.13 ± 0.07	1.04 ± 0.08	0.18 ± 0.05
1 - 10	TPA (m^2.g^{-1})	0.11 ± 0.04	0.24 ± 0.08	0.11 ± 0.07	0.10 ± 0.02	0.00 ± 0.00	0.09 ± 0.03	0.02 ± 0.00
	Porosity (%)	5.36 ± 1.54	8.93 ± 1.90	5.65 ± 2.01	4.69 ± 1.10	1.12 ± 0.37	3.58 ± 0.68	1.77 ± 0.43
10 - 50	TPA (m^2.g^{-1})	0.02 ± 0.00	0.03 ± 0.00	0.02 ± 0.00	0.03 ± 0.00	0.01 ± 0.00	0.01 ± 0.00	0.00 ± 0.00
	Porosity (%)	9.50 ± 0.53	9.00 ± 0.95	5.70 ± 0.90	11.37 ± 0.89	2.05 ± 0.40	10.58 ± 2.01	3.66 ± 2.98
50 - 100	TPA (m^2.g^{-1}) ×10^3	5.00 ± 0.70	3.50 ± 0.50	5.75 ± 1.09	6.00 ± 1.41	1.25 ± 0.43	13.00 ± 4.74	1.50 ± 0.87
	Porosity (%)	6.49 ± 1.08	4.00 ± 1.16	7.93 ± 1.82	8.48 ± 2.16	1.83 ± 0.84	13.30 ± 3.88	1.84 ± 0.43
100 - 150	TPA (m^2.g^{-1}) ×10^3	2.75 ± 0.83	2.25 ± 0.43	3.25 ± 0.11	2.00 ± 0.00	2.25 ± 1.09	4.67 ± 1.25	1.75 ± 0.83
	Porosity (%)	5.89 ± 2.09	4.12 ± 0.42	7.44 ± 2.90	4.70 ± 0.26	4.78 ± 1.38	8.55 ± 1.13	5.50 ± 1.70
150 - 360	TPA (m^2.g^{-1}) ×10^3	2.00 ± 0.00	1.00 ± 0.00	1.50 ± 0.87	1.25 ± 0.43	0.75 ± 0.43	2.75 ± 0.83	1.00 ± 0.00
	Porosity (%)	6.97 ± 0.43	2.27 ± 0.18	3.62 ± 1.00	4.79 ± 1.44	3.64 ± 0.49	6.56 ± 1.53	3.47 0.86±

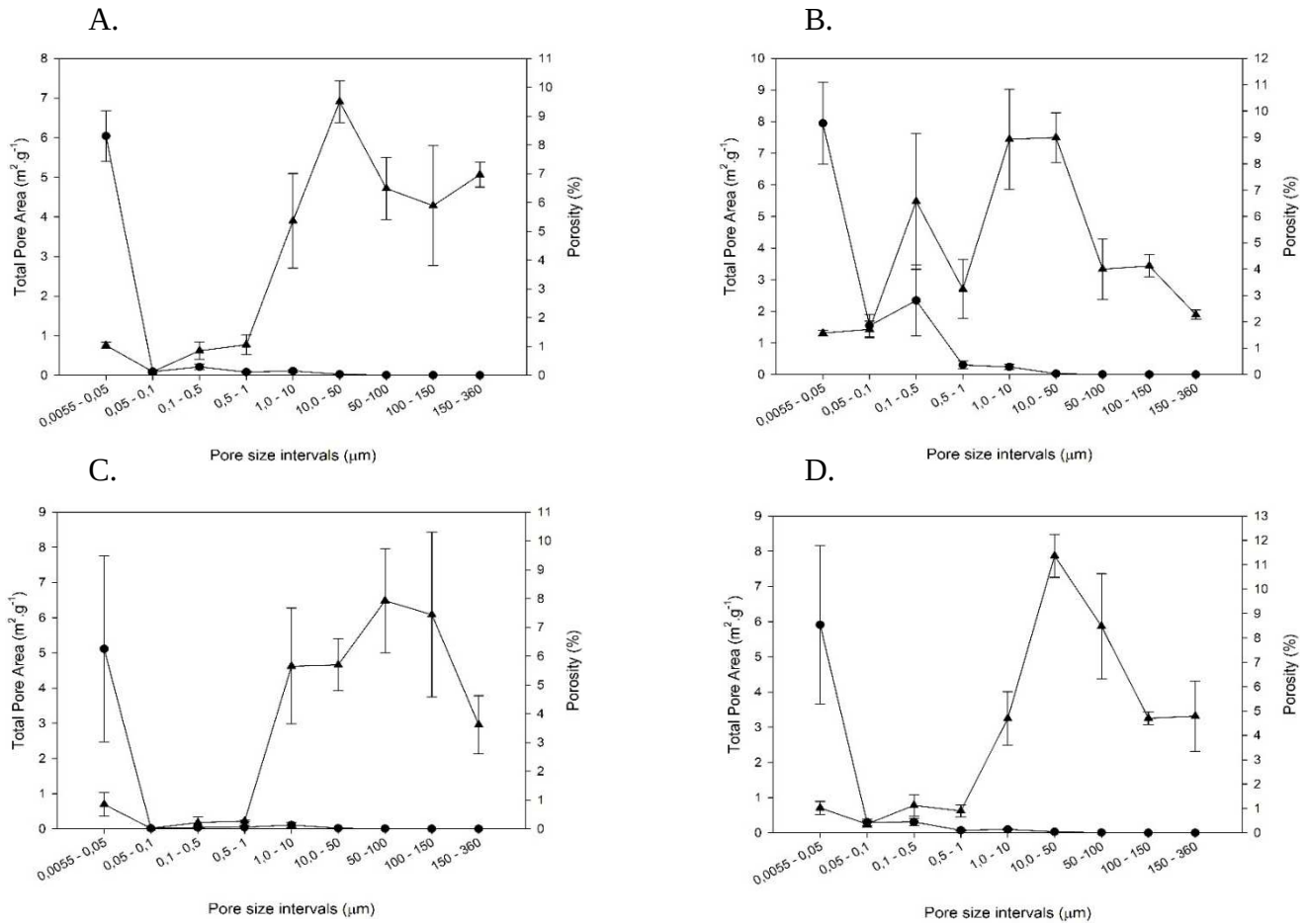

Figure D 1. *Total pore area (●) and porosity (▲) of the produced foams from the optimization assays, from mercury intrusion for every defined pore size interval. A – Foam produced at P = 20 MPa, T = 35ºC and $\Delta P/\Delta t$ = 0.3 MPa.min^{-1}; B - Foam produced at P = 20 MPa, T = 35ºC and $\Delta P/\Delta t$ = 1 MPa.min^{-1}; C - Foam produced at P = 20 MPa, T = 40ºC and $\Delta P/\Delta t$ = 0.3 MPa.min^{-1} and D - Foam produced at P = 20 MPa, T = 40ºC and $\Delta P/\Delta t$ = 1 MPa.min^{-1}, for 2h.*

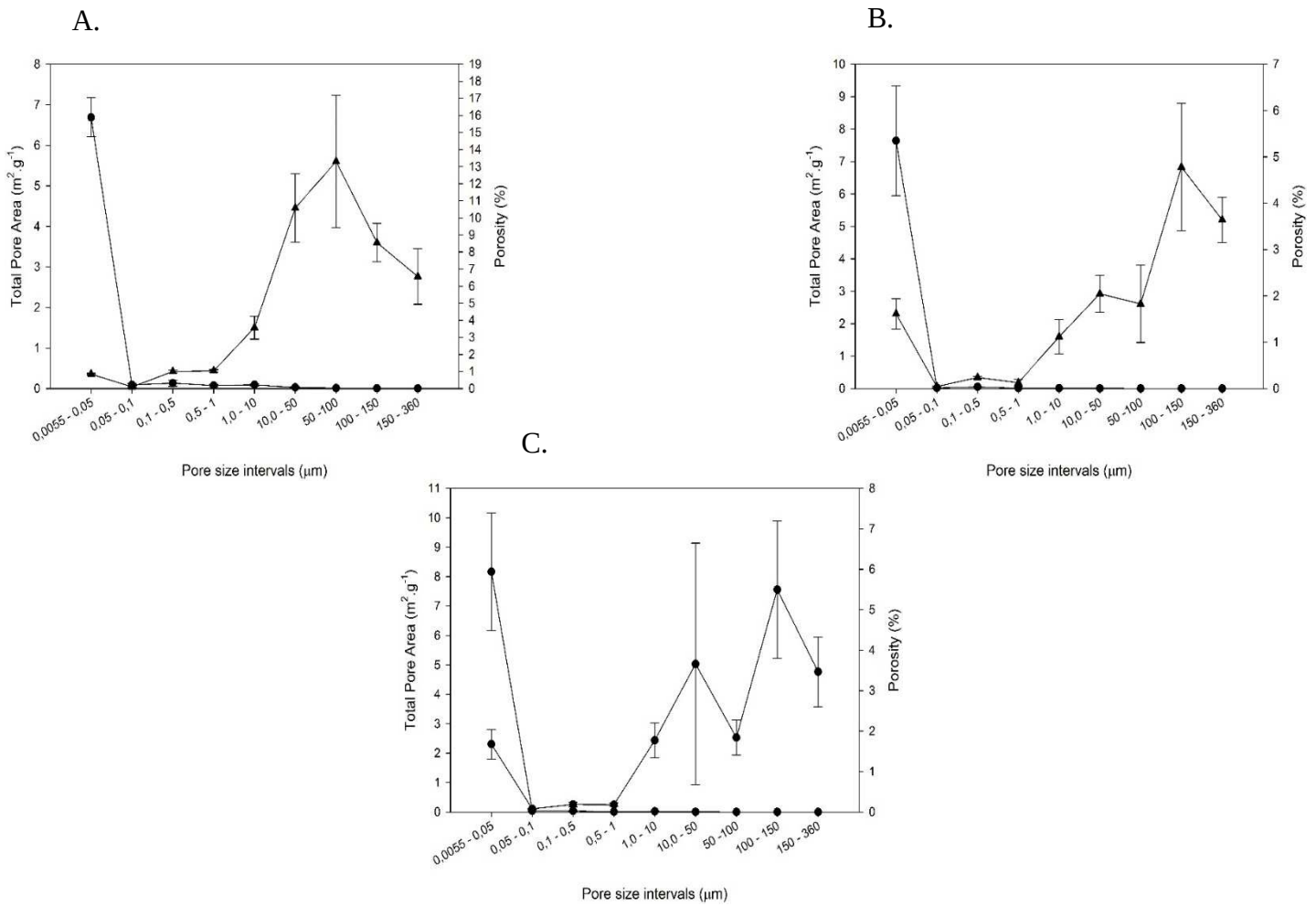

Figure D 2. *Total pore area (●) and porosity (▲) of the produced foams from the optimization assays, from mercury intrusion for every defined pore size interval. A – Foam produced at P = 20 MPa, T = 45ºC and $\Delta P/\Delta t$ = 0.3 MPa.min^{-1}; B - Foam produced at P = 20 MPa, T = 45ºC and $\Delta P/\Delta t$ = 1 MPa.min^{-1}; C - Foam produced at P = 20 MPa, T = 50ºC and $\Delta P/\Delta t$ = 0.3 MPa.min^{-1}, for 2h.*

***Table D 3**. Obtained values from Helium picnometry, Mercury intrusion and Nitrogen adsorption of the produced biomaterials for the additivated and composite assays. Prepared at $P = 20$ MPa $T = 40$ ºC, $\Delta P/\Delta t = 0.3$ MPa.min^{-1} for 2h.*

SBA-15 Composition (wt. %)	**Biomaterials Compostion**	**Helium Picnometry**	**Mercury Intrusion**				**Nitrogen Adsorption**			
		Real Density (g.cm^{-3})	Average Pore Diameter (µm)	Porosity (%)	Skeletal Density (g.cm^{-3})	Bulk Density (g.cm^{-3})	BET Surface Area (m^2.g^{-1})	BJH Surface Area (m^2.g^{-1})	Pore Volume (cm^3.g^{-1}) ×10^4	BET Average Pore Diameter (Å)
0	PCL	1.09 ± 0.01	0.16 ± 0.01	28.53±1.06	1.05±0.01	0.75±0.02	0.84 ± 0.10	0.60 ± 0.21	4.69 ± 1.40	21.89±4.02
	PCL+GF	1.09 ± 0.01	0.04 ± 0.01	8.68±1.64	1.09±0.01	1.00±0.01	1.51 ± 0.01	0.06 ± 0.06	5.45 ± 5.20	13.25±0.11
	PCL+TTPB	1.09 ± 0.00	0.25 ± 0.05	41.16±0.21	1.00±0.02	0.59±0.01	3.58 ± 0.5	3.00 ± 0.91	25.04 ± 5.88	27.62 ± 2.70
	PCL+GF+TTPB (2:1)	1.09 ± 0.01	0.04 ± 0.00	10.78±0.35	1.08±0.03	0.96±0.03	2.27 ± 0.38	1.93 ± 0.24	17.80± 7.09	30.22±7.49
	PCL+GF+TTPB (3:1)	1.09 ± 0.01	0.18 ± 0.03	30.45±3.87	1.13±0.01	0.79±0.05	1.91 ± 0.46	1.78 ± 0.47	56.00±45.20	100.32±70.39
	PCL+GF+TTPB (5:1)	1.11 ± 0.03	0.08 ± 0.03	19.52±5.65	1.09±0.01	0.87±0.07	1.23 ± 0.06	0.41 ± 0.23	6.63 ± 4.40	21.70±2.47
20	PCL	1.20 ± 0.00	0.35 ± 0.04	43.77±3.13	1.14±0.01	0.64±0.03	1.49 ± 0.03	1.70 ± 0.04	24.70 ± 1.32	66.16±2.11
	PCL+GF	1.19 ± 0.00	0.27 ± 0.05	28.56±4.68	1.19±0.01	0.85±0.06	0.64 ± 0.01	0.54 ± 0.06	33.08 ± 0.43	206.12±0.50
	PCL+TTPB	1.19 ± 0.01	0.21 ± 0.05	34.96±4.77	1.12±0.03	0.73±0.03	1.72 ± 0.13	1.66 ± 0.19	18.80 ± 2.92	43.28±3.52
	PCL+GF+TTPB (2:1)	1.18 ± 0.01	0.06 ± 0.01	15.85±0.86	1.14±0.01	0.96±0.00	0.54 ± 0.02	0.49 ± 0.04	8.89 ± 0.66	65.53±2.72
	PCL+GF+TTPB (3:1)	1.17 ± 0.00	0.15 ± 0.02	27.53±2.62	1.17±0.02	0.85±0.02	1.29 ± 0.07	0.37 ± 0.03	7.88 ± 0.48	24.41±0.21
	PCL+GF+TTPB (5:1)	1.19 ± 0.01	0.10 ± 0.01	23.16±0.91	1.18±0.03	0.91±0.01	0.27 ± 0.01	0.19 ± 0.03	14.20 ± 6.72	216.99±111.74

The distribution of porosity throughout the pore size ranges, can be used as another tool to understand the distribution of pore sizes in the produced biomaterials in order to choose the optimal processing conditions. To understand which operating conditions set, yields into biomaterials with a wide distribution of porosity throughout all the pore size ranges, since for hard tissue engineering applications are needed pores of almost every size, as shown in Table 1, section 1.1. Observing Figures D 1 and D 2, the obtained results of total pore area represent what was expected, smaller pores have much larger surface area, due to their high aspect ratio. The obtained high deviations are due to the fact that this property, total pore area, is an indirect measure of the mercury intrusion technique. In the obtained values of porosity, also high deviation values are obtained. This might be due to the used method to determine this property, and considering that the measured samples, were cut from different sections of the biomaterials and, as shown, the produced biomaterials presented pores of different sizes heterogeneously dispersed spatially.

Observing both Figures D 1 and D 2, it is visible that in the range between 0.1 and 1 µm, except the biomaterial produced at a temperature of 35 ºC and a depressurization rate of 1 $MPa.min^{-1}$, all the produced biomaterials presented very low porosity. This effect is not reported in literature. This results shows that with the used experimental apparatus for the SFM process, when nucleation of the cells CO_2 molecules preferentially diffused into larger cells and/or smaller, leading to the formation of larger and/or smaller pores. PCL could preferentially forms pores either larger or smaller, meaning that cells with size within this range are unstable and or either they grow yielding into larger pores and/or they collapse during depressurization. Despite the proposed explanation this phenomena is not quite understood.

All the produced biomaterials present porosity within all the other pore size ranges. Although, despite the biomaterial produced at a temperature of 40 ºC and a depressurization rate of 0.3 $MPa.min^{-1}$, all of them present one or two peaks in porosity which can be translated into biomaterials with more pores within the peaks range, *i.e.*, almost all of the produced biomaterials presented porosity concentrated in a few pore size ranges. Contrarily, in the biomaterial represented in Figure H 1 (C), a wider distribution of porosity is observed, meaning that with these operating conditions, biomaterials with wider distribution of pore sizes can be obtained. This finding confirms, once more, that these operating conditions are the optimal in order to produce biomaterials for hard tissue engineering applications. Although, and as seen previously, operating at a temperature of 45 ºC and a depressurization rate of 1 $MPa.min^{-1}$ yields into an almost similar distribution of porosity throughout the pore size ranges, although not so homogeneous as the considered optimal conditions, however, at these conditions higher porosity is obtained for very small pores, which could be interesting concerning surface area of the final porous material.

In Figure D 3, is showed, as an example, an obtained isotherm, from nitrogen adsorption, by the BET method, for a biomaterial of the optimization assays.

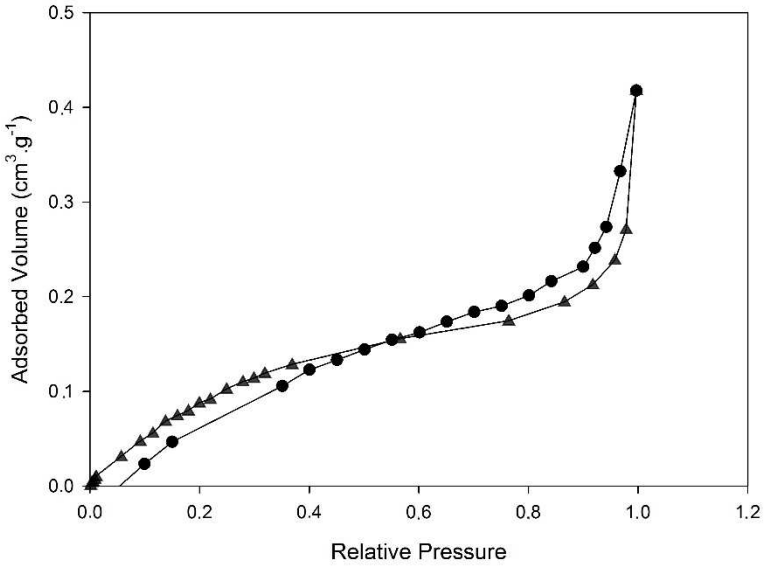

***Figure D 3**. Adsorption and desorption BET isotherms of a biomaterial prepared at P = 20 MPa, T = 35ºC, ΔP/Δt = 1 MPa.min-1 for 2h, of the optimization assays. Legend: ▲ - Adsorption Isotherm, ● - Desorption Isotherm.*

In Figure D 4, is shown an example of an obtained adsorption and desorption BET isotherm, from nitrogen adsorption, of a biomaterial from the additivated and composite assays.

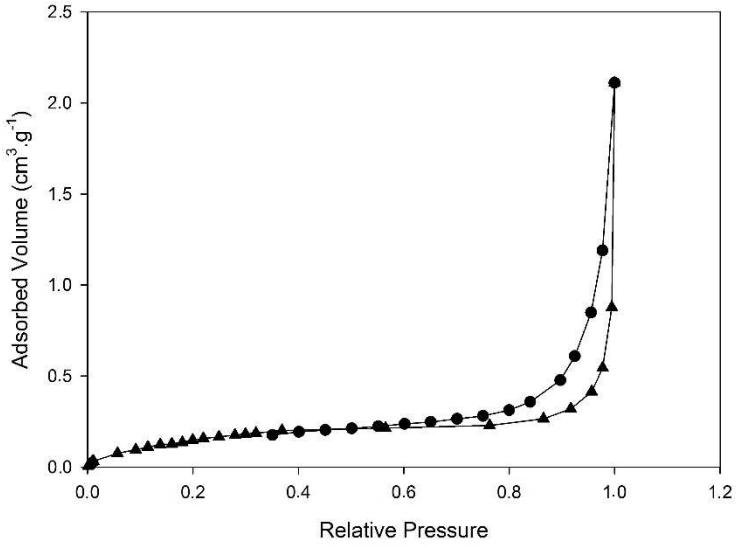

***Figure D 4**. Adsorption and desorption BET isotherms of a composite additivated biomaterial (PCL+GF+SBA-15 (20 wt. %)) prepared at P = 20 MPa, T = 40 ºC, $\Delta P/\Delta t$ = 0.3 MPa.min^{-1} for 2h of the additivated and composite assays. Legend: ▲ - Adsorption Isotherm, ● - Desorption Isotherm.*

Appendix E – Determination of the Average Pore Diameter and Pore Density with SEM Imaging

An example on how was determined the horizontal Feret's diameter of each observable pore in the photographs obtained by SEM, using Image J software, is shown in Figure E 1.

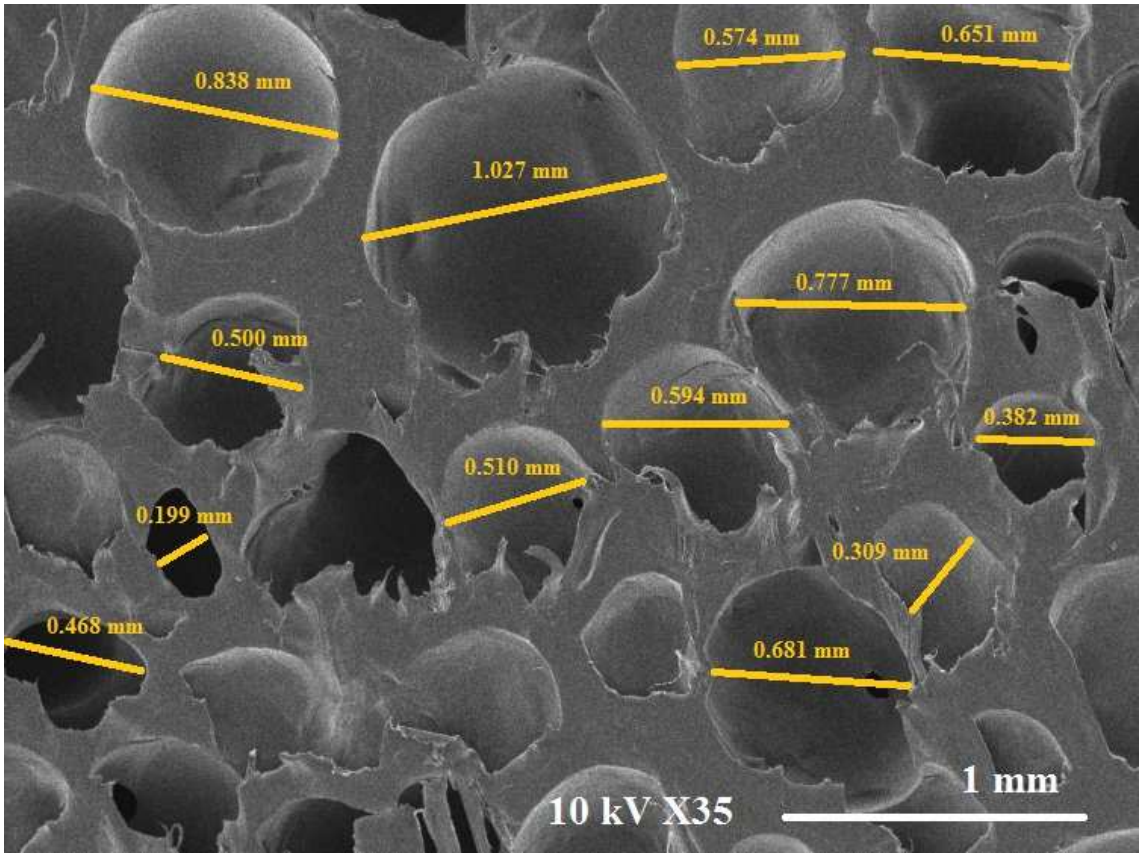

Figure E 1. *Example of determination of the Feret diameter of every observable pore on the photographs obtained by SEM, for pure PCL biomaterial produced at P = 20 MPa, T = 40 ºC, ΔP/Δt = 0.3 MPa.min-1 for 2h.*

In the pure PCL biomaterial about 80 pores were identified and measured, in composite biomaterials about 200 pores were identified and measured and in non-composite additivated biomaterials about 10 pores were identified and measured for each biomaterial.

The pore sizes were grouped into 20 groups, for every biomaterial, and then plot in a histogram. In Figure E 2 is shown an example of an obtained histogram for the non-additivated composite biomaterial (20 wt. %).

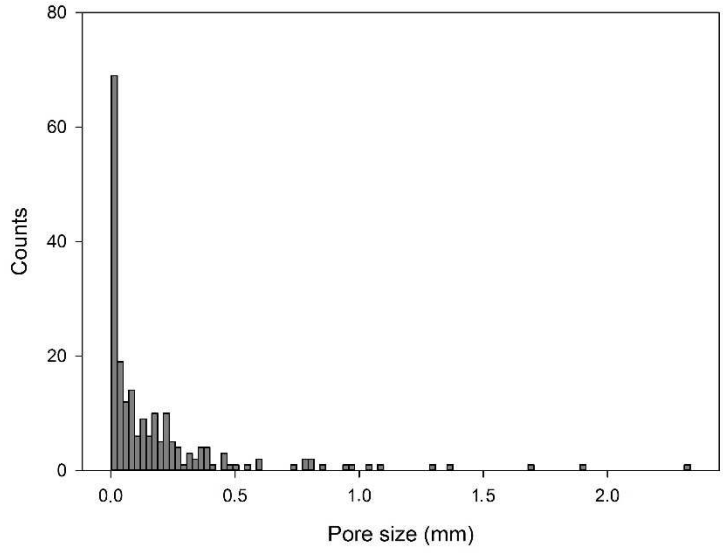

***Figure E 2**. Obtained histogram graph from the distribution of pore size measured by SEM imaging from the non-additivated composite biomaterial (20 wt. %) produced at P = 20 MPa, T = 40 ºC,ΔP/Δt = 0.3 MPa.min-1 for 2h.*

The average pore diameter and standard deviation, were determined based on the obtained results from the histogram distribution, using equations (E1) and (E2),

$$\bar{\phi} = \frac{\sum_{i=1}^{20} n_i}{\left(\sum_{i=1}^{20} \bar{\phi}_i \times n_i\right)} \quad \text{(E1)}$$

In which $\bar{\phi}$ represents the average pore diameter (µm), n_i the number of counts of the interval i (dimensionless) and $\bar{\phi}_i$ the average pore size of the i interval (bin) (µm).

$$\bar{\sigma} = \frac{\sum_{i=1}^{20}(n_i \times (\bar{\phi}_i - \bar{\phi})^2)}{\sum_{i=1}^{20} n_i - 1} \quad \text{(E2)}$$

Where $\bar{\sigma}$ represents the standard deviation.

Pore density

Pore density of the produced biomaterials for the additivated and composite assays, except biomaterials prepared with a filler composition of 30 wt. %, was determined by equation (E3) as proposed by Salerno and co-workers (Salerno *et al.*, 2013),

$$P_D = \left(\frac{n}{A_s}\right)^{\left(\frac{3}{2}\right)} \quad \text{(E3)}$$

In which P_D represents pore density of the biomaterial (pores.mm^{-2}), n the number of pores identified using Image J software and A_s the cross sectional area of the sample analysed by SEM. The obtained pore densities of the prepared biomaterials are presented in Table E 1.

***Table E 1**. Obtained values of pore density of the prepared biomaterials for the additivated and composite assays, at P = 20 MPa T = 40 ºC, $\Delta P/\Delta t$ = 0.3 MPa.min^{-1} for 2h.*

SBA-15 Composition (wt. %)	Biomaterials Composition	Pore Density (pores.mm^{-2})
0	PCL	5.47 ± 1.93
	PCL+GF	0.58 ± 0.28
	PCL+TTPB	15.77 ± 1.52
	PCL+GF+TTPB (2:1)	0.29 ± 0.16
	PCL+GF+TTPB (3:1)	4.80 ± 1.16
	PCL+GF+TTPB (5:1)	2.09 ± 1.10
20	PCL	37.32 ± 4.07
	PCL+GF	14.97 ± 6.25
	PCL+TTPB	83.32 ± 3.25
	PCL+GF+TTPB (2:1)	13.44 ± 2.09
	PCL+GF+TTPB (3:1)	12.76 ± 2.35
	PCL+GF+TTPB (5:1)	12.63 ± 1.80

As can be observed in Table E 1 pore density highly increases when TTPB is incorporated. This clearly shows the enhanced porogenic effect of TTPB compared to GF, which led to a decrease on pore density. TTPB yields into a greater CO_2 absorption by the polymeric chains, increasing their free movement, and therefore more bubbles are formed. Incorporating in PCL biomaterials a mixture of GF and TTPB yielded into a decrease on pore density, comparing to pure PCL biomaterial. The effect of both additives is not linear, as the amount of GF increases on the biomaterial from the mixture of 2:1 to the mixture of 3:1, an increase is verified from 0.29 ± 0.16 to 4.80 ± 1.16 pores.mm^{-2}. When adding a mixture of GF and TTPB in a molar proportion of 3:1 better values of pore density are obtained (comparing to the effects of the other molar proportions) towards an application requiring high pore density like biomedical/pharmaceutical applications. Incorporating SBA-15 (20 wt. %) pore density is highly increased to 37.32 ± 4.07, as expected, since this inorganic creates an interface with the polymer, this interface lowers the activation energy of nucleation favouring the heterogeneous mechanism. The presence of the filler leads to a high nucleant density resulting in an increased nucleation rate and therefore high pore density (Nalawade *et al*., 2006; Jacobs *et al*., 2008; Chen L. *et al*., 2013). Again adding to the composite biomaterial TTPB, pore density is even further increased, due to its porogenic/plasticizer action. GF lowers pore density, since its action as a blowing agent promotes homogeneous nucleation yielding into very large pores, decreasing pore density. In the composite biomaterials, the trend verified for the non-composite biomaterials, when a mixture of the two additives is incorporated, is not verified. Greater pore density is obtained when a mixture in a molar proportion of 2:1 is incorporated, tough the obtained values for all the three tested molar proportions are very similar to each other. From this analysis it stays clear that incorporating SBA-15, producing composite biomaterials, pore density is highly increased. It was found also, that TTPB has high porogenic action, yielding into the production of highly porous materials. GF can be added in order to obtain, larger pores, as seen by SEM analysis.

Appendix F –Obtained Results from Thermal and Crystallinity Analysis

Simultaneous Differential Thermal Analysis (SDT)

In Figure F 1 is shown an example of a SDT profile obtained from a composite biomaterial (20 wt. %).

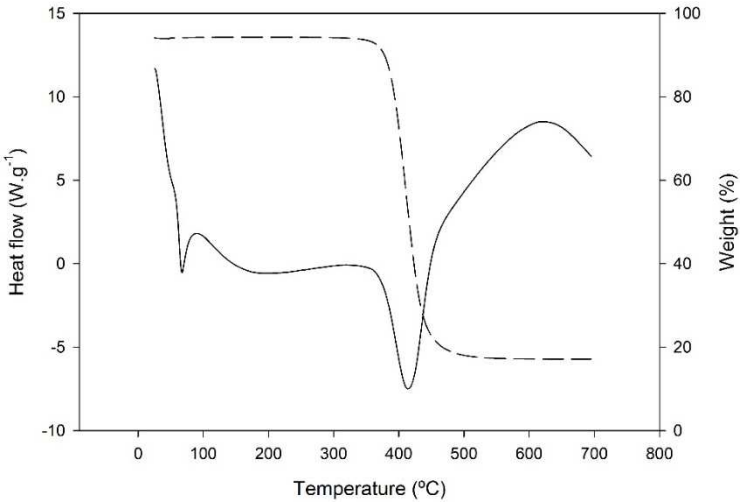

***Figure F 1**. SDT profile for a non-additivated composite biomaterial (20 wt. %) of the additivated and composite assays. Prepared at P = 20 MPa T = 40 ºC, $\Delta P/\Delta t$ = 0.3 MPa.min^{-1} for 2h. Legend: —— Heat flow, ----- sample weight.*

In Figure F 2 is shown an example of a SDT profile obtained from a biomaterial additivated with GF.

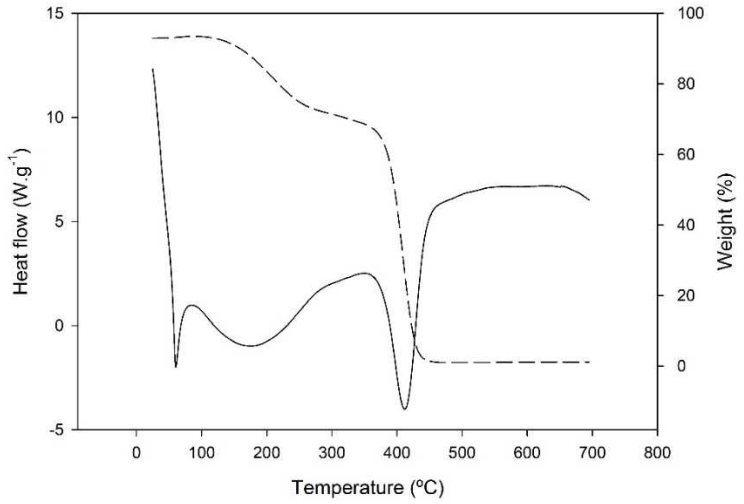

***Figure F 2.** SDT profile for a non-composite additivated biomaterial (GF) of the additivated and composite assays. Prepared at P = 20 MPa T = 40 ºC, $\Delta P/\Delta t$ = 0.3 MPa.min^{-1} for 2h. Legend: —— Heat flow, ----- sample weight.*

As stays clear, by observation of Figures F 1 and 2, in the first case, since no liquid additive was incorporated, the observed mass loss is constant until the polymer degrades leaving as

residual mass the initially incorporated inorganic content, in the second case, a liquid additive was incorporated which have a lower thermal stability than the polymer, degrading firstly. This is observed, in Figure F 2, as a small mass loss is observed between 200 and 300 ºC corresponding to the degradation of GF. In this case, since no inorganic content was incorporated, the mass loss is total reaching 0% weight at 700ºC, indicating that all the polymer and the additive were degraded.

In Figure F 3 is shown an example of the determination of peak area of the thermal events detected by SDT, as well as the melting and degradation temperatures. The same intervals for determination of the peak areas were used for every performed sample.

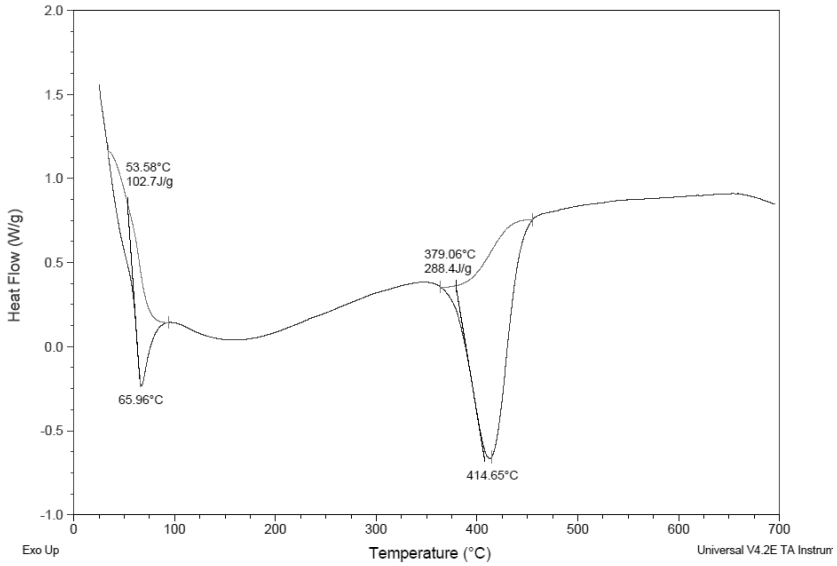

Figure F 3. *Example of determination of melting and degradation enthalpies as well as melting and degradation temperatures for pure PCL biomaterial of the additivated and composite assays prepared at P = 20 MPa T = 40 ºC, $\Delta P/\Delta t$ = 0.3 MPa.min^{-1} for 2h.*

In Figure F 4 is shown the determination of melting and degradation temperature and enthalpies for pure unprocessed PCL.

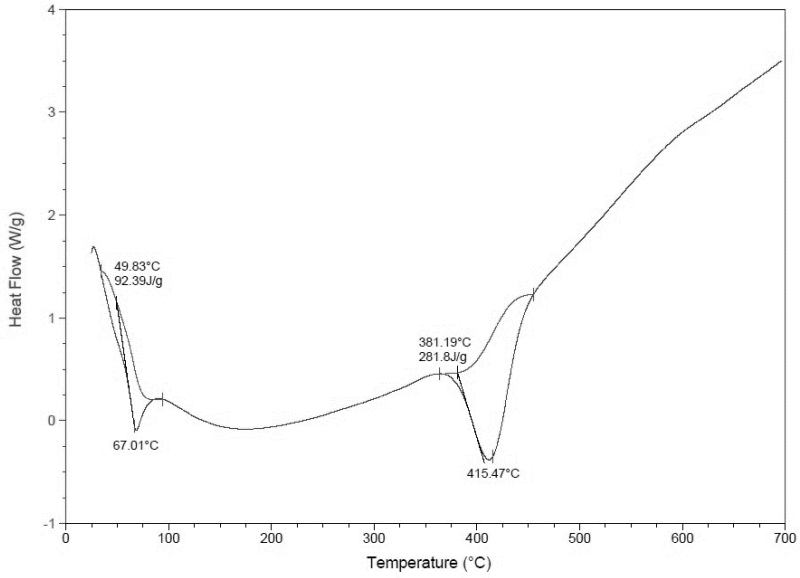

Figure F 4. *Example of determination of melting and degradation enthalpies as well as melting and degradation temperatures for pure and unprocessed PCL*

In Figure F 5 is shown an example on how the mass loss was determined based on the obtained SDT profile.

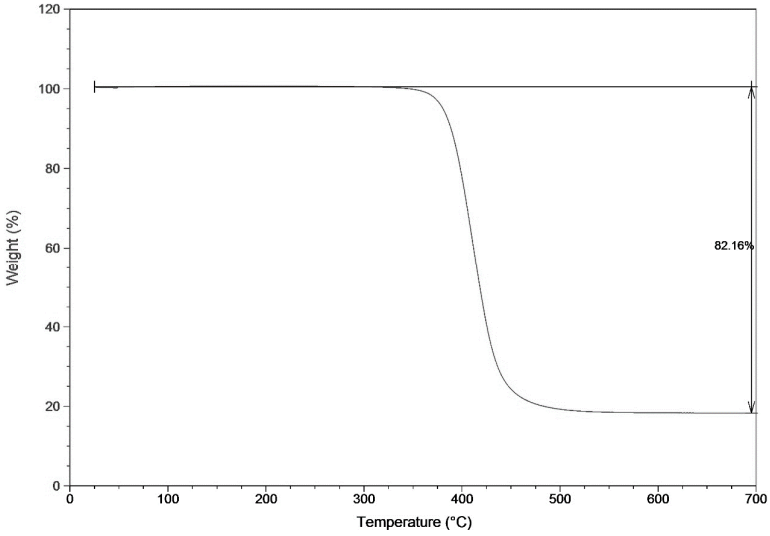

Figure F 5.*Example of determination of mass loss and real SBA-15 content from SDT analysis, for a non-additivated composite biomaterial (20 wt. %) from the additivated and composite assays prepared at P = 20 MPa T = 40 ºC,* $\Delta P/\Delta t$ *= 0.3 MPa.min*$^{-1}$ *for*

In Table F 1 are presented the obtained values from SDT of melting and degradation temperatures, melting enthalpy, as well as the crystallinity and mass loss of the produced biomaterials for the additivated and composites assays.

Table F 1. *Obtained values of melting and degradation temperatures, melting enthalpies, crystallinity and mass loss from SDT of the produced biomaterials for the additivated and composite assays*

SBA-15 content (wt. %)	Biomaterials Compostion	Melting Temperature (ºC)	Degradation Temperature (ºC)	Melting Enthalpy ($J.g^{-1}$)	Crystallinity (%)	Mass loss (%)
0	Pure TTPB	-	420.32 ± 7.39	-	-	99.62 ± 0.38
	Pure GF	-	180.29 ± 1.82	-	-	97.20 ± 0.97
	PCL powder	68.10 ± 0.14	416.34 ± 0.25	98.61 ± 1.90	70.79 ± 1.36	97.71 ± 0.34
	Unprocessed PCL	65.23 ± 1.79	415.86 ± 0.39	96.95 ± 4.56	69.59 ± 3.27	99.98 ± 0.02
	PCL	66.08 ± 0.12	414.67 ± 0.02	97.06 ± 5.64	69.68 ± 4.05	99.79 ± 0.16
	PCL+GF	60.06 ± 0.59	414.63 ± 0.32	66.17 ± 3.24	47.50 ± 2.32	98.49 ± 0.16
	PCL+TTPB	64.94 ± 0.86	403.97 ± 0.00	47.14 ± 2.44	33.84 ± 1.75	98.32 ± 0.23
	PCL+GF+TTPB (2:1)	63.58 ± 0.21	414.15 ± 1.20	67.12 ± 1.45	48.18 ± 1.04	95.16 ± 1.19
	PCL+GF+TTPB (3:1)	61.21 ± 0.44	410.27 ± 0.44	64.10 ± 5.59	46.02 ± 4.01	98.72 ± 0.13
	PCL+GF+TTPB (5:1)	63.26 ± 0.34	414.15 ± 1.19	73.87 ± 3.29	53.03 ± 2.36	99.99 ± 0.01
20	PCL	65.85 ± 0.11	416.41 ± 0.08	62.62 ± 3.24	56.19 ± 2.91	80.70 ± 0.88
	PCL+GF	59.07 ± 0.66	411.23 ± 0.11	76.15 ± 0.90	68.33 ± 0.81	86.46 ± 0.21
	PCL+TTPB	65.62 ± 0.40	417.26 ± 1.60	72.44 ± 4.05	65.00 ± 3.63	85.32 ± 0.09
	PCL+GF+TTPB (2:1)	61.37 ± 0.50	414.64 ± 4.97	50.54 ± 6.20	45.35 ± 5.56	89.39 ± 0.93
	PCL+GF+TTPB (3:1)	62.00 ± 0.46	411.57 ± 1.55	63.90 ± 1.77	57.34 ± 1.59	84.69 ± 1.73
	PCL+GF+TTPB (5:1)	59.51 ± 0.22	411.97 ± 0.07	57.85 ± 1.10	51.91 ± 0.98	87.65 ± 1.16
30	PCL	69.54 ± 0.03	416.35 ± 0.96	34.16 ± 2.05	35.03 ± 2.10	79.66 ± 0.90
	PCL+GF	57.82 ± 2.17	417.50 ± 0.22	47.72 ± 5.81	48.94 ± 5.96	80.36 ± 1.03
	PCL+GF+TTPB (2:1)	62.05 ± 0.08	422.87 ± 1.19	53.38 ± 3.79	54.74 ± 3.89	81.12 ± 0.22

X-Ray Diffraction (XRD)

In Figure F 6 is represented the obtained diffractogram of pure PCL biomaterial, with the crystalline peaks and Gaussian fit of the amorphous region identified.

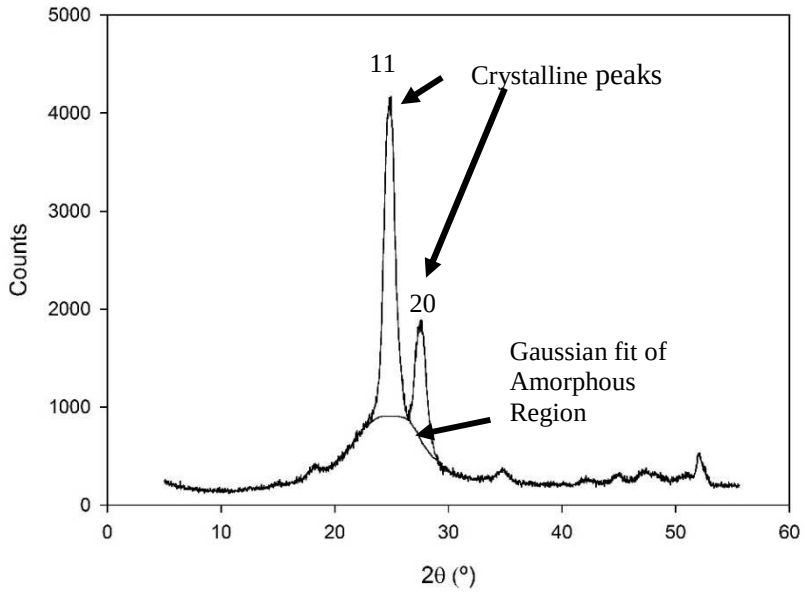

***Figure F 6**. Pure PCL biomaterial, prepared at P = 20 MPa, T = 40 ºC, $\Delta P/\Delta t$ = 0.3 MPa.min^{-1} for 2h, diffractogram with crystalline peaks, Gaussian fit of amorphous region and diffraction planes identified.*

In Table F 2 are presented the obtained values of crystallinity index from XRD and SDT for the prepared non-composite biomaterials of the composite and additivated biomaterials assays.

***Table F 2**. Obtained crystallinity indexes from XRD and SDT for non-composite biomaterials of the additivated and composite assays, prepared at P = 20 MPa, T = 40 ºC, $\Delta P/\Delta t$ = 0.3 MPa.min^{-1} for 2h.*

Biomaterials Composition	XRD Crystallinity index (χ_i(%))	SDT Crystallinity index (χ_c(%))
PCL	67.76 ± 0.19	69.68 ± 4.05
PCL+GF	62.55 ± 0.57	47.50 ± 2.32
PCL+TTPB	68.11 ± 0.48	33.84 ± 1.75
PCL+GF+TTPB (2:1)	63.06 ± 0.83	48.18 ± 1.04
PCL+GF+TTPB (3:1)	60.39 ± 0.10	46.02 ± 4.01
PCL+GF+TTPB (5:1)	65.70 ± 0.26	53.03 ± 2.36

As seen in Table F 2, the obtained values from XRD differ from the ones obtained from SDT. In literature a good correspondence between the two techniques is reported, when supercritical foamed PCL is analysed (de Matos *et al*., 2013; Yu and Dean, 2005). In this work, only a good correspondence was found for pure PCL biomaterial. The trend for the biomaterials additivated only with one additive found by SDT is not found by XRD, although once a mixture of the two additives is incorporated the trend found by SDT is confirmed by XRD.

Appendix G –Obtained Results from Mechanical Analysis

In Figure G 1 is shown an example of an obtained stress *versus* strain plot of a biomaterial for the optimization assays, with the three zones identified, linear elastic, collapse plateau and densification as well as the rupture and failure points.

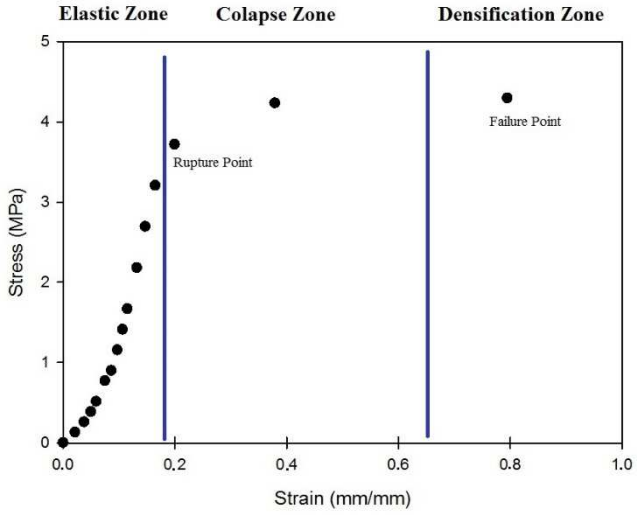

***Figure G 1**. Stress versus strain plot of a biomaterial prepared at P = 20 MPa, T = 35 ºC,$\Delta P/\Delta t$ = 1 MPa.min^{-1} for 2h for the optimization assays.*

In Figure G 2 is shown an example of an obtained stress versus strain plot of a composite biomaterial (20 wt. %) of the additivated and composite biomaterials.

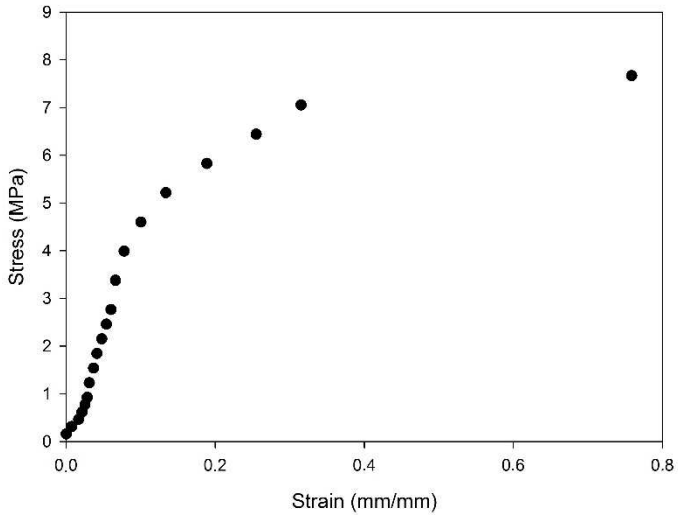

***Figure G 2.** Stress versus strain plot of a composite biomaterial (20 wt. %) prepared at P = 20 MPa T = 40 ºC, $\Delta P/\Delta t$ = 0.3 MPa.min^{-1} for 2h for the additivated and composite assays.*

In Table G 1 are shown the obtained results for compressive strength and Young's modulus of the produced biomaterials for the optimization assays, as well as the bone mechanical properties.

***Table G 1**. Obtained results of compressive strength and Young's modulus of the prepared biomaterials for the optimization assays.*

Temperature (ºC)	$\Delta P/\Delta t$ **(MPa.min^{-1})**	**Compressive Strength (MPa)**	**Young's Modulus (MPa)**	**Regression Coefficients**
35	0.3	6.87 ± 2.64	9.93 ± 1.42	1.00 ± 0.00*
	1	24.72 ± 0.83	13.27 ± 4.01	0.99 ± 0.01
40	0.3	1.90 ± 0.39	32.61 ± 3.01	0.99 ± 0.00*
	1	3.95 ± 0.01	35.91 ± 0.25	0.99 ± 0.01
45	0.3	0.62 ± 0.19	11.47 ± 1.62	0.99 ± 0.01
	1	2.67 ± 0.11	23.86 ± 2.13	0.99 ± 0.01
50	0.3	0.67 ± 0.02	5.35 ± 1.20	0.99 ± 0.00*
	1	0.34 ± 0.04	8.28 ± 0.47	1.00 ± 0.00*
References (Yang *et al.*, 2001)				
Cortical Bone		130-180	3000-30000	-
Trabecular Bone		4-12	20-50	-

*The obtained values for the replicas of these biomaterials were exactly the same until the fourth decimal place.

In Table G 2 are shown the obtained results for compressive strength and Young's modulus of the produced biomaterials for the additivated and composite assays.

Table G 2. Obtained results of compressive strength and Young's modulus of the prepared biomaterials for the additivated and composite assays.

SBA-15 content (wt. %)	Biomaterials Composition	Compressive Strength (MPa)	Young's Modulus (MPa)	Regression Coefficients
0	PCL	1.90 ± 0.39	32.61 ± 3.01	0.99 ± 0.00**
	PCL+GF	0.65 ± 0.13	9.68 ± 2.07	0.99 ± 0.03
	PCL+TTPB	1.18 ± 0.05	17.05 ± 2.26	0.99 ± 0.00**
	PCL+GF+TTPB (2:1)	0.47 ± 0.00*	4.26 ± 3.14	0.97 ± 0.03
	PCL+GF+TTPB (3:1)	0.47 ± 0.00*	14.30 ± 2.08	0.95 ± 0.05
	PCL+GF+TTPB (5:1)	0.39 ± 0.08	8.13 ± 1.68	0.98 ± 0.02
20	PCL	7.97 ± 0.31	60.17 ± 2.31	0.99 ± 0.00**
	PCL+GF	0.63 ± 0.01	11.51 ± 1.11	0.98 ± 0.01
	PCL+TTPB	3.38 ± 1.23	17.05 ± 2.26	0.97 ± 0.01
	PCL+GF+TTPB (2:1)	2.15	2.03	1.00
	PCL+GF+TTPB (3:1)	0.77 ± 0.00*	16.80 ± 4.40	0.96 ± 0.03
	PCL+GF+TTPB (5:1)	1.08 ± 0.15	8.75 ± 2.87	0.99 ± 0.01
30	PCL	3.12 ± 0.01	21.60 ± 6.69	0.99 ± 0.00**
	PCL+GF	3.33 ± 2.56	12.98 ± 2.67	0.99 ± 0.00**
	PCL+GF+TTPB (2:1)	0.52	6.55	0.98
References (Yang *et al.*, 2001)				
	Cortical Bone	130-180	3000-30000	-
	Trabecular Bone	4-12	20-50	-

*The obtained values for the replicas of these biomaterials were exactly the same, since they broke at the same load.
** The obtained values for the replicas of these biomaterials were exactly the same until the fourth decimal place.

The mechanical properties of the composite biomaterial (20 wt. %) additivated with a mixture of the two additives in a molar proportion of 2:1, was only measured once, since from all produced replicas it was only possible to achieve a homogeneous cross section for performing the assay, from one sample. nonetheless the assay was attempted to be conducted with the other replicas but the biomaterials were so fragile that they were destroyed only by applying the oedometer arm weight.

The composite biomaterials (30 wt. %) additivated with a mixture of the two additives in a molar proportion of 2:1, had a non-reproducible macroscopic structure. Several replicas were prepared but the same macroscopic results were never achieved. Moreover, this biomaterial presented always a very heterogeneous distribution of the filler, resulting in a very heterogeneous structure, as seen on section 3.3.1, Figure 16. In this biomaterial a phase separation occurred, since the polymer grown vertically on the side of the biomaterial and the SBA-15 particles were concentrated on the other side of the biomaterial. So, the mechanical analysis for this biomaterial was only performed once, due to the high heterogeneity and non-reproducible feature of the biomaterials.

Appendix H – Silica "Fibres"

As referred on section 3.3.1, the unexpected formation of "fibre"- like structures was verified in the prepared composite biomaterials (20 and 30 wt. %) additivated with GF, increasing the visible amount of those structures with the amount of SBA-15. When TTPB was added to the mixture, it was verified a larger dispersion of the presence of those structures throughout the polymeric matrix. In non-composite biomaterials, non-additivated and additivated with GF and/or TTPB, no such structure was visible.

As the amount of GF, in mixture with TTPB, increased, also the visible amount of these structures appeared to increase. So, the biomaterial prepared with a composition of SBA-15 of 20 wt. % additivated with a mixture of GF and TTPB in a molar proportion of 5:1 is the one presenting larger amount of these structures, of the composites with this inorganic content, and the biomaterial prepared with 30 wt. % of SBA-15 additivated with a mixture of GF and TTPB in a molar proportion of 2:1 is the biomaterial which presents the larger amount of these structures.

In Figure H 1 are shown some examples of the observed structures on the prepared biomaterials.

The presence and/or formation of such structures was thought to be due to several explanations, since in the literature no work reported the formation of such structures, despite the natural formation of spicules (but the obtained results in this work were much different). The first though was concerning a contamination of the prepared samples. Tough, a contamination of the entire sample was discarded, since on the samples analysed at the same time, without GF and/or SBA-15 no such structure was visible. Also, at another time, the same trend was visible, only the samples with GF and SBA-15 presented these structures. But nonetheless it could still be an organic contamination. Also, it was thought to be a contamination either of the SBA-15 nanoparticles and/or the PCL powder particles, although on the non-composite biomaterials no such structure was visible as well as on the non-additivated composite biomaterials. To confirm this speculation, SBA-15 nanoparticles and PCL powder particles were observed with SEM, which results are presented in Figure 18 on section 3.3.1. In this analysis no "fibre"-like structure and/or contamination were observed since EDS analysis was used. EDS was also employed on the samples, in which these structures were observed, as showed in Figure H 2.

Through EDS analysis of the composite (30 wt. %) and additivated biomaterial with GF, as seen in Figure H 2, the presence and/or formation of these "fibre"-like structures appears to be a contamination of Na. however, the obtained results are highly inconclusive since, and as seen on the obtained spectra (Figure H 2 (F)), the Na detections are very low (0.2 wt. % with a deviation of 0.0, which is indicative of very low detection and/or an analytical error. Observing the obtained mapping of O (Figure H 2 (D)) it is also clear that these "fibre"-like structures are composed by O. Since no conclusive result was obtained, other EDS analysis were performed, as shown in Figure H 3. In this spectra, showed in Figure H 3, Na was not identified, leading into more inconclusive results about a possible contamination of the biomaterials and/or the used compounds, such as GF and/or TTPB. Concerning that no additivated biomaterial with TTPB presented any "fibre"-like structure (composite and non-composite), the contamination, if any exists, could only be on GF, however, the composite and non-composite biomaterials additivated only with GF did not present any such structure.

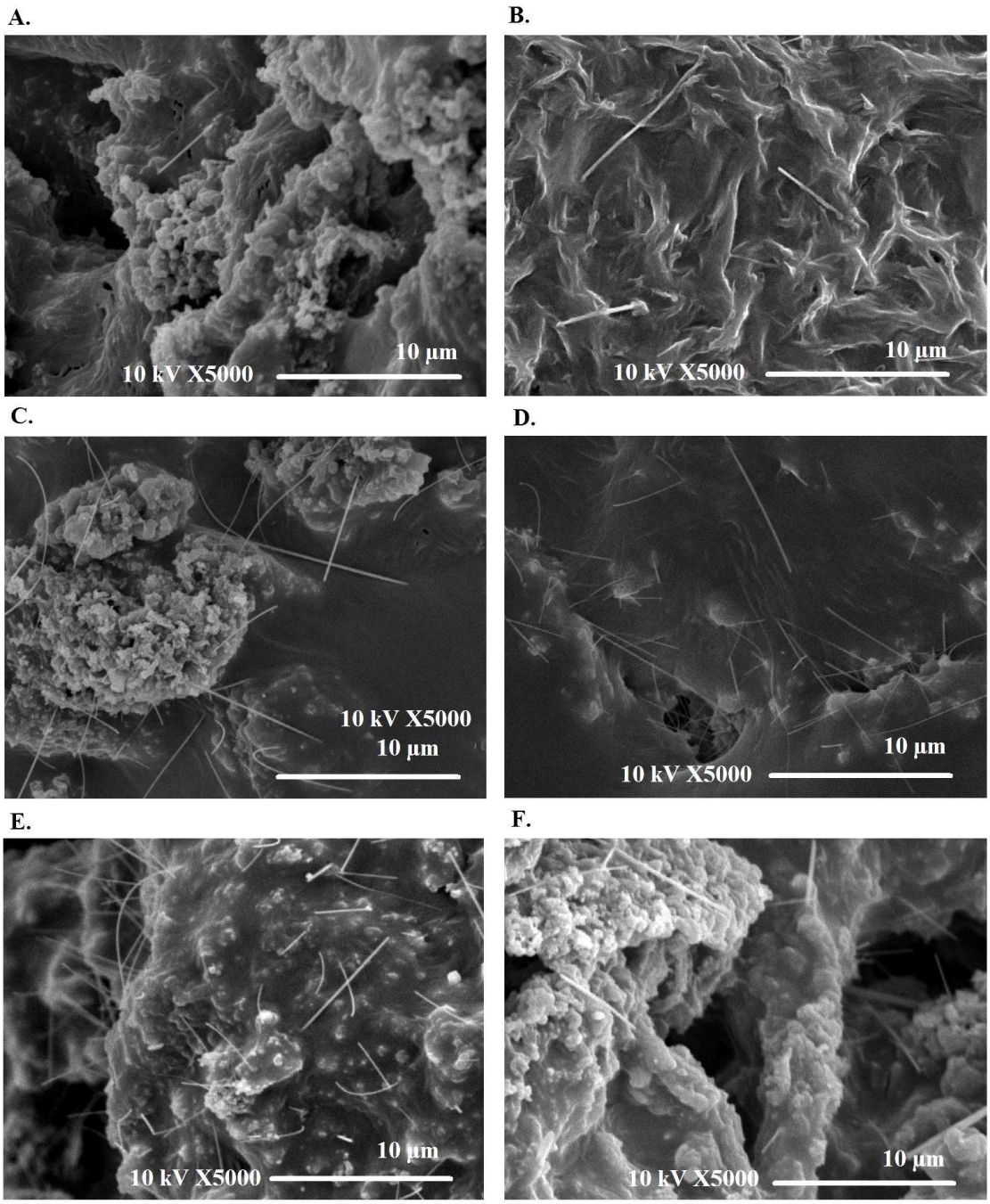

***Figure H 1**. Observed "fibre"-like structures on the prepared biomaterials from the composite and additivated assays. A – PCL+SBA-15 (20 wt. %)+GF; B - PCL+SBA-15 (20 wt. %)+GF+TTPB (2:1);C - PCL+SBA-15 (20 wt. %)+GF+TTPB (3:1); D - PCL+SBA-15 (20 wt. %)+GF+TTPB (5:1); E - PCL+SBA-15 (30 wt. %)+GF; F - PCL+SBA-15 (20 wt. %)+GF+TTPB (2:1). Biomaterials prepared at P = 20 MPa, T = 40ºC, $\Delta P/\Delta t$ = 0.3 MPa.min^{-1} for 2h.*

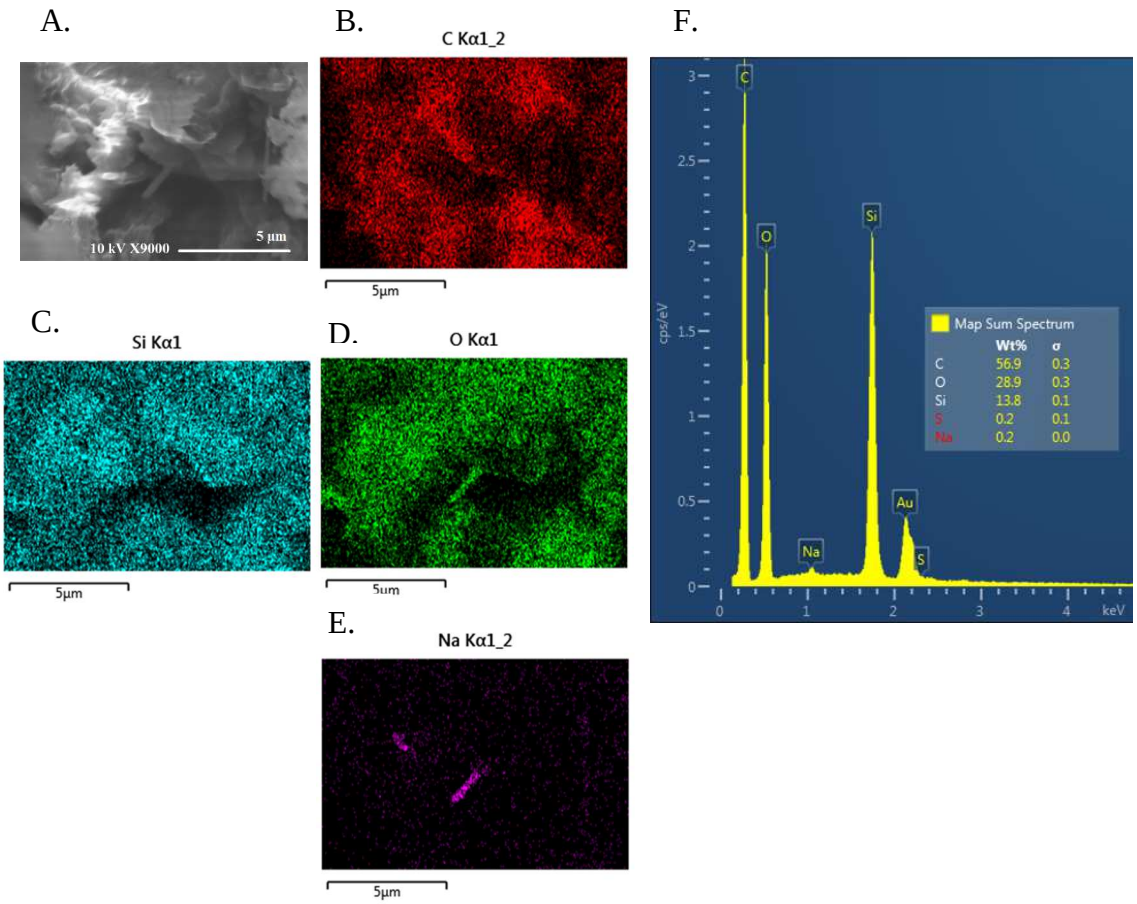

***Figure H 2**. EDS mapping of the composite (30 wt. %) additivated biomaterial with GF. A. – Obtained SEM image of the composite screw device at a magnification of X9000, scale bar – 5 µm; B. – mapping image of the chemical element C; C. – mapping image of the chemical element Si; D. – mapping image of the chemical element O; E – mapping image of the chemical element Na; F - EDS spectra of the identified chemical elements.*

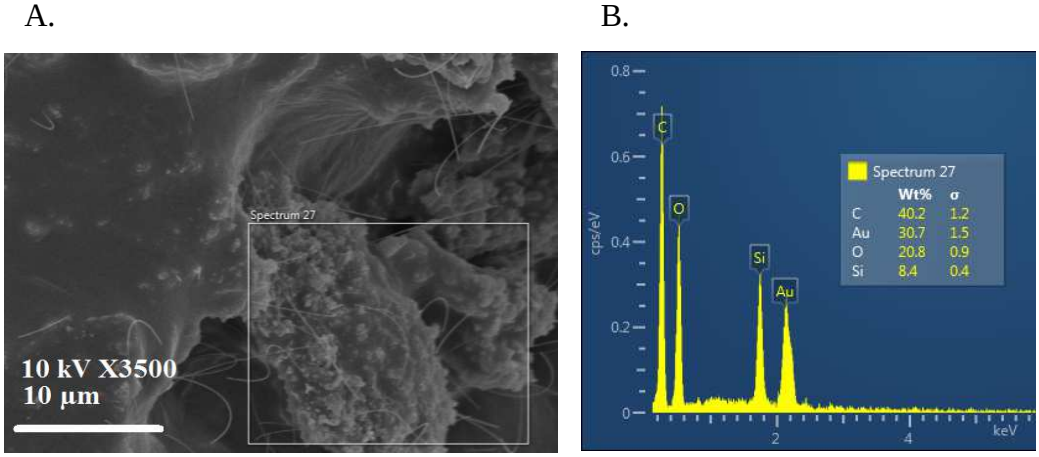

***Figure H 3**. EDS area spectrum of the prepared composite biomaterial (20 wt. %) additivated with a mixture of GF and TTPB (3:1). A – Obtained SEM image of the biomaterial at a magnification of X3500, scale bar – 10 µm; B – EDS spectra of the identified chemical elements.*

Since no conclusive result, concerning a possible Na contamination, was obtained, the next possible explanation was that the formed structures were silica-based structures. Silica is the

used name for silicon oxide, in which are present atoms of Si and O, as confirmed in both EDS analysis, as seen in Figures H 2 and H 3.

The biomaterials in which these structures were observed, suffered a thermal treatment, for SDT analysis, from room temperature until 700 ºC. Contrary to the other tested biomaterials, these leaved a powder-like residue (despite the SBA-15 content) with the shape of the sample as seen in Figure H 4 (A.), and the other biomaterials leaved all the residue "glued" to the sample bearer borders. This powder-like residue was analyzed with SEM, as seen in Figure H 4 (B.).

A.

B.

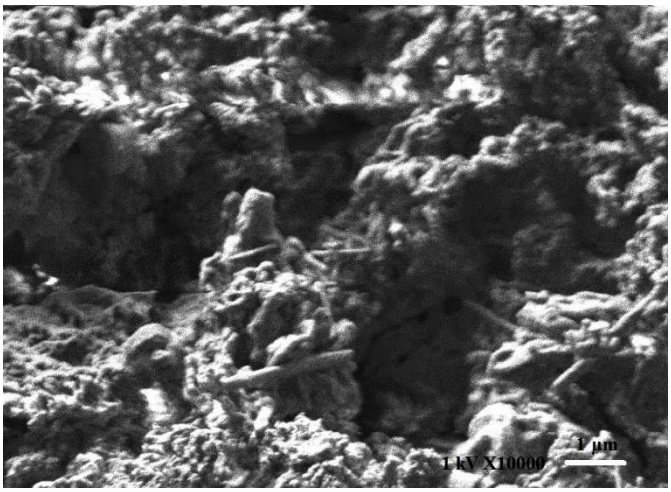

Figure H 4. *Obtained residue from thermal heating until 700ºC from SDT analysis (A) and SEM image of the obtained residue (B), obtained at a magnification of X10000, scale bar 1 µm.*

As seen on Figure H 4, even after heating of the biomaterial until 700 ºC, these "fibre"-like structures are found, which reveals that these structures are not any organic contamination, since after 700 ºC it would all be destroyed. So, these structures are inorganic, what could be indicative that they are of Silicon-nature.

In order to understand if the heating of the composite and the biomaterial additivated with GF led into inorganic residues with the presence of these "fibre"-like structures, a composite (30 wt. %) and additivated biomaterial with GF, was heated in a muffle furnace (Carbolite, Sheffiled, UK) from room temperature (~20 ºC) to 700 ºC with a heating rate of 10 $ºC.min^{-1}$. Then the sample was analysed with SEM in order to confirm the presence of these "fibre"-like structures. A composite (30 wt. %) and non-additivated biomaterial, was also heated in the muffle furnace until 700 ºC, in order to compare with the biomaterial in which the "fibre"-like structures were found. In Figure H 5 A is showed the composite (30 wt. %) and additivated with GF biomaterial after exposure to 700 ºC in the muffle furnace, in Figure H 5 B is showed the SEM image after exposure to 700 ºC in the muffle furnace and in Figure H 5 C is showed the SEM image of the non-additivated composite biomaterial (30 wt. %) after exposure until 700 ºC.

B.

A.

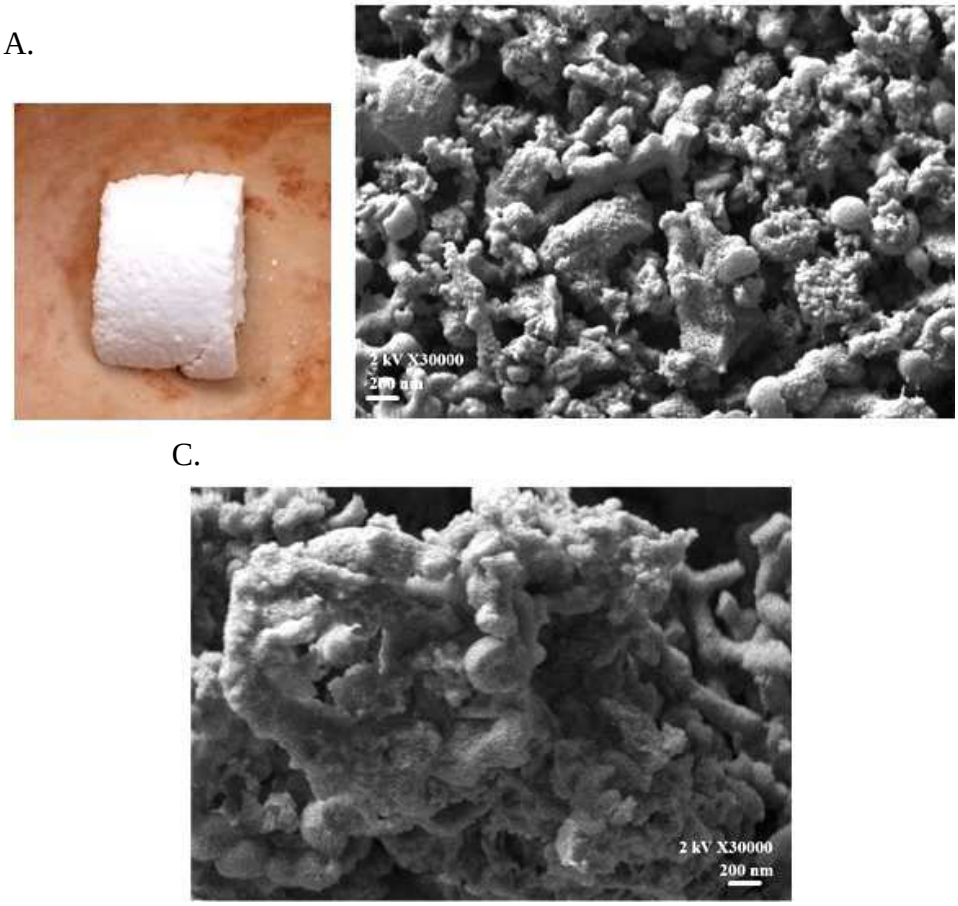

Figure H 5.*Obtained residue of the composite (30 wt. %) additivated biomaterial with GF after exposure until 700 ºC on the muffle furnace (A.), its SEM image (B.) at a magnification of X30000, scale bar 200 nm and the obtained SEM image at a magnification of X30000, scale bar 200 nm from a composite and non-additivated biomaterial after exposure until 700 ºC at the same conditions (C.)*

Observing Figure H 5 B., some "fibre"/spicules structures are observed on the inorganic residue. Tough, these observed structures are much smaller than the previous observed on the prepared biomaterial s and in the residue from the SDT analysis, since the used magnification to enable the observation of these structures is much higher. However, in the residue from the non-additivated biomaterial (Figure H 5 C), no such structure is found. Once more, these observations are not very conclusive, which can be indicative that no zone of the sample in which the "fibre"-like structures were found was analysed, which can be elucidative that the presence of these "fibres" is not homogeneous in this biomaterial (what could be indicative of a local contamination).

After all the observations, the explanation which is seen as the most accurate is that, somehow, during $scCO_2$ exposure and processing, and by action of GF, the inorganic nanoparticles assume this morphological conformation. So, in order to understand the effect of every variable (namely operating pressure), acetone (low polar and hydrophobic solvent) was used to mimic the effect of $scCO_2$ in PCL, and GF and SBA-15 (20 wt. %) were incorporated in the mixture in the same compositions of the prepared biomaterial s for the additivated and composite assays. Also, other tests were performed, one with only acetone, PCL and GF and other with GF and SBA-15. These mixtures were stirred until acetone, which was added for all the mixtures in a proportion

able to dissolve all the PCL, had dissolved all the employed PCL (1g). The obtained macroscopic results are shown in Figure H 6.

A. B. C. D.

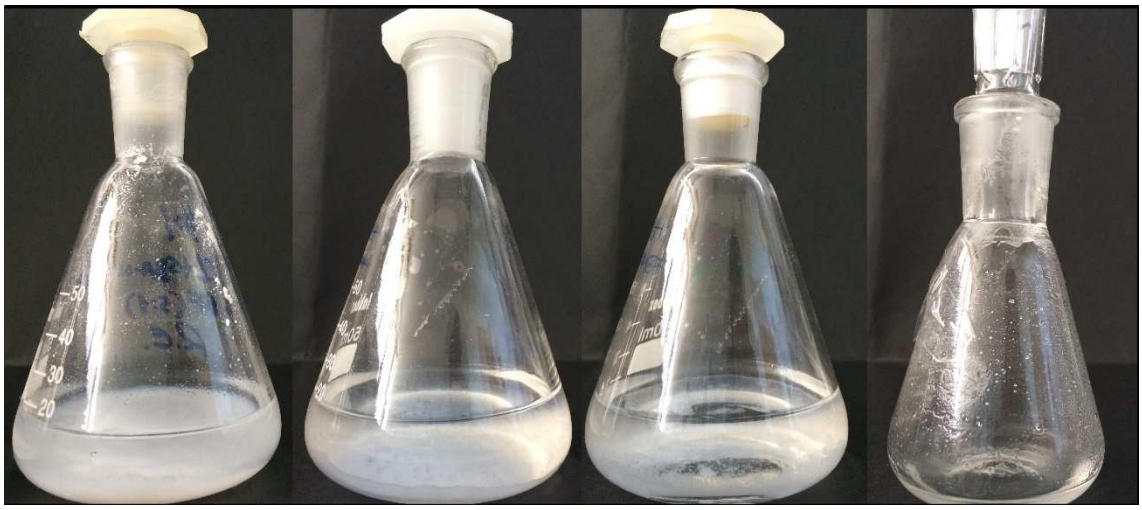

Figure H 6. *Obtained macroscopic results from the mixtures of Acetone+PCL+SBA-15+GF (98% molar) (A), Acetone+PCL+GF (98% molar) (B); Acetone+PCL and (C) GF+SBA-15.*

As observed, in all the mixtures prepared with PCL and acetone, PCL was totally dissolved. In the mixture of PCL and acetone, showed in Figure H 6 (C) after a week approximately, PCL started to precipitate. This could be due to some evaporation and loss of solvent mass. The same happened in the mixture of acetone + PCL + SBA-15 + GF, after total solubilization of PCL, it precipitated after a week approximately, as seen in Figure H 6 A. In Figure H 6 (C), SBA-15 appeared to be partially soluble on GF, although what could have happened is a reduction of particle size, as seen by the smaller particles on the walls of the Erlenmeyer flask, and so by the naked eye the SBA-15 particles are not visible.

In order to understand the effect of the molten polymer and GF on the possible formation of those “fibre”-like structures of SBA-15, as thought, using the solution shown in Figure H 6 A, acetone was evaporated (mimicking the depressurization step, and vitrification of the polymer) yielding into a composite film of PCL and SBA-15. This film was analysed using SEM, in order to confirm the presence of those “fibre”-like silica structures. In Figure H 7 are shown the obtained results.

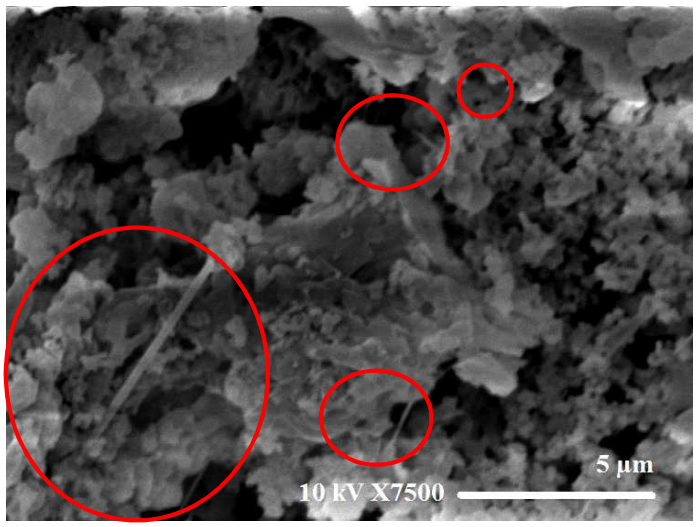

Figure H 7. *SEM image of the obtained composite film from solvent evaporation, obtained at a magnification of X7500, scale bar 5 µm. The red circles show the identified "fibre"-like structures.*

As seen, even by this method, several "fibre"-like structures were identified, although in much smaller number than in the prepared biomaterials. EDS analysis was performed in order to assess the chemical information of such structures. Once again, the obtained results from this analysis were not conclusive and these structures appear to be of silicon nature. The other prepared solutions, showed in Figure H 6 (B, C and D) were not analysed with SEM due to limitation of the available time, although in the future they will be analysed.

Even after all the attempts made to assess the origin and mechanism of formation of such structures no conclusive result was achieved, although all the obtained results appear to lead into the conclusion that these structures are of silicon nature, and are formed by action of GF. In the literature, as referred, no similar result was reported. Only the formation of spicules is reported in literature, although these structures are not similar to the ones found in this work (Müller *et al.*, 2013; Wang, 2015).

A possible explanation of formation of these "fibre"-like structures, since they are assumed to be of silicon nature, concerns the self-assembly of these structures by action of GF, acting this as a surfactant. It is supposed that SBA-15 can be partially soluble in GF, due to its hydrophilic end. Then, at the depressurization step, the other end of GF, which is hydrophobic, is guided and dragged by CO_2 molecules leaving the polymer + inorganic + GF mixture, self-assembling the silica particles yielding into "fibre"-like structures. The chemical mechanism is represented in Figure H 8. This "fibre"-like structures presented diameters of 100 ~150 nm (measured by image analysis using Image J software). Due to this feature these structures present great interest for development in silica nanotechnology, to disclose the proposed nature and formation mechanism.

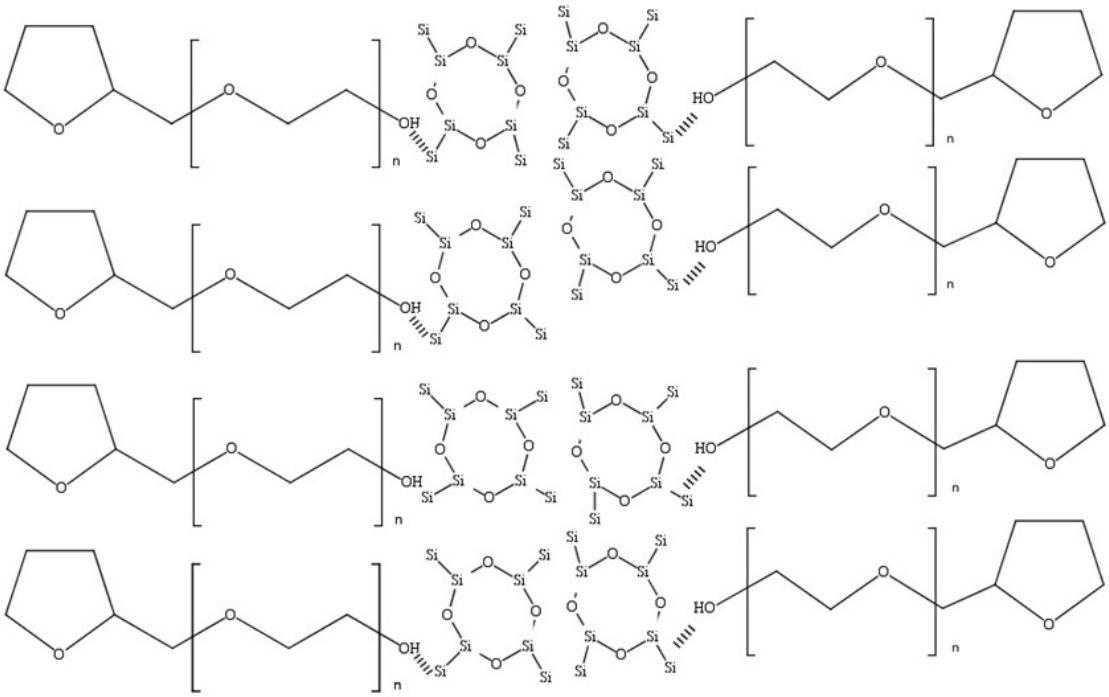

Figure H 8. *Proposed self-assembly mechanism of the silica "fibre"-like structures. Note – SBA-15 chemical structure is not fully represented, only the structure of a pore is.*

Cited References in this Appendix

Müller W.E.G., Schröder H.C., Muth S., Gietzen S., Korzhev M., Grebenjuk V.A., Wiens M., Schlomacher U., Wang X., The silicatein propeptide acts as inhibitor/modulator of self-organization during spicule axial filament formation, *Federation of European Biochemical Societies Journal*, 280 (2013) 1693-1708.

Wang X., Schröder H.C., Müller W.E.G., Enzymatically Synthesized Biosilica (Chapter 57) *in* Kim S-K. (Ed.), Handbook of Marine Biotechnology, 1st Edition, London, Elsevier Inc, 2015.

Appendix I –Pressure Behaviour during Depressurization

In Figure I 1 is shown the pressure behaviour during the depressurization step of the batch SFM process of a biomaterial for the filler selection assays.

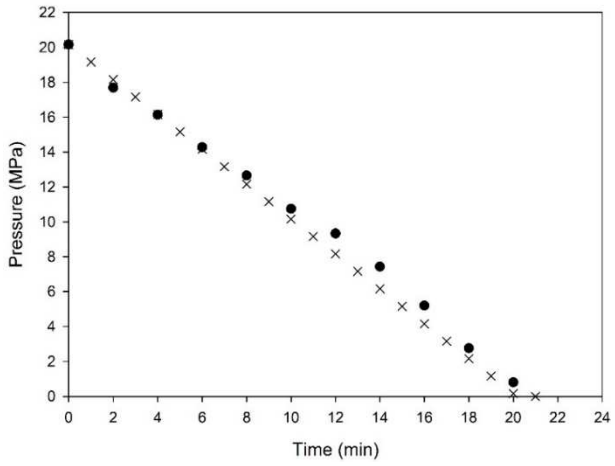

Figure I 1. *Pressure drop behavior during the depressurization step at a depressurization rate of 1 MPa.min^{-1}.*

In Figure I 2 is shown the pressure behaviour during the depressurization step of the batch SFM process of a biomaterial for the additivated and composite assays.

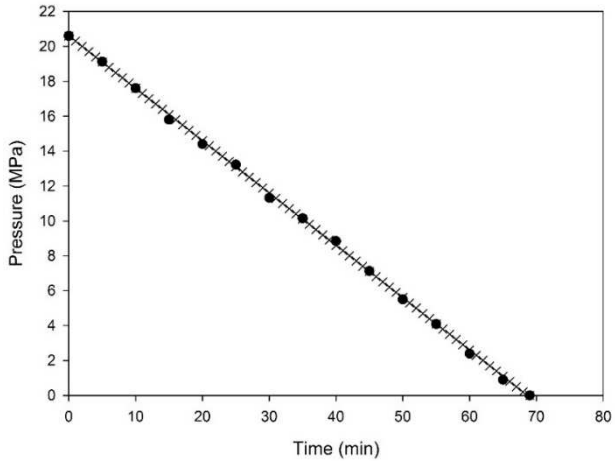

Figure I 2. *Pressure drop behavior during the depressurization step at a depressurization rate of 0.3 MPa.min^{-1}.*

As can be seen, on Figure I 1, when the critical point of CO_2 is reached there is an added difficulty to maintain the depressurization rate constant, due to the phase change. When the exit valve is opened, due to the large difference between the pressure inside the vessel and the ambient pressure the pressure drop is very fast, which is translated in a higher rate of depressurization within the first minutes.

Appendix J – Supplier Technical Data Sheet of SBA-15 and MCM-41

In Table J 1, are shown the physical properties of SBA-15, comparing to MCM-41, as supplied by the manufacturer (Claytec (USA)).

Table J 1. *Manufacturer information of morphological properties of SBA-15 and MCM-41.*

Claytec Number	**Framework Structure**	**Average BJH Framework Pore size (nm)**	**BET Surface Area ($m^2.g^{-1}$)**	**Framework Pore Volume ($cm^3.g^{-1}$)**	**Total Pore Volume ($cm^3.g^{-1}$)**
01-001	1D-Hexagonal MCM-41 Type	2.4	1050	0.79	0.92
01-002	1D-Hexagonal SBA-15 Type	8.5	718	0.90	0.93